Global Carbon Budget 2025

Pierre Friedlingstein[1,2], Michael O'Sullivan[1], Matthew W. Jones[3], Robbie M. Andrew[4], Dorothee C. E. Bakker[5], Judith Hauck[6,7], Peter Landschützer[8], Corinne Le Quéré[3], Hongmei Li[9,10], Ingrid T. Luijkx[11], Glen P. Peters[4], Wouter Peters[11,12], Julia Pongratz[13,10], Clemens Schwingshackl[13], Stephen Sitch[1], Josep G. Canadell[14], Philippe Ciais[15], Kjetil Aas[4], Simone R. Alin[16], Peter Anthoni[17], Leticia Barbero[18], Nicholas R. Bates[19,20], Nicolas Bellouin[21], Alice Benoit-Cattin[22], Carla F. Berghoff[23], Raffaele Bernardello[24], Laurent Bopp[2], Ida Bagus Mandhara Brasika[1,25], Matthew A. Chamberlain[26], Naveen Chandra[27], Frédéric Chevallier[15], Louise P. Chini[28], Nathan O. Collier[29], Thomas H. Colligan[30], Margot Cronin[31], Laique M. Djeutchouang[32,33,34], Xinyu Dou[35], Matt P. Enright[19,20], Kazutaka Enyo[36], Michael Erb[37,38], Wiley Evans[39], Richard A. Feely[16], Liang Feng[40,41], Daniel J. Ford[1], Adrianna Foster[42], Filippa Fransner[43,44], Thomas Gasser[45], Marion Gehlen[15], Thanos Gkritzalis[8], Jefferson Goncalves De Souza[1], Giacomo Grassi[46], Luke Gregor[47,48], Nicolas Gruber[47], Bertrand Guenet[49], Özgür Gürses[6], Kirsty Harrington[50], Ian Harris[51], Jens Heinke[52], George C. Hurtt[28], Yosuke Iida[36], Tatiana Ilyina[53,9,10], Akihiko Ito[54], Andrew R. Jacobson[55,56], Atul K. Jain[57], Tereza Jarníková[3], Annika Jersild[30], Fei Jiang[58], Steve D. Jones[8], Etsushi Kato[59], Ralph F. Keeling[60], Kees Klein Goldewijk[61], Jürgen Knauer[62], Yawen Kong[63,64], Jan Ivar Korsbakken[4], Charles Koven[65], Taro Kunimitsu[4], Xin Lan[55,56], Junjie Liu[66,67], Zhiqiang Liu[68], Zhu Liu[69], Claire Lo Monaco[70], Lei Ma[28], Gregg Marland[37,38], Patrick C. McGuire[71], Galen A. McKinley[72], Joe R. Melton[73], Natalie Monacci[74], Erwan Monier[75,76], Eric J. Morgan[60], David R. Munro[55,56], Jens D. Müller[77], Shin-Ichiro Nakaoka[78], Lorna R. Nayagam[78], Yosuke Niwa[78], Tobias Nutzel[13], Are Olsen[43,44], Abdirahman M. Omar[79,44], Naiqing Pan[80], Sudhanshu Pandey[66], Denis Pierrot[81], Zhangcai Qin[82], Pierre Regnier[83], Gregor Rehder[84], Laure Resplandy[85], Alizée Roobaert[8], Thais M. Rosan[1], Christian Rödenbeck[86], Jörg Schwinger[44,79], Ingunn Skjelvan[79,44], T. Luke Smallman[40,41], Victoria Spada[87], Mohanan G. Sreeush[6], Qing Sun[88], Adrienne J. Sutton[16], Colm Sweeney[56], Didier Swingedouw[89], Roland Séférian[90], Shintaro Takao[78], Hiroaki Tatebe[91,92], Hanqin Tian[80], Xiangjun Tian[93,94], Bronte Tilbrook[26,95], Hiroyuki Tsujino[96], Francesco Tubiello[97], Erik van Ooijen[26], Guido R. van der Werf[11], Sebastiaan J. van de Velde[98,99], Anthony P. Walker[100], Rik Wanninkhof[81], Xiaojuan Yang[100], Wenping Yuan[101], Xu Yue[102], Jiye Zeng[78]

1: Faculty of Environment, Science and Economy, University of Exeter, Exeter, EX4 4QF, UK
2: Laboratoire de Météorologie Dynamique, Institut Pierre-Simon Laplace, CNRS, École Normale Supérieure, Université PSL, Sorbonne Université, École Polytechnique, Paris, France
3: Tyndall Centre for Climate Change Research, School of Environmental Sciences, University of East Anglia, Norwich Research Park, Norwich NR4 7TJ, UK

4: CICERO Center for International Climate Research, Oslo 0349, Norway
5: School of Environmental Sciences, University of East Anglia, Norwich NR4 7TJ, UK
6: Alfred-Wegener-Institut, Helmholtz-Zentrum für Polar- und Meeresforschung, Am Handelshafen 12, 27570 Bremerhaven
7: Universität Bremen, FB02 Biology/Chemistry Bremen, Germany
8: Flanders Marine Institute (VLIZ), Jacobsenstraat 1, 8400, Ostend, Belgium
9: Helmholtz-Zentrum Hereon, Max-Planck-Straße 1, 21502 Geesthacht, Germany
10: Max Planck Institute for Meteorology, Bundesstraße 53, 20146 Hamburg, Germany
11: Wageningen University, Environmental Sciences Group, P.O. Box 47, 6700AA, Wageningen, The Netherlands
12: University of Groningen, Centre for Isotope Research, Groningen, The Netherlands
13: Ludwig-Maximilians-Universität München, Luisenstr. 37, 80333 München, Germany
14: CSIRO Oceans and Atmosphere, Canberra, ACT 2101, Australia
15: Laboratoire des Sciences du Climat et de l'Environnement, LSCE/IPSL, CEA-CNRS-UVSQ, Université Paris-Saclay, F-91198 Gif-sur-Yvette, France
16: National Oceanic and Atmospheric Administration, Pacific Marine Environmental Laboratory (NOAA/PMEL), 7600 Sand Point Way NE, Seattle, WA 98115, USA
17: Karlsruhe Institute of Technology, Institute of Meteorology and Climate Research/Atmospheric Environmental Research, 82467 Garmisch-Partenkirchen, Germany
18: Rosenstiel School of Marine Atmospheric and Earth Science, Cooperative Institute for Marine and Atmospheric Studies (CIMAS), University of Miami, 4600 Rickenbacker Causeway, Miami, FL, USA
19: Arizona State University, Tempe, Arizona, AZ 85287-5502, USA
20: Bermuda Institute of Ocean Sciences (BIOS), 17 Biological Lane, St. Georges, GE01, Bermuda
21: Department of Meteorology, University of Reading, Reading, RG6 6BB, UK
22: Marine and Freshwater Research Institute, Reykjavik, Iceland
23: Instituto Nacional de Investigación y Desarrollo Pesquero (INIDEP), Paseo Victoria Ocampo N°1, B7602HSA, Mar del Plata, Argentina
24: Barcelona Supercomputing Center, Barcelona, Spain
25: Faculty of Marine Science & Fisheries, Udayana University, Denpasar, Bali, 80361, Indonesia
26: CSIRO Environment, Castray Esplanade, Hobart, Tasmania 7004, Australia
27: Research Institute for Global Change, JAMSTEC, 3173-25 Showa-machi, Kanazawa, Yokohama, 236-0001, Japan
28: Department of Geographical Sciences, University of Maryland, College Park, MD 20742, USA
29: Computer Science and Engineering Division, Oak Ridge National Laboratory, Oak Ridge, TN 37831, USA
30: Earth System Science Interdisciplinary Center, University of Maryland, College Park, MD 20740, USA

31: Marine Institute, Rinville, Oranmore, Co Galway H91 R673, Ireland
32: School for Climate Studies, Stellenbosch University, Private Bag X1, Matieland, Stellenbosch, 7602, South Africa
33: Southern Ocean Carbon – Climate Observatory, CSIR, Rosebank, Cape Town, 7700, South Africa
34: Engr. Computer Science, University of California, Davis, CA 95616, USA
35: Department of Earth System Science, Stanford University, Stanford, CA 94305, USA
36: Japan Meteorological Agency, 3-6-9 Toranomon, Minato City, Tokyo, 105-8431, Japan
37: Research Institute for Environment, Energy, and Economics, Appalachian State University, Boone, North Carolina, USA
38: Department of Geological and Environmental Sciences, Appalachian State University, Boone, North Carolina, USA
39: Hakai Institute, 1713 Hyacinthe Bay Rd, Heriot Bay, BC, V0P 1H0, Canada
40: National Centre for Earth Observation, University of Edinburgh, Edinburgh, EH9 3FE, UK
41: School of Geosciences, University of Edinburgh, Edinburgh, EH9 3FE, UK
42: Climate and Global Dynamics Laboratory, National Center for Atmospheric Research
43: Geophysical Institute, University of Bergen, Allégaten 70, 5007 Bergen, Norway
44: Bjerknes Centre for Climate Research, Bergen, Norway
45: International Institute for Applied Systems Analysis (IIASA), Schlossplatz 1 A-2361 Laxenburg, Austria
46: European Commission, Joint Research Centre (JRC), Ispra, Italy
47: Environmental Physics Group, Institute of Biogeochemistry and Pollutant Dynamics and Center for Climate Systems Modeling (C2SM), ETH Zürich, Zurich, Switzerland
48: Swiss Data Science Center, 8050 Zurich, Switzerland
49: Laboratoire de Géologie, Ecole Normale Supérieure, CNRS UMR 8538, Institut Pierre-Simon Laplace, PSL Research University, Paris, France
50: Smith School for Enterprise and the Environment, University of Oxford, Oxford, UK
51: NCAS-Climate, Climatic Research Unit, School of Environmental Sciences, University of East Anglia, Norwich Research Park, Norwich, NR4 7TJ, UK
52: Potsdam Institute for Climate Impact Research (PIK), member of the Leibniz Association, P.O. Box 60 12 03, 14412 Potsdam, Germany
53: Universität Hamburg, Bundesstraße 55, 20146 Hamburg, Germany
54: Graduate School of Agricultural and Life Sciences, University of Tokyo, Tokyo, Japan
55: Cooperative Institute for Research in Environmental Sciences (CIRES), University of Colorado Boulder, Boulder, CO 80305, USA
56: National Oceanic and Atmospheric Administration Global Monitoring Laboratory (NOAA/GML), 325 Broadway R/GML, Boulder, CO 80305, USA

57: Department of Climate, Meteorology and Atmospheric Sciences, University of Illinois, Urbana, IL 61801, USA
58: Jiangsu Provincial Key Laboratory for Advanced Remote Sensing and Geographic Information Technology, International Institute for Earth System Science, Nanjing University, Nanjing, 210023, China.
59: Institute of Applied Energy (IAE), Minato-ku, Tokyo 105-0003, Japan
60: University of California, San Diego, Scripps Institution of Oceanography, La Jolla, CA 92093-0244, USA
61: Utrecht University, Faculty of Geosciences, Department IMEW, Copernicus Institute of Sustainable Development, Heidelberglaan 2, P.O. Box 80115, 3508 TC, Utrecht, the Netherlands
62: School of Life Sciences, Faculty of Science, University of Technology Sydney, Ultimo, NSW 2007, Australia
63: State Key Laboratory of Remote Sensing and Digital Earth, Aerospace Information Research Institute, Chinese Academy of Sciences, Beijing 100101, China
64: Ministry of Education Key Laboratory for Earth System Modeling, Department of Earth System Science, Tsinghua University, Beijing 100084, China
65: Lawrence Berkeley National Laboratory, USA
66: Jet Propulsion Laboratory, California Institute of Technology, Pasadena, CA, USA
67: Division of Geological and Planetary Sciences, California Institute of Technology, Pasadena, CA, USA
68: CMA Key Open Laboratory of Transforming Climate Resources to Economy, Chongqing Institute of Meteorological Sciences, Chongqing 401147, China
69: Department of Earth System Science, Tsinghua University, Beijing, China
70: LOCEAN Laboratory (Sorbonne Université, CNRS, IRD, MNHN), 4 Place Jussieu, F-75005 Paris, France
71: Department of Meteorology and National Centre for Atmospheric Science, University of Reading, Reading, UK
72: Lamont-Doherty Earth Observatory, Columbia University, New York, NY, USA
73: Climate Research Division, Environment and Climate Change Canada, Victoria, BC, Canada
74: College of Fisheries and Ocean Sciences, University of Alaska Fairbanks, Fairbanks, Alaska 99775-7220, USA
75: Department of Land, Air and Water Resources, University of California, Davis, CA 95616, USA
76: Climate Adaptation Research Center, University of California, Davis, CA 95616, USA
77: Carbon to Sea Initiative, Washington D.C., USA
78: Earth System Division, National Institute for Environmental Studies (NIES), 16-2 Onogawa, Tsukuba Ibaraki, 305-8506, Japan
79: NORCE Research, Jahnebakken 5, 5007 Bergen, Norway

80: Schiller Institute of Integrated Science and Society, Department of Earth and Environmental Sciences, Boston College, Chestnut Hill, MA 02467, USA
81: National Oceanic and Atmospheric Administration, Atlantic Oceanographic & Meteorological Laboratory (NOAA/AOML), 4301 Rickenbacker Causeway, Miami, FL 33149, USA
82: School of Atmospheric Sciences, Sun Yat-sen University, Zhuhai 519000, China
83: Department of Geoscience, Environment & Society-BGEOSYS, Université Libre de Bruxelles, 1050 Brussels, Belgium
84: Leibniz Institute for Baltic Sea Research Warnemünde (IOW), Seestrasse 15, 18119 Rostock, Germany
85: Princeton University, Department of Geosciences and Princeton Environmental Institute, Princeton, NJ, USA
86: Max Planck Institute for Biogeochemistry, P.O. Box 600164, Hans-Knöll-Str. 10, 07745 Jena, Germany
87: Canadian Centre for Climate Modelling and Analysis, Environment and Climate Change Canada, Victoria, BC, Canada
88: Institute for Climate and Environmental Physics, University of Bern, Bern, Switzerland
89: Environnements et Paléoenvironnements Océaniques et Continentaux (EPOC) UMR CNRS 5805 EPOC - OASU, Université de Bordeaux, Allée Geoffroy Saint Hilaire, 33615 Pessac, France
90: Centre National de Recherches Météorologiques, Université de Toulouse, Météo-France, CNRS, UMR 3589, Toulouse, France
91: Research Center for Environmental Modeling and Application, Japan Agency for Marine-Earth Science and Technology,Yokohama, Japan
92: Advanced Institute for Marine Ecosystem Change, Japan Agency for Marine-Earth Science and Technology, Yokohama, Japan
93: State Key Laboratory of Tibetan Plateau Earth System and Resource Environment, Institute of Tibetan Plateau Research, Chinese Academy of Sciences, Beijing 100101, China
94: University of Chinese Academy of Sciences, Beijing 101408, China
95: Australian Antarctic Partnership Program, University of Tasmania, Hobart, Australia
96: JMA Meteorological Research Institute, Tsukuba, Ibaraki, Japan
97: Statistics Division, Food and Agriculture Organization of the United Nations, Via Terme di Caracalla, Rome 00153, Italy
98: Earth Sciences New Zealand, Wellington, New Zealand
99: Department of Marine Science, University of Otago, Dunedin, New Zealand
100: Climate Change Science Institute and Environmental Sciences Division, Oak Ridge National Laboratory, Oak Ridge, TN 37831, USA
101: Institute of Carbon Neutrality, College of Urban and Environmental Sciences, Peking University, Beijing 100091, China

102: School of Environmental Science and Engineering, Nanjing University of Information Science and Technology (NUIST), Nanjing, 210044, China

Correspondence to: Pierre Friedlingstein (p.friedlingstein@exeter.ac.uk)

Abstract

Accurate assessment of anthropogenic carbon dioxide (CO_2) emissions and their redistribution among the atmosphere, ocean, and terrestrial biosphere in a changing climate is critical to better understand the global carbon cycle, support the development of climate policies, and project future climate change. Here we describe and synthesise datasets and methodologies to quantify the five major components of the global carbon budget and their uncertainties. Fossil CO_2 emissions (E_{FOS}) are based on energy and cement production data. Emissions from land-use change (E_{LUC}) are estimated by bookkeeping models based on land-use data. The global atmospheric CO_2 growth rate (G_{ATM}) is computed from changes in concentration measured at surface stations. The global net uptake of CO_2 by the ocean (S_{OCEAN}) is estimated with global ocean biogeochemistry models and observation-based fCO_2-products. The global net uptake of CO_2 by the land (S_{LAND}) is estimated with dynamic global vegetation models. Additional lines of evidence are provided by atmospheric inversions, atmospheric oxygen measurements, ocean interior observation-based estimates, and Earth System Models. This year, we introduced corrections on the E_{LUC}, S_{OCEAN} and S_{LAND} estimates. The sum of all sources and sinks results in the carbon budget imbalance (B_{IM}), a measure of imperfect data and incomplete understanding of the contemporary carbon cycle. All uncertainties are reported as ±1σ.

For the year 2024, E_{FOS} increased by 1.1% relative to 2023, with fossil emissions at 10.3 ± 0.5 GtC yr^{-1} (including the cement carbonation sink, 0.2GtC yr^{-1}), E_{LUC} was 1.3 ± 0.7 GtC yr^{-1}, for total anthropogenic CO_2 emissions of 11.6 ± 0.9 GtC yr^{-1} (42.4 ± 3.2 $GtCO_2$ yr^{-1}). Also, for 2024, G_{ATM} was 7.9 ± 0.2 GtC yr^{-1} (3.73 ± 0.1 ppm yr^{-1}), 2.2 GtC above the 2023 growth rate. S_{OCEAN} was 3.4 ± 0.4 GtC yr^{-1} and S_{LAND} was 1.9 ± 1.1 GtC yr^{-1}, leaving a large negative B_{IM} (-1.7 GtC yr^{-1}), suggesting that the total sink or G_{ATM} is strongly overestimated in 2024. The global atmospheric CO_2 concentration averaged over 2024 reached 422.8 ± 0.1 ppm. Preliminary data for 2025 suggest an increase in E_{FOS} relative to 2024 of +1.0% (0.2% to 1.7%) globally, and atmospheric CO_2 concentration increasing by 2.1 ppm reaching 425.6 ppm, 53% above the pre-industrial level (around 278 ppm in 1750). Overall, the mean and trend in the components of the global carbon budget are consistently estimated over the period 1959-2024, with a near-zero overall budget imbalance, although discrepancies of up to around 1 GtC yr^{-1} persist for the representation of annual to decadal variability in CO_2 fluxes. Comparison of estimates from multiple approaches and observations shows: (1) a persistent large uncertainty in the estimate of land-use change emissions, (2) a low agreement between the different methods on the

magnitude of the land CO_2 flux in the northern extra-tropics, and (3) a discrepancy between the different methods on the mean ocean sink.

This living data update documents changes in methods and datasets applied to this most-recent global carbon budget as well as evolving community understanding of the global carbon cycle. The data presented in this work are available at https://doi.org/10.18160/GCP-2025 (Friedlingstein et al., 2025c).

Executive Summary

Global fossil CO_2 emissions (including cement carbonation) are expected to further increase in 2025 by 1.0% relative to 2024 (range 0.2% to 1.7%), bringing fossil emissions to an expected 10.4 GtC yr^{-1} (38.1 $GtCO_2$ yr^{-1}) [1]. Emissions from coal, oil and gas in 2025 are all expected to be above their 2024 levels (by 1.0%, 1.1% and 1.3% respectively). These preliminary estimates are based on available data for 2025. Consolidated data confirm a growth of 1.1% in 2024 relative to 2023, with fossil CO_2 emissions of 10.3 ± 0.5 GtC yr^{-1} (37.8 ± 1.8 $GtCO_2$ yr^{-1}) in 2024.

Regionally, fossil emissions are projected to grow in 2025 in the USA and be nearly flat in the European Union, reversing long-term decreases, and to grow in China and India, albeit more slowly compared to recent trends. The increase in fossil emissions in 2025 relative to 2024 is projected to be 0.4% (-0.1% to 0.9%) for China, 2.5% (2.2% to 2.8%) for the United States, 1.1% for India. 2025 emissions for the European Union are projected to decrease by -0.1%. Projected emissions in Japan, provided this year for the first time, are for a decrease of -0.9%. Emissions are also projected to increase by 6.7% for international aviation and by 2.0% for international shipping, and to increase by 0.9% (-1.0% to 3.0%) for the rest of the world in aggregate. The global carbon intensity of energy has consistently decreased over the past decade (-0.7% yr^{-1}), indicating decarbonisation of the energy system in China (-1.4% yr^{-1}), the European Union (-1.5% yr^{-1}), and the USA (-1.3% yr^{-1}), but no decline in India and an increase in the rest of the world in aggregate. These trends are not sufficient to offset the growth in global energy demand, which is driven by growing GDP globally and a weakening decline in energy per GDP, particularly in China and the US.

Fossil CO_2 emissions decreased ($p<0.05$) in 35 economies with growing GDP ($p<0.05$) during the decade 2015-2024. The list of decarbonising economies nearly doubled since the previous decade (2005-2014; 18 countries). These 35 decarbonising economies contribute 2.7 GtC yr^{-1} (9.7 $GtCO_2$) fossil fuel CO_2 emissions over the last decade in aggregate, representing 27% of the world CO_2 fossil

[1] All growth rates use a leap year adjustment that corrects for the extra day in 2024.

emissions.

Global net CO_2 emissions from land use averaged 1.4 ± 0.7 GtC yr^{-1} (5.0 ± 2.6 $GtCO_2$ yr^{-1}) for the 2015-2024 period. Emissions from deforestation, the main driver of global gross emissions, remain high at around 1.9 GtC yr^{-1} over the 2015-2024 period, highlighting the strong potential of halting deforestation for emissions reductions. Sequestration of 1.3 GtC yr^{-1} through re-/afforestation and forest regrowth in shifting cultivation cycles offsets two third of the deforestation emissions. In addition, smaller net emissions are due to wood harvest & forest management, peat drainage and peat fire. Regionally, the highest net emitters during 2015-2024 were Brazil, Indonesia, and the Democratic Republic of the Congo, with these 3 countries contributing more than half of global land-use CO_2 emissions. Net carbon dioxide removals (CDR) from re-/afforestation were highest in China, the USA, and the EU27, with combined removals of 0.3 GtC yr^{-1} during 2015-2024.

Since the late-1990s, emissions from land use show a statistically significant decrease at a rate of around 0.2 GtC per decade, with a larger drop within the most recent decade. Preliminary data for 2025 suggest emissions decreased to around 1.1 GtC (4.1 $GtCO_2$ yr^{-1}), mainly attributable to the end of the El Niño conditions.

Total anthropogenic emissions (fossil and land use, including the carbonation sink) were 11.6 GtC yr^{-1} (42.4 $GtCO_2$ yr^{-1}) in 2024, with a slightly lower preliminary estimate of 11.5 GtC yr^{-1} (42.2 $GtCO_2$ yr^{-1}) for 2025. Total anthropogenic emissions have grown more slowly over the last decade (0.3% yr^{-1} over the 2015-2024 period) compared to the previous decade (1.9% yr^{-1} over 2005-2014).

The remaining carbon budget from the beginning of 2026 for a 50% likelihood to limit warming to 1.5°C is nearly exhausted (50 GtC, 170 $GtCO_2$ left, equivalent to around 4 years at the 2025 emissions levels), consistent with the warming of the planet attributed to human activities, which reached 1.36°C in 2024. Each additional cumulative emission of about 180 $GtCO_2$ will lead to approximately 0.1°C of warming. The remaining carbon budgets to limit warming to 1.7°C and 2°C above the 1850-1900 level have been reduced to 145 GtC (525 $GtCO_2$, 12 years) and 290 GtC (1055 $GtCO_2$, 25 years) respectively.

The concentration of CO_2 in the atmosphere is set to reach 425.6 ppm in 2025, 53% above pre-industrial levels. The atmospheric CO_2 growth rate was 5.6 ± 0.02 GtC yr^{-1} (2.6 ppm) during the decade 2015-2024 (50% of total CO_2 emissions). 2024 had a record-high growth rate of 7.9 ± 0.02 GtC yr^{-1} (3.7 ppm) mainly due to the 2023/2024 El Niño conditions. The preliminary 2025 growth rate estimate is 4.4 GtC (2.1 ppm).

The ocean sink, the global net uptake of CO_2 by the ocean, has taken up 29% of the total emissions in the past decade, after being re-evaluated upwards based on new evidence and process understanding. The ocean sink has been stagnant since 2016, largely in response to climate variability modulating the growing sink trend, but further affected by the ocean heatwave

of 2023-2024 in the Northern Hemisphere. The ocean CO_2 sink was 3.2 ± 0.4 GtC yr^{-1} during the decade 2015-2024, with a preliminary estimate of 3.2 GtC yr^{-1} for 2025, slightly below 2024 levels, due to the end of the El Niño conditions in 2024 and associated reduced atmospheric CO_2 growth rate.

The land sink, which is the global net uptake of CO_2 by the land excluding land use, has taken up 21% of the total emissions in the past decade, after being re-evaluated downwards based on improved process representation. The land sink has been relatively stagnant since 2000, largely in response to climate variability and climate change offsetting the CO_2 induced growth. The land CO_2 sink was 2.4 ± 0.8 GtC yr^{-1} during the 2015-2024 decade but was reduced to 1.9 GtC ± 0.8 GtC yr^{-1} in 2024. The preliminary estimate for the land sink in 2025 is an increase to 3.1 GtC, recovering entirely from its strong drop during the 2023-2024 El Niño conditions.

The effects of climate change and climate variability act to reduce the land and ocean CO_2 sinks by 25% and 7.1% respectively, on average for the 2015-2024 period. The land sink is negatively affected by warming with decreased tropical plant productivity and enhanced ecosystem respiration globally. The ocean sink is negatively affected by altered oceanic circulation and surface warming which decreases CO_2 solubility**.**

So far in 2025, global fire CO_2 emissions have been approximately 20% lower than the 2015-2024 average due to low fire activity in Africa and the tropics, reaching 1.2-1.4 GtC globally during January-September. This contrasts with the above average fire emissions in 2023 (1.7-2.1 GtC yr^{-1}) and 2024 (1.6-2.2 GtC yr^{-1}) due to extensive fires in Canada (2023) and Brazil and Bolivia (2024). These fire emissions estimates should not be directly compared with the land-use emissions or the land sink, because they represent a gross carbon flux to the atmosphere and do not account for post-fire recovery. They also do not distinguish between natural, climate-driven, and land-use-related fires.

1 Introduction

The concentration of carbon dioxide (CO_2) in the atmosphere has increased from approximately 278 parts per million (ppm) in 1750 (Gulev et al., 2021), the beginning of the Industrial Era, to 422.8 ± 0.1 ppm in 2024 (Lan et al., 2025; Figure 1). The atmospheric CO_2 increase above pre-industrial levels was, initially, primarily caused by the release of carbon to the atmosphere from deforestation and other land-use change activities (Canadell et al., 2021). While emissions from fossil fuels started before the Industrial Era, they became the dominant source of anthropogenic emissions to the atmosphere from around 1950 and their relative share has continued to increase until present. Anthropogenic emissions occur on top of an active natural carbon cycle that circulates carbon between the reservoirs of the atmosphere, ocean, and terrestrial biosphere on time scales from sub-daily to millennial, while exchanges with geologic reservoirs occur on longer timescales (Archer et al., 2009).

The global carbon budget (GCB) presented here refers to the mean, variations, and trends in the perturbation of CO_2 in the environment, referenced to the beginning of the Industrial Era (defined here as 1750). This paper describes the components of the global carbon cycle over the historical period with a stronger focus on the recent period (since 1959, onset of robust atmospheric CO_2 measurements), the last decade (2015-2024), the last year (2024) and the current year (2025). Finally, it provides cumulative emissions from fossil fuels and land-use change since the year 1750, and since the year 1850 (the reference year for historical simulations in IPCC).

We quantify the input of CO_2 to the atmosphere by emissions from human activities, the growth rate of atmospheric CO_2 concentration, and the resulting changes in the storage of carbon in the land and ocean reservoirs in response to increasing atmospheric CO_2 levels, climate change and variability, and other anthropogenic and natural changes (Figure 2). An understanding of this perturbation budget over time and the underlying variability and trends of the natural carbon cycle is necessary to understand the response of natural sinks to changes in climate, CO_2 and land-use change drivers, and to quantify emissions compatible with a given climate stabilisation target.

The components of the CO_2 budget that are reported annually in this paper include separate and independent estimates for the CO_2 emissions from (1) fossil fuel combustion and oxidation from all energy and industrial processes; also including cement production and carbonation (E_{FOS}; GtC yr^{-1}) and (2) the emissions resulting from deliberate human activities on land, including those leading to land-use change (E_{LUC}; GtC yr^{-1}); and their partitioning among (3) the growth rate of atmospheric CO_2 concentration (G_{ATM}; GtC yr^{-1}), and the uptake of CO_2 (the 'CO_2 sinks') in (4) the ocean (S_{OCEAN}; GtC yr^{-1}) and (5) on land (S_{LAND}; GtC yr^{-1}). The CO_2 sinks as defined here conceptually include the response of the land (including inland waters and estuaries) and ocean (including coastal and marginal seas) to

elevated CO_2 and changes in climate and other environmental conditions, although in practice not all processes are fully accounted for (see Section 2.10). Note that the term sink means that the net transfer of carbon is from the atmosphere to land or the ocean, but it does not imply any permanence of that sink in the future.

Global emissions and their partitioning among the atmosphere, ocean and land are in mass balance in the real world. Due to the combination of imperfect spatial and/or temporal data coverage, errors in each estimate, and smaller terms not included in our budget estimate (discussed in Section 2.10), the GCB independent estimates (1) to (5) above do not necessarily add up to zero. We hence estimate a budget imbalance (B_{IM}), which is a measure of the mismatch between the estimated emissions and the estimated changes in the atmosphere, land, and ocean, as follows:

$$B_{IM} = E_{FOS} + E_{LUC} - (G_{ATM} + S_{OCEAN} + S_{LAND}) \quad (1)$$

G_{ATM} is usually reported in ppm yr^{-1}, which we convert to units of carbon mass per year, GtC yr^{-1}, using 1 ppm = 2.124 GtC (Ballantyne et al., 2012; Table 1). Units of gigatonnes of CO_2 (or billion tonnes of CO_2) used in policy are equal to 3.664 multiplied by the value in units of GtC.

We also assess a set of additional lines of evidence derived from global atmospheric inversion system results (Section 2.7), observed changes in oxygen concentration (Section 2.8) and Earth System Models (ESMs) simulations (Section 2.9), all these methods closing the global carbon balance (zero B_{IM}).

We further quantify E_{FOS} and E_{LUC} by country, including both territorial and consumption-based accounting for E_{FOS} (see Section 2), and discuss missing terms from sources other than the combustion of fossil fuels (see Section 2.10). We also assess carbon dioxide removal (CDR) (see Sect. 2.2 and 2.3). Land-based CDR is significant, but already accounted for in E_{LUC} in equation (1) (Sect 3.2.2). Other CDR methods, not based on vegetation, are currently several orders of magnitude smaller than the other components of the budget (Sect. 3.3), hence these are not included in equation (1), or in the global carbon budget tables or figures (except for Figure 2 where CDR is shown primarily for illustrative purpose).

The global CO_2 budget has been assessed by the Intergovernmental Panel on Climate Change (IPCC) in all assessment reports (Watson et al., 1990; Schimel et al., 1995; Prentice et al., 2001; Denman et al., 2007; Ciais et al., 2013; Canadell et al., 2021), and by others (e.g., Ballantyne et al., 2012). The Global Carbon Project (GCP, www.globalcarbonproject.org, last access: 23 October 2025) has coordinated this cooperative community effort for the annual publication of global carbon budgets for the year 2005 (Raupach et al., 2007; including fossil emissions only), year 2006 (Canadell et al., 2007), year 2007 (GCP, 2008), year 2008 (Le Quéré et al., 2009), year 2009 (Friedlingstein et al., 2010), year 2010 (Peters et al., 2012a), year 2012 (Le Quéré et al., 2013; Peters et al., 2013), year 2013 (Le Quéré et al., 2014), year 2014 (Le Quéré et al., 2015a; Friedlingstein et al., 2014), year 2015 (Jackson et al., 2016;

Le Quéré et al., 2015b), year 2016 (Le Quéré et al., 2016), year 2017 (Le Quéré et al., 2018a; Peters et al., 2017a), year 2018 (Le Quéré et al., 2018b; Jackson et al., 2018), year 2019 (Friedlingstein et al., 2019; Jackson et al., 2019; Peters et al., 2020), year 2020 (Friedlingstein et al., 2020; Le Quéré et al., 2021), year 2021 (Friedlingstein et al., 2022a; Jackson et al., 2022), year 2022 (Friedlingstein et al., 2022b), the year 2023 (Friedlingstein et al., 2023), and most recently the year 2024 (Friedlingstein et al., 2025a). Each of these papers updated previous estimates with the latest available information for the entire time series.

We adopt a range of ±1 standard deviation (σ) to report the uncertainties in our global estimates, representing a likelihood of 68% that the true value will be within the provided range if the errors have a gaussian distribution, and no bias is assumed. Note that when less than 10 individual data are available for an estimate (e.g., atmospheric inversions, *f*-CO_2 products), we provide the full range, as opposed to the standard deviation. The choice of reporting a ±1 σ r reflects the difficulty of characterising the uncertainty in the CO_2 fluxes between the atmosphere and the ocean and land reservoirs individually, particularly on an annual basis, as well as the difficulty of updating the CO_2 emissions from land-use change. A likelihood of 68% provides an indication of our current capability to quantify each term and its uncertainty given the available information. The uncertainties reported here combine statistical analysis of the underlying data, assessments of uncertainties in the generation of the datasets, and expert judgement of the likelihood of results lying outside this range. The limitations of current information are discussed in the paper and have been examined in detail elsewhere (Ballantyne et al., 2015; Zscheischler et al., 2017). We also use a qualitative assessment of confidence level to characterise the annual estimates from each term based on the type, amount, quality, and consistency of the different lines of evidence as defined by the IPCC (Stocker et al., 2013).

This paper provides a detailed description of the datasets and methodology used to compute the global carbon budget estimates for the industrial period, from 1750 to 2025, and in more detail for the recent period since 1959. This paper is updated every year using the format of 'living data' to keep a record of budget versions and the changes in new data, revision of data, and changes in methodology that lead to changes in estimates of the carbon budget. All underlying data used to produce the budget and additional materials associated with the release of each new version are available via the Global Carbon Budget website (https://globalcarbonbudget.org/ , last access: 23 October 2025), with emissions also available through the Global Carbon Atlas (http://www.globalcarbonatlas.org, last access: 23 October 2025). With this approach, we aim to provide the highest transparency and traceability in the reporting of CO_2, the key driver of climate change.

2 Methods

Multiple organisations and research groups around the world generated the original measurements and data used to complete the global carbon budget. The effort presented here is thus mainly one of

synthesis, where results from individual groups are collated, analysed, and evaluated for consistency. We facilitate access to original data with the understanding that primary datasets will be referenced in future work (see Table 2 for how to cite the datasets, and Section on data availability). Descriptions of the measurements, models, and methodologies follow below, with more detailed descriptions of each component provided as Supplementary Information (Supplement Tables S1 to S5). In the GCB, when possible, we account for adjustments and corrections to the components estimates. We refer to 'adjustments' when accounting for known processes not included in one estimate (ex. river correction for fCO2 products), while we refer to 'corrections' when addressing known biases in one estimate (ex. replaced sinks and sources for DGVMs).

This is the 20th version of the global carbon budget and the 14th revised version in the format of a living data update in Earth System Science Data. It builds on the latest published global carbon budget of Friedlingstein et al. (2025a). The main changes this year are: the inclusion of (1) data to year 2024 and a projection for the global carbon budget for year 2025; (2) transient carbon densities in the estimate of E_{LUC}, (3) a correction on S_{LAND} to account for the historical changes in forest cover, (4) a correction on S_{OCEAN} to account for the underestimation of the sink by GOBMs and for the ocean temperature gradients in the *f*CO_2-products estimate, (5) an estimate of the atmospheric CO_2 growth rate derived from satellite observations, and (6) decadal estimates of change in the dissolved inorganic carbon inventory in the interior ocean. Other methodological differences are summarised in Table 3 and previous changes since 2006 are provided in Table S10.

2.1 Fossil CO_2 emissions (E_{FOS})

2.1.1 Historical period 1850-2024

The estimates of global and national fossil CO_2 emissions (E_{FOS}) include the oxidation of fossil fuels through both combustion (e.g., transport, heating) and chemical oxidation (e.g., carbon anode decomposition in aluminium refining) activities, and the decomposition of carbonates in industrial processes (e.g. the production of cement). We also include CO_2 uptake from the cement carbonation process. Several emissions sources are not estimated or not fully covered: coverage of emissions from lime production are not global, and decomposition of carbonates in glass and ceramic production are included only for the "Annex 1" countries of the United Nations Framework Convention on Climate Change (UNFCCC) for lack of activity data. These omissions are considered to be minor. Short-cycle carbon emissions - for example from combustion of biomass - are not included here but are accounted for in the CO_2 emissions from land use (see Section 2.2).

Our estimates of fossil CO_2 emissions rely on data collection by many other parties. Our goal is to produce the best estimate of this flux, and we therefore use a prioritisation framework to combine data from different sources that have used different methods, while being careful to avoid double counting

and undercounting of emissions sources. The CDIAC-FF emissions dataset, derived largely from UN energy data, forms the foundation, and we extend emissions to 2024 using energy growth rates reported by the Energy Institute (a dataset formerly produced by BP). We then proceed to replace estimates using data from what we consider to be superior sources, for example Annex 1 countries' official submissions to the UNFCCC. All data points are potentially subject to revision, not just the latest year. For full details see Andrew and Peters (2025).

Other estimates of global fossil CO_2 emissions exist, and these are compared by Andrew (2020a). The most common reason for differences in estimates of global fossil CO_2 emissions is a difference in which emissions sources are included in the datasets. Datasets such as those published by the Energy Institute, the US Energy Information Administration, and the International Energy Agency's 'CO_2 emissions from fuel combustion' are all generally limited to emissions from combustion of fossil fuels. In contrast, datasets such as PRIMAP-hist, CEDS, EDGAR, and GCP's dataset aim to include all sources of fossil CO_2 emissions. See Andrew (2020a) for detailed comparisons and discussion.

Cement products absorb CO_2 from the atmosphere over their lifetimes, a process known as 'cement carbonation'. We estimate this CO_2 sink, from 1931 onwards, as the average of two studies in the literature (Cao et al., 2020; Guo et al., 2021). Both studies use the same model, developed by Xi et al. (2016), with different parameterisations and input data, with the estimate of Guo and colleagues being a revision of Xi et al. (2016). The trends of the two studies are very similar. Since carbonation is a function of both current and previous cement production, we extend these estimates to 2024 by using the growth rate derived from the smoothed cement emissions (10-year smoothing) fitted to the carbonation data. In the present budget, we always include the cement carbonation carbon sink in the fossil CO_2 emission component (E_{FOS}) unless explicitly stated otherwise.

We use the Kaya Identity for a simple decomposition of CO_2 emissions into the key drivers (Raupach et al., 2007). While there are variants (Peters et al., 2017b), we focus here on a decomposition of CO_2 emissions into population, GDP per person, energy use per GDP, and CO_2 emissions per energy. Multiplying these individual components together returns the CO_2 emissions. Using the decomposition, it is possible to attribute the change in CO_2 emissions to the change in each of the drivers. This method gives a first order understanding of what causes CO_2 emissions to change each year.

2.1.2 2025 projection

We provide a projection of global fossil CO_2 emissions in 2025 by combining separate projections for China, USA, EU, India, Japan, and for all other countries combined. The methods are different for each of these. For China we use growth rates from the 2026 edition of the National Bureau of Statistics' Statistical Communique along with cement clinker trade data and estimated changes in lime production. For the USA our projection is taken directly from the Energy Information Administration's (EIA)

Short-Term Energy Outlook (EIA, 2026), combined with the year-to-date growth rate of cement clinker production. For the EU we use monthly energy data from Eurostat to derive estimates of monthly CO_2 emissions through December (Andrew, 2021). EU cement emissions are based on available production data through December from three of the largest producers, Germany, Poland, and Spain as well as production indices for Italy and France. India's projected emissions are derived from monthly estimates through December using the methods of Andrew (2020b). Japan's emissions are based on monthly estimates through December. Emissions from international transportation (bunkers) are estimated separately for aviation and shipping. Changes in aviation emissions are derived primarily from OECD monthly estimates, extrapolated using the growth rates of global flight miles from Airportia. Shipping emissions are derived from estimates of sales of bunker fuels provided by Ship and Bunker (Ship and Bunker, 2026). Emissions for the rest of the world are derived for coal and cement using projected growth in economic production from the IMF (2025) combined with extrapolated changes in emissions intensity of economic production; for oil using a global constraint from EIA; and for natural gas using a global constraint from IEA. More details on the E_{FOS} methodology and its 2025 projection can be found in Supplement S.1.

We compare our 2025 projection with the Carbon Monitor (2025). Carbon Monitor is a dataset of daily emissions constructed using hourly to daily proxy data (e.g., electricity consumption, travel patterns, etc) instead of energy use data (Liu et al., 2020a; Liu et al., 2020b). Emissions estimates from January to December are combined to give a full-year 2025 estimate.

2.2 CO_2 emissions from land-use, land-use change and forestry (E_{LUC})

2.2.1 Historical period 1850-2024

The net CO_2 flux from land-use, land-use change and forestry (E_{LUC}, called land-use change emissions in the rest of the text) includes CO_2 fluxes from deforestation, afforestation, logging, and forest degradation (including harvest activity), shifting cultivation (cycle of cutting forest for agriculture, then abandoning), regrowth of forests (following wood harvest or agriculture abandonment), peat burning, and peat drainage.

Updated estimates from three bookkeeping models are used to quantify gross emissions, gross removals, and the resulting net E_{LUC}: BLUE (Hansis et al., 2015), LUCE (Qin et al. 2024), and OSCAR (Gasser et al., 2020). An important improvement compared to previous GCBs is the use of transient carbon densities by all three bookkeeping models, i.e., they consider the effects of environmental changes, such as atmospheric CO_2 increase, on vegetation and soil carbon densities, to estimate E_{LUC} (Gasser et al., 2020; Dorgeist et al., 2024). The GCB assessments have for a long time also (and initially exclusively) used estimates from the bookkeeping model H&C2023 (Houghton and Castanho, 2023), its predecessor H&N2017 (Houghton and Nassikas, 2017), and earlier versions. However,

H&C2023 does not consider transient carbon densities and only provides data up to 2020, which implies the need to extrapolate its data to the time after 2020. As the model does thus not incorporate the most recent developments in bookkeeping modeling, it is not used anymore in GCB2025.

Emissions from peat burning and peat drainage are added from external datasets (see Supplement S.2.2): peat fire emissions from the Global Fire Emission Database (GFED4s; van der Werf et al., 2017) and peat drainage emissions averaged from estimates of the Food Agriculture Organization (Conchedda and Tubiello, 2020; FAO, 2025a) and from simulations with the DGVM ORCHIDEE-PEAT (Qiu et al., 2021) and the DGVM LPX-Bern (Lienert and Joos, 2018; Müller and Joos, 2021).

Uncertainty estimates were derived from the Dynamic Global Vegetation Models (DGVMs) ensemble for the time period prior to 1960, and using for the recent decades an uncertainty range of ±0.7 GtC yr^{-1}, which is a semi-quantitative measure for annual and decadal emissions and reflects our best value judgement that there is at least 68% chance (±1σ) that the true land-use change emission lies within the given range, for the range of processes considered here.

The GCB E_{LUC} estimates follow the CO_2 flux definition of global carbon cycle models and differ from IPCC definitions adopted in National GHG Inventories (NGHGI) for reporting under the UNFCCC. The latter typically include terrestrial fluxes occurring on all land that countries define as managed, following the IPCC managed land proxy approach (Grassi et al., 2018). This partly includes fluxes due to environmental change (e.g., atmospheric CO_2 increase), which are part of S_{LAND} in our definition. As a result, global emission estimates are smaller for NGHGI than for the global carbon budget definition (Grassi et al., 2023). The same is the case for the FAO estimates of carbon fluxes on forest land, which include both anthropogenic and natural fluxes on managed land (Tubiello et al., 2025; FAO, 2025b). Using the NGHGI data collected and processed in the LULUCF data hub V3.1 (Melo et al. 2025), we translate the GCB and NGHGI definitions to each other, to provide a comparison of the anthropogenic carbon budget as reported in GCB to the official country reporting to the UNFCCC convention. We further compare these estimates with the net atmosphere-to-land flux from atmospheric inversion systems (see Section 2.7), averaged over managed land only.

E_{LUC} contains a range of fluxes that are related to Carbon Dioxide Removal (CDR). CDR is defined as the set of anthropogenic activities that remove CO_2 from the atmosphere, in addition to the Earth's natural processes (such as carbon uptake in response to atmospheric CO_2 increase), and store it in durable form, such as in forest biomass, soils, long-lived products, oceans or geological reservoirs. Here, we quantify vegetation-based CDR that is implicitly or explicitly captured by land-use fluxes (CDR not based on vegetation is discussed in Section 2.3). We quantify CDR through re/afforestation from the three bookkeeping estimates by separating permanent increases in forest cover, which counts as CDR, from forest regrowth in shifting cultivation cycles (not part of CDR; see Supplement S.2.2). It should be noted that the permanence of the storage under climate risks such as fire is increasingly

questioned. Other CDR activities related to land use but not fully accounted for in our E_{LUC} estimate include the transfer of carbon to harvested wood products (HWP), bioenergy with carbon capture and storage (BECCS), and biochar production (Babiker et al., 2022; Smith et al., 2024). The different bookkeeping models all represent HWP but with varying details concerning product usage and their lifetimes. BECCS and biochar are currently only represented in bookkeeping and DGVM models regarding the CO_2 removal through photosynthesis, without accounting for the durable storage. HWP, BECCS, and biochar are typically counted as CDR once the transfer to the durable storage site occurs and not when the CO_2 is removed from the atmosphere, which complicates a direct comparison to the GCB approach to quantify annual fluxes to and from the atmosphere. We provide estimates for CDR through HWP, BECCS, and biochar based on independent studies in Section 3.2.2. HWP and BECCS estimates reflect updated 2024 data of the State of CDR report (Smith et al., 2024), while biochar estimates correspond to 2023 due to unavailability of newer data. We do not add them to our E_{LUC} estimate to avoid potential double-counting that arises from the partial consideration of HWP, BECCS, and biochar in the bookkeeping and DGVM models and to avoid inconsistencies from the temporal discrepancy between transfer to storage and removal from the atmosphere. More details on the E_{LUC} methodology can be found in Supplement S.2.

2.2.2 2025 Projection

We project the 2025 land-use emissions for BLUE, OSCAR, and LUCE based on their E_{LUC} estimates for 2023 and adding the anomalies in carbon emissions from peat fires in equatorial Asia and tropical deforestation and degradation fires (2025 emissions relative to 2023 emissions) from GFED4s (van der Werf et al., 2017) estimated using active fire data (MCD14ML; Giglio et al., 2016). 2023 is used as base year since the E_{LUC} estimate for the year 2024 is informed by extrapolated land-use data (Supplement S.2.1). Peat drainage is assumed to be unaltered as it has low interannual variability.

2.3 Carbon Dioxide Removal (CDR) not based on vegetation

Some CDR involves CO_2 fluxes via land use, which is included in our estimate of E_{LUC} (re/afforestation) or provided separately in Section 3.2.2 (biochar, HWP, and BECCS). Other CDR occurs through CO_2 fluxes directly from the air to the geosphere, which is reported in Section 3.3. The majority of this derives from bio-oil storage in geological reservoirs, enhanced weathering through the application of crushed rock to soils, and the production of solid mineral products with CO_2 captured from the atmosphere, with smaller contributions from Direct Air Carbon Capture and Storage (DACCS), sinking of terrestrial (e.g., straw) or marine (e.g., macroalgae) biomass into the deep ocean through human intervention, and others like intentional ocean or river alkalinity enhancement. For these methods, we use updated 2024 data (Smith et al., 2024), which compiles and harmonises reported CDR from a combination of existing databases, surveys, and novel research. Currently, there are no internationally agreed methods for reporting these types of CDR, implying that estimates are based on

self-disclosure by projects following their own protocols or protocols produced by third party registries. As such, the fractional uncertainty on these numbers should be viewed as substantial, and numbers are liable to change in future years as protocols are harmonised and improved.

2.4 Growth rate in atmospheric CO_2 concentration (G_{ATM})

2.4.1 Historical period 1850-2024

The rate of growth of the atmospheric CO_2 concentration is provided for years 1959-2024 by the US National Oceanic and Atmospheric Administration Global Monitoring Laboratory (NOAA/GML; Lan et al., 2025), which includes recent revisions to the calibration scale of atmospheric CO_2 measurements (WMO-CO2-X2019; Hall et al., 2021). For the 1959-1979 period, the global growth rate is based on measurements of atmospheric CO_2 concentration averaged from the Mauna Loa and South Pole stations, as observed by the CO_2 Program at Scripps Institution of Oceanography (SIO, Keeling et al., 1976). For the 1980-2024 period, the global growth rate is based on the average of multiple stations selected from the marine boundary layer sites with well-mixed background air (Lan et al., 2024), after fitting a smooth curve through the data for each station as a function of time, and averaging by latitude band (Masarie and Tans, 1995). The annual growth rate is estimated by Lan et al. (2025) from atmospheric CO_2 concentration by taking the average of the most recent December-January months corrected for the average seasonal cycle and subtracting this same average one year earlier. To obtain G_{ATM}, the observation-based growth rate in units of ppm yr^{-1} is converted to units of GtC yr^{-1} by multiplying by a factor of 2.124 GtC per ppm, assuming instantaneous mixing of CO_2 throughout the atmosphere (Ballantyne et al., 2012; Table 1). There is high confidence in the observations because they are based on direct measurements from stations distributed around the world (Lan et al., 2024) with all CO_2 measurements consistently measured against the same CO_2 standard scale (WMO X2019) defined by a suite of gas standards (Hall et al., 2021). However, the conversion to estimates of G_{ATM} in GtC yr^{-1} incurs large uncertainty on annual time scale as discussed next.

The uncertainty around G_{ATM} is due to three main factors. First, the network composition of the marine boundary layer sites with some sites being introduced or removed over time, gaps in sites time series, etc. This uncertainty was estimated with a bootstrap method by constructing 100 "alternative" networks (Steele et al., 1992; Masarie and Tans, 1995; Lan et al., 2025). Second, the analytical uncertainty that describes the short- and long-term uncertainties associated with the CO_2 analyzers. A Monte Carlo method was used to estimate the total analytical uncertainty by randomly selecting errors to add to each observation from a normal distribution of combined short- and long-term uncertainties. Prior to the 1980s when analyzers were less precise and CO_2 measurement scale was slightly less well defined, larger analytical errors were assigned to account for these factors. However, the network uncertainty remains the larger term of uncertainty. The first and second uncertainties are reported as 1-sigma standard deviations (i.e., 68% confidence interval), and summed in quadrature to determine the global

surface growth rate uncertainty, which averaged to 0.085 ppm (Lan et al., 2024). Third, the uncertainty associated with using the average CO_2 concentration from a surface network to approximate the true atmospheric average CO_2 concentration (mass-weighted, in 3 dimensions) as needed to assess the total atmospheric CO_2 burden. In reality, CO_2 variations measured at the stations will not exactly track changes in total atmospheric burden, with offsets in magnitude and phasing due to vertical and horizontal mixing (Pandey et al., 2025). This effect must be very small on decadal and longer time scales, when the atmosphere can be considered well mixed. The long-term CO_2 increase in the stratosphere lags the increase (meaning lower concentrations) that we observe in the marine boundary layer, while the continental boundary layer (where most of the emissions take place) leads the marine boundary layer with higher concentrations. These effects nearly cancel each other on decadal time scales, when the growth rate is nearly the same everywhere (Ballantyne et al., 2012). We therefore maintain an uncertainty around the annual growth rate based on the multiple stations dataset ranges between 0.11 and 0.72 GtC yr^{-1}, with a mean of 0.61 GtC yr^{-1} for 1959-1979 and 0.17 GtC yr^{-1} for 1980-2024, when more measurement sites were available (Lan et al., 2025). We estimate the uncertainty of the decadal averaged growth rate after 1980 at 0.02 GtC yr^{-1} based on the annual growth rate uncertainty but stretched over a 10-year interval. For years prior to 1980, we estimate the decadal averaged uncertainty to be 0.07 GtC yr^{-1} based on a factor proportional to the annual uncertainty prior and after 1980 (0.02 * [0.61/0.17] GtC yr^{-1}).

To estimate the total carbon accumulated in the atmosphere since 1750 or 1850, we use an atmospheric CO_2 concentration of 278.0 ± 3 ppm or 287.7 ± 3 ppm, respectively (Gulev et al., 2021). For the construction of the historical budget shown in Figure 3, we use the fitted estimates of CO_2 concentration from Joos and Spahni (2008) to estimate the annual atmospheric growth rate (see Supplement S.7). The uncertainty of ±3 ppm (converted to ±1σ) is taken directly from the IPCC's AR5 assessment (Ciais et al., 2013). Typical uncertainties in the growth rate in atmospheric CO_2 concentration from ice core data are equivalent to ±0.1-0.15 GtC yr^{-1} as evaluated from the Law Dome data (Etheridge et al., 1996) for individual 20-year intervals over the period from 1850 to 1960 (Bruno and Joos, 1997).

2.4.2 Satellite-based (2015-present)

Further opportunities to estimate global CO_2 growth rates are offered by space-based platforms such as GOSAT (since 2010) and OCO-2 (since 2015). Their recorded short-wave infrared spectra allow retrieval of column CO_2 abundances (XCO_2) over cloud-free scenes over land and ocean with footprints of 80 (GOSAT) and 3 (OCO-2) km^2 respectively. The columns are not full integrals; the sensitivity to surface and lower-tropospheric CO_2 mole fractions is much higher than to upper tropospheric and stratospheric CO_2. However, for the purpose of calculating atmospheric growth rates, the sensitivity is not limiting, as the pressure-weighted sensitivity is still above 0.5 in the stratosphere (Pandey et al.

2024) and priors used in OCO-2 account for the slow stratospheric-tropospheric exchanges using the age of air (Laughner et al. 2023). Here, we use OCO-2 based whole atmosphere growth rates using the Growth Rate from Satellite Observations (GRESO) approach (Pandey et al., 2024). We specifically note that their retrievals are evaluated against surface-based remote sensing (Total Column Carbon Observing Network) data, which in turn are tied to atmospheric observations (from aircraft and using aircore) (Wunch et al., 2017). Furthermore, OCO-2 retrievals use a priori CO_2 mole fraction profiles tied to NOAA GML in-situ flask records at Mauna Loa (MLO) and American Samoa (SMO) measurement stations (Laughner et al., 2023). For details on evaluation, bias-correction, and spatiotemporal coverage of OCO-2 we refer to O'Dell et al (2018).

Relative to surface observations, the GRESO product typically reflects tropical growth rate anomalies earlier and sees whole atmosphere carbon stock changes with a lower latency. The GRESO growth rates presented here use both land and ocean observations of OCO-2 providing global sampling of the atmosphere. We used GRESO post 2015 to present an alternative quantification of the atmospheric carbon stock changes in G_{ATM}, using the reported 1-sigma uncertainty of 0.08 ppm yr^{-1}. The mean differences between GRESO and surface-data derived G_{ATM} is 0.05±0.26 ppm yr^{-1} over the 2015-2024 (n=10 years) period.

2.4.3 2025 projection

We provide an assessment of G_{ATM} for 2025 as the average of two methods. First, the GCB regression method models monthly global-average atmospheric CO_2 concentrations and derives the increment and annual average from these. The model uses lagged observations of concentration (Lan et al., 2025): both a 12-month lag, and the lowest lag that will allow model prediction to produce an estimate for the following January, recalling that the G_{ATM} increment is derived from December/January pairs. The largest driver of interannual changes is the ENSO signal (Betts et al., 2016), so the monthly ENSO 3.4 index (Huang et al., 2023) is included in the model. Given the natural lag between sea-surface temperatures and effects on the biosphere, and in turn effects on globally mixed atmospheric CO_2 concentration, a lagged ENSO index is used, and we use both a 5-month and a 6-month lag. The combination of the two lagged ENSO values helps reduce possible effects of noise in a single month. To help characterise the seasonal variation, we add month as a categorical variable. Finally, we flag the period affected by the Pinatubo eruption (August 1991 - November 1993) as a categorical variable.

The second method uses the multi-model mean and uncertainty of the 2025 G_{ATM} estimated by the ESMs prediction system (see Section 2.9). We then take the average of the GCB regression and ESMs G_{ATM} estimates, with their respective uncertainty combined quadratically.

Similarly, the projection of the 2025 global average CO_2 concentration (in ppm), is calculated as the average of the estimates from the two methods. For the GCB regression method, it is the annual average

of global concentration over the 12 months of 2025; for the ESMs, it is the observed global average CO_2 concentration for 2024 plus the annual increase in 2025 of the global average CO_2 concentration, which is an average of NOAA/GML measurements from January to June (Lan et al., 2025) and predictions of the ESMs multi-model mean from July to December (see Section 2.9).

2.5 Ocean CO_2 sink

2.5.1 Historical period 1850-2024

The reported estimate of the global ocean anthropogenic CO_2 sink S_{OCEAN} is derived as the average of two estimates. The first estimate is derived as the mean over an ensemble of ten global ocean biogeochemistry models (GOBMs, Table 4 and Table S2). The second estimate is obtained as the mean over an ensemble of nine surface ocean fCO_2-observation-based data-products (Table 4 and Table S3).

The GOBMs simulate both the natural and anthropogenic CO_2 cycles in the ocean. They constrain the anthropogenic air-sea CO_2 flux (the dominant component of S_{OCEAN}) by the transport of carbon into the ocean interior, which is also the controlling factor of present-day ocean carbon uptake in the real world. They cover the full globe and all seasons and were evaluated against surface ocean carbon observations, suggesting they are suitable to estimate the annual ocean carbon sink (Hauck et al., 2020). We derive S_{OCEAN} from GOBMs by using a simulation (sim A) with historical forcing of climate and atmospheric CO_2 from GCB (Section 2.4), accounting for model biases and drift from a control simulation (sim B) with constant atmospheric CO_2 and normal year climate forcing. A third simulation (sim C) with historical atmospheric CO_2 increase and normal year climate forcing is used to attribute the ocean sink to CO_2 (sim C minus sim B) and climate (sim A minus sim C) effects. A fourth simulation (sim D; historical climate forcing and constant atmospheric CO_2) is used to compare the change in anthropogenic carbon inventory in the interior ocean (sim A minus sim D) to the observation-based estimates of Gruber et al. (2019) and Müller et al. (2023) with the same flux components (steady state and non-steady state anthropogenic carbon flux).

As there is accumulating evidence for a 10-20% underestimation of S_{OCEAN} by the GOBMs based on ocean interior data (section 3.6.5), atmospheric oxygen (section 3.6.2), atmospheric inversions (section 3.8) and supported by eddy-covariance measurements (Dong et al., 2024), we scale up the global GOBM multi-model mean estimates by 10% when estimating S_{OCEAN} (Friedlingstein et al., 2025b) (see Supplement S3.3). Analysis of Earth System Models and GOBMs indicate that an underestimation by about 10% may be due to biases in ocean carbon transport and mixing from the surface mixed layer to the ocean interior (Goris et al., 2018, Terhaar et al., 2021, Bourgeois et al., 2022, Terhaar et al., 2022), biases in the chemical buffer capacity (Revelle factor) of the ocean (Vaittinada Ayar et al., 2022; Terhaar et al., 2022) and partly due to a late starting date of the simulations (mirrored in atmospheric CO_2 chosen for the pre-industrial control simulation, Table S2, Bronselaer et al., 2017, Terhaar et al.,

2022; 2024). GOBMs are evaluated against key metrics and their capability to reproduce various statistical measures of physical and biogeochemical fields using the International Ocean Model Benchmarking (IOMB) Scheme (Fu et al., 2022, Text S3.3).

The fCO_2-products are tightly linked to observations of fCO_2 (fugacity of CO_2, which equals pCO_2 corrected for the non-ideal behaviour of the gas; Pfeil et al., 2013), which carry imprints of temporal and spatial variability, but are also sensitive to uncertainties in gas-exchange parameterizations and data-sparsity (Fay et al., 2021, Gloege et al., 2021, Hauck et al., 2023a). Their asset is the assessment of the mean spatial pattern of variability and its seasonality (Hauck et al., 2020, Gloege et al. 2021, Hauck et al., 2023a). To benchmark biases and trends derived from the fCO_2-products, we update a model subsampling exercise following Hauck et al. (2023a, see section S3) and use independent measurements from the SOCAT (Surface Ocean CO_2 Atlas) flag E dataset (uncertainty less than 10 µatm) (Bakker et al., 2016) and calculated fCO_2 from the Global Ocean Data Analysis Project GLODAP (Lauvset et al., 2024). New in GCB2025, we now also include the UExP-FNN-U product in the ensemble mean, which was previously shown but not included. We include it since new evidence emerged from field and modelling studies, recommending adopting a temperature correction to the fCO_2 from measurement depth to the surface skin layer where the gas exchange takes place (Dong et al., 2024, Ford et al., 2024a, Bellenger et al., 2022). Furthermore, a second fCO_2-product submitted temperature corrected fCO_2 (JMA-MLR) this year, so we now include these corrected estimates in the ensemble mean. Additionally, following Friedlingstein et al (2025b), we now also add 0.18 GtC yr^{-1} (multiplied by 7/9 as two products already include a temperature correction) to the multi fCO_2-product average when calculating S_{OCEAN} to account for the warm layer and cool skin effect (See Supplement S3.1). This correction is based on a recent field study (Ford et al., 2024a) and broadly consistent in magnitude with a GOBM study (Bellenger et al 2022).

The global fCO_2-based flux estimates were adjusted to remove the pre-industrial natural ocean source of CO_2 to the atmosphere of 0.65 ± 0.3 GtC yr^{-1}, arising from the transfer of carbon from land to ocean via rivers (Regnier et al., 2022), to satisfy our definition of S_{OCEAN} (Hauck et al., 2020). This CO_2 outgassing adjustment was distributed over the latitudinal bands using the regional distribution of Lacroix et al. (2020; North: 0.14 GtC yr^{-1}, Tropics: 0.42 GtC yr^{-1}, South: 0.09 GtC yr^{-1}). Acknowledging that this distribution is based on only one model, the advantage is that a gridded field is available, and the adjustment can be calculated for the three latitudinal bands and the RECCAP regions (REgional Carbon Cycle Assessment and Processes (RECCAP2; Ciais et al., 2020, Poulter et al., 2022, DeVries et al., 2023). This dataset suggests that more of the river-induced outgassing occurs in the tropics than in the Southern Ocean and is thus opposed to the previously used dataset of Aumont et al. (2001). Accordingly, the regional distribution is associated with an additional uncertainty in addition to the large uncertainty around the global estimate (Crisp et al., 2022; Gruber et al., 2023). Anthropogenic perturbations of river carbon and nutrient transport to the ocean are not represented in the process

models used to quantify S_{OCEAN}, but an a-posteriori correction is applied to the global S_{OCEAN} estimate (see Section 2.10 and Supplement S.8.3). We calculate S_{OCEAN} as the average of the GOBM ensemble mean and the fCO_2-product ensemble mean from 1990 onwards, including the corrections on the GOBM and fCO_2-product ensemble means as described above. For the 1959-1989 period, it is calculated as the GOBM ensemble mean plus half of the offset between GOBMs and fCO_2-products ensemble means over 1990-2001, also including the above corrections. In addition, two diagnostic ocean models are used to estimate S_{OCEAN} over the industrial era (1781-1958, Khatiwala et al. (2013) and DeVries (2014)).

S_{OCEAN} is evaluated against the change in the total dissolved inorganic carbon inventory in the interior ocean from the observation-based estimates of Keppler et al. (2023) with the same flux components.

We assign an uncertainty of ± 0.4 GtC yr^{-1} to the ocean sink based on a combination of random (ensemble standard deviation) and systematic uncertainties (GOBMs bias in anthropogenic carbon accumulation, previously reported uncertainties in fCO_2-products; see Supplement S.3.4). While this approach is consistent within the GCB, an independent uncertainty assessment of the fCO_2-products alone suggests a somewhat larger uncertainty of up to 0.7 GtC yr^{-1} (Ford et al. 2024). We assess a medium confidence level to the annual ocean CO_2 sink and its uncertainty because it is based on multiple lines of evidence, it is consistent with ocean interior carbon estimates (see Section 3.6.5) and the interannual variability in the GOBMs and data-based estimates is largely consistent and can be explained by climate variability. We refrain from assigning a high confidence because of the deviation between the GOBM and fCO_2-product trends between around 2002 and 2020 and the higher S_{OCEAN} estimate from O_2:N_2 (section 2.8). More details on the S_{OCEAN} methodology can be found in Supplement S.3.

2.5.2 2025 Projection

The S_{OCEAN} forecast for the year 2025 is based on (a) the historical (Lan et al., 2025) and our 2025 estimate of atmospheric CO_2 concentration, (b) the historical and our 2025 estimate of global fossil emissions, and (c) the boreal spring (March, April, May) Oceanic Niño Index (ONI) (NCEP, 2025). Using a non-linear regression approach, i.e., a feed-forward neural network, atmospheric CO_2, ONI, and the fossil emissions are used as training data to best match the corrected S_{OCEAN} from 1959 through 2024 from this year's carbon budget. Using this relationship, the 2025 S_{OCEAN} can then be estimated from the projected 2025 input data using the non-linear relationship established during the network training. To avoid overfitting, the neural network training was done using a Monte Carlo approach, with a variable number of artificial neurons (varying between 2-5) and 20% of the randomly selected training data were withheld for independent internal testing.

Based on the best output performance (tested using the 20% withheld input data), the best performing number of neurons was selected. In a second step, we trained the network 10 times using the best number of neurons identified in step 1 and different sets of randomly selected training data. The mean of the 10 trainings is considered our best forecast, whereas the standard deviation of the 10 ensembles provides a first order estimate of the forecast uncertainty. This uncertainty is then combined with the S_{OCEAN} uncertainty (0.4 GtC yr^{-1}) to estimate the overall uncertainty of the 2025 projection. As an additional line of evidence, we also assess the 2025 atmosphere-ocean carbon flux from the ESM prediction system (see Section 2.9).

2.6 Land CO_2 sink

2.6.1 Historical Period 1850-2024

The terrestrial land sink (S_{LAND}) is thought to be due to the combined effects of rising atmospheric CO_2, increasing N inputs, and climate change, on plant growth and terrestrial carbon storage. S_{LAND} does not include land sinks directly resulting from land-use and land-use change (e.g., regrowth of vegetation) as these are part of the land-use change emissions (E_{LUC}), although system boundaries make it difficult to attribute exactly CO_2 fluxes on land between S_{LAND} and E_{LUC} (Erb et al., 2013).

S_{LAND} is derived from the multi-model mean of 22 DGVMs (Table 4 and Table S1). DGVMs simulations include all climate variability and CO_2 effects over land. In addition to the carbon cycle represented in all DGVMs, 15 models also account for the nitrogen cycle and hence can include the effect of N inputs on S_{LAND}. The DGVMs estimates of S_{LAND} do not explicitly include the export of carbon to aquatic systems or its historical perturbation, which is discussed in Supplement S.8.3. DGVMs need to meet several criteria to be included in this assessment (see Supplement S.4.2). In addition, we use the International Land Model Benchmarking system (ILAMB; Collier et al., 2018) for the DGVMs evaluation (see Supplement S.4.2), with an additional comparison of DGVMs with a data-informed, Bayesian model-data fusion framework (CARDAMOM) (Bloom and Williams, 2015; Bloom et al., 2016). The uncertainty on S_{LAND} is taken from the DGVMs standard deviation.

New to GCB2025 is a correction applied to the S_{LAND} estimate to account for its overestimation resulting from the assumption of pre-industrial land-use in the DGVM simulations, when in reality a large portion of the land surface has been converted to pasture and cropland, with a lower sink capacity. This bias is termed the Replaced Sinks and Sources (RSS) (Gitz and Ciais, 2003; Sitch et al., 2005, Pongratz et al., 2009; Gasser et al., 2021; Obermeier et al. 2021; Dorgeist et al., 2024). The correction, which is only applied when estimating the global S_{LAND}, utilises results from a subset of DGVMs that were able to supply Net Biome Productivity estimates at a Plant Functional Type basis combined with time-varying PFT area fractions from the simulation with land use and land use change considered (O'Sullivan et al., 2025; Friedlingstein et al. 2025b), see S.4.1 for details on methodology. The

corrected S_{LAND} is reduced by 19% globally when accounting for the RSS. More details on the S_{LAND} methodology can be found in Supplement S.4.

2.6.2 2025 Projection

In previous versions of the GCB, the land sink projection was, like the ocean sink forecast, based on a non-linear regression approach with a feed-forward neural network. This approach, however, resulted in a large uncertainty and underestimated the land sink variability in the past. This year, we update the projection and simply calculate the land sink for 2025 as the residual of the projection of the other components of the carbon cycle ($S_{LAND}=E_{FOS}+E_{LUC}-G_{ATM}-S_{OCEAN}$). Hence, by construction the 2025 B_{IM} is set to zero.

2.7 Atmospheric inversion estimate

The world-wide network of in-situ atmospheric measurements and satellite derived atmospheric CO_2 column (XCO_2) observations put a strong constraint on changes in the atmospheric abundance of CO_2. This allows atmospheric inversion methods to constrain the magnitude and location of the combined total surface CO_2 fluxes from all sources, including fossil and land-use change emissions and land and ocean CO_2 fluxes. The inversions assume E_{FOS} to be well known, and they solve for the spatial and temporal distribution of land and ocean fluxes from the residual gradients of CO_2 between stations that are not explained by fossil fuel emissions. By design, such systems thus close the carbon balance (B_{IM} = 0) and provide an additional perspective on the independent estimates of the ocean and land fluxes.

This year's release includes fourteen inversion systems that are described in Table S4. Each system is rooted in Bayesian inversion principles but uses different methodologies. These differences concern the selection of atmospheric CO_2 data or XCO_2, and the choice of a-priori fluxes to refine. They also differ in spatial and temporal resolution, assumed correlation structures, and mathematical approach of the models (see references in Table S4 for details). Importantly, the systems use a variety of transport models, which was demonstrated to be a driving factor behind differences in atmospheric inversion-based flux estimates, and specifically their distribution across latitudinal bands (Gaubert et al., 2019; Schuh et al., 2019). Six inversion systems used surface observations from the global measurement network (Schuldt et al., 2024, 2025). Eight inversion systems used satellite XCO_2 retrievals from GOSAT and/or OCO-2, scaled to the WMO 2019 calibration scale, of which three inversions this year used these XCO_2 datasets in addition to the in-situ observational CO_2 mole fraction records.

The original products delivered by the inverse modellers were modified to facilitate the comparison to the other elements of the budget, specifically on two accounts: (1) global total fossil emissions including cement carbonation CO_2 uptake, and (2) riverine CO_2 transport. We note that with these

adjustments the inverse results no longer represent the net atmosphere-surface exchange over land/ocean areas as sensed by atmospheric observations. Instead, for land, they become the net uptake of CO_2 by vegetation and soils that is not exported by fluvial systems, similar to the DGVMs estimates. For oceans, they become the net uptake of anthropogenic CO_2, similar to the GOBMs estimates.

The inversion systems prescribe global fossil emissions based on e.g., the GCP's Gridded Fossil Emissions Dataset versions 2025.1 (GCP-GridFED; Jones et al., 2025), which are updates to GCP-GridFEDv2021 presented by Jones et al. (2021b). GCP-GridFEDv2025.1 scales gridded estimates of CO_2 emissions from EDGARv4.3.2 (Janssens-Maenhout et al., 2019) within national territories to match national emissions estimates provided by the GCB for the years 1959-2024, which were compiled following the methodology described in Section 2.1. Small differences between the systems due to for instance regridding to the transport model resolution, or use of different fossil fuel emissions than GCP-GridFEDv2025.1, are adjusted in the latitudinal partitioning we present, to ensure agreement with the estimate of E_{FOS} in this budget. We also note that the ocean fluxes used as prior by 8 out of 14 inversions are part of the suite of the ocean process model or fCO_2-products listed in Section 2.5. Although these fluxes are further adjusted by the atmospheric inversions (except for Jena CarboScope), it makes the inversion estimates of the ocean fluxes not completely independent of S_{OCEAN} assessed here.

To facilitate comparisons to the independent S_{OCEAN} and S_{LAND}, we used the same adjustments for transport and outgassing of carbon transported from land to ocean, as done for the observation-based estimates of S_{OCEAN} (see Supplement S.5.1).

The atmospheric inversions are evaluated using vertical profiles of atmospheric CO_2 concentrations (Figure S13). More than 50 aircraft programs over the globe, either regular programs or repeated surveys over at least 9 months (except for SH programs), have been used to assess system performance (with space-time observational coverage sparse in the SH and tropics, and denser in NH mid-latitudes; Table S9). The fourteen systems are compared to the independent aircraft CO_2 measurements between 2 and 7 km above sea level between 2001 and 2024. Results are shown in Figure S13 and discussed in Supplement S.5.2.

We note that as of GCB2025, the ensemble of inverse models covering a full decade is deemed sufficiently large to report the 1-sigma standard deviation as uncertainty, following the convention of the other components in GCB. More details on the atmospheric inversion methodology can be found in Supplement S.5.

2.8 Atmospheric oxygen based estimate

Long-term atmospheric O_2 and CO_2 observations allow estimation of the global ocean and land carbon sinks, due to the coupling of O_2 and CO_2 with distinct exchange ratios for fossil fuel emissions and land

uptake, and uncoupled O_2 and CO_2 ocean exchange (Keeling and Manning, 2014). The global ocean and net land carbon sinks were calculated following methods and constants used in Keeling and Manning (2014) but modified to also include the effective O_2 source from metal refining (Battle et al., 2023). For the exchange ratio of the net land sink a value of 1.05 is used, following Resplandy et al. (2019). For fossil fuels, the following values are used: gas: 1.95 (+/-) 0.04, liquid: 1.44, (+/-) 0.03, solid: 1.17 (+/-) 0.03, cement: 0 (+/-) 0, gas flaring: 1.98 (+/-) 0.07 (Keeling, 1988). Atmospheric O_2 is observed as $\delta(O_2/N_2)$ and combined with CO_2 mole fraction observations into Atmospheric Potential Oxygen (APO, Stephens et al., 1998). The APO observations from 1990 to 2024 were taken from a weighted average of flask records from three stations in the Scripps O_2 program network (Alert, Canada (ALT), La Jolla, California (LJO), and Cape Grim, Australia (CGO), weighted per Keeling and Manning (2014). Observed CO_2 was taken from the globally averaged marine surface annual mean growth rate from the NOAA/GML Global Greenhouse Gas Reference Network (Lan et al., 2025). The O_2 source from ocean warming is based on ocean heat content from updated data from NOAA/NCEI (Levitus et al., 2012). The effective O_2 source from metal refining is based on production data from Bray (2020), Flanagan (2021), and Tuck (2022). Uncertainty was determined through a Monte Carlo approach with 20,000 iterations, using uncertainties prescribed in Keeling and Manning (2014), including observational uncertainties from Keeling et al. (2007) and autoregressive errors in fossil fuel emissions (Ballantyne et al., 2015). The reported uncertainty is 1 standard deviation of the ensemble. As for the atmospheric inversions, the O_2 based estimates also closes the carbon balance ($B_{IM} = 0$) by design and provides another independent estimate of the ocean and land fluxes. Note that the O_2 method requires a correction for global air-sea O_2 flux, which has the largest uncertainty at annual time scales, but which is still non-negligible for decadal estimates (Nevison et al., 2008).

2.9 Earth System Models estimate

Reconstructions and predictions from decadal prediction systems based on Earth system models (ESMs) provide a novel line of evidence in assessing the atmosphere-land and atmosphere-ocean carbon fluxes in the past decades and predicting their changes for the current year and years to come. By assimilating physical atmospheric and oceanic data products into the ESMs, the models are able to reproduce the historical variations of the atmosphere-sea CO_2 fluxes, atmosphere-land CO_2 fluxes, and atmospheric CO_2 growth rate (Li et al., 2016, 2019; Lovenduski et al., 2019a,b; Ilyina et al., 2021; Li et al., 2023). Furthermore, the ESM-based predictions have proven their skill in predicting the air-sea CO_2 fluxes for up to 6 years, the air-land CO_2 fluxes and atmospheric CO_2 growth for 2 years (Lovenduski et al., 2019a,b; Ilyina et al., 2021; Li et al., 2023). The reconstructions from the fully coupled model simulations ensure a closed budget within the Earth system, i.e., no budget imbalance term.

Six ESMs have performed the set of prediction simulations. The ensemble size of initialized prediction simulations is 10, and the ensemble mean for each individual model is used here. Each ESM uses a

different assimilation method and combination of data products incorporated in the system, more details on the models configuration can be found in Table 4 and Supplement Table S5. Reconstructions of atmosphere-ocean CO_2 fluxes (S_{OCEAN}) and atmosphere-land CO_2 fluxes (S_{LAND}-E_{LUC}) for the time period from 1960-2024 are assessed here. Predictions of the atmosphere-ocean CO_2 flux, atmosphere-land CO_2 flux, and atmospheric CO_2 growth for 2025 are calculated based on the predictions at lead year 1. The predictions of atmosphere-ocean CO_2 flux and atmosphere-land CO_2 flux are bias corrected by removing the climatological mean and linear trend biases from 1981-2021 referring to GCB2022 (Friedlingstein et al., 2022), the atmospheric CO_2 growth (G_{ATM}) is then calculated as the residual of the CO_2 emissions subtracting the carbon sinks into the ocean and the land. With the ESMs simulations, we also compute the G_{ATM} in another way based on monthly atmospheric CO_2 concentrations at 1000hPa level over the oceans to be comparable to the NOAA/GML global measurements of atmospheric CO_2 concentrations (Lan et al., 2025). The bias correction is done referring to NOAA/GML monthly CO_2 concentrations in recent 10 years from 2015-2024 regarding mean state and linear trend, a shorter period is used because a non-linear trend for the whole period is observed from both NOAA/GML measurements and model simulations. The 2025 G_{ATM} is then calculated by the increment of atmospheric CO_2 concentration in December 2025 minus that in December 2024 multiplied by 2.124 to convert the unit from ppm to GtC. The prediction of 2025 atmospheric CO_2 concentration is an average of the available NOAA/GML measurements from January to June (Lan et al., 2025) and ESMs' predictions from July to December. Note that the two methods, i.e., one based on the residual of carbon sources and sinks and another based on atmospheric concentration increment, of calculation of G_{ATM} result in different magnitudes, which suggests the consideration of variable ratio rather than a constant value in converting CO_2 concentration to mass. More details on methods of bias correction of decadal predictions can be found in Kharin et al. (2012), Boer et al. (2016) and Li et al. (2023). The ESMs are used here to support the assessment of S_{OCEAN} and net atmosphere-land CO_2 flux (S_{LAND} - E_{LUC}) over the 1960-2024 period, and to provide an estimate of the 2025 prediction of G_{ATM} and atmospheric CO_2 concentration.

2.10 Processes not fully included in the global carbon budget

The contribution of anthropogenic CO and CH_4 to the global carbon budget is not fully accounted for in Eq. (1) and is described in Supplement S.8.1. The contributions to CO_2 emissions of decomposition of carbonates not accounted for is described in Supplement S.8.2. The contribution of anthropogenic changes in river fluxes is conceptually included in Eq. (1) in S_{OCEAN} and in S_{LAND}, but it is not represented in the process models used to quantify these fluxes. However, a correction of -0.07 GtC yr^{-1} is applied a posteriori to the S_{LAND} estimate for the 2015-2024 period, as proposed in Friedlingstein et al. (2025b). This effect is discussed in Supplement S.8.3. Similarly, the Replaced Sinks and Sources effect from reduced forest cover over the historical period is missing from the DGVMs used here to estimate S_{LAND}. However, a correction (-19%) is applied a posteriori to the S_{LAND} estimate from DGVMs, based on O'Sullivan et al. (2025; see Section 2.6 and Supplement S.4.1).

3 Results

For each component of the global carbon budget, we present results for three different time periods: the full historical period, from 1850 to 2024, the decades in which we have atmospheric concentration records from Mauna Loa (1959-2024), a specific focus on last year (2024), and the projection for the current year (2025). Subsequently, we assess the estimates of the budget components of the last decades against the top-down constraints from inverse modelling of atmospheric observations and the land/ocean partitioning derived from the atmospheric O_2 measurements. Atmospheric inversions further allow for an assessment of the budget components with a regional breakdown of land and ocean sinks.

3.1 Fossil CO_2 Emissions

3.1.1 Historical period 1850-2024

Cumulative fossil CO_2 emissions for 1850-2024 were 495 ± 25 GtC, including the cement carbonation sink (Table 8, with all cumulative numbers rounded to the nearest 5GtC). In this period, 46% of global fossil CO_2 emissions came from coal, 35% from oil, 15% from natural gas, 3% from decomposition of carbonates for cement production, and 1% from flaring. In 1850, the UK stood for 62% of global fossil CO_2 emissions. In 1893 the combined cumulative emissions of the current members of the European Union reached and subsequently surpassed the level of the UK. Since 1917 US cumulative emissions have been the largest. Over the entire period 1850-2024, US cumulative emissions amounted to 120 GtC (24% of world total), the EU's to 80 GtC (16%), China's to 80 GtC (15%), and India's to 18 GtC (4%).

In addition to the estimates of fossil CO_2 emissions that we provide here (see Section 2.1), there are three global datasets with long time series that include all sources of fossil CO_2 emissions: CDIAC-FF (Erb and Marland, 2025), CEDS version 2024_07_08 (Hoesly et al., 2024) and PRIMAP-hist version 2.6 (Gütschow et al., 2016; Gütschow et al., 2024), although these datasets are not entirely independent from each other (Andrew, 2020a). CEDS has cumulative emissions over 1750-2022 at 480 GtC, CDIAC-FF has 481 GtC, GCP 484 GtC, PRIMAP-hist CR 490 GtC, and PRIMAP-hist TR 492 GtC. CDIAC-FF excludes emissions from lime production. CEDS estimates higher emissions from international shipping in recent years, while PRIMAP-hist has higher fugitive emissions than the other datasets. However, in general these four datasets are in relative agreement as to total historical global emissions of fossil CO_2.

3.1.2 Recent period 1959-2024

Global fossil CO_2 emissions, E_{FOS} (including the cement carbonation sink), have increased every decade from an average of 3.0 ± 0.2 GtC yr^{-1} for the decade of the 1960s to an average of 9.8 ± 0.5 GtC yr^{-1}

during 2015-2024 (Table 7, Figure 2 and Figure 4). The growth rate in these emissions decreased between the 1960s and the 1990s, from 4.3% yr^{-1} in the 1960s (1960-1969), 3.1% yr^{-1} in the 1970s (1970-1979), 1.5% yr^{-1} in the 1980s (1980-1989), to 1.0% yr^{-1} in the 1990s (1990-1999). After this period, the growth rate began increasing again in the 2000s at an average growth rate of 2.8% yr^{-1}, decreasing to 1.2% yr^{-1} in the 2010s, and 0.8% yr^{-1} for the last decade (2015-2024). China's emissions increased by 2.5% yr^{-1} on average over the last 10 years dominating the global trend, and India's emissions increased by 3.6% yr^{-1}, while emissions decreased in EU27 (-2.5% yr^{-1}), and in the USA (-1.2% yr^{-1}) (Figure 5a). Figure 6 illustrates the spatial distribution of fossil fuel emissions for the 2015-2024 period.

E_{FOS} reported here includes the uptake of CO_2 by cement via carbonation which has increased with increasing stocks of cement products, from an average of 20 MtC yr^{-1} (0.02 GtC yr^{-1}) in the 1960s to an average of 210MtC yr^{-1} (0.21 GtC yr^{-1}) during 2015-2024 (Figure 5b).

3.1.3 Final year 2024

Global fossil CO_2 emissions were slightly higher, 1.1%, in 2024 than in 2023, with an increase of 0.11 GtC to reach 10.3 ± 0.5 GtC (including the 0.22 GtC cement carbonation sink) in 2024 (Figure 4), distributed among coal (41%), oil (32%), natural gas (21%), cement (4%), flaring (1%), and others (1%). Compared to 2023, the 2024 emissions from coal, oil, and gas increased by 0.8%, 1.3%, and 2.4% respectively, while emissions from cement decreased by 4.6%. All annual growth rates presented are adjusted for the leap year, unless stated otherwise.

In 2024, the largest absolute contributions to global fossil CO_2 emissions were from China (32%), the USA (13%), India (8%), and the EU27 (6%). These four regions account for 59% of global fossil CO_2 emissions, while the rest of the world contributed 41%, including international aviation and marine bunker fuels (3% of the total). Growth rates for these countries from 2023 to 2024 were 0.7% (China), -0.6% (USA), -2.6% (EU27), and 4.0% (India), with +1.3% for the rest of the world, including international aviation and marine bunker fuels (9.8%). The per-capita fossil CO_2 emissions in 2024 were 1.3 tC $person^{-1}$ yr^{-1} for the globe, and were 3.9 (USA), 2.4 (China), 1.5 (EU27) and 0.6 (India) tC $person^{-1}$ yr^{-1} for the four highest emitters (Figure 5c).

3.1.4 Year 2025 Projection

Globally, we estimate that global fossil CO_2 emissions (including cement carbonation, -0.21 GtC) grew by 1.0% in 2025 (0.2% to 1.7%) to 10.4 GtC (38.1 $GtCO_2$), an historical record high[2]. The estimates of changes in 2025 emissions per fuel types, relative to 2024, are projected to be 1.0% (range 0.2% to

[2] Growth rates in this section use a leap year adjustment that corrects for the extra day in 2024.

1.7%) for coal, 1.1% (range 0.7% to 1.5%) for oil, 1.3% (range 0.1% to 2.4%) for natural gas, and -0.9% (range -2.5% to 0.8%) for cement (Figure 5b).

The uncertainty presented for projections relates only to the estimated growth rate, and excludes the uncertainty of the baseline (i.e., 2024) level. Given that our projection is effectively of what the data will show when observations are first available, the uncertainty drops to zero for any country where we already have data reported for all of 2025. This is the case below for both India and Japan, and for Carbon Monitor's estimates of growth in 2025, since they report data through December 2025.

For China, projected fossil emissions in 2025 are expected to have increased slightly by 0.4% (range -0.1% to 0.9%) compared with 2024 emissions, bringing 2024 emissions for China around 3.4 GtC yr^{-1} (12.3 $GtCO_2$ yr^{-1}). Our projected changes by fuel for China are 0.3% for coal, 3.8% for oil, 2.3% for natural gas, and -7.3% for cement.

For the USA, using the Energy Information Administration (EIA) emissions estimate for 2025 combined with cement clinker data from USGS, we estimate an increase of 2.5% (range 2.2% to 2.8%) compared to 2024, bringing USA 2025 emissions to around 1.4 GtC yr^{-1} (5.0 $GtCO_2$ yr^{-1}). Our estimated changes by fuel are 10.4% for coal, 1.1% for oil, 1.4% for natural gas, and -3.1% for cement.

For India, our estimate for 2025 is an increase of 1.1% over 2024, with 2025 emissions around 0.9 GtC yr^{-1} (3.2 $GtCO_2$ yr^{-1}). Our projected changes by fuel are 1.3% for coal, -0.5% for oil, -5.7% for natural gas, and 10.5% for cement.

For the European Union, our projection for 2025 is for a decrease of -0.1% (range -2.6% to 2.3%) relative to 2024, with 2025 emissions around 0.7 GtC yr^{-1} (2.4 $GtCO_2$ yr^{-1}). Our projected changes by fuel are -2.6% for coal, -0.7% for oil, 2.8% for natural gas, and -0.8% for cement.

New this year, we provide a projection for Japan, with a 2025 decrease of 0.9%, with 2025 emissions around 0.3 GtC yr^{-1} (0.9 $GtCO_2$ yr^{-1}). Our projected changes by fuel are -0.7% for coal, -0.8% for oil, -1.2% for natural gas, and -2.9% for cement.

International aviation and shipping are expected to have increased by 4.3% in 2025, reaching 0.3 GtC yr^{-1} (1.2 $GtCO_2$ yr^{-1}), with international aviation and international shipping projected to be respectively 6.7% and 2.0% over 2024. For the rest of the world, the expected change for 2025 is an increase of 0.9% (range -1.1% to 3.0%) with 2025 emissions around 3.7 GtC yr^{-1} (13.7 $GtCO_2$ yr^{-1}). The fuel-specific projected 2025 growth rates for the rest of the world are: 1.3% for coal, 0.3% for oil, 1.2% for natural gas, 2.6% for cement.

Compared to the GCB estimate, Carbon Monitor estimates an increase in global fossil CO_2 emissions of 0.7% for 2025, lower than GCB but with overlapping uncertainties. In contrast to GCB, Carbon Monitor projects the 2025 emissions from China to decline by -0.6%. Conversely, Carbon Monitor

projects the 2025 emissions to increase by 1.4% for the USA, by 0.7% for India, by 0.8% for the EU27, but to decrease by -0.3% for Japan. The Carbon Monitor estimates that international aviation and shipping increased by 3.4% in 2025. For the rest of the world, the estimated change is an increase of 1.3%.

For traceability, Table S6 provides a comparison of annual projections from GCB since 2015 with the actual emissions assessed in the subsequent GCB annual report.

3.2 Emissions from Land-Use Change

3.2.1 Historical period 1850-2024

Cumulative net CO_2 emissions from land-use change (E_{LUC}) for 1850-2024 are 250 ± 60 GtC (Table 8) with a large spread among individual bookkeeping estimates of 210 GtC (OSCAR), 240 GtC (LUCE) and 290 GtC (BLUE). DGVMs show a lower estimate of 160 ± 60 GtC. Vegetation biomass observations provide independent constraints on the E_{LUC} estimates over the 1901-2012 period (Li et al., 2017). Over that period, the GCB bookkeeping models' cumulative E_{LUC} amounts to 180 GtC [155 to 210 GtC] and the DGVM cumulative E_{LUC} to 121 ± 45 GtC, both not significantly different from the observation-based estimate of 155 ± 50 GtC (Li et al., 2017). The substantially lower cumulative E_{LUC} estimates from DGVMs compared to GCB2024 are due to the correction for the RSS bias, which is implemented in this assessment (see Section 2.6.1; O'Sullivan et al., 2025).

3.2.2 Recent period 1959-2024

In contrast to growing fossil emissions, net CO_2 emissions from land use, land-use change, and forestry remained relatively constant (around 1.8 GtC yr^{-1}) over the 1959-1999 period. Since then, they have shown a statistically significant decrease of about 0.2 GtC per decade ($p<0.001$), reaching 1.4 ± 0.7 GtC yr^{-1} for the 2015-2024 period (Table 7), with a spread from 1.3 to 1.6 GtC yr^{-1} across the three bookkeeping estimates (Table 5, Figure 4b). Different from the bookkeeping average, the DGVM average grows slightly larger over the 1980-2010 period, but as bookkeeping models, DGVMs show decreasing emissions in the most recent decade, 2015-2024 (Table 5).

Compared to GCB2024, the overall trends in E_{LUC} remained similar but the E_{LUC} estimates increased. The main reason for the larger estimates in this assessment is that the H&C2023 model, included up to GCB2024, is not included anymore (see Section 2.2). H&C2023 had the lowest E_{LUC} estimates among all bookkeeping models (Figure S3). Larger E_{LUC} estimates in the last few decades (compared to GCB2024) are also due to the consideration of transient, instead of constant, carbon densities by all three bookkeeping models (Section 2.2.1). The inclusion of transient carbon densities increases gross fluxes for all E_{LUC} components in the last few decades (Figure S3). Net E_{LUC} increases because emissions from deforestation are still the dominating term.

We separate E_{LUC} into five component fluxes to gain further insight into the drivers of net emissions: deforestation, forest (re-)growth, wood harvest and other forest management, peat drainage and peat fires, and all other transitions, with CO_2 emissions to the atmosphere being positive and CO_2 removals from the atmosphere being negative (Figure 7b; Supplement S.2.2). We further decompose the deforestation and the forest (re-)growth term into contributions from shifting cultivation vs permanent forest cover changes (Figure 7c). Averaged over the 2015-2024 period and over the three bookkeeping estimates, fluxes from deforestation amount to an emission of 1.9 [1.5 to 2.3] GtC yr^{-1} (Table 5), of which 1.1 [0.9, 1.2] GtC yr^{-1} are from permanent deforestation. Fluxes from forest (re-)growth amount to a removal of -1.3 [-1.5, -1.0] GtC yr^{-1} (Table 5), of which -0.6 [-0.7, -0.5] GtC yr^{-1} is from re/afforestation and the remainder from forest regrowth in shifting cultivation cycles. Wood harvest and other forest management causes net emissions of 0.4 [0.1, 0.7] GtC yr^{-1} (with substantial gross fluxes largely compensating each other; see Figure S2). Emissions from peat drainage and peat fires (0.2 [0.2, 0.3] GtC yr^{-1}) and the net flux from other transitions (0.1 [0.1, 0.1] GtC yr^{-1}) are of smaller magnitude globally (Table 5).

The split into component fluxes clarifies the potentials for emission reduction and carbon dioxide removal: emissions from permanent deforestation - the largest of our component fluxes - could be halted (largely) without compromising carbon uptake by forests, contributing substantially to emissions reduction. By contrast, reducing wood harvesting would have limited potential to reduce net emissions as it would be associated with less forest regrowth; removals and emissions cannot be decoupled here on long timescales. A similar conclusion applies to removals and emissions from shifting cultivation, which we have therefore separated out. Carbon Dioxide Removal (CDR) in forests could instead be increased by permanently increasing the forest cover through re/afforestation. Currently, re/afforestation creates a removal of -0.6 GtC yr^{-1} from the atmosphere averaged over 2015-2024. This value is similar to independent estimates derived from NGHGIs for CDR in managed forests (through re/afforestation plus forest management) for 2013-2022 (-0.5 GtC yr^{-1}, Pongratz et al., 2024). In contrast to NGHGIs, bookkeeping estimates do not consider the impacts from natural disturbances (like fires, windthrow, insect outbreaks), which may lead to an overestimation of removals from re/afforestation. Re/afforestation constitutes most of all current CDR (Pongratz et al., 2024). Though they cannot be compared directly to annual fluxes from the atmosphere and are thus not included in our estimate of E_{LUC}, CDR through transfers between non-atmospheric reservoirs such as in durable HWPs, biochar, or BECCS comprise much smaller amounts of carbon. 218 MtC yr^{-1} have been estimated to be transferred to HWPs, averaged over 2013-2022 (Pongratz et al., 2024). The net flux of HWPs, considering the re-release of CO_2 through their decay, amounts to 91 MtC yr^{-1} over that period (Pongratz et al., 2024). Note that some double accounting between the CDR through HWPs and the CDR through re/afforestation exists if the HWPs are derived from newly forested areas. CDR from Biochar and BECCS in 2024 amount to 0.31 MtC yr^{-1} and 0.18 MtC yr^{-1} respectively. “Blue carbon”, i.e., coastal wetland management such as restoration of mangrove forests, saltmarshes, and seagrass

meadows, though at the interface of land and ocean carbon fluxes, are counted towards the land-use sector as well. Currently, bookkeeping models do not include blue carbon; however, current CDR deployment in coastal wetlands is small globally, less than 0.003 MtC yr^{-1} (Powis et al., 2023).

The statistically significant decrease in E_{LUC} since the late-1990s, including the larger drop within the most recent decade, is due to the combination of decreasing emissions from deforestation (in particular permanent deforestation) and increasing removals from forest regrowth (with those from re/afforestation stagnating globally in the last decade). Net emissions in 2015-2024 are 23% lower than in the late-1990s (1995-2004) and 19% lower than in 2005-2014. The steep drop in E_{LUC} after 2015 is due to the combined effect from a peak in peat fire emissions in 2015 and a long-term decline in deforestation emissions in many countries over the 2010-2020 period. The processes behind gross removals, foremost forest regrowth and soil recovery, are all slow, while gross emissions include a large instantaneous component. Short-term changes in gross emissions dynamics, such as a temporary decrease in deforestation, influences E_{LUC} faster than a change in gross removals, which rather act on longer-term timescales. Component fluxes often differ more across the bookkeeping estimates than the net flux (Figure 7b), which is expected due to different process representation; in particular, the treatment of shifting cultivation, which increases both gross emissions and gross removals, differs across models, but also net and gross wood harvest fluxes show high model spread (Figure S2). By contrast, models agree relatively well for emissions from permanent deforestation.

Overall, highest net land-use emissions occur in the tropical regions of all three continents. The top three emitters over 2015-2024 are Brazil (in particular the Amazon Arc of Deforestation), Indonesia, and the Democratic Republic of the Congo, with these 3 countries contributing 0.8 GtC yr^{-1} or 57% of the global net land-use emissions (average over 2015-2024; Figure 6b, Figure 7a). This is related to massive expansion of cropland (FAO, 2025c), particularly in the last few decades in Latin America, Southeast Asia, and sub-Saharan Africa (Hong et al., 2021), to a substantial part for export of agricultural products (Pendrill et al., 2019). Emission intensity is high in many tropical countries, particularly of Southeast Asia, due to high rates of land conversion in regions of carbon-dense and often still pristine, undegraded natural forests (Hong et al., 2021). Emissions are further increased by peat fires in equatorial Asia (GFED4s, van der Werf et al., 2017), contributing substantially to emissions in individual years, typically related to dry conditions during El Niño (0.2 GtC in 2015; 0.03 GtC yr^{-1} averaged over 2015-2024). Uptake due to land-use change occurs in several regions of the world (Figure 6b) particularly due to re/afforestation. Highest nature-based CDR in the last decade is seen in China, the USA, and the EU27, partly related to expanding forest area as a consequence of the forest transition in the 19th and 20th century and subsequent regrowth of forest (Mather 2001; McGrath et al., 2015). Substantial uptake through re/afforestation also exists in other regions such as Brazil, Russia, or Indonesia, where, however, emissions from deforestation and other land-use changes dominate the net land-use flux. While the mentioned patterns are robust and supported by independent literature, we

acknowledge that model spread is substantially larger on regional than global levels, as has been shown for bookkeeping models (Bastos et al., 2021) as well as DGVMs (Obermeier et al., 2021). Independent assessments exist for selected regions (e.g., for Europe by Petrescu et al., 2020; for Brazil by Rosan et al., 2021; for China by Zhu et al., 2025; and for 8 selected countries/regions in comparison to inventory data by Schwingshackl et al., 2022).

The NGHGI data under the land-use, land-use change, and forestry (LULUCF) sector (Melo et al. 2025) and the LULUCF estimates from FAOSTAT (FAO, 2025d) differ from the global models' definition of E_{LUC} (see Section 2.2.1). In the NGHGI reporting, natural land fluxes (S_{LAND}) are counted towards E_{LUC} when they occur on managed land (Grassi et al., 2018) whereas FAOSTAT LULUCF estimates generally include natural fluxes in managed and unmanaged forests (Tubiello et al., 2021). To compare our results to the NGHGI approach, we perform a translation of our E_{LUC} estimates by adding S_{LAND} in managed forest from the DGVMs simulations (1.9 GtC yr^{-1} in 2015-2024) to the bookkeeping E_{LUC} estimate (following the methodology described in Grassi et al., 2023; see Supplement S.2.4). Adding this sink changes E_{LUC} from being a source of 1.4 GtC yr^{-1} to a sink of 0.5 GtC yr^{-1}, much closer to the NGHGI estimate reporting a sink of 1.0 GtC yr^{-1} (Figure 8a, Table S11). Remaining differences in the bookkeeping and NGHGI estimates are mainly stemming from fluxes due to other transitions and permanent deforestation, whereas peat emissions and the net flux in managed forests agree well (Figure 8b,c). We further apply a mask of managed land to the net atmosphere-to-land flux estimate from atmospheric inversions to obtain inverse estimates that are comparable to the NGHGI estimates and to the translated E_{LUC} estimates from bookkeeping models (see Supplement S.2.4). The inversion-based net flux in managed land indicates a sink of 0.7 GtC yr^{-1} for 2015-2024, which is in broad agreement with the NGHGI and the translated E_{LUC} estimates (Figure 8, Table S11). Additionally, the interannual variability of the inversion estimates and the translated E_{LUC} estimates show a remarkable agreement (Pearson correlation of 0.71 in 2000-2024), which supports the suggested translation approach. Though estimates of NGHGI, FAOSTAT, and atmospheric inversions and the translated bookkeeping estimates still differ in value and need further analysis, the approach suggested by Grassi et al. (2023), which we adopt here, provides a feasible way to relate the global models' and NGHGI approach to each other and thus link the anthropogenic carbon budget estimates of land-use CO_2 fluxes directly to the Global Stocktake, as part of the UNFCCC Paris Agreement. The translation approach has been shown to be generally applicable also at the country-level (Grassi et al., 2023; Schwingshackl et al., 2022).

3.2.3 Final year 2024

The global CO_2 emissions from land-use change are estimated as 1.3 ± 0.7 GtC in 2024, similar to the 2023 estimate. However, confidence in the annual change remains low, as the land-use forcing underlying the E_{LUC} estimates was informed directly by data only up to and including 2023, with a trend

extrapolation to 2024 (see Supplement Section S.2.1). The impacts of the 2023/2024 droughts linked to El Niño on the 2024 E_{LUC} estimate are thus not captured - while natural fires are not counted towards E_{LUC}, deforestation fires spreading further or drained peatlands burning more vastly because of dry conditions would be part of E_{LUC}. The extent of degradation was anomalously high in the Amazon in 2024 and partly masked relatively low deforestation rates (https://terrabrasilis.dpi.inpe.br). However, this is not captured by our approach that is based on forest cover changes. For degradation it is currently impossible to be separated into effects of land-use activity versus effects of climate variability.

3.2.4 Year 2025 Projection

In equatorial Asia, peat fire emissions remained low (1 MtC in 2025 through October 15, 2025, after 2 MtC in 2024; GFED4.1s, van der Werf et al., 2017), as did deforestation and degradation fires (4 MtC in 2025; 8 MtC in 2024). South America saw a big reduction in emissions from deforestation and degradation fires, from 334 MtC in 2024 to 35 MtC until October 15, 2025. Pantropical 2025 fire emission estimates from deforestation and degradation through October 15 are 105 MtC, which is not just a massive drop compared to the anomalously high 2024 emissions, but also only about one third of the long-term average (1997-2024). The reduction in emissions is mainly attributable to anomalously low deforestation and degradation fire emissions in South America, likely connected to the ceasing of the El Niño conditions and their impacts on ecosystems.

Since the E_{LUC} estimate for the year 2024 is not informed directly by data on land-use dynamics (Section 3.2.3), we estimate the 2025 projection based on fire anomalies over the year 2023. We expect E_{LUC} emissions of around 1.1 GtC (4.1 $GtCO_2$) in 2025, 0.1 GtC below the 2024 level (0.3 GtC below the 2015-2024 average). Note that the confidence in the 2025 E_{LUC} projection remains low, as it is based on deforestation, degradation and peat fire emissions, which are only a proxy for land-use change. Projections in past GCB assessments are only partially confirmed by updated E_{LUC} estimates based on bookkeeping models in the following GCB assessments (Figure S4). Although our extrapolation includes tropical deforestation and degradation fires, the degradation attributable to selective logging, edge-effects or fragmentation is not captured. Further, deforestation and fires in deforestation zones may become more disconnected, partly due to changes in legislation in some regions. For example, Van Wees et al. (2021) found that the contribution from fires to forest loss decreased in the Amazon and in Indonesia over the period of 2003-2018.

3.3 CDR not based on vegetation

Besides the CDR through land use (Sec. 3.2), the atmosphere-to-geosphere flux of carbon resulting from carbon dioxide removal (CDR) activities in 2024 is estimated at 0.011 MtC yr^{-1}. This results primarily from 0.0048 MtC yr^{-1} of biomass direct storage (compressing waste biomass to store underground), 0.003 MtC yr^{-1} and 0.002 MtC yr^{-1} of mineralisation and enhanced weathering projects

respectively, and 0.0004 MtC yr^{-1} of DACCS (Pongratz et al., 2024). This represents an increase (267%) in the anthropogenic sink compared to revised estimates for 2023 (0.003 MtC yr^{-1}), although it remains roughly a million times smaller than current fossil CO_2 emissions. Note that the lower DACCS estimates, as well as revised 2023 values, reflect updated CDR tracking methodologies which include drawing on more accurate annual data from registries, indicating that operational projects are currently removing less CO_2 than their expected capacities. Similarly, reported CDR via Enhanced Rock Weathering decreased in 2024; however, this may not indicate a real decline in activity. The decline likely reflects a transition toward third party verification, with some removals not yet appearing on registries. Other novel CDR methods, including ocean and river alkalinity enhancement (0.0003 MtC yr^{-1} and 0.00001 MtC yr^{-1} in 2024 respectively), and bio-oil geological storage (0.0002 MtC yr^{-1}, jointly contributed just over 0.0005 MtC yr^{-1} according to updated 2024 estimates of the State of CDR report (Smith et al., 2024). CDR through intentional biomass sinking into the deep ocean was reported at 0.001 MtC yr^{-1} for 2023, but no activities have been identified for 2024.

3.4 Total anthropogenic emissions

Cumulative anthropogenic CO_2 emissions (fossil, including cement carbonation, and land-use change) for 1850-2024 totalled 745 ± 65 GtC (2730 ± 240 $GtCO_2$), of which 71% (530 GtC) occurred since 1959 and 35% (260GtC) since 2000 (Table 7 and 8). Total anthropogenic emissions more than doubled since the 1960s, from 4.9 ± 0.7 GtC yr^{-1} for the decade of the 1960s to an average of 11.2 ± 0.9 GtC yr^{-1} during 2015-2024 and reaching 11.6 ± 0.9 GtC (42.4 ± 3.2 $GtCO_2$) in 2024. However, total anthropogenic CO_2 emissions have been almost stable over the last decade (0.3% yr^{-1} average growth rate over the 2015-2024 period), much lower than the 1.9% growth rate over the previous decade (2005-2014). This slower growth is due both to the reduced growth in E_{FOS} between the two decades, and to the decrease in emissions from E_{LUC} over the past decade.

During the historical period 1850-2024, 67% of historical emissions were from fossil emissions and 33% from land-use change. However, fossil emissions have grown significantly since the 1960s while net land-use change emissions have not, and consequently the contributions of land-use change to total anthropogenic emissions were smaller during recent periods, 21% during the period 1959-2024 and down to 12% over the last decade (2015-2024).

For 2025 we project global total anthropogenic CO_2 emissions from fossil and land-use changes to be around 11.5 GtC (42.2 $GtCO_2$), marginally below the 2024 level due to lower net land-use emissions (-0.13 GtC) compensating the growth in fossil emission (+0.09 GtC).

3.5 Atmospheric CO_2

3.5.1 Historical period 1850-2024

Atmospheric CO_2 concentration was approximately 278 parts per million (ppm) in 1750, reaching 300 ppm in the late 1900s, 350 ppm in the late 1980s, and reaching 422.80 ± 0.1 ppm in 2024 (Lan et al., 2025; Figure 1). The mass of carbon in the atmosphere increased by 52% from 590 GtC in 1750 to 898 GtC in 2024. Current CO_2 concentrations in the atmosphere are unprecedented in the last 2 million years and the current rate of atmospheric CO_2 increase is at least 10 times faster than at any other time during the last 800,000 years (Canadell et al., 2021).

3.5.2 Recent period 1959-2024

The growth rate in atmospheric CO_2 level increased from 1.7 ± 0.07 GtC yr^{-1} in the 1960s to 5.6 ± 0.02 GtC yr^{-1} during 2015-2024 with important decadal variations (Table 7, Figure 3 and Figure 4c). During the last decade (2015-2024), the growth rate in atmospheric CO_2 concentration continued to increase, albeit with large interannual variability (Figure 9). This interannual variability is highly consistent between the surface-based CO_2 growth rate and GRESO, the XCO_2-based growth rate (Pearson correlation of 0.84), but substantial differences are seen in 2019 and 2022-2024. These reflect differences in the total atmospheric carbon stock seen within the set boundaries of Jan-1 and Dec-31 used to create an annual growth rate, as discussed in Section 2.4.2. Especially with large anomalies in tropical regions and close to January 1st, the calculation becomes sensitive to when the change is detected. This affected the 2023 and 2024 growth rates most strongly as they originated from tropical regions, and late in the calendar year (see next section). Figure 9 also shows the total annual fluxes (in GtC yr^{-1}) from the inverse models, which are derived to match the observed atmospheric increase while numerically accounting for the atmospheric transport-related delay in detection. The inversely modeled values generally match the GRESO growth rate better than the surface observations-based growth rate, indicating that the latter is more strongly influenced by the delay between the fluxes occurring and the actual observation of these signals. Note that this effect is mainly important on the annual timescale, and not over longer periods.

3.5.3 Final year 2024

The growth rate in the surface based atmospheric CO_2 concentration was 7.9 ± 0.2 GtC (3.73 ± 0.08 ppm) in 2024 (Figure 4c; Lan et al., 2025), well above the 2023 growth rate (5.7 ± 0.2 GtC, 2.7± 0.08 ppm) or the 2015-2024 average (5.6 ± 0.02 GtC, 2.6 ± 0.008 ppm), as to be expected during an El Niño year. The 2024 atmospheric CO_2 growth rate was the largest over the 1959-2024 atmospheric observational record, more than 1.5 GtC above the growth rates of 1998, 2015, and 2016 and 1998, all strong El Niño years.

In contrast, the satellite-based GRESO growth rate was 6.8±0.2 GtC yr^{-1} (3.20±0.09 ppm yr^{-1}) for 2024 which was also above its 2023 growth rate (6.5±0.2 GtC yr^{-1}, 3.06±0.07 ppm yr^{-1}) and the highest on its 10-year record. But it shows a more equal split of the anomaly between both years (2023-2024). This likely reflects more accurately that a substantial fraction of the flux anomaly occurred in 2023, but this was only detected by the surface network in 2024. For the interpretation of the annual global budget this has strong implications, as 2024 surface fluxes would need to add up to a smaller anomaly (by 1.1 GtC yr^{-1}) than when using the surface-based annual growth rate. Hence the budget imbalance in 2024 (Table 7) would be reduced from -1.7 GtC to -0.6 GtC if the GRESO growth rate was used for the budget estimate.

As the satellite-based GRESO growth rate is more evenly split between 2023 and 2024, so would be the B_{IM}, -0.3 GtC in 2023 and -0.6 GtC in 2024 with GRESO, compared to +0.4 GtC in 2023 and -1.7 GtC in 2024 with the GATM from the surface based network.

3.5.4 Year 2025 Projection

The 2025 atmospheric CO_2 concentration, averaged over the year reached the level of 425.64 ppm, 53% over the pre-industrial level (Lan et al., 2025). We estimate the annual growth in atmospheric CO_2 (G_{ATM}) to be about 4.4 GtC (equivalent to a 2.1 ppm increase in the global mean concentration), in line with a neutral ENSO year (ENSO 3.4 Index between -0.5 and 0.5). The projected growth rate estimated by the ESMs multi-model mean is slightly larger (5.5 GtC, 2.6 ppm).

For traceability, Table S7 provides a comparison of annual projections of the G_{ATM}, S_{OCEAN} and S_{LAND} from GCB since 2021 with the actual estimate assessed in the subsequent GCB annual report.

3.6 Ocean Sink

3.6.1 Historical period 1850-2024

Cumulated since 1850, the ocean sink S_{OCEAN} adds up to 200 ± 35 GtC, with more than 70% of this amount (145 ± 25 GtC) being taken up by the global ocean since 1959. Over the historical period, the ocean sink increased in pace with the anthropogenic emissions exponential increase (Figure 3). Since 1850, the ocean has removed 27% of total anthropogenic emissions.

3.6.2 Recent period 1959-2024

S_{OCEAN} increased from 1.3 ± 0.4 GtC yr^{-1} in the 1960s to 3.2 ± 0.4 GtC yr^{-1} during 2015-2024 (Table 7), with interannual variations of the order of a few tenths of GtC yr^{-1} (Figure 4d, Figure 10b). As described in section 2.5.1, S_{OCEAN} is now corrected for identified biases in the GOBMs and fCO_2

products estimates. Compared to the uncorrected estimate, S_{OCEAN} is increased by 0.2 GtC yr^{-1} for the 2015-2024 period.

The ocean-borne fraction ($S_{OCEAN}/(E_{FOS}+E_{LUC})$) has been remarkably constant around 27% on average, with variations around this mean illustrating the decadal variability of the ocean carbon sink. So far, there is no evidence of a sustained decrease in the ocean-borne fraction from 1959 to 2024 (Figure S16).

The increase of the ocean sink is primarily driven by the increased atmospheric CO_2 concentration, with the strongest CO_2 induced signal in the North Atlantic and the Southern Ocean (Figure 12a, Figure S10). The effect of climate change is much weaker, reducing the ocean sink globally by 0.20 ± 0.05 GtC yr^{-1} (-7.1% relative to the simulation that only accounts for the effect of atmospheric CO_2 increase) during 2015-2024 (all models simulate a weakening of the ocean sink by climate change, range -4.2 to -10.7%). The climate change effect leading to a reduced ocean sink is evident in all large-scale latitudinal bands (north, tropics, south, Figure 12b, Figure S10). This is the combined effect of change and variability in all atmospheric forcing fields, previously attributed to wind and temperature changes (Le Quéré et al., 2010, Bunsen et al., 2024). The effect of warming is smaller than expected from offline calculation due to stabilising feedback from limited exchange between surface and deep waters (Bunsen et al., 2024; Müller et al., 2025).

The global net air-sea CO_2 flux is a residual of large natural and anthropogenic CO_2 fluxes into and out of the ocean with distinct regional and seasonal variations (Figure 6c and Figure S5). Natural fluxes dominate on regional scales, but largely cancel out when integrated globally (Gruber et al., 2009; DeVries et al., 2023). Mid-latitudes in all basins and the high-latitude North Atlantic dominate the ocean CO_2 uptake where low temperatures and high wind speeds facilitate CO_2 uptake at the surface (Takahashi et al., 2009). In these regions, formation of mode, intermediate and deep-water masses transport anthropogenic carbon into the ocean interior, thus allowing for continued CO_2 uptake at the surface. Outgassing of natural CO_2 occurs mostly in the tropics, especially in the equatorial upwelling region, and to a lesser extent in the North Pacific and polar Southern Ocean, mirroring a well-established understanding of regional patterns of air-sea CO_2 exchange (e.g., Takahashi et al., 2009, Gruber et al., 2009; DeVries et al., 2023). These patterns are also noticeable in the Surface Ocean CO_2 Atlas dataset, where an ocean fCO_2 value above the atmospheric level indicates outgassing (Figure S5). This map further illustrates the data-sparsity in the Indian Ocean and the Southern Hemisphere in general.

The largest variability in the ocean sink occurs on decadal timescales (Figure 10b). The ensemble means of GOBMs and fCO_2-products show the same patterns of decadal variability, although with a larger amplitude of variability in the fCO_2-products than in the GOBMs. The ocean sink stagnated in the 1990s and strengthened between the early 2000s and the mid-2010s (Figure 10b; Le Quéré et al.,

2007; Landschützer et al., 2015, 2016; DeVries et al., 2017; Hauck et al., 2020; McKinley et al., 2020, Gruber et al., 2023). Different explanations have been proposed for the decadal variability in the 1990s and 2000s, ranging from the ocean's response to changes in atmospheric wind systems (e.g., Le Quéré et al., 2007, Keppler and Landschützer, 2019), including variations in upper ocean overturning circulation (DeVries et al., 2017) to the eruption of Mount Pinatubo in the 1990s (McKinley et al., 2020, Fay et al., 2023). The main origin of the decadal variability is a matter of debate with several studies initially pointing to the Southern Ocean (see review in Canadell et al., 2021 and Gruber et al., 2023), but also contributions from the North Atlantic and North Pacific (Landschützer et al., 2016, DeVries et al., 2019), or a global signal (McKinley et al., 2020) were proposed. The GOBM decomposition into climate and CO_2 effects emphasizes the role of the climate effect (that would include cooling signals from volcanic eruptions) for the stagnation in the 1990s until 2002, which are seemingly more pronounced in the tropics and north than in the south (Figure S10). The atmospheric pCO_2 growth rate is a spatially uniform driver that amplifies with large-scale averaging, while climate exerts spatially heterogeneous effects that cancel with averaging. Thus, climate dominates small-scale flux variability, but is matched on the global mean by the impact of the pCO_2 growth rate (Fay et al., 2024).

More recently, the sink seems to have entered a phase of stagnation 2016 - 2022, largely in response to large inter-annual climate variability. The first-order effect of interannual variability stems from a stronger ocean sink during large El Niño events leading to a reduction in CO_2 outgassing from the Tropical Pacific (e.g., 1997/98, 2015/16) and a weaker sink in neutral years following El Niño (2017) and during La Niña events (2020-2022, Figure 10b; Rödenbeck et al., 2014, Hauck et al., 2020; McKinley et al. 2017). After the triple La Niña event 2020-2022, the ocean sink rebound in 2023 linked to the onset of an El Niño event. Warming in the extratropics, in particular in the Northern Hemisphere, however, weakened the overall increase in the ocean carbon sink (Müller et al., 2025). In the GOBMs, the ocean sink stagnation 2016-2022 is associated with a period of a stronger climate effect reducing the ocean sink, mostly stemming from the tropics, in line with the expected patterns from El Niño and La Niña (Figure S10). The CO_2 effect has also shown a lower growth rate since around 2016.

The ensemble means of GOBMs, and fCO_2-products (adjusted for the riverine flux) show a mean offset increasing from 0.28 GtC yr^{-1} in the 1990s (first decade available) to 0.59 GtC yr^{-1} in the decade 2015-2024. The offset is larger than in previous GCB versions, because two fCO_2-products (UExP-FNN-U, JMA-MLR), that use an adjusted version of the Surface Ocean CO_2 Atlas data to represent the sea surface fCO_2 within the surface skin layer where gas exchange takes place (Ford et al., 2025), are now included in the fCO_2-product mean. Additionally, an update in the SOCAT dataset with regards to Southern Ocean data led to an increase in the sink strength in three of the fCO_2-products (VLIZ-SOMFFN, LDEO-HPD, CMEMS-LSCE-FFNN - see section S3.1, Fay et al., 2025). In this version of the GCB, the positive trends in the ocean sink estimated by the GOBMs and the fCO_2-products diverges

over time by a factor of 1.6 since 2002 (GOBMs: 0.27 ± 0.05 GtC yr^{-1} per decade, fCO_2-products: 0.46 GtC yr^{-1} per decade [0.22 to 0.81 GtC yr^{-1} per decade], corrected S_{OCEAN}: 0.38 GtC yr^{-1} per decade), but the uncertainty ranges overlap. A hybrid approach recently constrained the trend for 2000 to 2022 to 0.42 ± 0.06 GtC yr^{-1} $decade^{-1}$ (Mayot et al., 2024), which aligns with the updated trend of S_{OCEAN} (0.46 GtC yr^{-1} $decade^{-1}$), while the fCO_2-products exhibit a larger (0.54 [0.29, 0.85] GtC yr^{-1} $decade^{-1}$) and the GOBMs a lower trend (0.34 ± 0.05 GtC yr^{-1} per decade) over the same period.

In the current budget, the discrepancy between the two types of estimates stems from a persistently larger ocean sink in the fCO_2-products in the northern and southern extra-tropics since around 2002 (Figure 14). Note that the discrepancy in the mean flux, which was located in the Southern Ocean in GCB2022 and earlier, was reduced due to the choice of the regional river flux adjustment (Lacroix et al., 2020 instead of Aumont et al., 2001). This comes at the expense of a discrepancy in the mean S_{OCEAN} of about 0.2-0.3 GtC yr^{-1} in the tropics. Likely explanations for the discrepancy in the trends and decadal variability in the high latitudes are data sparsity and uneven data distribution (Bushinsky et al., 2019, Gloege et al., 2021, Hauck et al., 2023a, Mayot et al., 2024). In particular, two fCO_2-products were shown to overestimate the Southern Ocean CO_2 flux trend by 50 and 130% based on current sampling in a model subsampling experiment (Hauck et al., 2023a) and the largest trends in the fCO_2-products occurred in a data devoid region in the North Pacific (Mayot et al., 2024). In Supplement S3 we show that the strength of the trends in fCO_2 products may be linked to reconstruction biases of the true trend signal. In this respect it is highly worrisome that the coverage of fCO_2 observations has declined since 2016/17 (Dong et al., 2022, 2024; Bakker et al., 2025b) and is now down to that of the mid-2000s (Figure 10b). The temperature correction applied in two products further worsens the agreement in trends between GOBMs and fCO_2-products. Similarly, model biases likely contribute to the discrepancy between GOBMs and fCO_2-products (as indicated by the comparison with Mayot et al., 2024, and by the large model spread in the South, Figure 14).

The S_{OCEAN} estimate is 2.9 ± 0.4 GtC yr^{-1} over the period 2004 to 2019, which agrees within the ranges of uncertainty with the ocean interior estimate of 3.2 ± 0.7 GtC yr^{-1} obtained with the MOBO-DIC approach (Keppler et al., 2023). The carbon flux components of the observation-based ocean interior estimate match the definition of S_{OCEAN} used here (Hauck et al., 2020). Furthermore, the decadal S_{OCEAN} estimates agree well with the corresponding ocean interior estimates for all decades from the 1960s to the 2010s, which represent a composite estimate of three observation-based products (Table 6).

The S_{OCEAN} estimate agrees within uncertainties with other lines of evidence from atmospheric oxygen-based estimates, atmospheric inversions, and ocean interior observation-based constraints (Table 6). The atmospheric oxygen-based estimate shows a lower estimate than S_{OCEAN} in the 1990s, but a larger estimate over the 2015-2024 period, indicating a strong growth of >1.5 GtC yr^{-1} over that period. ESMs with data assimilation result in lower estimates of the ocean sink than all other estimates (Table 6).

Also, the atmospheric inversion estimates of the ocean sink are generally lower than S_{OCEAN} on average but are within the uncertainties of the GOBMs and fCO_2 products.

3.6.3 Final year 2024

The estimated ocean CO_2 sink is 3.4 ± 0.4 GtC for 2024. This is an increase of 0.1 GtC compared to 2023 (Figure 4d). The sink strengthening was expected from the atmospheric CO_2 growth and El Niño conditions in the beginning of the year (January to April). However, the continuation of the anomalous warm conditions in the extra tropics, especially of the Atlantic Ocean, led to a weaker than expected increase in the sink (Figure 11c). The GOBMs suggest that the increase is driven by the anomalously high atmospheric CO_2 growth rate and dampened by climate effects, thus suggesting that warming overcompensated the effect from El Niño (Figure S10). GOBMs and fCO_2-products largely agree on patterns of ocean sink anomalies with a reduced sink in parts of the subtropical and subpolar North Atlantic and North Pacific that coincides with regions of anomalously warm sea surface temperatures (Figure S9). GOBM and fCO_2-product ensemble mean estimates consistently result in an ocean sink increase in 2024 (GOBMs: 0.13 ±0.14 GtC, fCO_2-products: 0.08 [-0.34,0.43] GtC). Eight GOBMs and six fCO_2-products show an increase in S_{OCEAN}, while only two GOBMs and three fCO_2-products show a decrease in S_{OCEAN}. The fCO_2-products have a larger uncertainty at the end of the reconstructed time series, potentially linked to uncertainties related to fewer available observations in the final year (see e.g. Watson et al 2020, Pérez et al 2024). Specifically, the fCO_2-products' estimate of the last year is regularly adjusted in the following release owing to the tail effect and an incrementally increasing data availability. While the monthly grid cells covered may have a lag of only about a year (Figure 10b inset), the values within grid cells may change with 1-5 years lag (see absolute number of observations plotted in previous GCB releases), potentially resulting in annual changes in the flux magnitude from fCO_2-products.

3.6.4 Year 2025 projection

Using a feed-forward neural network method (see Section 2.5.2) we project an ocean sink of 3.3 ±0.4 GtC for 2025, which is a declining sink of -0.1 GtC compared to 2024 and can be explained by the generally lower ocean CO_2 uptake following the El Niño event ending in 2024, consistent with the projected recovery of the atmospheric CO_2 growth rate after a record high in 2024. The set of ESMs predictions support this estimate with a 2025 ocean sink of around 3.1 [3.0, 3.2] GtC. Taking the average of both estimates, we project an ocean sink of 3.2 ±0.4 GtC for 2025.

3.6.5 Evaluation of ocean models and fCO_2-products

The process-based model evaluation draws a generally positive picture with GOBMs scattered around the observational values for Southern Ocean sea-surface salinity, Southern Ocean stratification index,

albeit outliers exist (Section S3.3 and Table S12). The Revelle factor is high in most GOBMs when compared to GLODAP but appears less biased when compared to OceanSODA. However, the Atlantic Meridional Overturning Circulation at 26°N is underestimated by 8 out of 10 GOBMs and overestimated by one GOBM. IOMB summarizes the GOBMs' performance across physical and biogeochemical data sets and various statistics relative to the GOBM ensemble (Figure S6). All GOBMs perform better in some variables compared to the other models, and worse in other variables. Despite the indication that GOBMs underestimate the ocean sink, low sink models do not perform generally worse than the other models; and similarly, high sink models do not perform better than the others.

The model simulations allow to separate the anthropogenic carbon component and to compare the GOBMs DIC inventory change directly to the interior ocean estimates of Gruber et al. (2019), Müller et al. (2023) and the GOBM anthropogenic surface fluxes to DeVries (2022) without further assumptions (Table S12). The GOBMs ensemble average of anthropogenic carbon inventory changes 1994-2007 amounts to 2.3 GtC yr^{-1} and is thus 10.5% lower than the 2.6 ± 0.3 GtC yr^{-1} estimated by Gruber et al. (2019) although within the uncertainty. Five models fall within the range reported by Gruber et al. (2019). Comparison to the decadal estimates of anthropogenic carbon accumulation (Müller et al., 2023) are close to the interior ocean data based estimate for the decade 2004-2014 (GOBMs sim D minus sim A, 2.6 ± 0.4 GtC yr^{-1}, Müller et al. 2.7 ± 0.3 GtC yr^{-1}), but do not reproduce the supposedly higher anthropogenic carbon accumulation in the earlier period 1994-2004 (GOBMs sim D minus sim A, 2.2 ± 0.3 GtC yr^{-1}, Müller et al. 2.9 ± 0.3 GtC yr^{-1}). Finally, the mean anthropogenic carbon uptake in GOBMs from 1985 to 2018 amounts to 2.3 GtC yr^{-1}, slightly lower than the corresponding observation-based uptake rate of 2.4 ± 0.2 Gt yr^{-1} based on OCIM (DeVries, 2022; DeVries et al., 2023). The underestimation of anthropogenic carbon accumulation by 10% in the period 1994 to 2007, in the 1990s and 2000s (Table 6) and by 15% in the 2010s (Table 6) justifies the correction of GOBMs by 10% (Friedlingstein et al., 2025a, section 2.5.1). Interestingly, and in contrast to the uncertainties in the surface CO_2 flux, we find the largest mismatch in interior ocean carbon accumulation in the tropics, with smaller contributions from the north and the south (Table S12). The large discrepancy in accumulation in the tropics highlights the role of interior ocean carbon redistribution for those inventories (Khatiwala et al., 2009, DeVries et al., 2023).

Additional benchmarking of the fCO_2-products with independent data generally shows low and consistent biases and RMSEs, with the exception of the comparison with SOCAT flag E data in the tropics where the biases range from -6.6 µatm in JMA-MLR to -10.29 µatm in OceanSODA_ETHv2 , (Figure S7) and the Northern Hemisphere, where biases range from -2.68 µatm in VLIZ-SOMFFN to -40.47 µatm in UExP-FNN-U (Figure S7), although with few measurements covering the latter area. Furthermore, we evaluate the trends derived from a subset of fCO_2-products by subsampling five GOBMs used in Friedlingstein et al. (2023; covering the period up to the year 2022) following the

approach of Hauck et al. (2023a) and evaluating the air-sea CO_2 flux trend for the 2001-2021 period, i.e. the period of strong divergence in the air-sea CO_2 exchange excluding the tail effect, against trend biases identified by the GOBM reconstruction. The results indicate a relationship between reconstruction bias and strength of the decadal trends (Figure S8), indicating a tendency of the fCO_2-products ensemble to overestimate the air-sea CO_2 flux trends in agreement with Mayot et al. (2024). This relationship, however, remains uncertain and its sensitivity to the GOBM used needs further investigation.

3.7 Land Sink

3.7.1 Historical period 1850-2024

Cumulated since 1850, the terrestrial carbon sink S_{LAND} amounts to 175 ± 50 GtC, 24% of total anthropogenic emissions, with more than two thirds of this amount (120 ± 40 GtC) being taken up by the terrestrial ecosystems since 1959. Over the historical period, the land sink increased in pace with the anthropogenic emissions exponential increase (Figure 3). As described in section 2, S_{LAND} estimate now includes the RSS correction.

3.7.2 Recent period 1959-2024

S_{LAND} increased from 0.9 ± 0.3 GtC yr^{-1} in the 1960s to 2.4 ± 0.8 GtC yr^{-1} during 2015-2024, with important interannual variations of up to 2 GtC yr^{-1} generally showing a decreased land sink during El Niño events (Figure 10a), responsible for the corresponding enhanced growth rate in atmospheric CO_2 concentration. The larger land CO_2 sink during 2015-2024 compared to the 1960s is reproduced by all the DGVMs in response to the increase in both atmospheric CO_2, nitrogen deposition, and the changes in climate, and is broadly consistent with the residual estimated from the other budget terms, that is E_{FOS}+E_{LUC}-G_{ATM}-S_{OCEAN} which amounts to 2.4 GtC for the last decade (See Table 5). As described in section 2.6.1, S_{LAND} is now corrected for the Replaced Sinks and Sources (RSS) bias. Compared to the uncorrected estimate, S_{LAND} is reduced by 0.6 GtC yr^{-1} for the 2015-2024 period.

Over the historical period, the increase in the global terrestrial CO_2 sink is largely attributed to the CO_2 fertilisation effect (Prentice et al., 2001, Piao et al., 2009, Schimel et al., 2015) and increased nitrogen deposition (Huntzinger et al., 2017, O'Sullivan et al., 2019), directly stimulating plant photosynthesis and increased plant water use in water limited systems, with a smaller negative contribution of climate change (Figure 12). There is a range of evidence to support a positive terrestrial carbon sink in response to increasing atmospheric CO_2 (Walker et al., 2021), including a new synthesis of free-air CO_2-enrichment experiments across forests and ages, which concluded that Net Primary Productivity increased by 22% for a common 41% CO_2 enrichment (Norby 2025). As expected from theory, the greatest CO_2 effect is simulated in the tropical forest regions, associated with warm temperatures and

long growing seasons (Hickler et al., 2008) (Figure 12a). However, evidence from tropical intact forest plots indicate an overall decline in the land sink across Amazonia (1985-2011), attributed to enhanced mortality offsetting productivity gains (Brienen et al., 2015, Hubau et al., 2020). During 2015-2024 the land sink is positive in all regions (Figure 6d) with the exception of eastern Brazil, Bolivia, northern Venezuela, Southwest USA, central Europe and Central Asia, North and South Africa, and eastern Australia, where the negative effects of climate variability and change (i.e. reduced rainfall and/or increased temperature) counterbalance CO_2 effects. This is clearly visible in Figure 12 where the effects of CO_2 (Figure 12a) and climate (Figure 12b) as simulated by the DGVMs are isolated (see also Figure S12). The negative effect of climate can be seen across the globe, and is particularly strong in most of South America, Central America, Southwest US, Central Europe, western Sahel, southern Africa, Southeast Asia and southern China, and eastern Australia (Figure 12b, Figure S12). Globally, over the 2015-2024 period, climate change reduces the land sink by 0.8 ± 0.7 GtC yr^{-1} (25% of the CO_2 effect, which is 3.2 ± 1.1 GtC yr^{-1} for the corresponding period, see Supplement S4.1).

Most DGVMs have similar S_{LAND} averaged over 2015-2024, and 14/22 models fall within the 1σ range of the residual land sink [1.4 to 3.3 GtC yr^{-1}] (see Table 5), and all models but one are within the 2σ range [0.5 to 4.3 GtC yr^{-1}]. The ED model is an outlier, with a land sink estimate of 4.9 GtC yr^{-1} for the 2015-2024 period (accounting for the RSS correction), driven by a strong CO_2 fertilisation effect (6.4 GtC yr^{-1} in the CO_2 only (S1) simulation). There are no direct global observations of the land sink (S_{LAND}), or the CO_2 fertilisation effect, and so we are not yet able to rule out models based on component fluxes if their net land sink (S_{LAND}-E_{LUC}) is within the observational uncertainty provided by O_2 measurements. The important role of non-living carbon pools in carbon budgets has also been recently highlighted from an Earth-observation (EO) perspective, where contrary to DGVMs, EO products do not show an increase in biomass, thus inferring a larger role of dead carbon in land carbon cycle dynamics (Bar-On et al., 2025).

Since 2020 the globe has experienced La Niña conditions which would be expected to lead to an increased land carbon sink. This 3-year long period of La Niña conditions came to an end by the second half of 2023 and transitioned to an El Niño which lasted until mid-2024. A clear transition from maximum to a minimum in the global land sink is evident in S_{LAND}, from 2022 to 2023 and we find that an El Niño-driven decrease in tropical land sink is offset by a smaller increase in the high-latitude land sink. In the past years several regions experienced record-setting fire events (see also section 3.8.3). While global burned area has declined over the past decades mostly due to declining fire activity in savannas (Andela et al., 2017), forest fire emissions are rising and have the potential to counter the negative fire trend in savannas (Zheng et al., 2021). Noteworthy extreme fire events include the 2019-2020 Black Summer event in Australia (emissions of roughly 0.2 GtC; van der Velde et al., 2021), Siberia in 2021, where emissions approached 0.4 GtC or three times the 1997-2020 average according to GFED4s, Canada in 2023 and 2024 (Byrne et al., 2024), and unprecedented wildfires in Brazil and

Bolivia in 2024 (partly related to land-use activity, see Sec. 3.2.3 and 3.2.4) (Bourgoin et al., 2025), partially offset by a negative trend in wildfire over Northern Hemisphere Africa. While other regions, including Western US and Mediterranean Europe, also experienced intense fire seasons in 2021 their emissions are substantially lower.

Despite these regional negative effects of climate change on S_{LAND}, the efficiency of land to remove anthropogenic CO_2 emissions has remained broadly constant over the last six decades at around 23% (including the RSS correction) (Figure S16).

3.7.3 Final year 2024

The terrestrial CO_2 sink from the DGVMs ensemble S_{LAND} was 1.9 ± 0.9 GtC in 2024, 37% below the 2022 La Niña induced strong sink of 3.1 ± 1.0 GtC, and below the 2015-2024 average of 2.4 ± 0.8 GtC yr^{-1} (Figure 4e, Table 7). We estimate that the 2024 land sink was the lowest since 2015. The severe reduction in the land sink in 2024 is likely driven by the El Niño conditions, leading to a 66% reduction in S_{LAND} in the tropics (30N-30S) from 2.8 GtC in 2022 to 1.0 GtC in 2024. This is combined with intense wildfires in Canada, Bolivia and Brazil that led to a significant CO_2 source (see also Section 3.8.3). We note that the S_{LAND} estimate for 2024 of 1.9 ± 0.9 GtC is much larger than the 0.3 ± 1.0 GtC yr^{-1} estimate from the residual sink from the global budget (E_{FOS}+E_{LUC}-G_{ATM}-S_{OCEAN}, Table 5), although the residual sink would be substantially larger (at around 1.4 GtC yr^{-1}) if using the satellite-based GRESO in this equation. A large budget imbalance is often associated with El Niño years (e.g. 1986/87, 1997/98, 2005/06, 2023/24), and the possible underestimation in DGVMs of the tropical land carbon losses in response to drought, high temperature extremes, and fires. Few DGVMs have explicit representation of drought-mortality and only 8 from 22 include some form of forest demography, although recent efforts are underway to fill these critical research gaps (Eckes-Shephard et al., 2025 Yao et al., 2022, 2023).

An overestimate in S_{LAND} in 2024 can in part be attributed to the inability in DGVMs to reproduce extreme fire emissions in 2024. Globally fire emissions as calculated by GFED were 0.43 GtC yr^{-1} higher in 2024 compared to the decadal average (2015-2024), similar to the anomaly in 2023 (0.44 GtC yr^{-1}). This was mainly due to an increase in fire over forests in Boreal North America (0.16 GtC yr^{-1}) and forests, savannahs and grasslands over Southern Hemisphere South America (0.35 GtC yr^{-1}) in 2024, partly offset by a negative trend in fires over Northern Hemisphere Africa (-0.05 GtC yr^{-1} anomaly). In fact, across the Amazon basin emissions from degradation fires (two thirds Brazil, one third Bolivia) surpassed those from deforestation fires in 2024 (Bourgoin et al., 2025). In contrast DGVMs simulate an anomaly of 0.2 GtC yr^{-1} in 2024, i.e., an underestimate of 0.23 GtC yr^{-1} in fire emissions for 2024. Fire enabled DGVMs simulate a larger reduction in S_{LAND} in 2024 compared to non-fire models (0.6 vs 0.3 GtC), indicating the importance of representing fire extremes when explaining reductions in the land sink.

Finally, a large uncertainty relates to climate forcing datasets, particularly over the critical carbon-rich tropical forest regions with poor coverage of meteorological stations. For example, there are large differences in climate forcing (e.g., CRUJRA-3Q and ERA5) and downstream DGVM carbon simulations over the Congo basin and tropical central and northern Africa in 2024 (Ke et al., 2025).

3.7.4 Year 2025 projection

Calculating the land sink as the residual of the other projections for 2025, we project a land sink of 3.1 GtC for 2025, 1.1 GtC larger than the 2024 estimate, consistent with an expected recovery of the land sink after an El Niño event. The ESMs do not provide an additional estimate of S_{LAND} as they only simulate the net atmosphere-land carbon flux (S_{LAND}-E_{LUC}).

3.7.5 Evaluation of land models

The evaluation of the DGVMs shows generally higher agreement across models for runoff, and to a lesser extent for GPP, and ecosystem respiration. These conclusions are supported by a more comprehensive analysis of DGVM performance in comparison with benchmark data (Sitch et al., 2024). A relative comparison of DGVM performance (Figure S11) suggests several DGVMs (CABLE-POP, CLASSIC, OCN, ORCHIDEE) may outperform others at multiple carbon and water cycle benchmarks. However, results from Seiler et al., 2022, also show how DGVM differences are often of similar magnitude compared with the range across observational datasets. All models score high enough over the metrics tests to support their use here. There are a few anomalously low scores for individual metrics from a single model, and these can direct the effort to improve models for use in future budgets (See also Supplement S.4.2).

3.8 Partitioning the carbon sinks

3.8.1 Global sinks and spread of estimates

In the period 2015-2024, the bottom-up view of global net ocean and land carbon sinks provided by the GCB, S_{OCEAN} for the ocean and S_{LAND}– E_{LUC} for the land, agrees closely with the top-down global carbon sinks delivered by the atmospheric inversions. This is shown in Figure 13, which visualises the individual decadal mean atmosphere-land and atmosphere-ocean fluxes from each, along with the constraints on their sum offered by the global fossil CO_2 emissions flux minus the atmospheric growth rate (E_{FOS} – G_{ATM}, 4.2 ± 0.5 Gt C yr^{-1}, Table 7, shown as diagonal line in Figure 13). The GCB estimate for net atmosphere-to-surface flux (S_{OCEAN} + S_{LAND} - E_{LUC}) during 2015-2024 is 4.2 ± 1.1 Gt C yr^{-1} (Table 7), implying a zero budget imbalance (B_{IM}) (see Section 3.9). The atmospheric inversions estimate of the net atmosphere-to-surface flux during 2015-2024 is 4.3 Gt C yr^{-1}, with a < 0.1 GtC yr^{-1} imbalance, and thus scatter across the diagonal, with inverse models trading land for ocean fluxes in

their solution. The independent constraint on the net atmosphere-to-surface flux based on atmospheric O_2 by design also closes the balance and is 4.2 ± 0.9 GtC yr^{-1} over the 2015-2024 period (orange symbol on Figure 13), while the ESMs estimate for the net atmosphere-to-surface flux over that period is 4.8 [2.4, 6.0] GtC yr^{-1} (Tables 5 and 6).

The distributions based on the individual models and fCO_2-products reveal substantial spread but converge near the decadal means quoted in Tables 5 to 7. Sink estimates for S_{OCEAN} are mostly non-Gaussian, while the ensemble of DGVMs and inverse models appears more normally distributed justifying the use of a multi-model mean and standard deviation for their errors in the budget. Noteworthy is that the tails of the distributions provided by the land and ocean bottom-up estimates would not agree with the global constraint provided by the fossil fuel emissions and the observed atmospheric CO_2 growth rate. This illustrates the power of the atmospheric joint constraint from the global CO_2 observation capacity.

3.8.1.1 Net atmosphere-to-land flux

The GCB estimate of the net atmosphere-to-land flux ($S_{LAND} - E_{LUC}$), calculated as the difference between S_{LAND} from the DGVMs and E_{LUC} from the bookkeeping models, amounts to a 1.0 ± 1.0 GtC yr^{-1} sink during 2015-2024 (Table 5). The estimate of net atmosphere-to-land flux ($S_{LAND} - E_{LUC}$) from the DGVMs alone (1.4 ± 0.7 GtC yr^{-1}, Table 5, green symbols on Figure 13) is slightly larger, although within the uncertainty of the GCB estimate and within uncertainty of the global carbon budget constraint ($E_{FOS} - G_{ATM} - S_{OCEAN}$, 1.0 ± 0.6 GtC yr^{-1}; Table 7). Also, for 2015-2024, the inversions estimate the net atmosphere-to-land flux is a 1.3 ± 0.3 GtC yr^{-1} sink, similar to the mean of the DGVMs estimates (purple versus grey symbols on Figure 13). The independent constraint based on atmospheric O_2 is slightly lower, 0.7 ± 0.8 GtC yr^{-1} (orange symbol in Figure 13), although its uncertainty overlaps with the uncertainty range from other approaches. Last, the ESMs estimate for the net atmosphere-to-land flux during 2014-2023 is a 2.3 [-0.1, 3.6] GtC yr^{-1} sink, larger than all other estimates (Table 5).

As discussed in Section 3.5.3, the atmospheric growth rate of CO_2 derived from the NOAA surface stations was very high in 2024, 7.9 GtC (3.73 ppm) the largest on the 65 years long observational record. Both DGVMs and inversions assign this large CO_2 growth rate to a continued reduction of the net atmosphere to land flux since 2023, in particular in the tropics (Figures 11 and 14), especially pronounced in the inversions. DGVMs simulate a 2024 global net atmosphere-to-land flux of 1.1 GtC yr^{-1}, a 50% decline relative to the 2.2 GtC yr^{-1} sink in 2022, primarily driven by the severe reduction in S_{LAND} (-37%, see Section 3.7.3). The tropics (30°N-30°S) are recording a dramatic decrease in the net atmosphere-to-land flux from a 1.3 GtC yr^{-1} sink in 2022 to a 0.2 GtC yr^{-1} source in 2024. The atmospheric inversions show a continued reduction with the global net atmosphere-to-land flux declining from 2.9 GtC yr^{-1} in 2022 to 0.8 GtC yr^{-1} in 2023 to 0.2 GtC yr^{-1} in 2024 (-94% from 2022 to 2024), with the tropics turning from a 1.3 GtC yr^{-1} sink in 2022 to a 1.2 GtC yr^{-1} source in 2024. This

discrepancy between the DGVMs and inversions estimates of the tropical and hence global atmosphere-land flux largely explains the negative B_{IM} in 2024, (see also Section 3.8.2.2 below).

3.8.1.2 Net atmosphere-to-ocean flux

For the 2015-2024 period, the GOBMs (2.7 ± 0.4 GtC yr^{-1}) produce a lower estimate of the ocean sink than the fCO_2-products with 3.3 [2.9, 3.8] GtC yr^{-1}, which shows up in Figure 13 as separate peaks in the distribution from the GOBMs (dark blue symbols) and from the fCO_2-products (light blue symbols). Atmospheric inversions (3.0 ± 0.3 GtC yr^{-1}) suggest an ocean uptake more in line with the average of the GOBMs and fCO_2-products for the recent decade (Table 6). The inversions are not fully independent as 7 out of 14 inversions covering the last decade use fCO_2-products as ocean priors and one uses a GOBM (Table S4). The independent constraint based on atmospheric O_2 (3.5 ± 0.5 GtC yr^{-1}) is at the high end of the distribution of the other methods. However, as mentioned in section 2.8, the O_2 method requires a correction for global air-sea O_2 flux, which induces a non-negligible uncertainty on the decadal estimates (about 0.5 GtC yr^{-1}). The large growth in the ocean carbon sink from O_2 is compatible with the GOBMs and fCO_2-products estimates when accounting for their uncertainty ranges. Lastly, the ESMs estimate, 2.5 [2.2, 2.8] GtC yr^{-1}, suggest a lower average ocean carbon sink than the other estimates. We caution that the riverine transport of carbon taken up on land and outgassing from the ocean, accounted for here, is a substantial (0.65 ± 0.3 GtC yr^{-1}) and uncertain term (Crisp et al., 2022; Gruber et al., 2023; DeVries et al., 2023) that separates the GOBMs, ESMs and oxygen-based estimates on the one hand from the fCO_2-products and atmospheric inversions on the other hand.

3.8.2 Regional partitioning

Figure 14 shows the latitudinal partitioning of the global atmosphere-to-ocean (S_{OCEAN}), atmosphere-to-land ($S_{LAND} - E_{LUC}$), and their sum ($S_{OCEAN} + S_{LAND} - E_{LUC}$) according to the estimates from GOBMs and ocean fCO_2-products (S_{OCEAN}), DGVMs ($S_{LAND} - E_{LUC}$), and from atmospheric inversions (S_{OCEAN} and $S_{LAND} - E_{LUC}$). S_{OCEAN} estimates were not corrected for the regional analysis.

3.8.2.1 North

Despite being one of the most densely observed and studied regions of our globe, annual mean carbon sink estimates in the northern extra-tropics (north of 30°N) continue to differ. The atmospheric inversions suggest an atmosphere-to-surface sink ($S_{OCEAN} + S_{LAND} - E_{LUC}$) for 2015-2024 of 2.7 ± 0.4 GtC yr^{-1}, which is higher than the process models' estimate of 2.0 ± 0.4 GtC yr^{-1} (Figure 14). The GOBMs (1.1 ± 0.2 GtC yr^{-1}), fCO_2-products (1.4 [1.2-1.6] GtC yr^{-1}), and inversion systems (1.2 ± 0.1 GtC yr^{-1}) produce largely consistent estimates of the ocean sink. However, the larger flux in the fCO_2-products may be related to data sparsity (Mayot et al., 2024). Thus, the difference mainly arises from

the net land flux ($S_{LAND} - E_{LUC}$) estimate, which is 0.9 ± 0.3 GtC yr^{-1} in the DGVMs compared to 1.5 ± 0.4 GtC yr^{-1} in the atmospheric inversions (Figure 14, second row).

Discrepancies in the northern land fluxes conform with persistent issues surrounding the quantification of the drivers of the global net land CO_2 flux (Arneth et al., 2017; Huntzinger et al., 2017; O'Sullivan et al., 2022) and the distribution of atmosphere-to-land fluxes between the tropics and high northern latitudes (Baccini et al., 2017; Schimel et al., 2015; Stephens et al., 2007; Ciais et al., 2019; Gaubert et al., 2019; O'Sullivan et al. 2024).

In the northern extra-tropics, the process models, inversions, and *f*CO_2-products consistently suggest that most of the interannual variability stems from the land (Figure 14). Inversions generally agree on the magnitude of interannual variations (IAV) over land, more so than DGVMs (0.27-0.38 vs 0.07-0.55 GtC yr^{-1}, averaged over 1990-2024).

3.8.2.2 Tropics

In the tropics (30°S-30°N), both the atmospheric inversions and process models estimate a net carbon balance ($S_{OCEAN} + S_{LAND} - E_{LUC}$) that is relatively close to neutral over the past decade (inversions: 0.05 ± 0.5 GtC yr^{-1}, process models: 0.4±0.6 GtC yr^{-1}). The GOBMs (-0.003 ± 0.3 GtC yr^{-1}), *f*CO_2-products (0.3 [0.1, 0.6] GtC yr^{-1}), and inversion systems (0.3 ± 0.1 GtC yr^{-1}) indicate a neutral to positive tropical ocean flux (see Figure S5 for spatial patterns). DGVMs indicate a net land sink ($S_{LAND} - E_{LUC}$) of 0.4 ±0.5 GtC yr^{-1}, whereas the inversion systems indicate a small source in the net land flux although with larger model spread (-0.2 ± 0.6 GtC yr^{-1}, Figure 14, third row).

A continuing conundrum is the partitioning of the global atmosphere-land flux between the Northern Hemisphere land and the tropical land (Stephens et al., 2017; Pan et al., 2011; Gaubert et al., 2019). It is of importance because each region has its own history of land-use change, climate drivers, and impact of increasing atmospheric CO_2 and nitrogen deposition. Quantifying the magnitude of each sink is a prerequisite to understanding how each individual driver impacts the tropical and mid/high-latitude carbon balance. We define the North-South (N-S) difference as net atmosphere-land flux north of 30°N minus the net atmosphere-land flux south of 30°N. For the inversions, the N-S difference is 1.7 ± 1.0 GtC yr^{-1} across this year's inversion ensemble. In the ensemble of DGVMs the N-S difference is 0.6 ± 0.5 GtC yr^{-1}, a much narrower range than the one from atmospheric inversions. The smaller spread across DGVMs than across inversions is to be expected as there is no correlation between Northern and Tropical land sinks in the DGVMs as opposed to the inversions where the sum of the two regions being well-constrained by atmospheric observations leads to an anti-correlation between these two regions.

The tropical lands are the origin of most of the atmospheric CO_2 interannual variability (Ahlström et al., 2015), consistently among the process models and inversions (Figure 14). The interannual variability in

the tropics is similar among the ocean fCO_2-products (0.06-0.18 GtC yr^{-1}) and the GOBMs (0.07-0.16 GtC yr^{-1}). The DGVMs and inversions indicate that atmosphere-to-land CO_2 fluxes are more variable than atmosphere-to-ocean CO_2 fluxes in the tropics, with interannual variability of 0.3 to 1.13 and 0.96 GtC yr^{-1} for DGVMs and inversions, respectively for 1990-2024. The year 2024 saw the largest growth rate in the atmosphere so far, largely caused by reductions in the tropical land sink, similar to earlier extreme years, such as during the 2015-2016 El Niño period. The inversions seem to capture the response of the tropical land sink to a larger degree than the DGVMs, with a 2024 tropical land source of 1.2 ± 0.9 GtC yr^{-1} for the inversions versus a 0.2 ± 0.7 sink for the DGVMs.

3.8.2.3 South

In the southern extra-tropics (south of 30°S), the atmospheric inversions suggest a net atmosphere-to-surface sink (S_{OCEAN}+S_{LAND}-E_{LUC}) for 2015-2024 of 1.6 ± 0.2 GtC yr^{-1}, similar to the process models' estimate of 1.5 ± 0.4 GtC yr^{-1} (Figure 14). An approximately neutral net land flux (S_{LAND}-E_{LUC}) for the southern extra-tropics is estimated by both the DGVMs (0.05 ± 0.1 GtC yr^{-1}) and the inversion systems (0.01 ± 0.1 GtC yr^{-1}). This means nearly all carbon uptake is due to oceanic sinks south of 30°S. The Southern Ocean flux in the fCO_2-products (1.6 [1.5, 1.9 GtC] yr^{-1}) and inversion estimates (1.6 ± 0.2 GtC yr^{-1}) is marginally higher than in the GOBMs (1.5 ± 0.4 GtC yr^{-1}) (Figure 14, bottom row). This agreement is subject to the choice of the river flux adjustment (Lacroix et al., 2020, Hauck et al., 2023b). Nevertheless, the time-series of atmospheric inversions and fCO_2-products diverge from the GOBMs. A substantial overestimation of the trends in the fCO_2-products could be explained by sparse and unevenly distributed observations, especially in wintertime (Figure S5; Hauck et al., 2023a; Gloege et al., 2021). Model biases likely contribute as well, with biases in mode water formation, stratification, and the chemical buffer capacity known to play a role in Earth System Models (Terhaar et al., 2021, Bourgeois et al., 2022, Terhaar et al., 2022).

The interannual variability in the southern extra-tropics is low because of the dominance of ocean areas with low variability compared to land areas. The split between land (S_{LAND}-E_{LUC}) and ocean (S_{OCEAN}) shows a substantial contribution to variability in the south coming from the land, with no consistency between the DGVMs and the inversions or among inversions. This is expected due to the difficulty of separating exactly the land and oceanic fluxes when viewed from atmospheric observations alone. The S_{OCEAN} interannual variability was found to be higher in the fCO_2-products (0.04-0.18 GtC yr^{-1}) compared to GOBMs (0.03 to 0.06 GtC yr^{-1}) in 1990-2024. Inversions give an interannual variability of 0.13 to 0.15 GtC yr^{-1}. Model subsampling experiments recently illustrated that fCO_2-products may overestimate decadal variability in the Southern Ocean carbon sink by 30% and the trend since 2000 by 50-130% due to data sparsity, based on one and two fCO_2-products with strong variability (Gloege et al., 2021, Hauck et al., 2023a). The trend benchmark test using the method of Hauck et al., (2023a) and a subset of 6 fCO_2-products confirms the sensitivity of the decadal trends in fCO_2-products to

reconstruction biases, particularly in the Southern Ocean, indicating an overestimation of the ensemble mean trend (See Supplement S.3.4). However, we also find compensating positive biases in the ensemble so that the ensemble mean bias is smaller than the bias from some individual fCO_2-products.

3.8.2.4 RECCAP2 regions

Aligning with the RECCAP-2 initiative (Ciais et al., 2022; Poulter et al., 2022; DeVries et al., 2023), we provide a breakdown of this GCB paper estimate of the E_{LUC}, S_{LAND}, Net land (S_{LAND} - E_{LUC}), and S_{OCEAN} fluxes over the 10 land, and 5 ocean RECCAP-2 regions, averaged over the period 2015-2024 (Figure 15). The DGVMs and inversions suggest a positive net land sink in all regions, except for South America, Africa, and Southeast Asia, where the inversions indicate a small net source of respectively -0.1±0.5 GtC yr^{-1}, -0.3±0.3 GtC yr^{-1}, and -0.1±0.3 GtC yr^{-1} compared to a small sink of 0.1±0.3 GtC yr^{-1}, 0.1±0.3 GtC yr^{-1}, and 0.03±0.1 GtC yr^{-1} for the DGVMs. The uncertainty in the sign of net tropical carbon fluxes is driven by opposing gross fluxes and relatively large uncertainty in the gross fluxes themselves. For South America, DGVMs estimate S_{LAND} of 0.4±0.4 GtC yr^{-1} and E_{LUC} of 0.3±0.2 GtC yr^{-1}. Bookkeeping models suggest a larger E_{LUC} source of around 0.5 GtC yr^{-1}. Similarly, in Southeast Asia, the DGVMs estimate an E_{LUC} of 0.2±0.1 GtC yr^{-1}, compared with the bookkeeping model estimate of 0.4±0.02 GtC yr^{-1}. Therefore, DGVMs may underestimate E_{LUC} in these regions, which could explain the net sink discrepancy with inversions. In Africa, E_{LUC} is similar for DGVMs and bookkeeping models (~0.4 GtC yr^{-1}), and DGVMs estimate an S_{LAND} of 0.5±0.2 GtC yr^{-1}.

The inversions suggest the largest net land sinks are in North America (0.4±0.3 GtC yr^{-1}), Russia (0.6±0.2 GtC yr^{-1}), Europe (0.3±0.2 GtC yr^{-1}), and East Asia (0.2±0.3 GtC yr^{-1}). This agrees well with the DGVMs in North America (0.4±0.1 GtC yr^{-1}), which indicate a large natural land sink (S_{LAND}) of 0.4±0.2 GtC yr^{-1}, and near-zero net land-use related carbon losses (0.02±0.1 GtC yr^{-1}). The DGVMs suggest a smaller net land sink in Russia compared to inversions (0.3±0.1 GtC yr^{-1}), and a similar net sink in East Asia (0.2±0.1 GtC yr^{-1}).

There is generally a higher level of agreement in the estimates of regional S_{OCEAN} between the different data streams (GOBMs, fCO_2-products and atmospheric inversions) on decadal scale, compared to the agreement between the different land flux estimates. All data streams agree that the largest contribution to S_{OCEAN} stems from the Southern Ocean due to a combination of high flux density and large surface area, but with important contributions also from the Atlantic (high flux density) and Pacific (large area) basins. In the Southern Ocean, GOBMs suggest a sink of 1.1±0.4 GtC yr^{-1}, in line with the fCO_2-products (1.1 [1.0,1.2] GtC yr^{-1}) and atmospheric inversions (1.1±0.2 GtC yr^{-1}). There is similar agreement in the Pacific Ocean, with GOBMs, fCO_2-products, and atmospheric inversions indicating a sink of 0.6±0.1 GtC yr^{-1}, 0.7 [0.6,0.9] GtC yr^{-1}, and 0.6±0.2 GtC yr^{-1}, respectively. However, in the

Atlantic Ocean, GOBMs simulate a sink of 0.5±0.1 GtC yr^{-1}, noticeably lower than both the fCO_2-products (0.8 [0.7,0.9] GtC yr^{-1}) and atmospheric inversions (0.8±0.1 GtC yr^{-1}). It is important to note the fCO_2-products and atmospheric inversions have a substantial and uncertain river flux adjustment in the Atlantic Ocean (0.3 GtC yr^{-1}) that also leads to a mean offset between GOBMs and fCO_2-products/inversions in the latitude band of the tropics (Figure 14). The Indian Ocean due its smaller size and the Arctic Ocean due to its size and sea-ice cover that prevents air-sea gas-exchange are responsible for smaller but non negligible S_{OCEAN} fluxes (Indian Ocean: (0.3±0.1 GtC yr^{-1}, 0.3 [0.3,0.4] GtC yr^{-1}, and 0.3±0.1 GtC yr^{-1} for GOBMs, fCO_2-products, and atmospheric inversions, respectively, and Arctic Ocean: (0.1±0.03 GtC yr^{-1}, 0.2 [0.1,0.3] GtC yr^{-1}, and 0.1±0.04 GtC yr^{-1} for GOBMs, fCO_2-products, and atmospheric inversions, respectively). Note that the S_{OCEAN} numbers presented here deviate from numbers reported in RECCAP-2 where the net air-sea CO_2 flux is reported (i.e. without river flux adjustment for fCO_2-products and inversions, and with river flux adjustment subtracted from GOBMs in most chapters, or comparing unadjusted datasets with discussion of uncertain regional riverine fluxes as major uncertainty, e.g. Sarma et al., 2023, DeVries et al., 2023).

3.8.3 Fire emissions in 2025

Fire emissions so far in 2025 have been below the average of recent decades, chiefly due to the lowest emissions on record since 2003 across the tropics. Figure S14 shows global and regional emissions estimates for the period 1st Jan-30th September in each year 2003-2025. Estimates derive from two global fire emissions products: the global fire emissions database (GFED, version 4.1s; van der Werf et al., 2017), and the global fire assimilation system (GFAS, operated by the Copernicus Atmosphere Service; Kaiser et al., 2012). The two products estimate that global emissions from fires were 1.2-1.4 GtC (the range reflecting the difference between the two fire emission datasets, actual uncertainties are larger, and estimates are likely conservative, see Chen et al. (2023)) during January-September 2025. These estimates are 19-20% below the 2015-2024 average for the same months (1.5-1.7 GtC). Both the GFED4.1s and GFAS products show the second-lowest January-September fire emissions since 2003 (2022 is the lowest year in both products).

Notably, the year 2025 follows two years with above-average global fire emissions (Figure S14), with global emissions through September totalling 1.7-2.1 GtC in 2023 and 1.6-2.2 GtC in 2024. These high emissions totals were caused by high emissions in North America in 2023 principally in Canada; Jones et al., 2024b), and in both North America and South America in 2024 (principally in Canada and Brazil; Kelley et al., 2025). For example, in January-September 2024, GFED4.1s suggests that global emissions totalled 2.2 GtC, the highest total on record for these months and 32% above the average for the decade prior (2014-2023; GFAS also suggests that emissions were 11% above the average for January-September).

Despite low global fire emissions so far in 2025, a pattern of extremely high fire emissions from Canada has now persisted for three consecutive years commencing with the record-breaking year in 2023 (Jones et al., 2024b, Byrne et al., 2024; Kelley et al., 2025). In January-September 2025, fire emissions from Canada (0.3-0.4 GtC) were slightly greater than in the same months of 2024 (0.2-0.3 GtC yr^{-1}) and around half as large as those in the same months of 2023 (0.5-0.8 GtC). The emissions totals for Canada in January-September 2025 were 2.2 times the average of January-September periods during the prior decade 2015-2024 and 4-6 times greater than the average of those months in 2003-2022 [excluding the record-breaking year in 2023]; Figure S14). According to GFED4.1s, January-September fire emissions from Canada in just the past three years (1.5 GtC) exceeded the country's total January-September fire emissions throughout the 20 years prior (1.2 GtC during 2003-2022). The continued anomaly in Canada propagated to the Northern Hemisphere, where January-September 2025 emissions of 0.4-0.5 GtC were 13-21% above the average of 2015-2024.

Fire emissions anomalies in Africa strongly influence global fire emissions totals because the continent typically contributed near 50% of global fire emissions during 2015-2024 (average of January-September periods). For 2025, fire emissions in Africa through September were 0.4-0.6 GtC, 19-25% below the average of 2015-2024 (0.6-0.8 GtC). Synchronously, emissions through September from South America were around 0.1 GtC in both GFED4.1s and GFAS systems, less than half of the average for 2015-2024 (0.2-0.3 GtC), and emissions from Southeast Asia were around 0.05 GtC, also less than half of the average for 2015-2024 (0.1 GtC in both GFED4.1s and GFAS). Low emissions from the tropical parts of Africa, South America, and Southeast Asia contribute to low emissions across the global tropics so far in 2025 (0.7-0.9 GtC), which were only around two-thirds of the average for 2015-2024 (1.1-1.3 GtC) in both GFED4.1s and GFAS.

We caution that the fire emissions fluxes presented here should not be compared directly with other fluxes of the budget (e.g., S_{LAND} or E_{LUC}) due to incompatibilities between the observable fire emission fluxes and what is quantified in the S_{LAND} and E_{LUC} components of the budget. The fire emission estimates from global fire products relate to all fire types that can be observed in Earth Observations (Giglio et al., 2018; Randerson et al., 2012; Kaiser et al., 2012), including (i) fires occurring as part of natural disturbance-recovery cycles that would also have occurred in the pre-industrial period (Yue et al., 2016; Keeley and Pausas, 2019; Zou et al., 2019), (ii) fires occurring above and beyond natural disturbance-recovery cycle due to changes in climate, CO_2 and N fertilisation and to an increased frequency of extreme drought and heatwave events (Abatzoglou et al., 2019; Jones et al., 2022; Zheng et al., 2021; Burton et al., 2024), and (iii) fires occurring in relation to land use and land use change, such as deforestation fires and agricultural fires (van der Werf et al., 2010; Magi et al., 2012). In the context of the global carbon budget, fire emissions associated with (ii) should be included in the S_{LAND} component, fire emissions associated with (iii) should already be accounted for in the E_{LUC} component, while fire emissions associated with (i) should not be included in the global carbon budget as part of the

natural carbon cycle. However, it is not currently possible to derive specific estimates for fluxes (i), (ii), and (iii) using global fire emission products such as GFED or GFAS. In addition, the fire emissions estimates from global fire emissions products represent a gross flux of carbon to the atmosphere, whereas the S_{LAND} component of the budget is a net flux that should also include post-fire recovery fluxes. Even if emissions from fires of type (ii) could be separated from those of type (i), these fluxes may be partially or wholly offset in subsequent years by post-fire fluxes as vegetation recovers, sequestering carbon from the atmosphere to the terrestrial biosphere (Yue et al., 2016; Jones et al., 2024c). Increases in forest fire emissions and severity (emissions per unit area) globally during the past two decades have highlighted the increasing potential for fire emissions fluxes to outweigh post-fire recovery fluxes, though long-term monitoring of vegetation recovery is required to quantify the net effect on terrestrial C storage (Jones et al., 2024c).

3.9 Closing the global carbon cycle

3.9.1 Partitioning of cumulative emissions and sink fluxes

Emissions during the period 1850-2024 amounted to 745 ± 65 GtC and were partitioned among the atmosphere (290 ± 5 GtC; 39%), ocean (200 ± 40 GtC; 27%), and land (175 ± 50 GtC; 24%). The cumulative land sink is lower than the cumulative land-use emissions (250 ± 65 GtC), making the global land a source of 75 ± 80 GtC over the whole 1850-2024 period (Table 8).

The use of nearly independent estimates for the individual terms of the global carbon budget shows a cumulative budget imbalance of 80 GtC (11% of total emissions) during 1850-2024 (Table 8), which suggests that emissions could be slightly too high by the same proportion or that the combined land and ocean sinks are underestimated (by up to 20%). A large part of the B_{IM} occurs over the first half of the 20th century (Figure 3, red dashed line) and could originate from the estimation of significant increase in E_{FOS} and E_{LUC} between the mid 1920s and the mid 1960s which is unmatched by a similar growth in atmospheric CO_2 concentration as recorded in ice cores (Figure 3). Also, we now correct the S_{LAND} estimate for historical reduction in forest cover (RSS, see Section 2.6). This reduces the S_{LAND} estimate by about 40 GtC over the 1850-2024 period, contributing to the increase of the historical budget imbalance in comparison to GCB2024 (Friedlingstein et al., 2025a).

For the more recent 1959-2024 period where direct atmospheric CO_2 measurements are available, total emissions (E_{FOS} + E_{LUC}) amounted to 530 ± 50 GtC, of which 420 ± 20 GtC (79%) were caused by fossil CO_2 emissions, and 110 ± 45 GtC (21%) by land-use change (Table 8). The total emissions were partitioned among the atmosphere (230 ± 5 GtC; 44%), ocean (145 ± 30 GtC; 27%), and the land (120 ± 30 GtC; 23%), with a budget imbalance of 35 GtC (7% of total emissions). All components except land-use change emissions have significantly grown since the 1960s, with important interannual variability in the growth rate in atmospheric CO_2 concentration primarily mirrored in the land CO_2 sink

(Figure 4), and some decadal variability in all terms (Table 7). Differences with previous budget releases are documented in Figure S15.

The global carbon budget averaged over the last decade (2015-2024) is shown in Figure 2 and Table 7. For this period, 88% of the total emissions ($E_{FOS} + E_{LUC}$) were from fossil CO_2 emissions (E_{FOS}), and 12% from land-use change (E_{LUC}). The total emissions were partitioned among the atmosphere (50%), ocean (29%) and land (21%), with a near zero budget imbalance (0.1%, <0.1 GtC yr^{-1}). We note that, compared to GCB2024, the corrections on S_{OCEAN} and S_{LAND} largely reduced the B_{IM} over the 2015-2024 period, by about 0.4 GtC, but at the cost of increasing the cumulated B_{IM} over the longer 1959-2024 period, from 17 GtC (uncorrected estimate) to 37 GtC (corrected estimate).

For single years, the budget imbalance can be larger (Figure 4f). For 2024, the combination of our estimated anthropogenic sources (11.6 ± 0.9 GtC yr^{-1}) and partitioning in atmosphere, land and ocean (13.3 ± 0.9 GtC yr^{-1}) leads to a large negative B_{IM} of -1.7 GtC (Table 7), indicating that, despite the lower than average S_{LAND} in 2024, the land sink is still too large to explain the record-high atmospheric CO_2 growth rate of 2024. We note that using the 2024 GRESO atmospheric growth rate of 6.8±0.2 GtC yr^{-1} (Section 3.5.3) would reduce the 2024 B_{IM} to about -0.6 GtC.

3.9.2 Trend and variability in the carbon budget imbalance

The carbon budget imbalance (B_{IM}; Eq. 1, Figure 4f) quantifies the mismatch between the estimated total emissions and the estimated changes in the atmosphere, land, and ocean reservoirs. The budget imbalance from 1959 to 2024 is small (35 GtC cumulated over the period, i.e. 0.5 GtC yr^{-1} on average) and shows no significant trend over the 1959-2024 period (Figure 4). The process models (GOBMs and DGVMs) and *f*CO_2-products have been selected to match observational constraints in the 1990s, but no further constraints have been applied to their representation of trend and variability. Therefore, the small mean and trend in the budget imbalance can be seen as evidence of a coherent community understanding of the emissions and their partitioning on those time scales (Figure 4). However, the budget imbalance shows substantial variability of the order of ±1 GtC yr^{-1}, particularly over semi-decadal time scales, although most of the variability is within the uncertainty of the estimates.

We cannot attribute the cause of the budget imbalance with our analysis, we only note that the budget imbalance is unlikely to be explained by errors in the emissions alone because of its large semi-decadal variability component, a variability that is atypical of emissions, and also because the budget imbalance has not increased in the past 60 years despite a near tripling in anthropogenic emissions (Figure 4). Errors in S_{LAND} and S_{OCEAN} are more likely to be the main cause for the budget imbalance, especially on interannual to semi-decadal timescales. For example, underestimation of the S_{LAND} by DGVMs has been reported following the eruption of Mount Pinatubo in 1991 possibly due to missing responses to changes in diffuse radiation (Mercado et al., 2009). Although we account for aerosol effects on solar

radiation quantity and quality (diffuse vs direct), most DGVMs only used the former as input (i.e., total solar radiation) (Table S1). Thus, the ensemble mean may not capture the full effects of volcanic eruptions, i.e., associated with high light scattering sulphate aerosols, on the land carbon sink (O'Sullivan et al., 2021), potentially explaining the large positive B_{IM} in 1991-1992. DGVMs are suspected to underestimate the land sink reduction in response to El Niño events (see Section 3.7.3), which could explain the large negative B_{IM} in 1986-1987, 1997-1998 or 2023-2024). Quasi-decadal variability in the ocean sink has also been reported, with all methods agreeing on smaller than expected ocean CO_2 sink in the 1990s and a larger than expected sink in the 2000s (Figure 10b; Landschützer et al., 2016, DeVries et al., 2019, Hauck et al., 2020, McKinley et al., 2020, Gruber et al., 2023) and the climate-driven variability could be substantial but is not well constrained (DeVries et al., 2023, Müller et al., 2023). Errors in sink estimates could also be partly driven by errors in the climatic forcing data, particularly precipitation for S_{LAND} and wind for S_{OCEAN}.

Although the budget imbalance is near zero for the most recent decade, it could be due to a compensation of errors. We cannot exclude an overestimation of CO_2 emissions, particularly from land-use change, given their large uncertainty, as has been suggested elsewhere (Piao et al., 2018), and/or an underestimate of the land or ocean sinks. A larger estimate of the atmosphere-land CO_2 flux (S_{LAND}-E_{LUC}) over the extra-tropics would reconcile bottom-up model results with inversion estimates (Figure 14). Likewise, a larger S_{OCEAN} is also possible given the higher estimates from the fCO_2-products and the oxygen-based estimates (see Table 6 and Figure 10b), the underestimation of interior ocean anthropogenic carbon accumulation in the GOBMs (Section 3.6.5, Müller et al., 2023), or known biases of ocean models (e.g., Terhaar et al., 2022; 2024). More integrated use of observations in the global carbon budget, either on their own or for further constraining model results, should help resolve some of the budget imbalance.

4 Tracking progress towards mitigation targets

The average growth in global fossil CO_2 emissions peaked at nearly +3% per year during the 2000s, driven by the rapid growth in emissions in China. In the last decade, however, the global growth rate has slowly declined, reaching a low +0.8% per year over 2015-2024. While this slowdown in global fossil CO_2 emissions growth is welcome, global fossil CO_2 emissions continue to grow, far from the rapid emission decreases needed to be consistent with the temperature goals of the Paris Agreement.

Since the 1990s, the average growth rate of fossil CO_2 emissions has continuously declined across the group of developed countries of the Organisation for Economic Co-operation and Development (OECD), with emissions peaking in around 2005 and declining at 1.5% yr^{-1} in the decade 2015-2024, compared to a decline of 0.9% yr^{-1} during the 2005-2014 period (Table 9). In the non-OECD countries, emissions rose 4.6% yr^{-1} from 2005-2014, but growth has lowered to 2.1% yr^{-1} from 2015-2024. In the decade 2015-2024, territorial fossil CO_2 emissions decreased significantly (at the 95% confidence level)

in 35 economies whose gross domestic product (GDP) grew significantly (also at the 95% confidence level): Andorra, Australia, Austria, Belgium, Bulgaria, Czechia, Denmark, Estonia, Finland, France, Germany, Greece, Hungary, Ireland, Israel, Jordan, Latvia, Luxembourg, Netherlands, New Zealand, Norway, Poland, Portugal, South Korea, Romania, Serbia, Slovakia, Slovenia, Spain, Sweden, Switzerland, Taiwan, Thailand, United Kingdom, and USA (updated from Le Quéré et al., 2019). Altogether, these 35 economies emitted 2.7 GtC yr^{-1} (9.7 $GtCO_2$ yr^{-1}) on average over the last decade, about 27% of world CO_2 fossil emissions. For comparison, over the previous decade (2005-2014), 18 economies showed a significant decrease in territorial fossil CO_2 emissions while significantly growing their GDP (Austria, Belgium, Bulgaria, Czechia, France, Germany, Luxembourg, North Macedonia, Netherlands, New Zealand, Romania, Serbia, Slovakia, Sweden, Switzerland, United Kingdom, USA, Uzbekistan). These 18 economies emitted an average 2.0 GtC yr^{-1} over 2005–2014, or 20% of the global total.

Decomposing emission changes into the components of growth, a Kaya decomposition, helps give an initial understanding of the drivers of emission changes (Peters et al., 2017b). The reduction in growth in global fossil CO_2 emissions in the last decade (2015-2024, 0.8% yr^{-1}) relative to the previous decade (2005-2014, 2.2% yr^{-1}) is due to slightly weaker economic growth (3.5% yr^{-1} to 2.4% yr^{-1}), increasing declines in CO_2 emissions per unit energy (0% yr^{-1} to 0.7% yr^{-1}), and weakening declines in energy per unit GDP (1.6% yr^{-1} to 1.3% yr^{-1}) (Figure S17). Fossil CO_2 emission declines in the USA and the EU27 are primarily driven by sustained or increasing declines in energy per GDP and CO_2 emissions per unit energy. China has seen emissions growth decline from 6.7% yr^{-1} in the 2005-2014 decade to 2.5% yr^{-1} from 2015-2024, driven by weaker economic growth (five percentage points), offset by a considerable weakening in the rate of reduction in the energy per GDP (four percentage points), with sustained improvements in CO_2 emissions per unit energy (Figure S17). India has had strong economic growth that is not offset by declines in energy per GDP or declines in CO_2 emissions per unit energy, driving up fossil CO_2 emissions. In the rest of the world, economic growth has slowed considerably in the last decade, and carbon intensity has increased, with declines in energy per GDP unable to counteract these increases leading to growing emissions. Despite the high deployment of renewables in some countries (e.g., China, India), fossil energy sources continue to grow to meet growing energy demand (Le Quéré et al., 2019). In summary, the carbon intensity of energy has consistently decreased over the past decade globally (-0.7% yr^{-1}), indicating decarbonisation of the global energy system, with declines in China (-1.4% yr^{-1}), the European Union (-1.5% yr^{-1}), the USA (-1.3% yr^{-1}), but no change in India and increases (carbonisation) in the Rest of the World. The global decarbonation trends are not sufficient to offset the growth in global energy demand, with energy demand growing faster than expected due to weakening declines in energy per GDP in China, US, and globally.

The slower growth of global fossil CO_2 emissions in the last decade is due in part to the emergence of climate policy (Eskander and Fankhauser 2020; Le Quere et al 2019; Hoppe et al., 2023) and

technological change, which is leading to a shift from coal to gas and growth in renewable energies, and reduced expansion of coal capacity. At the aggregated global level, decarbonisation shows a strong and growing signal in the last decade, with smaller contributions from lower economic growth and declines in energy per GDP. Altogether, global fossil CO_2 emissions are still growing, far from the reductions needed to meet the ambitious climate goals of the UNFCCC Paris agreement.

Last, we update the remaining carbon budget (RCB) based on two studies, the IPCC AR6 (Canadell et al., 2021) and the revision of the IPCC AR6 estimates (Forster et al., 2025, Lamboll et al., 2023). We update the RCB assessed by the IPCC AR6 (Canadell et al., 2021), accounting for the 2020 to 2025 GCB estimated anthropogenic emissions from fossil combustion (E_{FOS}) and land use change (E_{LUC}). From January 2026, the IPCC AR6 RCB (50% likelihood) for limiting global warming to 1.5°C, 1.7°C and 2°C is estimated to amount to 70, 165, and 300 GtC (250, 600, 1100 $GtCO_2$). The Forster et al. (2025) study proposed a significantly lower RCB than IPCC AR6, with the largest reduction being due to an update of the climate emulator (MAGICC) used to estimate the warming contribution of non-CO_2 agents, and to the warming (i.e. emissions) that occurred over the 2020-2024 period. We update the Forster et al., budget accounting for the 2025 GCB estimated anthropogenic emissions. From January 2026, the Forster et al., (2025) RCB (50% likelihood) for limiting global warming to 1.5°C, 1.7°C and 2°C is estimated to amount to 25, 120, and 275 GtC (90, 450, 1010 $GtCO_2$), significantly smaller than the updated IPCC AR6 estimate. Both the original IPCC AR6 and Forster et al. (2025) estimates include the Earth System uncertainty on the climate response to cumulative CO_2 emissions, which is reflected through the percent likelihood of exceeding the given temperature threshold, an additional uncertainty of ±220$GtCO_2$ due to alternative non-CO_2 emission scenarios, and other sources of uncertainties (see Canadell et al., 2021). The two sets of estimates overlap when considering all uncertainties.

Here, we take the average of our update of both IPCC AR6 and Forster et al. (2025) estimates, giving a remaining carbon (50% likelihood) for limiting global warming to 1.5°C, 1.7°C and 2°C of respectively 45, 145, and 290 GtC (170, 525, 1055 $GtCO_2$) starting from January 2026. We emphasise the large uncertainties, particularly when close to the global warming limit of 1.5°C. These 1.5°C, 1.7°C and 2°C remaining carbon budgets correspond respectively to about 4, 12 and 25 years from the beginning of 2026, at the 2025 level of total anthropogenic CO_2 emissions. Reaching net-zero CO_2 emissions by 2050 entails cutting total anthropogenic CO_2 emissions by about 0.5 GtC (1.7 $GtCO_2$), 4% of 2025 emissions, each year on average, comparable to the decrease in E_{FOS} observed in 2020 during the COVID-19 pandemic. However, this would lead to cumulative emissions over 2025-2050 of 140 GtC (520 $GtCO_2$), well above the remaining carbon budget of 50 GtC to limit global warming to 1.5°C, but still within the remaining budget of 145 GtC to limit warming to 1.7°C (in phase with the “well below 2°C” ambition of the Paris Agreement).

5 Discussion

Each year when the global carbon budget is published, each flux component is updated for all previous years to consider corrections that are the result of further scrutiny and verification of the underlying data in the primary input datasets. Annual estimates may be updated with improvements in data quality and timeliness (e.g., to eliminate the need for extrapolation of forcing data such as land use). Of all terms in the global budget, only the fossil CO_2 emissions and the growth rate in atmospheric CO_2 concentration are based primarily on empirical inputs supporting annual estimates in this carbon budget. The carbon budget imbalance, yet an imperfect measure, provides a strong indication of the limitations in observations, in understanding and representing processes in models, and/or in the integration of the carbon budget components.

The persistent unexplained variability in the carbon budget imbalance limits our ability to verify reported emissions (Peters et al., 2017a) and suggests we do not yet have a complete understanding of the underlying carbon cycle dynamics on annual to decadal timescales. Resolving most of this unexplained variability should be possible through different and complementary approaches. First, as intended with our annual updates, the imbalance as an error term should be reduced by improvements of individual components of the global carbon budget that follow from improving the underlying data and statistics and by improving the models through the resolution of some of the key uncertainties detailed in Table 10. Second, additional clues to the origin and processes responsible for the variability in the budget imbalance could be obtained through a closer scrutiny of carbon variability in light of other Earth system data (e.g., heat balance, water balance), and the use of a wider range of biogeochemical observations to better understand the land-ocean partitioning of the carbon imbalance such as the constraint from atmospheric oxygen. Finally, additional information could also be obtained through better inclusion of process knowledge at the regional level. The limit for reducing the carbon budget imbalance is yet unclear, but most certainly not yet reached given the possibilities for improvements that lie ahead.

Estimates of global fossil CO_2 emissions from different datasets are in relatively good agreement when the different system boundaries of these datasets are considered (Andrew, 2020a). While estimates of E_{FOS} are derived from reported activity data requiring much fewer complex transformations than some other components of the budget, uncertainties remain, and one reason for the apparently low variation between datasets is precisely the reliance on the same underlying reported energy data. The budget excludes some sources of fossil CO_2 emissions, which available evidence suggests are relatively small (<1%) (see Supplement S.8.2). We have added emissions from lime production in China and the US, but these are still absent in reporting from most other non-Annex I countries, and before 1990 in other Annex I countries.

Estimates of E_{LUC} suffer from a range of intertwined issues (Obermeier et al., 2025), including the poor knowledge of historical land-cover and land-use change (particularly before the 1960s when FAO reporting started), the rudimentary representation of management processes in most models, and the diversity in methodologies and boundary conditions used across methods (e.g., Arneth et al., 2017; Pongratz et al., 2014; Bastos et al., 2021). Uncertainties in current and historical carbon stocks in soils and vegetation also contribute to uncertainty in E_{LUC} estimates. Major efforts are thus necessary to resolve the different issues concerning E_{LUC} (Obermeier et al., 2025). The large uncertainty and limited reliability of E_{LUC} estimates are particularly concerning given the growing importance of E_{LUC} for climate mitigation strategies, and the large issues in the quantification of the cumulative emissions over the historical period that arise from large uncertainties in E_{LUC}.

By adding the natural land sink in managed forests estimated by DGVMs (part of S_{LAND} in this budget) to the budget E_{LUC} estimate, we reconcile most of the large gap between our E_{LUC} estimate and the land-use flux estimates from NGHGIs (Figure 8). This reconciliation (translation) can be used as potential adjustment in the policy context, for instance to help assess the collective countries' progress towards the goal of the Paris Agreement avoiding double-accounting for the natural sink in managed forests. In the absence of this translation, collective progress would appear better than it is (Grassi et al., 2021). A clear understanding of these implications is thus essential for policymakers for developing effective climate targets (Grassi et al., 2025). The application of this translation is also recommended in the UNFCCC Synthesis report for the first Global Stocktake (UNFCCC, 2022) whenever a comparison between LULUCF fluxes reported by countries and the global emission estimates of the IPCC is conducted. However, this translation should be seen as a short-term and pragmatic fix based on existing data, rather than a definitive solution to bridge the differences between global models and national inventories. Platforms for dataset comparisons (e.g., Melo et al., 2025) help strengthening the dialogue across communities and identify the additional steps needed to understand and reconcile the remaining differences, some of which are relevant at the country level (Grassi, et al., 2023, Schwingshackl, et al., 2022).

The comparison of GOBMs, fCO_2-products, and inversions highlights discrepancies in the temporal evolution of S_{OCEAN} in the Southern Ocean and northern high-latitudes (Figure 14, Hauck et al., 2023a) and in the mean S_{OCEAN} in the tropics. A large part of the uncertainty in the mean fluxes stems from the regional distribution of the river flux adjustment term. The current distribution simulates the largest share of the outgassing to occur in the tropics (Lacroix et al., 2020). The long-standing sparse data coverage of fCO_2 observations in the Southern compared to the Northern Hemisphere (e.g., Takahashi et al., 2009) continues to exist (Bakker et al., 2016, 2025a, Figure S5) and to lead to substantially higher uncertainty in the S_{OCEAN} estimate for the Southern Hemisphere (Watson et al., 2020, Gloege et al., 2021, Hauck et al., 2023a). This discrepancy, which also hampers model improvement, points to the need for increased high-quality fCO_2 observations especially in the Southern Ocean. At the same time,

model uncertainty is illustrated by the large spread of individual GOBM estimates (indicated by shading in Figure 14) and highlights the need for model improvement, now also supported by the IOMB benchmarking. The issue of diverging trends in S_{OCEAN} from different methods remains a matter of concern. Recent and on-going work suggests that the fCO_2-products may overestimate the trend although biases in the fCO_2-product ensemble may partly cancel out (Supplement section S3.4). A data-constrained model approach suggests that the GOBMs underestimate the amplitude of decadal variability, but that the fCO_2-products overestimate the trend (Mayot et al., 2024). The various methods, now also including ocean interior observation-based estimates, agree within uncertainties on the mean ocean sink in the last decade, although the independent estimate from atmospheric oxygen measurements still shows the largest sink estimate for the past decade and has a steeper trend (Table 6). However, the estimate is consistent within uncertainties with S_{OCEAN}, with the relatively larger ocean sink in the fCO_2-products and some of the GOBMs. The assessment of the net land-atmosphere exchange from DGVMs and atmospheric inversions also shows substantial discrepancy, particularly for the estimate of the net land flux over the northern extra-tropic. This discrepancy highlights the difficulty to quantify complex processes (CO_2 fertilisation, nitrogen deposition and fertilisers, climate change and variability, land management, etc.) that collectively determine the net land CO_2 flux. Resolving the differences in the Northern Hemisphere land sink will require the consideration and inclusion of larger volumes of observations.

The adjustments introduced in this budget for S_{LAND} and S_{OCEAN} to account for known biases (RSS for DGVMs, cold skin/warm layer for fCO_2 products, ocean sink underestimation for GOBMs) lead to a smaller net land sink (S_{LAND}-E_{LUC}) and a larger ocean sink (S_{OCEAN}), more in line with the atmospheric inversions and independent oxygen based estimates (Table 7), and also consistent with a recent study based on satellite derived changes in aboveground biomass over the 2000-2019 period (Randerson et al., 2025).

We provide metrics for the evaluation of the ocean and land models and the atmospheric inversions (Figure S6-S8 and S13, Table S12). These metrics expand the use of observations in the global carbon budget, helping 1) to support improvements in the ocean and land carbon models that produce the sink estimates, and 2) to constrain the representation of key underlying processes in the models and to allocate the regional partitioning of the CO_2 fluxes. The use of process-based metrics in an objective evaluation framework (IOMB) targeted to evaluate the simulation of S_{OCEAN} in the ocean biogeochemistry models is an important advance. This is another step in the endeavour to use a broader range of observations and more stringent model evaluation that we hope will support continued improvements in the models and in the annual estimates of the global carbon budget.

We assessed before that a sustained decrease of –1% in global emissions could be detected at the 66% likelihood level after a decade only (Peters et al., 2017a). Similarly, a change in behaviour of the land and/or ocean carbon sink would take as long to detect, and much longer if it emerges more slowly. To

continue reducing the carbon imbalance on annual to decadal time scales, regionalising the carbon budget, and integrating multiple variables are powerful ways to shorten the detection limit and ensure the research community can rapidly identify issues of concern in the evolution of the global carbon cycle under the current rapid and unprecedented changing environmental conditions.

6 Conclusions

The estimation of global CO_2 emissions and sinks is a major effort by the carbon cycle research community that requires a careful compilation and synthesis of measurements, statistical estimates, and model results. The delivery of an annual carbon budget serves two purposes. First, there is a large demand for up-to-date information on the state of the anthropogenic perturbation of the climate system and its underpinning causes. A broad stakeholder community relies on the datasets associated with the annual carbon budget including scientists, policy makers, businesses, journalists, and non-governmental organisations engaged in adapting to and mitigating human-driven climate change. Second, over the last decades we have seen unprecedented changes in the human and biophysical environments (e.g., changes in the growth of fossil fuel emissions, impact of COVID-19 pandemic, Earth's warming, extreme events, and strength of the carbon sinks), which call for frequent assessments of the state of the planet, a better quantification of the causes of changes in the contemporary global carbon cycle, and an improved capacity to anticipate its evolution in the future. Building this scientific understanding to meet the extraordinary climate mitigation challenge requires frequent, robust, transparent, and traceable datasets and methods that can be scrutinised and replicated. This paper via 'living data' helps to keep track of new budget updates.

7 Data availability

The data presented here are made available in the belief that their wide dissemination will lead to greater understanding and new scientific insights of how the carbon cycle works, how humans are altering it, and how we can mitigate the resulting human-driven climate change. Full contact details and information on how to cite the data shown here are given at the top of each page in the accompanying database and summarised in Table 2.

The accompanying database includes three Excel files organised in the following spreadsheets:

File Global_Carbon_Budget_2025v1.0.xlsx includes the following:

1. Summary
2. The global carbon budget (1959-2024);
3. The historical global carbon budget (1750-2024);

4. Global CO_2 emissions from fossil fuels and cement production by fuel type, and the per-capita emissions (1850-2024);
5. CO_2 emissions from land-use change from the individual bookkeeping models (1959-2024);
6. Ocean CO_2 sink from the individual global ocean biogeochemistry models and fCO_2-products (1959-2024);
7. Terrestrial CO_2 sink from the individual DGVMs (1959-2024);
8. Cement carbonation CO_2 sink (1959-2024).

File National_Fossil_Carbon_Emissions_2025v1.0.xlsx includes the following:

1. Summary
2. Territorial country CO_2 emissions from fossil fuels and cement production (1850-2024);
3. Consumption country CO_2 emissions from fossil fuels and cement production and emissions transfer from the international trade of goods and services (1990-2020) using CDIAC/UNFCCC data as reference;
4. Emissions transfers (Consumption minus territorial emissions; 1990-2020);
5. Country definitions.

File National_LandUseChange_Carbon_Emissions_2024v1.0.xlsx includes the following:

1. Summary
2. Territorial country CO_2 emissions from Land Use Change (1850-2024) from three bookkeeping models;

All three spreadsheets are published by the Integrated Carbon Observation System (ICOS) Carbon Portal and are available at https://doi.org/10.18160/GCP-2025 (Friedlingstein et al., 2025c). National emissions data are also available at https://doi.org/10.5281/zenodo.5569234 (Andrew and Peters, 2025), from the Global Carbon Atlas (http://www.globalcarbonatlas.org/, last access: 23 October 2025) and from Our World in Data (https://ourworldindata.org/co2-emissions, last access: 23 October 2025).

Author contributions

PF, MOS, MWJ, DCEB, RMA, JH, PL, CLQ, HL, ITL, GPP, WP, JP, CSc, and SS designed the study, conducted the analysis, and wrote the paper with input from JGC and PC. RMA, GPP, JIK and TK

produced the fossil CO_2 emissions and their uncertainties and analysed the emissions data. ME and GM provided fossil fuel emission data. ZL provided the Carbon Monitor fossil emission projection. JP, CSc, TG and ZQ provided the bookkeeping land-use change emissions with synthesis by JP and CSc. KH and JDM provided the estimates of non-vegetation CDR fluxes. LB, MAC, ÖG, NG, TI, TJ, LR, JS, RS, and HTs provided an update of the global ocean biogeochemical models; LD, DJF, MG, LG, YI, AJ, GMK, CR, JZ, and PC provided an update of the ocean fCO_2-data products, with synthesis on both streams by JH, PL and AR. SRA, LBa, NRB, AB, CFB, MC, MPE, KE, WE, RAF, TGk, CL, NM, DRM, SN, AO, AMO, DP, GR, IS, AJS, CSw, ST, BT, SJvdV, EVO, and RW provided ocean fCO_2 measurements for the year 2024, with synthesis by DCEB and SDJ. KA, PA, THC, JHE, AFo, BG, JG, AI, AKJ, EK, JK, EM, JM, LM, TN, QS, TLS, HT, APW, WY, XYa, XYu and CK provided an update of the Dynamic Global Vegetation Models, with synthesis by SS and MOS. RB, FF, HL, VS, DS, and HiT provided estimates of land and ocean sinks from Earth System Models, as well as a projection of the atmospheric growth rate for 2025, with synthesis by HL. FC, NC, LF, ARJ, FJ, ITL, JL, LRN, YN, CR, XT, YK, and ZL provided an updated atmospheric inversion, WP, FC, and ITL developed the protocol and produced the synthesis and evaluation of the atmospheric inversions. EJM and RFK provided the atmospheric oxygen estimate of surface net carbon sinks. RMA provided projections of the 2025 fossil emissions and atmospheric CO2 growth rate. PL provided the predictions of the 2025 ocean sink. IBMB, LPC, KKG, GCH, TMR and GRvdW provided forcing data for land-use change. FT and GG provided data for the land-use change NGHGI harmonisation. XL provided the atmospheric CO_2 data. SP provided the satellite OCO-2 atmospheric CO_2 growth rate. MWJ provided the historical atmospheric CO_2 concentration and growth rate. IH provided the climate forcing data for the DGVMs. NP provided the nitrogen fertilizer forcing data for the DGVMs. MOS and NB produced the aerosol diffuse radiative forcing for the DGVMs. PCM provided the iLAMB evaluation of the DGVMs. NOC and MGS provided the iOMB evaluation of the GOBMs. PR provided the historical land carbon export estimate, MWJ provided the emissions prior for use in the inversion systems. XD provided seasonal emissions data, based on GRACED (Global gridded daily CO_2 emissions dataset), for most recent years for the emission prior. PF, MO and MWJ coordinated the effort, revised all figures, tables, text and

numbers to ensure the update was clear from the 2024 edition and in line with the globalcarbonatlas.org.

Competing interests.

At least one of the authors is a member of the editorial board of Earth System Science Data

Acknowledgements

First, we wish to thank Richard 'Skee' Houghton for his tremendous contribution to the Global Carbon Budget since its inception, pioneering the estimate of land use change emissions with bookkeeping models. We thank all people and institutions who provided the data used in this global carbon budget 2025 and the Global Carbon Project members for their input throughout the development of this publication. We thank Christian Ethé, Xavier Perrot, Damian Loher, Fatemeh Chegini, Fabrice Lacroix, Yangyang Zhao, Paridhi Rustogi, Sarah Berthet, Aurore Voldoire, Laurent Oziel, T. Toyoda, Y. Kitamura, K. Toyama, H. Nakano, L. S. Urakawa, Philip Townsend, Nathaniel O. Collier, Min Xu, James D. Shutler, Andrew J. Watson, T. Holding, I.G.C. Ashton, D. K. Woolf, Lonneke Goddijn-Murphy, Richard Sims, Stefanie Falk, Pengyue Du, Peter Lawrence, Sean Swenson, Daniel Kennedy, Sam Levis, Erik Kluzek, Lachlan Whyborn, Drew Holzworth, Ian Harman, Naiqing Pan, Shufen Pan for their involvement in the development, use, and analysis of the models and data products used here. We thank Kim Currie, Hannelore Theetaert, and Coraline Leseurre who contributed to the provision of surface ocean CO_2 observations for the year 2024 (see Table S8). We also thank Kevin O'Brien and Eugene Burger of NOAA's Pacific Marine Environmental Laboratory and Alex Kozyr of NOAA's National Centers for Environmental Information, for their contribution to surface ocean CO_2 data and metadata management. We thank the scientists, institutions, and funding agencies responsible for the collection and quality control of the data in SOCAT as well as the International Ocean Carbon Coordination Project (IOCCP) and the Surface Ocean Lower Atmosphere Study (SOLAS) program for their support. ITL and WP thank the CarbonTracker Europe team at Wageningen University, including Remco de Kok, Joram Hooghiem and Auke van der Woude. The inverse modelling team thanks all data providers of atmospheric CO_2 data provided through multiple ObsPack products. HL thanks Tatiana Ilyina for supporting the coordination of ESMs' contributions to GCBs, and Sebastian Brune and Kristina Frölich for helping with the MPI-ESM1-2-LR assimilation. Zhangcai Qin thanks Ziwang Fu and Dr. Yakun Zhu for contributing to LUCE modeling. We thank Ram Alkama and Simone Rossi for helping in filtering SLAND data from DGVMs with managed forest area and Joana Melo for extracting and processing data

from NGHGIs. FT acknowledges support of member countries to the FAO regular budget and FAOSTAT. The conclusions in this paper are the authors' only and do not represent FAO views and position on the subject matter. This is PMEL contribution 5802. MC thanks Tobias Steinhoff (MACID), Lukasz Pawlikowski, Ian Murphy and Gordon Furey (P&O Maritime Services), and Aodhan Fitzgerald (Marine Institute) for their support. TG and the VLIZ team are thankful to the management group and crew of the research vessels Simon Stevin, Skagerak and Neil Armstrong for all the support and help they provided. pCO_2 measurements on the Marion Dufresne were collected in the frame of the French COOL/OISO long-term monitoring program with support from the National Institute of Sciences of the Universe (INSU), the French Polar Institute (IPEV) and the French Oceanographic Fleet (FOF). AMO thanks the captain and crew on the Sea-Cargo Express for their help. DP would like to thank Kevin Sullivan for processing and quality controlling AOML data and facilitating submission to SOCATv2025. GR thanks the "Finnmaid science and tech-teams" at IOW and SYKE for their support, and is indebted to the crew of the ship and the people involved at Finnlines. IS thanks the captain and crew on the G. O. Sars for their help. BT and EvO thank Australia's Integrated Marine Observing System (IMOS) for sourcing CO_2 data. IMOS is enabled by the National Collaborative Research Infrastructure Strategy (NCRIS). SJV thanks Andrew Marriner for maintaining the pCO_2 underway system on the RV Tangaroa. PCM thanks Tristan Quaife, Eddy Robertson, Emily Black and Anthony Walker for support. FC thanks Adrien Martinez who maintained the atmospheric transport model for the CAMS inversion. We acknowledge the contributions of Jeongmin Yun, Anthony Bloom, and Kevin Bowman to the CMS-Flux inversion submission. YN thanks Suman Maity who performed the NISMON-GOSAT inversion. LF thanks Paul I. Palmer and acknowledges ongoing support from the National Centre for Earth Observation. Xiangjun Tian thanks Zhe Jin, Yilong Wang, Hongqin Zhang, Min Zhao, Tao Wang, Jinzhi Ding, and Shilong Piao for their contributions to the GONGGA inversion system. We thank Ning Zeng, Yun Liu, Eugenia Kalnay, and Gassem Asrar for their contributions to the COLA system. CarbonTracker CT2025 results provided by NOAA GML, Boulder, Colorado, USA from the website at http://carbontracker.noaa.gov. FJ thanks Weimin Ju for running the BEPS model. LN thanks Shamil Maksyutov, Rajesh Janardanan and Tsuneo Matsunaga for contributing to NTFVAR inverse model study. YK acknowledges Bo Zheng from Tsinghua University for his contribution to the THU inversion system. RSA thanks William Merryfield, Woosung Lee, Jason Cole for their help to set up and produce the model runs. The IPSL contribution was achieved thanks to the valuable contributions of Patricia Cadule, Juliette Mignot and Olivier Torres. GAM acknowledges contributions from Amanda Fay to updating the LDEO-HPD fCO2 product. JRM thanks Gesa Meyer for assistance setting up the DGVM simulations. LMD thanks Pedro. M. S. Monteiro (SCS-SU) and Sandy Thomalla (SOCCO-CSIR) for their continued support to make the CSIR-ML6 fCO2-product up-to-date. CFB is grateful to the technicians and crew of the research vessel Víctor Angelescu for all the support and assistance they provided. This is INIDEP contribution 2460.

Financial and computing support

This research was supported by the following sources of funding: Instituto Nacional de Investrigación y Desarrollo Pesquero (INIDEP) (Argentina); Joint Technical Commission of the Maritime Front (CTMFM, Argentina-Uruguay) (Argentina); Integrated Marine Observing System (IMOS) (Australia); National Environmental Science Program (NESP) (Australia); Research Foundation Flanders (grant no. I001821N) (Belgium); ICOS (Integrated Carbon Observing System) Belgium (Belgium); Tula Foundation (Canada); National Key Research and Development Program of China (grant no. 2023YFF0805400) (China); Copernicus Atmosphere Monitoring Service, implemented by ECMWF on behalf of the European Commission (Grant no. CAMS2 55 bis) (EC); European Research Council (ERC-2022-STG OceanPeak, grant 101077209) (EC); Horizon Europe (NextGenCarbon: grant no. 101184989) (EC); Horizon Europe (RESCUE: grant no. 101056939) (EC); Horizon 2020 (ESM2025: grant no. 101003536) (EC); Horizon Europe (TRICUSO: grant no. 101199028) (EC); Horizon Europe (GreenFeedBack: grant no. 101056921) (EC); H2020 (JERICO-S3: grant no. 871153) (EC); Horizon Europe (GEORGE: grant no. 101094716) (EC); Horizon Europe (AI4PEX: grant no.101137682) (EC); ; MOB TAC project of the European Copernicus Marine Environment Monitoring Service (EC); Horizon Europe (TipESM: grant no. 101137673) (EC); European Union under grant agreement no. 101083922 (OceanICU) and UK Research and Innovation (UKRI) under the UK government's Horizon Europe funding guarantee [grant number 10054454, 10063673, 10064020, 10059241, 10079684, 10059012, 10048179]. Views and opinions expressed are however those of the author(s) only and do not necessarily reflect those of the European Union or European Research Executive Agency. Neither the European Union nor the granting authority can be held responsible for them; Climate Space RECCAP-2 (grant no. 4000144908/24/1-LR) (European Space Agency); EO-LINCS (European Space Agency); Ocean Carbon for Climate (grant no. 3-18399/24/I-NB) (European Space Agency); Satellite-based observations of Carbon in the Ocean: Pools, Fluxes and Exchanges (grant no. 4000142532/23/I-DT) (European Space Agency); THRAC3E (grant no. 4000149569/25/I-AG) (European Space Agency); ; ICOS Germany (Germany); Federal Ministry of Education and Research (BMBF) (STEPSEC: grant no. 01LS2102A) (Germany); Marine Institute (Ireland); Japan Meteorological Agency (Japan); Global Environmental Research Coordination System, Ministry of the Environment (grant nos. E2152 and E2252) (Japan); NIES GOSAT Project (Japan); the Environment Research and Technology Development Fund (JPMEERF24S12200) of the Environmental Restoration and Conservation Agency provided by Ministry of the Environment of Japan (Japan); Environment Research and Technology Development Fund (grant no. JPMEERF24S12205, Co-PI: P. K. Patra) of the Environmental Restoration and Conservation Agency of Japan, and the Arctic Challenge for Sustainability phase III project (ArCS-3; grant no. JPMXD1720251001; Co-PI: P. K. Patra) (Japan); Environment Research and Technology Development Fund (grant no. JPMEERF24S12206) of the Environmental Restoration and Conservation Agency of Japan (Japan); Ministry of Business, Innovation and Employment (Strategic Science Investment Fund via the NIWA Ocean-Climate Interaction programme) (New Zealand); Research Council of Norway

(ICOS-3, grant no. 350341) (Norway); Research Council of Norway (grant no. 352474) (Norway); Research Council of Norway (grant no. 352204) (Norway); South African Department of Science, Technology and Innovation (grant no. DSI/CON C3184/2023) (South Africa); UK Research and Innovation (Horizon Europe GreenFeedBack: grant no. 10040851) (UK); NCAS at the University of Reading (UK); NERC NE/V011103/1 “Frontiers of instability in marine ecosystems and carbon export”UK Natural Environment Research Council (NE/V01417X/1) (UK); Department of Energy, Office of Science, Office of Biological and Environmental Research (USA); NOAA (Global Ocean Monitoring and Observing Program: Open Funder Registry no. 100018302) (USA); NOAA (Ocean Acidification Program: Open Funder Registry no. 100018228) (USA); NOAA (Cooperative Agreement NA20OAR4320472) (USA); NOAA (Cooperative Agreement NA-03-AR4320179) (USA); Alaska Ocean Observing System (USA); NASA Carbon Monitoring System (grant no. 80NSSC25K7221) (USA); NASA Early Career Investigator Program in Earth Science (grant no. 80NSSC24K1632) (USA); NASA Land Cover and Land Use Change Program (Grants: 80NSSC24K0920 and 80NSSC25K7497) (USA); NSF (Cooperative Agreement No. 1852977) (USA); NASA Orbiting Carbon Observatory Science Team Program (grant no. NNH23ZDA001N-OCOST) (USA); NASA Carbon Monitoring System (grant no.NNH22ZDA001N-CMS) (USA); Work of J.L. and S.P. was conducted at the Jet Propulsion Laboratory, California Institute of Technology, under a contract with the National Aeronautics and Space Administration (80NM0018D0004) (USA); NOAA (Cooperative Institute for Marine, Earth and Atmospheric Systems, Award No. NA25NMFX432C0003-T1-01) (USA); NSF (OPP-2329254) (USA); ORNL is managed by UT-Battelle, LLC, for the DOE (grant no. DE-AC05-1008 00OR22725) (USA); Schmidt Sciences (VESRI CALIPSO) (USA); Schmidt Sciences (OBVI InMOS) (USA); NSF (OPP-1922922) (USA); NOAA grant NA24NESX432C0001 (Cooperative Institute for Satellite Earth System Studies - CISESS) (USA); NOAA cooperative agreement NA22OAR4320151 (CIRES: Andrew Jacobson and Xin Lan) (USA); Schmidt Sciences (CLARiTy project, part of the Virtual Institute for the Carbon Cycle) (USA); Schmidt Sciences (COCO2 project, part of the Virtual Institute for the Carbon Cycle) (USA); NSF (LEAP STC Award no 2019625) (USA); NASA (grant no. 80NSSC22K0150) (USA); NOAA (GOMO, grant no. NA24OARX431G0151-T1-01) (USA).

The US National Science Foundation (grant nos. OPP-1922922, OPP-2329254), a NOAA cooperative agreement, the Cooperative Institute for Marine, Earth and Atmospheric Systems (CIMEAS, grant nos. NA20OAR4320278-T1-01 and NA25NMFX432C0003-T3-01S022); although NSF grants 1922922 and 2329254 and NOAA grants NA20OAR4320278-T1-01 and NA25NMFX432C0003-T3-01S022 have been identified for conflict of interest management based on the overall scope of the project and its potential benefit to the Keeling Curve Foundation, the research findings included in this particular publication may not necessarily relate to the interests of Keeling Curve Foundation. The terms of this arrangement have been reviewed and approved by the University of California, San Diego in accordance with its conflict of interest policies.

We also acknowledge support from the following computing facilities: Australian Community Climate and Earth System Simulator – National Research Infrastructure (ACCESS-NRI) (Australia); National Computational Infrastructure (NCI) (Australia); High-Performance Computing Center (HPCC) of Nanjing University for doing the inversions on its blade cluster system (China); HPC computing and storage resources by GENCI at IDRIS and TGCC thanks to the grant 2024-2201 on the supercomputers Jean Zay's V100 and Joliot Curie's SKL and V100 partitions. (France); The ORCHIDEE simulations were performed using HPC resources from GENCi-TGCC on grant 2024-00006328 (France); IPSL Climate Modelling Centre (https://mesocentre.ipsl.fr) (France); HPC resources from GENCI - TGCC (Grant A005-017403) (France); Deutsches Klimarechenzentrum (DKRZ) (Projects: bm0891, bm1124 and bg1446) (Germany); NIES Supercomputer system, GOSAT Supercomputing Facility (GOCF) (Japan); NEC SX-Aurora TSUBASA at NIES (Japan);Fugaku provided by the RIKEN Center for Computational Science (Project ID: hp250024) (Japan); JAMSTEC's ES4 Super Computer system (Japan); Sigma2 - the National Infrastructure for High-Performance Computing and Data Storage in Norway (Norway); NICIS Centre for High-Performance Computing (South Africa); UK CEDA JASMIN supercomputer (UK); Compute and Data Environment for Science (CADES) at the Oak Ridge National Laboratory (USA); LEAP Pangeo cloud platform (USA);NASA Ames Supercomputers (USA).

References

Andela, N., Morton, D. C., Giglio, L., Chen, Y., van der Werf, G. R., Kasibhatla, P. S., DeFries, R. S., Collatz, G. J., Hantson, S., Kloster, S., Bachelet, D., Forrest, M., Lasslop, G., Li, F., Mangeon, S., Melton, J. R., Yue, C., and Randerson, J. T.: A human-driven decline in global burned area, Science, 356, 1356–1362, https://doi.org/10.1126/science.aal4108, 2017.

Andrew, R. M.: A comparison of estimates of global carbon dioxide emissions from fossil carbon sources, Earth Syst. Sci. Data, 12, 1437–1465, https://doi.org/10.5194/essd-12-1437-2020, 2020a.

Andrew, R. M.: Timely estimates of India's annual and monthly fossil CO2 emissions, Earth Syst. Sci. Data, 12, 2411–2421, https://doi.org/10.5194/essd-12-2411-2020, 2020b.

Andrew, R. M.: Towards near real-time, monthly fossil CO2 emissions estimates for the European Union with current-year projections, Atmospheric Pollution Research, 12, 101229, https://doi.org/10.1016/j.apr.2021.101229, 2021.

Andrew, R. M., & Peters, G. P.:The Global Carbon Project's fossil CO2 emissions dataset (Version 251022) [Data set]. Zenodo. https://doi.org/10.5281/zenodo.5569234, 2025.

Aragão, L. E. O. C., Anderson, L. O., Fonseca, M. G., Rosan, T. M., Vedovato, L. B., Wagner, F. H., Silva, C. V. J., Silva Junior, C. H. L., Arai, E., Aguiar, A. P., Barlow, J., Berenguer, E., Deeter, M. N., Domingues, L. G., Gatti, L., Gloor, M., Malhi, Y., Marengo, J. A., Miller, J. B., Phillips, O. L., and Saatchi, S.: 21st Century drought-related fires counteract the decline of Amazon deforestation carbon emissions, Nat Commun, 9, 536, https://doi.org/10.1038/s41467-017-02771-y, 2018.

Archer, D., Eby, M., Brovkin, V., Ridgwell, A., Cao, L., Mikolajewicz, U., Caldeira, K., Matsumoto, K., Munhoven, G., Montenegro, A., and Tokos, K.: Atmospheric Lifetime of Fossil Fuel Carbon Dioxide, Annu. Rev. Earth Planet. Sci., 37, 117–134, https://doi.org/10.1146/annurev.earth.031208.100206, 2009.

Arneth, A., Sitch, S., Pongratz, J., Stocker, B. D., Ciais, P., Poulter, B., Bayer, A. D., Bondeau, A., Calle, L., Chini, L. P., Gasser, T., Fader, M., Friedlingstein, P., Kato, E., Li, W., Lindeskog, M., Nabel, J. E. M. S., Pugh, T. A. M., Robertson, E., Viovy, N., Yue, C., and Zaehle, S.: Historical carbon dioxide emissions caused by land-use changes are possibly larger than assumed, Nature Geosci, 10, 79–84, https://doi.org/10.1038/ngeo2882, 2017.

Asaadi, A., Arora, V. K., Melton, J. R., and Bartlett, P.: An improved parameterization of leaf area index (LAI) seasonality in the Canadian Land Surface Scheme (CLASS) and Canadian Terrestrial Ecosystem Model (CTEM) modelling framework, 15, 6885–6907, https://doi.org/10.5194/bg-15-6885-2018, 2018.

Aumont, O., Orr, J. C., Monfray, P., Ludwig, W., Amiotte-Suchet, P., and Probst, J.-L.: Riverine-driven interhemispheric transport of carbon, Global Biogeochem. Cycles, 15, 393–405, https://doi.org/10.1029/1999GB001238, 2001.

Aumont, O., Ethé, C., Tagliabue, A., Bopp, L., and Gehlen, M.: PISCES-v2: an ocean biogeochemical model for carbon and ecosystem studies, 8, 2465–2513, https://doi.org/10.5194/gmd-8-2465-2015, 2015.

Babiker, M., G. Berndes, K. Blok, B. Cohen, A. Cowie, O. Geden, V. Ginzburg, A. Leip, P. Smith, M. Sugiyama, F. Yamba, Al Khourdajie, A., Arneth, A., Lima de Azevedo, I. M., Bataille, C., Beerling, D., Bezner Kerr, R., Bradley, J., Buck, H. J., Cabeza, L. F., Calvin, K., Campbell, D., Carnicer Cols, J., Daioglou, V., Harmsen, M., Höglund-Isaksson, L., House, J. I., Keller, D., de Kleijne, K., Kugelberg, S., Makarov, I., Meza, F., Minx, J. C., Morecroft, M., Nabuurs, G. J., Neufeldt, H., Novikova, A., Nugroho, S. B., Oschlies, A., Parmesan, C., Peters, G. P., Poore, J., Portugal-Pereira, J., Postigo, J. C., Pradhan, P., Renforth, P., Rivera-Ferre, M. G., Roe, S., Singh, P. K., Slade, R., Smith, S. M., Tirado von der Pahlen, M. C., and Toribio Ramirez, D.: Cross sectoral perspectives. In: Climate Change 2022: Mitigation of Climate Change. Contribution of Working Group III to the Sixth Assessment Report of the Intergovernmental Panel on Climate Change [P.R. Shukla, J. Skea, R. Slade, A. Al Khourdajie, R. van Diemen, D. McCollum, M. Pathak, S. Some, P. Vyas, R. Fradera, M. Belkacemi, A. Hasija, G. Lisboa, S. Luz, J. Malley, (eds.)]. Cambridge University Press, Cambridge, UK and New York, NY, USA. doi: 10.1017/9781009157926.014, 2022.

Baccini, A., Walker, W., Carvalho, L., Farina, M., Sulla-Menashe, D., and Houghton, R. A.: Tropical forests are a net carbon source based on aboveground measurements of gain and loss, Science, 358, 230–234, https://doi.org/10.1126/science.aam5962, 2017.

Bakker, D. C. E., Pfeil, B., Landa, C. S., Metzl, N., O'Brien, K. M., Olsen, A., Smith, K., Cosca, C., Harasawa, S., Jones, S. D., Nakaoka, S., Nojiri, Y., Schuster, U., Steinhoff, T., Sweeney, C., Takahashi, T., Tilbrook, B., Wada, C., Wanninkhof, R., Alin, S. R., Balestrini, C. F., Barbero, L., Bates, N. R., Bianchi, A. A., Bonou, F., Boutin, J., Bozec, Y., Burger, E. F., Cai, W.-J., Castle, R. D., Chen, L., Chierici, M., Currie, K., Evans, W., Featherstone, C., Feely, R. A., Fransson, A., Goyet, C., Greenwood, N., Gregor, L., Hankin, S., Hardman-Mountford, N. J., Harlay, J., Hauck, J., Hoppema, M., Humphreys, M. P., Hunt, C. W., Huss, B., Ibánhez, J. S. P., Johannessen, T., Keeling, R., Kitidis, V., Körtzinger, A., Kozyr, A., Krasakopoulou, E., Kuwata, A., Landschützer, P., Lauvset, S. K., Lefèvre, N., Lo Monaco, C., Manke, A., Mathis, J. T., Merlivat, L., Millero, F. J., Monteiro, P. M. S., Munro, D. R., Murata, A., Newberger, T., Omar, A. M., Ono, T., Paterson, K., Pearce, D., Pierrot, D., Robbins, L. L., Saito, S., Salisbury, J., Schlitzer, R., Schneider, B., Schweitzer, R., Sieger, R., Skjelvan, I., Sullivan, K. F., Sutherland, S. C., Sutton, A. J., Tadokoro, K., Telszewski, M., Tuma, M., van Heuven, S. M. A. C., Vandemark, D., Ward, B., Watson, A. J., and Xu, S.: A multi-decade record of high-quality CO2 data in version 3 of the Surface Ocean CO2 Atlas (SOCAT), Earth Syst. Sci. Data, 8, 383–413, https://doi.org/10.5194/essd-8-383-2016, 2016.

Bakker, D. C. E., Alin, S. R., Aramaki, T., Barbero, L., Bates, N. R., Gkritzalis, T., Jones, S. D., Kozyr, A., Lauvset, S. K., Macovei, V., Metzl, N., Munro, D. R., Nakaoka, S.-i., O'Brien, K. M., Olsen, A., Pierrot, D., Steinhoff, T., Sullivan, K. F., Sutton, A. J., Sweeney, C., Wada, C., Wanninkhof, R., Akl, J., Arbilla, L. A., Azetsu-Scott, K., Battisti, R., Beatty, C. M., Becker, M., Benoit-Cattin, A., Berghoff, C. F., Bittig, H. C., Bonin, J. A., Bott, R., Bozzano, R., Burger, E. F., Brunetti, F., Cantoni, C., Castelli, G., Chambers, D. P., Chierici, M., Corbo, A., Cronin, M., Cross, J. N., Currie, K. I., Dentico, C., Emerson, S. R., Enochs, I., Enright, M. P., Enyo, K., Ericson, Y., Evans, W., Fay, A. R., Feely, R. A., Fragiacomo, E., Fransson, A., Gehrung, M., Giani, M., Glockzin, M., Hamnca, S., Holodkov, N., Hoppema, M., Ibánhez, J. S. P., Kadono, K., Kamb, L., Kralj, M., Kristensin, T. O., Laudicella, V. A., Lefèvre, N., Leseurre, C., Lo Monaco, C., Maenner Jones, S. M., Maenza, R. A., McAuliffe, A. M., Mdokwana, B. W., Monacci, N. M., Musielewicz, S., Neill, C., Newberger, T., Nojiri, Y., Ohman, M. D., Ólafsdóttir, S. R., Olivier, L., Omar, A., Osborne, J., Pensieri, S., Petersen, W., Plueddemann, A. J., Rehder, G., Roden, N. P., Rutgersson, A., Sallée, J.-B., Sanders, R., Sarpe, D., Schirnik, C., Schlitzer, R., Send, U., Skjelvan, I., Sutherland, S., C., T'Jampens, M., Tamsitt, V., Telszewski, M., Theetaert, H., Tilbrook, B., Trull, T., Tsanwani, M., Van de Velde, S., Van Heuven, S. M. A. C., Veccia, M. H., Voynova, Y. G., Weller, R. A., Williams, N. L.: Surface Ocean CO2 Atlas Database Version 2025 (SOCATv2025) (NCEI Accession 0304549), NOAA National Centers for Environmental Information, Dataset, https://doi.org/10.25921/648f-fv35, 2025a.

Bakker, D. C. E., Alin, S. R., Aramaki, T., Barbero, L., Bates, N. R., Gkritzalis, T., Jones, S. D., Kozyr, A., Lauvset, S. K., Macovei, V. A., Metzl, N., Munro, D. R., Nakaoka, S.i., O'Brien, K. M., Olsen, A., Pierrot, D., Steinhoff, T., Sullivan, K. F., Sutton, A. J., Sweeney, C., Wada, C., Wanninkhof, R: SOCAT version 2025: Open ocean CO2 data submissions stabilise, https://socat.info/index.php/posters/, Poster published on 05/06/2025. Last access 23 October 2025, 2025b.

Ballantyne, A. P., Alden, C. B., Miller, J. B., Tans, P. P., and White, J. W. C.: Increase in observed net carbon dioxide uptake by land and oceans during the past 50 years, Nature, 488, 70–72, https://doi.org/10.1038/nature11299, 2012.

Ballantyne, A. P., Andres, R., Houghton, R., Stocker, B. D., Wanninkhof, R., Anderegg, W., Cooper, L. A., DeGrandpre, M., Tans, P. P., Miller, J. B., Alden, C., and White, J. W. C.: Audit of the global carbon budget: estimate errors and their impact on uptake uncertainty, Biogeosciences, 12, 2565–2584, https://doi.org/10.5194/bg-12-2565-2015, 2015.

Bar-On, Y. M.,Li, X., O'Sullivan, M., Wigneron, J-P., Sitch, S., Ciais, P., Frankenberg, C., Fischer, W. W.: Recent gains in global terrestrial carbon stocks are mostly stored in nonliving pools, Science 387, 1291–1295, 2025.

Bastos, A., Hartung, K., Nützel, T. B., Nabel, J. E. M. S., Houghton, R. A., and Pongratz, J.: Comparison of uncertainties in land-use change fluxes from bookkeeping model parameterisation, 12, 745–762, https://doi.org/10.5194/esd-12-745-2021, 2021.

Battle, M. O., Raynor, R., Kesler, S., and Keeling, R.: Technical Note: The impact of industrial activity on the amount of atmospheric O2, Atmospheric Chem. Phys. Discuss., 1–17, https://doi.org/10.5194/acp-2022-765, 2023.

Bellenger, H., Bopp, L., Ethé, C., Ho, D., Duvel, J. P., Flavoni, S., Guez, L., Kataoka, T., Perrot, X., Parc, L., and Watanabe, M.: Sensitivity of the Global Ocean Carbon Sink to the Ocean Skin in a Climate Model, J. Geophys. Res. Oceans, 128, e2022JC019479, https://doi.org/10.1029/2022JC019479, 2023.

Bennington, V., Gloege, L., and McKinley, G. A.: Variability in the Global Ocean Carbon Sink From 1959 to 2020 by Correcting Models with Observations, Geophys. Res. Lett., 49, e2022GL098632, https://doi.org/10.1029/2022GL098632, 2022.

Bernardello, R., Sicardi, V., Lapin, V., Ortega, P., Ruprich-Robert, Y., Tourigny, E. and Ferrer, E.: Ocean biogeochemical reconstructions to estimate historical ocean CO 2 uptake. Earth System Dynamics, 15(5), pp.1255-1275, https://doi.org/10.5194/esd-15-1255-2024, 2024.

Berthet, S., Séférian, R., Bricaud, C., Chevallier, M., Voldoire, A., and Ethé, C.: Evaluation of an Online Grid-Coarsening Algorithm in a Global Eddy-Admitting Ocean Biogeochemical Model, J. Adv. Model Earth Sy., 11, 1759–1783, https://doi.org/10.1029/2019MS001644, 2019.

Bethke, I., Wang, Y., Counillon, F., Keenlyside, N., Kimmritz, M., Fransner, F., Samuelsen, A., Langehaug, H., Svendsen, L., Chiu, P.-G., Passos, L., Bentsen, M., Guo, C., Gupta, A., Tjiputra, J., Kirkevåg, A., Olivié, D., Seland, Ø., Solsvik Vågane, J., Fan, Y., and Eldevik, T.: NorCPM1 and its contribution to CMIP6 DCPP, Geosci. Model Dev., 14, 7073–7116, https://doi.org/10.5194/gmd-14-7073-2021, 2021.

Betts, R. A., Jones, C. D., Knight, J. R., Keeling, R. F., and Kennedy, J. J.: El Niño and a record CO2 rise, Nat. Clim. Change, 6, 806–810, https://doi.org/10.1038/nclimate3063, 2016.

Bilbao, R., Wild, S., Ortega, P., Acosta-Navarro, J., Arsouze, T., Bretonnière, P.A., Caron, L.P., Castrillo, M., Cruz-García, R., Cvijanovic, I. and Doblas-Reyes, F.J.: Assessment of a full-field initialised decadal climate prediction system with the CMIP6 version of EC-Earth. Earth System Dynamics Discussions, 2020, pp.1-30, https://doi.org/10.5194/esd-12-173-2021, 2020.

Bloom, A. A. and Williams, M.: Constraining ecosystem carbon dynamics in a data-limited world: integrating ecological “common sense” in a model–data fusion framework, Biogeosciences, 12, 1299–1315, https://doi.org/10.5194/bg-12-1299-2015, 2015.

Bloom, A. A., Exbrayat, J.-F., van der Velde, I. R., Feng, L., and Williams, M.: The decadal state of the terrestrial carbon cycle: Global retrievals of terrestrial carbon allocation, pools, and residence times, Proc. Natl. Acad. Sci., 113, 1285–1290, https://doi.org/10.1073/pnas.1515160113, 2016.

Boer, G. J., Smith, D. M., Cassou, C., Doblas-Reyes, F., Danabasoglu, G., Kirtman, B., Kushnir, Y., Kimoto, M., Meehl, G. A., Msadek, R., Mueller, W. A., Taylor, K. E., Zwiers, F., Rixen, M., Ruprich-Robert, Y., and Eade, R.: The Decadal Climate Prediction Project (DCPP) contribution to CMIP6, Geosci. Model Dev., 9, 3751–3777, https://doi.org/10.5194/gmd-9-3751-2016, 2016.

Boucher, O., Servonnat, J., Albright, A. L., Aumont, O., Balkanski, Y., Bastrikov, V., Bekki, S., Bonnet, R., Bony, S., Bopp, L., Braconnot, P., Brockmann, P., Cadule, P., Caubel, A., Cheruy, F., Codron, F., Cozic, A., Cugnet, D., D’Andrea, F., Davini, P., de Lavergne, C., Denvil, S., Deshayes, J., Devilliers, M., Ducharne, A., Dufresne, J.-L., Dupont, E., Éthé, C., Fairhead, L., Falletti, L., Flavoni, S., Foujols, M.-A., Gardoll, S., Gastineau, G., Ghattas, J., Grandpeix, J.-Y., Guenet, B., Guez, E., Lionel, Guilyardi, E., Guimberteau, M., Hauglustaine, D., Hourdin, F., Idelkadi, A., Joussaume, S., Kageyama, M., Khodri, M., Krinner, G., Lebas, N., Levavasseur, G., Lévy, C., Li, L., Lott, F., Lurton, T., Luyssaert, S., Madec, G., Madeleine, J.-B., Maignan, F., Marchand, M., Marti, O., Mellul, L., Meurdesoif, Y., Mignot, J., Musat, I., Ottlé, C., Peylin, P., Planton, Y., Polcher, J., Rio, C., Rochetin, N., Rousset, C., Sepulchre, P., Sima, A., Swingedouw, D., Thiéblemont, R., Traore, A. K., Vancoppenolle, M., Vial, J., Vialard, J., Viovy, N., and Vuichard, N.: Presentation and Evaluation of the IPSL-CM6A-LR Climate Model, J. Adv. Model. Earth Syst., 12, e2019MS002010, https://doi.org/10.1029/2019MS002010, 2020.

Bourgeois, T., Goris, N., Schwinger, J., and Tjiputra, J. F.: Stratification constrains future heat and carbon uptake in the Southern Ocean between 30°S and 55°S, Nat. Commun., 13, 340, https://doi.org/10.1038/s41467-022-27979-5, 2022.

Bourgoin, C., Beuchle, R., Branco, A., Carreiras, J., Ceccherini, G., Oom, D., San-Miguel-Ayanz, J., and Sedano, F.: Extensive fire-driven degradation in 2024 marks worst Amazon forest disturbance in over 2 decades, Biogeosciences, 22, 5247–5256, https://doi.org/10.5194/bg-22-5247-2025, 2025.

Bray, E.: 2017 Minerals Yearbook: Aluminum [Advance Release], Tech. rep., U.S. Geological Survey, https://d9-wret.s3-us-west-2.amazonaws.com/assets/palladium/production/atoms/files/myb1-2017-alumi.pdf, 2020.

Brienen, R. J. W., Caldwell, L., Duchesne, L., Voelker, S., Barichivich, J., Baliva, M., Ceccantini, G., Di Filippo, A., Helama, S., Locosselli, G. M., Lopez, L., Piovesan, G., Schöngart, J., Villalba, R., and Gloor, E.: Forest carbon sink neutralized by pervasive growth-lifespan trade-offs, Nat. Commun., 11, 4241, https://doi.org/10.1038/s41467-020-17966-z, 2020.

Brienen, R. J. W., Phillips, O. L., Feldpausch, T. R., Gloor, E., Baker, T. R., Lloyd, J., Lopez-Gonzalez, G., Monteagudo-Mendoza, A., Malhi, Y., Lewis, S. L., Vásquez Martinez, R., Alexiades, M., Álvarez Dávila, E., Alvarez-Loayza, P., Andrade, A., Aragão, L. E. O. C., Araujo-Murakami, A., Arets, E. J. M. M., Arroyo, L., Aymard C., G. A., Bánki, O. S., Baraloto, C., Barroso, J., Bonal, D., Boot, R. G. A., Camargo, J. L. C., Castilho, C. V., Chama, V., Chao, K. J., Chave, J., Comiskey, J. A., Cornejo Valverde, F., da Costa, L., de Oliveira, E. A., Di Fiore, A., Erwin, T. L., Fauset, S., Forsthofer, M., Galbraith, D. R., Grahame, E. S., Groot, N., Hérault, B., Higuchi, N., Honorio Coronado, E. N., Keeling, H., Killeen, T. J., Laurance, W. F., Laurance, S., Licona, J., Magnussen, W. E., Marimon, B. S., Marimon-Junior, B. H., Mendoza, C., Neill, D. A., Nogueira, E. M., Núñez, P., Pallqui Camacho, N. C., Parada, A., Pardo-Molina, G., Peacock, J., Peña-Claros, M., Pickavance, G. C., Pitman, N. C. A., Poorter, L., Prieto, A., Quesada, C. A., Ramírez, F., Ramírez-Angulo, H., Restrepo, Z., Roopsind, A., Rudas, A., Salomão, R. P., Schwarz, M., Silva, N., Silva-Espejo, J. E., Silveira, M., Stropp, J., Talbot, J., ter Steege, H., Teran-Aguilar, J., Terborgh, J., Thomas-Caesar, R., Toledo, M., Torello-Raventos, M., Umetsu, R. K., van der Heijden, G. M. F., van der Hout, P., Guimarães Vieira, I. C., Vieira, S. A., Vilanova, E., Vos, V. A., and Zagt, R. J.: Long-term decline of the Amazon carbon sink, 519, 344–348, https://doi.org/10.1038/nature14283, 2015.

Bronselaer, B., Winton, M., Russell, J., Sabine, C. L., and Khatiwala, S.: Agreement of CMIP5 Simulated and Observed Ocean Anthropogenic CO2 Uptake, Geophys. Res. Lett., 44, 12,298-12,305, https://doi.org/10.1002/2017GL074435, 2017.

Bruno, M. and Joos, F.: Terrestrial carbon storage during the past 200 years: A Monte Carlo Analysis of CO 2 data from ice core and atmospheric measurements, Global Biogeochem. Cycles, 11, 111–124, https://doi.org/10.1029/96GB03611, 1997.

Burrows, S. M., Maltrud, M., Yang, X., Zhu, Q., Jeffery, N., Shi, X., Ricciuto, D., Wang, S., Bisht, G., Tang, J., Wolfe, J., Harrop, B. E., Singh, B., Brent, L., Baldwin, S., Zhou, T., Cameron-Smith, P., Keen, N., Collier, N., Xu, M., Hunke, E. C., Elliott, S. M., Turner, A. K., Li, H., Wang, H., Golaz, J.-C., Bond-Lamberty, B., Hoffman, F. M., Riley, W. J., Thornton, P. E., Calvin, K., and Leung, L. R.: The DOE E3SM v1.1 Biogeochemistry Configuration: Description and Simulated Ecosystem-Climate Responses to Historical Changes in Forcing, J. Adv. Model. Earth Syst., 12, e2019MS001766, https://doi.org/10.1029/2019MS001766, 2020.

Bunsen, F., Nissen, C., and Hauck, J.: The Impact of Recent Climate Change on the Global Ocean Carbon Sink. Geophysical Research Letters, 51(4), e2023GL107030, https://doi.org/10.1029/2023GL107030, 2024.

Burton, C., Betts, R., Cardoso, M., Feldpausch, T. R., Harper, A., Jones, C. D., Kelley, D. I., Robertson, E., and Wiltshire, A.: Representation of fire, land-use change and vegetation dynamics in the Joint UK Land Environment Simulator vn4.9 (JULES), Geosci. Model Dev., 12, 179–193, https://doi.org/10.5194/gmd-12-179-2019, 2019.

Burton, C., Lampe, S., Kelley, D. I., Thiery, W., Hantson, S., Christidis, N., Gudmundsson, L., Forrest, M., Burke, E., Chang, J., Huang, H., Ito, A., Kou-Giesbrecht, S., Lasslop, G., Li, W., Nieradzik, L., Li, F., Chen, Y., Randerson, J., Reyer, C. P. O., and Mengel, M.: Global burned area increasingly explained by climate change, Nature Climate Change, https://doi.org/10.1038/s41558-024-02140-w, 2024.

Bushinsky, S. M., Landschützer, P., Rödenbeck, C., Gray, A. R., Baker, D., Mazloff, M. R., Resplandy, L., Johnson, K. S., and Sarmiento, J. L.: Reassessing Southern Ocean Air-Sea CO 2 Flux Estimates With the Addition of Biogeochemical Float Observations, Global Biogeochem. Cycles, 33, 1370–1388, https://doi.org/10.1029/2019GB006176, 2019.

Byrne, B., Liu, J., Bowman, K.W., Pascolini-Campbell, M., Chatterjee, A., Pandey, S., Miyazaki, K., van der Werf, G.R., Wunch, D., Wennberg, P.O., Roehl, C.M., and Sinha, S.: Carbon emissions from the 2023 Canadian wildfires. Nature, 633, 835–839, https://doi.org/10.1038/s41586-024-07878-z, 2024.

Canadell, J. G., Le Quere, C., Raupach, M. R., Field, C. B., Buitenhuis, E. T., Ciais, P., Conway, T. J., Gillett, N. P., Houghton, R. A., and Marland, G.: Contributions to accelerating atmospheric CO2 growth from economic

activity, carbon intensity, and efficiency of natural sinks, Proceedings of the National Academy of Sciences, 104, 18866–18870, https://doi.org/10.1073/pnas.0702737104, 2007.

Canadell, J. G., Monteiro, P. M. S., Costa, M. H., Cotrim da Cunha, L., Cox, P. M., Eliseev, A. V., Henson, S., Ishii, M., Jaccard, S., Koven, C., Lohila, A., Patra, P. K., Piao, S., Rogelj, J., Syampungani, S., Zaehle, S., and Zickfeld, K.: Global Carbon and other Biogeochemical Cycles and Feedbacks. In: Climate Change 2021: The Physical Science Basis. Contribution of Working Group I to the Sixth Assessment Report of the Intergovernmental Panel on Climate Change [Masson-Delmotte, V., P. Zhai, A. Pirani, S. L. Connors, C. Péan, S. Berger, N. Caud, Y. Chen, L. Goldfarb, M. I. Gomis, M. Huang, K. Leitzell, E. Lonnoy, J.B.R. Matthews, T. K. Maycock, T. Waterfield, O. Yelekçi, R. Yu and B. Zhou (eds.)]. Cambridge University Press, Cambridge, United Kingdom and New York, NY, USA, pp. 673–816, https://doi.org/10.1017/9781009157896.007., 2021.

Cao, Z., Myers, R. J., Lupton, R. C., Duan, H., Sacchi, R., Zhou, N., Reed Miller, T., Cullen, J. M., Ge, Q., and Liu, G.: The sponge effect and carbon emission mitigation potentials of the global cement cycle, Nat Commun, 11, 3777, https://doi.org/10.1038/s41467-020-17583-w, 2020.

Carbon Monitor: Year in Review: Global carbon emissions and decarbonization in 2024, available at: https://carbonmonitor.org/ , last access: 23 October 2025, 2025.

Centro Nacional de Monitoramento e Alertas de Desastres Naturais (CEMADEN): Monitoramento de secas e impactos no Brasil - Agosto 2024, available at: https://www.gov.br/cemaden/pt-br/assuntos/monitoramento/monitoramento-de-seca-para-o-brasil/monitoramento-de-secas-e-impactos-no-brasil-agosto-2024, last access: 23 October 2025.

Céspedes, J., Sylvester, J. M., Pérez-Marulanda, L., Paz-Garcia, P., Reymondin, L., Khodadadi, M., Tello, J. J., and Castro-Nunez, A.: Has global deforestation accelerated due to the COVID-19 pandemic?, J. For. Res., 34, 1153–1165, https://doi.org/10.1007/s11676-022-01561-7, 2023.

Chandra, N., Patra, P. K., Niwa, Y., Ito, A., Iida, Y., Goto, D., Morimoto, S., Kondo, M., Takigawa, M., Hajima, T., and Watanabe, M.: Estimated regional CO2 flux and uncertainty based on an ensemble of atmospheric CO2 inversions, Atmospheric Chem. Phys., 22, 9215–9243, https://doi.org/10.5194/acp-22-9215-2022, 2022.

Chatfield, C.: The Holt-Winters Forecasting Procedure, J. Roy. Stat. Soc. C., 27, 264–279, https://doi.org/10.2307/2347162, 1978.

Chau, T. T. T., Gehlen, M., and Chevallier, F.: A seamless ensemble-based reconstruction of surface ocean pCO2 and air–sea CO2 fluxes over the global coastal and open oceans, Biogeosciences, 19, 1087–1109, https://doi.org/10.5194/bg-19-1087-2022, 2022.

Chen, Y., Hall, J., Van Wees, D., Andela, N., Hantson, S., Giglio, L., Van Der Werf, G. R., Morton, D. C., and Randerson, J. T.: Multi-decadal trends and variability in burned area from the fifth version of the Global Fire Emissions Database (GFED5), Earth Syst. Sci. Data, 15, 5227–5259, https://doi.org/10.5194/essd-15-5227-2023, 2023.

Chevallier, F., Fisher, M., Peylin, P., Serrar, S., Bousquet, P., Bréon, F.-M., Chédin, A., and Ciais, P.: Inferring CO 2 sources and sinks from satellite observations: Method and application to TOVS data, J. Geophys. Res., 110, D24309, https://doi.org/10.1029/2005JD006390, 2005.

Chevallier, F., Martinez, A., Lloret, Z., Takache, S., and Cozic, A.: Offline Atmospheric Transport on a Global Mesh of Hexagons, JGR Atmospheres, 130, e2025JD043579, https://doi.org/10.1029/2025JD043579, 2025.

Ciais, P., Sabine, C., Bala, G., Bopp, L., Brovkin, V., Canadell, J. G., Chhabra, A., DeFries, R., Galloway, J., Heimann, M., Jones, C., Le Quéré, C., Myneni, R., Piao, S., Thornton, P., Willem, J., Friedlingstein, P., and Munhoven, G.: Carbon and Other Biogeochemical Cycles, in Climate Change 2013: The Physical Science Basis, Contribution of Working Group I to the Fifth Assessment Report of the Intergovernmental Panel on Climate Change, edited by: Intergovernmental Panel on Climate Change, Cambridge University Press, Cambridge, United Kingdom and New York, NY, USA, https://doi.org/10.1017/CBO9781107415324.015, 2013.

Ciais, P., Tan, J., Wang, X., Roedenbeck, C., Chevallier, F., Piao, S.-L., Moriarty, R., Broquet, G., Le Quéré, C., Canadell, J. G., Peng, S., Poulter, B., Liu, Z., and Tans, P.: Five decades of northern land carbon uptake revealed by the interhemispheric CO2 gradient, Nature, 568, 221–225, https://doi.org/10.1038/s41586-019-1078-6, 2019.

Ciais, P., Bastos, A., Chevallier, F., Lauerwald, R., Poulter, B., Canadell, P., Hugelius, G., Jackson, R. B., Jain, A., Jones, M., Kondo, M., Luijkx, I. T., Patra, P. K., Peters, W., Pongratz, J., Petrescu, A. M. R., Piao, S., Qiu, C., Von Randow, C., Regnier, P., Saunois, M., Scholes, R., Shvidenko, A., Tian, H., Yang, H., Wang, X., and Zheng, B.: Definitions and methods to estimate regional land carbon fluxes for the second phase of the REgional Carbon Cycle Assessment and Processes Project (RECCAP-2), Geosci. Model Dev., 15, 1289–1316, https://doi.org/10.5194/gmd-15-1289-2022, 2022.

Ciais, P., Ke, P., Yao, Y., Sitch, S., Li, W., Xu, Y., Du, X., Gui, X., Bastos, A., Zaehle, S., Poulter, B., Colligan, T., van der Woude, A. M., Peters, W., Liu, Z., Jin, Z., Tian, X., Wang, Y., Liu, J., Pandey, S., O'Dell, C., Bian, J., Zhou, C., Miller, J., Lan, X., Goncalves De Souza, J., O'Sullivan, M., Friedlingstein, P., van der Werf, G. R., Peters, G. P., and Chevallier, F.: Low latency global carbon budget indicates reduced land carbon sink in the year 2024, National Science Review, Volume 13, Issue 2, January 2026, nwaf594, https://doi.org/10.1093/nsr/nwaf594.

Collier, N., Hoffman, F. M., Lawrence, D. M., Keppel-Aleks, G., Koven, C. D., Riley, W. J., Mu, M., and Randerson, J. T.: The International Land Model Benchmarking (ILAMB) System: Design, Theory, and Implementation, J. Adv. Model. Earth Syst., 10, 2731–2754, https://doi.org/10.1029/2018MS001354, 2018.

Conchedda, G. and Tubiello, F. N.: Drainage of organic soils and GHG emissions: Validation with country data, Biosphere – Biogeosciences, https://doi.org/10.5194/essd-2020-202, 2020.

Cox, P. M., Pearson, D., Booth, B. B., Friedlingstein, P., Huntingford, C., Jones, C. D., and Luke, C. M.: Sensitivity of tropical carbon to climate change constrained by carbon dioxide variability, Nature, 494, 341–344, https://doi.org/10.1038/nature11882, 2013.

De Kauwe, M. G., Medlyn, B. E., Zaehle, S., Walker, A. P., Dietze, M. C., Wang, Y.-P., Luo, Y., Jain, A. K., El-Masri, B., Hickler, T., Wårlind, D., Weng, E., Parton, W. J., Thornton, P. E., Wang, S., Prentice, I. C., Asao, S., Smith, B., McCarthy, H. R., Iversen, C. M., Hanson, P. J., Warren, J. M., Oren, R., and Norby, R. J.: Where does the carbon go? A model–data intercomparison of vegetation carbon allocation and turnover processes at two temperate forest free-air CO2 enrichment sites, New Phytol., 203, 883–899, https://doi.org/10.1111/nph.12847, 2014.

Delire, C., Séférian, R., Decharme, B., Alkama, R., Calvet, J.-C., Carrer, D., Gibelin, A.-L., Joetzjer, E., Morel, X., Rocher, M., and Tzanos, D.: The Global Land Carbon Cycle Simulated With ISBA-CTRIP: Improvements Over the Last Decade, J. Adv. Model. Earth Syst., 12, e2019MS001886, https://doi.org/10.1029/2019MS001886, 2020.

Denman, K. L., Brasseur, G., Chidthaisong, A., Ciais, P., Cox, P. M., Dickinson, R. E., Hauglustaine, D., Heinze, C., Holland, E., Jacob, D., Lohmann, U., Ramachandran, S., Leite da Silva Dias, P., Wofsy, S. C., and Zhang, X.: Couplings Between Changes in the Climate System and Biogeochemistry, in: Climate Change 2007: The Physical Science Basis. Contribution of Working Group I to the Fourth Assessment Report of the Intergovernmental Panel on Climate Change, edited by: Solomon, S., Qin, D., Manning, M., Marquis, M., Averyt, K., Tignor, M. M. B., Miller, H. L., and Chen, Z. L., Cambridge University Press, Cambridge, UK and New York, USA, 499–587, ISBN: 9780521705967, 2007.

Denvil-Sommer, A., Gehlen, M., and Vrac, M.: Observation system simulation experiments in the Atlantic Ocean for enhanced surface ocean pCO2 reconstructions, Ocean Sci., 17, 1011–1030, https://doi.org/10.5194/os-17-1011-2021, 2021.

DeVries, T., Holzer, M., and Primeau, F.: Recent increase in oceanic carbon uptake driven by weaker upper-ocean overturning, Nature, 542, 215–218, https://doi.org/10.1038/nature21068, 2017.

DeVries, T.: The oceanic anthropogenic CO 2 sink: Storage, air-sea fluxes, and transports over the industrial era, Global Biogeochem. Cycles, 28, 631–647, https://doi.org/10.1002/2013GB004739, 2014.

DeVries, T., Quéré, C. L., Andrews, O., Berthet, S., Hauck, J., Ilyina, T., Landschützer, P., Lenton, A., Lima, I. D., Nowicki, M., Schwinger, J., and Séférian, R.: Decadal trends in the ocean carbon sink, PNAS, 116, 11646–11651, https://doi.org/10.1073/pnas.1900371116, 2019.

DeVries, T.: Atmospheric CO2 and Sea Surface Temperature Variability Cannot Explain Recent Decadal Variability of the Ocean CO2 Sink, Geophysical Research Letters, 49, e2021GL096018, https://doi.org/10.1029/2021GL096018, 2022.

DeVries, T., Yamamoto, K., Wanninkhof, R., Gruber, N., Hauck, J., Müller, J. D., Bopp, L., Carroll, D., Carter, B., Chau, T.-T.-T., Doney, S. C., Gehlen, M., Gloege, L., Gregor, L., Henson, S., Kim, J. H., Iida, Y., Ilyina, T., Landschützer, P., Le Quéré, C., Munro, D., Nissen, C., Patara, L., Pérez, F. F., Resplandy, L., Rodgers, K. B., Schwinger, J., Séférian, R., Sicardi, V., Terhaar, J., Triñanes, J., Tsujino, H., Watson, A., Yasunaka, S., and Zeng, J.: Magnitude, trends, and variability of the global ocean carbon sink from 1985-2018, Glob. Biogeochem. Cycles, n/a, e2023GB007780, https://doi.org/10.1029/2023GB007780, 2023.

Döscher, R., Acosta, M., Alessandri, A., Anthoni, P., Arneth, A., Arsouze, T., Bergmann, T., Bernadello, R., Bousetta, S., Caron, L.P. and Carver, G.: The EC-earth3 Earth system model for the climate model intercomparison project 6. Geoscientific Model Development Discussions, 2021, pp.1-90, https://doi.org/10.5194/gmd-15-2973-2022, 2021.

Doney, S. C., Lima, I., Feely, R. A., Glover, D. M., Lindsay, K., Mahowald, N., Moore, J. K., and Wanninkhof, R.: Mechanisms governing interannual variability in upper-ocean inorganic carbon system and air–sea CO2 fluxes: Physical climate and atmospheric dust, Deep Sea Research Part II: Topical Studies in Oceanography, 56, 640–655, https://doi.org/10.1016/j.dsr2.2008.12.006, 2009.

Dong, Y., Bakker, D. C. E., Bell, T. G., Huang, B., Landschützer, P., Liss, P. S., and Yang, M.: Update on the Temperature Corrections of Global Air-Sea CO2 Flux Estimates, Glob. Biogeochem. Cycles, 36, e2022GB007360, https://doi.org/10.1029/2022GB007360, 2022.

Dong, Y., Bakker, D. C. E., Bell, T. G., Yang, M., Landschützer, P., Hauck, J., Rödenbeck, C., Kitidis, V., Bushinsky, S. M., and Liss, P. S. (2024). Direct observational evidence of strong CO2 uptake in the Southern Ocean. Science Advances, 10(30), eadn5781, https://doi.org/10.1126/sciadv.adn5781, 2024a.

Dong, Y., Bakker, D. C. E., and Landschützer, P.: Accuracy of ocean CO2 uptake estimates at a risk by a reduction in the data collection. Geophysical Research Letters, 51, e2024GL108502, https://doi.org/10.1029/2024GL108502, 2024b.

Dorgeist, L., Schwingshackl, C., Bultan, S., and Pongratz, J.: A consistent budgeting of terrestrial carbon fluxes. Nature Communications, 15(1), 7426, https://doi.org/10.1038/s41467-024-51126-x, 2024.

Dou, X., Wang, Y., Ciais, P., Chevallier, F., Davis, S. J., Crippa, M., Janssens-Maenhout, G., Guizzardi, D., Solazzo, E., Yan, F., Huo, D., Zheng, B., Zhu, B., Cui, D., Ke, P., Sun, T., Wang, H., Zhang, Q., Gentine, P., Deng, Z., and Liu, Z.: Near-real-time global gridded daily CO2 emissions, The Innovation, 3, 100182, https://doi.org/10.1016/j.xinn.2021.100182, 2022.

Eckes-Shephard, A. H., Argles, A. P. K., Brzeziecki, B., Cox, P. M., De Kauwe, M. G., Esquivel-Muelbert, A., Fisher, R. A., Hurtt, G. C., Knauer, J., Koven, C. D., Lehtonen, A., Luyssaert, S., Marqués, L., Ma, L., Marie, G., Moore, J. R., Needham, J. F., Olin, S., Peltoniemi, M., Piltz, K., Sato, H., Sitch, S., Stocker, B. D., Weng, E., Zuleta, D., and Pugh, T. A. M. Pugh: Demography, dynamics and data: building confidence for simulating changes in the world's forests, New Phytologist, doi: 10.1111/nph.70643, 2025.

Edson, J. B., Jampana, V., Weller, R. A., Bigorre, S. P., Plueddemann, A. J., Fairall, C. W., Miller, S. D., Mahrt, L., Vickers, D., and Hersbach, H.: On the Exchange of Momentum over the Open Ocean, J. Phys. Oceanogr., 43, 1589–1610, https://doi.org/10.1175/JPO-D-12-0173.1, 2013.

EIA: Short-Term Energy Outlook: March 2026. U.S. Energy Information Administration [Data set]. Available at: http://www.eia.gov/forecasts/steo/outlook.cfm, last access: 23 March 2026, 2023.

Embury, O., Merchant, C.J., Good, S.A., Rayner, N.A., Høyer, J.L., Atkinson, C., Block, T., Alerskans, E., Pearson, K.J., Worsfold, M. and McCarroll, N. and Donlon, C.: Satellite-based time-series of sea-surface temperature since 1980 for climate applications. Scientific Data, 11(1), 326, https://doi.org/10.1038/s41597-024-03147-w, 2024.

Erb, K.-H., Kastner, T., Luyssaert, S., Houghton, R. A., Kuemmerle, T., Olofsson, P., and Haberl, H.: Bias in the attribution of forest carbon sinks, Nature Clim Change, 3, 854–856, https://doi.org/10.1038/nclimate2004, 2013.

Erb, K.-H., Kastner, T., Plutzar, C., Bais, A. L. S., Carvalhais, N., Fetzel, T., Gingrich, S., Haberl, H., Lauk, C., Niedertscheider, M., Pongratz, J., Thurner, M., and Luyssaert, S.: Unexpectedly large impact of forest management and grazing on global vegetation biomass, Nature, 553, 73–76, https://doi.org/10.1038/nature25138, 2018.

Erb, M. and Marland G.: Global, Regional, and National Fossil-Fuel CO2 Emisisons: 1751-2022 CDIAC-FF, Research Institute for Environment, Energy, and Economics, Appalachian State University. https://rieee.appstate.edu/projects-programs/cdiac/, last access: 23 October 2025, 2025.

Eskander, S. M. S. U. and Fankhauser, S.: Reduction in greenhouse gas emissions from national climate legislation, Nat. Clim. Chang., 10, 750–756, https://doi.org/10.1038/s41558-020-0831-z, 2020.

Etheridge, D. M., Steele, L. P., Langenfelds, R. L., Francey, R. J., Barnola, J.-M., and Morgan, V. I.: Natural and anthropogenic changes in atmospheric CO 2 over the last 1000 years from air in Antarctic ice and firn, J. Geophys. Res., 101, 4115–4128, https://doi.org/10.1029/95JD03410, 1996.

FAO, Food and Agriculture Organization of the United Nations (FAO): Impact of the Ukraine-Russia conflict on global food security and related matters under the mandate of the Food and Agriculture Organization of the United Nations (FAO), Hundred and Seventieth Session of the Council, https://www.fao.org/3/nj164en/nj164en.pdf, last access: 23 October 2025, 2023.

FAO: FAOSTAT Emissions from drained organic soils. Available at http://www.fao.org/faostat/en/#data/GV, last access: 23 October 2025, 2025a.

FAO: Forest emissions and removals – Global, regional and country trends 1990–2025.FAOSTAT Analytical Briefs, No. 114. Rome., available at: https://doi.org/10.4060/cd7163en, last access: 23 October 2025, 2025b.

FAO: Land statistics 2001–2023 – Global, regional and country trends. FAOSTAT Analytical Briefs, No.107. Rome, available at: https://doi.org/10.4060/cd5765en, last access: 23 October 2025, 2025c.

FAO: FAOSTAT Emissions totals database, available at: https://faostat.fao.org/internal/en/#data/GT, FAO, Rome, , last access: 23 October 2025, 2025d.

Fay, A. R., Gregor, L., Landschützer, P., McKinley, G. A., Gruber, N., Gehlen, M., Iida, Y., Laruelle, G. G., Rödenbeck, C., Roobaert, A., and Zeng, J.: SeaFlux: harmonization of air–sea CO2 fluxes from surface pCO2 data products using a standardized approach, Earth System Science Data, 13, 4693–4710, https://doi.org/10.5194/essd-13-4693-2021, 2021.

Fay, A. R., McKinley, G. A., Lovenduski, N. S., Eddebbar, Y., Levy, M. N., Long, M. C., Olivarez, H. C., and Rustagi, R. R.: Immediate and Long-Lasting Impacts of the Mt. Pinatubo Eruption on Ocean Oxygen and Carbon Inventories. Global Biogeochemical Cycles, 37(2). https://doi.org/10.1029/2022gb007513, 2023.

Fay, A. R., Carroll, D., McKinley, G. A., Menemenlis, D., and Zhang, H.: Scale-Dependent Drivers of Air-Sea CO2 Flux Variability, Geophysical Research Letters, 51, e2024GL111911, https://doi.org/10.1029/2024GL111911, 2024.

Fay, A. R., Heimdal, T. H., Acquaviva, V., Shaum, A. P., and McKinley, G. A.: Sensitivity of Ocean Carbon Sink Estimates to Rare Observations, Geophysical Research Letters, 52, e2025GL117961, https://doi.org/10.1029/2025GL117961, 2025.

Felzer, B. S.: Carbon, nitrogen, and water response to climate and land use changes in Pennsylvania during the 20th and 21st centuries, Ecological Modelling, 240, 49–63, https://doi.org/10.1016/j.ecolmodel.2012.05.003, 2012.

Felzer, B. S. and Jiang, M.: Effect of Land Use and Land Cover Change in Context of Growth Enhancements in the United States Since 1700: Net Source or Sink?, JGR Biogeosciences, 123, 3439–3457, https://doi.org/10.1029/2017JG004378, 2018.

Felzer, B. S., Cronin, T. W., Melillo, J. M., Kicklighter, D. W., and Schlosser, C. A.: Importance of carbon-nitrogen interactions and ozone on ecosystem hydrology during the 21st century, J. Geophys. Res., 114, 2008JG000826, https://doi.org/10.1029/2008JG000826, 2009.

Felzer, B. S., Cronin, T. W., Melillo, J. M., Kicklighter, D. W., Schlosser, C. A., and Dangal, S. R. S.: Nitrogen effect on carbon-water coupling in forests, grasslands, and shrublands in the arid western United States, J. Geophys. Res., 116, G03023, https://doi.org/10.1029/2010JG001621, 2011.

Feng, L., Palmer, P. I., Bösch, H., and Dance, S.: Estimating surface CO2 fluxes from space-borne CO2 dry air mole fraction observations using an ensemble Kalman Filter, Atmospheric Chem. Phys., 9, 2619–2633, https://doi.org/10.5194/acp-9-2619-2009, 2009.

Feng, L., Palmer, P. I., Parker, R. J., Deutscher, N. M., Feist, D. G., Kivi, R., Morino, I., and Sussmann, R.: Estimates of European uptake of CO2 inferred from GOSAT XCO2 retrievals: sensitivity to measurement bias inside and outside Europe, Atmos. Chem. Phys., 16, 1289–1302, https://doi.org/10.5194/acp-16-1289-2016, 2016.

Fisher, R. A., Muszala, S., Verteinstein, M., Lawrence, P., Xu, C., McDowell, N. G., Knox, R. G., Koven, C., Holm, J., Rogers, B. M., Spessa, A., Lawrence, D., and Bonan, G.: Taking off the training wheels: the properties of a dynamic vegetation model without climate envelopes, CLM4.5(ED), Geosci. Model Dev., 8, 3593–3619, https://doi.org/10.5194/gmd-8-3593-2015, 2015.

Flanagan, D.: 2017 Minerals Yearbook: Copper [Advance Release], Tech. rep., U.S. Geological Survey, https://pubs.usgs.gov/myb/vol1/2017/myb1-2017-copper.pdf, 2021.

Ford, D. J., Blannin, J., Watts, J., Watson, A. J., Landschützer, P., Jersild, A., and Shutler, J. D.: A Comprehensive Analysis of Air-Sea CO2 Flux Uncertainties Constructed From Surface Ocean Data Products, Global Biogeochemical Cycles, 38, e2024GB008188, https://doi.org/10.1029/2024GB008188, 2024.

Ford, D.J., Shutler, J.D., Blanco-Sacristán, J. et al. Enhanced ocean CO2 uptake due to near-surface temperature gradients. Nat. Geosci. 17, 1135–1140 . https://doi.org/10.1038/s41561-024-01570-7, 2024a

Ford, D. J., Shutler, J. D., Ashton, I., Sims, R. P., and Holding, T.: Recalculated (depth and temperature consistent) surface ocean CO_2 atlas (SOCAT) version 2025 (v0-1), https://doi.org/10.5281/ZENODO.15656803, 2025.

Forster, P. M., Smith, C., Walsh, T., Lamb, W. F., Lamboll, R., Cassou, C., Hauser, M., Hausfather, Z., Lee, J.-Y., Palmer, M. D., Von Schuckmann, K., Slangen, A. B. A., Szopa, S., Trewin, B., Yun, J., Gillett, N. P., Jenkins, S., Matthews, H. D., Raghavan, K., Ribes, A., Rogelj, J., Rosen, D., Zhang, X., Allen, M., Aleluia Reis, L., Andrew, R. M., Betts, R. A., Borger, A., Broersma, J. A., Burgess, S. N., Cheng, L., Friedlingstein, P., Domingues, C. M., Gambarini, M., Gasser, T., Gütschow, J., Ishii, M., Kadow, C., Kennedy, J., Killick, R. E., Krummel, P. B., Liné, A., Monselesan, D. P., Morice, C., Mühle, J., Naik, V., Peters, G. P., Pirani, A., Pongratz, J., Minx, J. C., Rigby, M., Rohde, R., Savita, A., Seneviratne, S. I., Thorne, P., Wells, C., Western, L. M., Van Der Werf, G. R., Wijffels, S. E., Masson-Delmotte, V., and Zhai, P.: Indicators of Global Climate Change 2024: annual update of key indicators of the state of the climate system and human influence, Earth Syst. Sci. Data, 17, 2641–2680, https://doi.org/10.5194/essd-17-2641-2025, 2025.

Friedlingstein, P., Houghton, R. A., Marland, G., Hackler, J., Boden, T. A., Conway, T. J., Canadell, J. G., Raupach, M. R., Ciais, P., and Le Quéré, C.: Update on CO2 emissions, Nature Geosci, 3, 811–812, https://doi.org/10.1038/ngeo1022, 2010.

Friedlingstein, P., Andrew, R. M., Rogelj, J., Peters, G. P., Canadell, J. G., Knutti, R., Luderer, G., Raupach, M. R., Schaeffer, M., van Vuuren, D. P., and Le Quéré, C.: Persistent growth of CO2 emissions and implications for reaching climate targets, Nature Geosci, 7, 709–715, https://doi.org/10.1038/ngeo2248, 2014.

Friedlingstein, P., Jones, M. W., O'Sullivan, M., Andrew, R. M., Hauck, J., Peters, G. P., Peters, W., Pongratz, J., Sitch, S., Le Quéré, C., Bakker, D. C. E., Canadell, J. G., Ciais, P., Jackson, R. B., Anthoni, P., Barbero, L., Bastos, A., Bastrikov, V., Becker, M., Bopp, L., Buitenhuis, E., Chandra, N., Chevallier, F., Chini, L. P., Currie, K. I., Feely, R. A., Gehlen, M., Gilfillan, D., Gkritzalis, T., Goll, D. S., Gruber, N., Gutekunst, S., Harris, I., Haverd, V., Houghton, R. A., Hurtt, G., Ilyina, T., Jain, A. K., Joetzjer, E., Kaplan, J. O., Kato, E., Klein Goldewijk, K., Korsbakken, J. I., Landschützer, P., Lauvset, S. K., Lefèvre, N., Lenton, A., Lienert, S., Lombardozzi, D., Marland, G., McGuire, P. C., Melton, J. R., Metzl, N., Munro, D. R., Nabel, J. E. M. S., Nakaoka, S.-I., Neill, C., Omar, A. M., Ono, T., Peregon, A., Pierrot, D., Poulter, B., Rehder, G., Resplandy, L., Robertson, E., Rödenbeck, C., Séférian, R., Schwinger, J., Smith, N., Tans, P. P., Tian, H., Tilbrook, B., Tubiello, F. N., van der Werf, G. R., Wiltshire, A. J., and Zaehle, S.: Global Carbon Budget 2019, Earth Syst. Sci. Data, 11, 1783–1838, https://doi.org/10.5194/essd-11-1783-2019, 2019.

Friedlingstein, P., O'Sullivan, M., Jones, M. W., Andrew, R. M., Hauck, J., Olsen, A., Peters, G. P., Peters, W., Pongratz, J., Sitch, S., Le Quéré, C., Canadell, J. G., Ciais, P., Jackson, R. B., Alin, S., Aragão, L. E. O. C., Arneth, A., Arora, V., Bates, N. R., Becker, M., Benoit-Cattin, A., Bittig, H. C., Bopp, L., Bultan, S., Chandra, N., Chevallier, F., Chini, L. P., Evans, W., Florentie, L., Forster, P. M., Gasser, T., Gehlen, M., Gilfillan, D., Gkritzalis, T., Gregor, L., Gruber, N., Harris, I., Hartung, K., Haverd, V., Houghton, R. A., Ilyina, T., Jain, A. K., Joetzjer, E., Kadono, K., Kato, E., Kitidis, V., Korsbakken, J. I., Landschützer, P., Lefèvre, N., Lenton, A., Lienert, S., Liu, Z., Lombardozzi, D., Marland, G., Metzl, N., Munro, D. R., Nabel, J. E. M. S., Nakaoka, S.-I., Niwa, Y., O'Brien, K., Ono, T., Palmer, P. I., Pierrot, D., Poulter, B., Resplandy, L., Robertson, E., Rödenbeck, C., Schwinger, J., Séférian, R., Skjelvan, I., Smith, A. J. P., Sutton, A. J., Tanhua, T., Tans, P. P., Tian, H., Tilbrook,

B., van der Werf, G., Vuichard, N., Walker, A. P., Wanninkhof, R., Watson, A. J., Willis, D., Wiltshire, A. J., Yuan, W., Yue, X., and Zaehle, S.: Global Carbon Budget 2020, Earth Syst. Sci. Data, 12, 3269–3340, https://doi.org/10.5194/essd-12-3269-2020, 2020.

Friedlingstein, P., Jones, M. W., O'Sullivan, M., Andrew, R. M., Bakker, D. C. E., Hauck, J., Le Quéré, C., Peters, G. P., Peters, W., Pongratz, J., Sitch, S., Canadell, J. G., Ciais, P., Jackson, R. B., Alin, S. R., Anthoni, P., Bates, N. R., Becker, M., Bellouin, N., Bopp, L., Chau, T. T. T., Chevallier, F., Chini, L. P., Cronin, M., Currie, K. I., Decharme, B., Djeutchouang, L. M., Dou, X., Evans, W., Feely, R. A., Feng, L., Gasser, T., Gilfillan, D., Gkritzalis, T., Grassi, G., Gregor, L., Gruber, N., Gürses, Ö., Harris, I., Houghton, R. A., Hurtt, G. C., Iida, Y., Ilyina, T., Luijkx, I. T., Jain, A., Jones, S. D., Kato, E., Kennedy, D., Klein Goldewijk, K., Knauer, J., Korsbakken, J. I., Körtzinger, A., Landschützer, P., Lauvset, S. K., Lefèvre, N., Lienert, S., Liu, J., Marland, G., McGuire, P. C., Melton, J. R., Munro, D. R., Nabel, J. E. M. S., Nakaoka, S.-I., Niwa, Y., Ono, T., Pierrot, D., Poulter, B., Rehder, G., Resplandy, L., Robertson, E., Rödenbeck, C., Rosan, T. M., Schwinger, J., Schwingshackl, C., Séférian, R., Sutton, A. J., Sweeney, C., Tanhua, T., Tans, P. P., Tian, H., Tilbrook, B., Tubiello, F., van der Werf, G. R., Vuichard, N., Wada, C., Wanninkhof, R., Watson, A. J., Willis, D., Wiltshire, A. J., Yuan, W., Yue, C., Yue, X., Zaehle, S., and Zeng, J.: Global Carbon Budget 2021, Earth Syst. Sci. Data, 14, 1917–2005, https://doi.org/10.5194/essd-14-1917-2022, 2022a.

Friedlingstein, P., O'Sullivan, M., Jones, M. W., Andrew, R. M., Gregor, L., Hauck, J., Le Quéré, C., Luijkx, I. T., Olsen, A., Peters, G. P., Peters, W., Pongratz, J., Schwingshackl, C., Sitch, S., Canadell, J. G., Ciais, P., Jackson, R. B., Alin, S. R., Alkama, R., Arneth, A., Arora, V. K., Bates, N. R., Becker, M., Bellouin, N., Bittig, H. C., Bopp, L., Chevallier, F., Chini, L. P., Cronin, M., Evans, W., Falk, S., Feely, R. A., Gasser, T., Gehlen, M., Gkritzalis, T., Gloege, L., Grassi, G., Gruber, N., Gürses, Ö., Harris, I., Hefner, M., Houghton, R. A., Hurtt, G. C., Iida, Y., Ilyina, T., Jain, A. K., Jersild, A., Kadono, K., Kato, E., Kennedy, D., Klein Goldewijk, K., Knauer, J., Korsbakken, J. I., Landschützer, P., Lefèvre, N., Lindsay, K., Liu, J., Liu, Z., Marland, G., Mayot, N., McGrath, M. J., Metzl, N., Monacci, N. M., Munro, D. R., Nakaoka, S., Niwa, Y., O'Brien, K., Ono, T., Palmer, P. I., Pan, N., Pierrot, D., Pocock, K., Poulter, B., Resplandy, L., Robertson, E., Rödenbeck, C., Rodriguez, C., Rosan, T. M., Schwinger, J., Séférian, R., Shutler, J. D., Skjelvan, I., Steinhoff, T., Sun, Q., Sutton, A. J., Sweeney, C., Takao, S., Tanhua, T., Tans, P. P., Tian, X., Tian, H., Tilbrook, B., Tsujino, H., Tubiello, F., van der Werf, G. R., Walker, A. P., Wanninkhof, R., Whitehead, C., Willstrand Wranne, A., Wright, R., Yuan, W., Yue, C., Yue, X., Zaehle, S., Zeng, J., and Zheng, B.: Global Carbon Budget 2022, Earth Syst. Sci. Data, 14, 4811–4900, https://doi.org/10.5194/essd-14-4811-2022, 2022b.

Friedlingstein, P., O'Sullivan, M., Jones, M. W., Andrew, R. M., Bakker, D. C. E., Hauck, J., Landschützer, P., Le Quéré, C., Luijkx, I. T., Peters, G. P., Peters, W., Pongratz, J., Schwingshackl, C., Sitch, S., Canadell, J. G., Ciais, P., Jackson, R. B., Alin, S. R., Anthoni, P., Barbero, L., Bates, N. R., Becker, M., Bellouin, N., Decharme, B., Bopp, L., Brasika, I. B. M., Cadule, P., Chamberlain, M. A., Chandra, N., Chau, T.-T.-T., Chevallier, F., Chini, L. P., Cronin, M., Dou, X., Enyo, K., Evans, W., Falk, S., Feely, R. A., Feng, L., Ford, D. J., Gasser, T., Ghattas, J., Gkritzalis, T., Grassi, G., Gregor, L., Gruber, N., Gürses, Ö., Harris, I., Hefner, M., Heinke, J., Houghton, R. A., Hurtt, G. C., Iida, Y., Ilyina, T., Jacobson, A. R., Jain, A. K., Jarníková, T., Jersild, A., Jiang, F., Jin, Z., Joos, F., Kato, E., Keeling, R. F., Kennedy, D., Klein Goldewijk, K., Knauer, J., Korsbakken, J. I., Körtzinger, A., Lan, X., Lefèvre, N., Li, H., Liu, J., Liu, Z., Ma, L., Marland, G., Mayot, N., McGuire, P. C., McKinley, G. A., Meyer, G., Morgan, E. J., Munro, D. R., Nakaoka, S., Niwa, Y., O'Brien, K. M., Olsen, A., Omar, A. M., Ono, T., Paulsen, M., Pierrot, D., Pocock, K., Poulter, B., Powis, C. M., Rehder, G., Resplandy, L., Robertson, E., Rödenbeck, C., Rosan, T. M., Schwinger, J., Séférian, R., Smallman, T. L., Smith, S. M., Sospedra-Alfonso, R., Sun, Q., Sutton, A. J., Sweeney, C., Takao, S., Tans, P. P., Tian, H., Tilbrook, B., Tsujino, H., Tubiello, F., van der Werf, G. R., van Ooijen, E., Wanninkhof, R., Watanabe, M., Wimart-Rousseau, C., Yang, D., Yang, X., Yuan, W., Yue, X., Zaehle, S., Zeng, J., and Zheng, B.: Global Carbon Budget 2023, Earth Syst. Sci. Data, 15, 5301–5369, https://doi.org/10.5194/essd-15-5301-2023, 2023.

Friedlingstein, P., O'Sullivan, M., Jones, M. W., Andrew, R. M., Hauck, J., Landschützer, P., Le Quéré, C., Li, H., Luijkx, I. T., Olsen, A., Peters, G. P., Peters, W., Pongratz, J., Schwingshackl, C., Sitch, S., Canadell, J. G., Ciais, P., Jackson, R. B., Alin, S. R., Arneth, A., Arora, V., Bates, N. R., Becker, M., Bellouin, N., Berghoff, C. F., Bittig, H. C., Bopp, L., Cadule, P., Campbell, K., Chamberlain, M. A., Chandra, N., Chevallier, F., Chini, L. P., Colligan, T., Decayeux, J., Djeutchouang, L. M., Dou, X., Duran Rojas, C., Enyo, K., Evans, W., Fay, A. R., Feely, R. A., Ford, D. J., Foster, A., Gasser, T., Gehlen, M., Gkritzalis, T., Grassi, G., Gregor, L., Gruber, N., Gürses, Ö., Harris, I., Hefner, M., Heinke, J., Hurtt, G. C., Iida, Y., Ilyina, T., Jacobson, A. R., Jain, A. K., Jarníková, T., Jersild, A., Jiang, F., Jin, Z., Kato, E., Keeling, R. F., Klein Goldewijk, K., Knauer, J., Korsbakken, J. I., Lan, X., Lauvset, S. K., Lefèvre, N., Liu, Z., Liu, J., Ma, L., Maksyutov, S., Marland, G., Mayot, N., McGuire, P. C., Metzl, N., Monacci, N. M., Morgan, E. J., Nakaoka, S.-I., Neill, C., Niwa, Y., Nützel, T., Olivier, L., Ono, T., Palmer, P. I., Pierrot, D., Qin, Z., Resplandy, L., Roobaert, A., Rosan, T. M., Rödenbeck, C., Schwinger, J., Smallman, T. L., Smith, S. M., Sospedra-Alfonso, R., Steinhoff, T., Sun, Q., Sutton, A. J., Séférian, R., Takao, S., Tatebe, H., Tian,

H., Tilbrook, B., Torres, O., Tourigny, E., Tsujino, H., Tubiello, F., van der Werf, G., Wanninkhof, R., Wang, X., Yang, D., Yang, X., Yu, Z., Yuan, W., Yue, X., Zaehle, S., Zeng, N., and Zeng, J.: Global Carbon Budget 2024, Earth Syst. Sci. Data, 17, 965–1039, https://doi.org/10.5194/essd-17-965-2025, 2025a.

Friedlingstein, P. ,Le Quéré, C., O'Sullivan, M., Hauck, J., Landschützer, P., Luijkx, I.T., Li, H., van der Woude, A., Schwingshackl, C., Pongratz, P., Regnier, P., Andrew, R.M., Bakker, D.C.E., Canadell, J.G., Ciais, P., Gasser, T., Jones, M.W., Lan, X., Morgan, E., Olsen, A., Peters, G.P., Peters, W., Sitch, S., and Tian, H.: Emerging climate impact on carbon sinks in a consolidated carbon budget, Nature, https://doi.org/10.1038/s41586-025-09802-5, 2025b.

Friedlingstein, P., O'Sullivan, M., Jones, M. W., Andrew, R. M., Bakker, D. C. E., Hauck, J., Landschützer, P., Le Quéré, C., Li, H., Luijkx, I. T., Peters, G. P., Peters, W., Pongratz, J., Schwingshackl, C., Sitch, S., Canadell, J. G., Ciais, P., Aas, K., Alin, S. R., Anthoni, P., Barbero, L., Bates, N. R., Bellouin, N., Benoit-Cattin, A., Berghoff, C. F., Bernardello, R., Bopp, L., Brasika, I. B. M., Chamberlain, M. A., Chandra, N., Chevallier, F., Chini, L. P., Collier, N. O., Colligan, T. H., Cronin, M., Djeutchouang, L. M., Dou, X., Enright, M. P., Enyo, K., Erb, M., Evans, W., Feely, R. A., Feng, L., Ford, D. J., Foster, A., Fransner, F., Gasser, T., Gehlen, M., Gkritzalis, T., Goncalves De Souza, J., Grassi, G., Gregor, L., Gruber, N., Guenet, B., Gürses, Ö., Harrington, K., Harris, I., Heinke, J., Hurtt, G. C., Iida, Y., Ilyina, T., Ito, A., Jacobson, A. R., Jain, A. K., Jarníková, T., Jersild, A., Jiang, F., Jones, S. D., Kato, E., Keeling, R. F., Klein Goldewijk, K., Knauer, J., Kong, Y., Korsbakken, J. I., Koven, C., Kunimitsu, T., Lan, X., Liu, J., Liu, Z., Liu, Z., Lo Monaco, C., Ma, L., Marland, G., McGuire, P. C., McKinley, G. A., Melton, J. R., Monacci, N., Monier, E., Morgan, E. J., Munro, D. R., Müller, J. D., Nakaoka, S., Nayagam, L. R., Niwa, Y., Nutzel, T., Olsen, A., Omar, A. M., Pan, N., Pandey, S., Pierrot, D., Qin, Z., Regnier, P., Rehder, G., Resplandy, L., Roobaert, A., Rosan, T. M., Rödenbeck, C., Schwinger, J., Skjelvan, I., Smallman, T. L., Spada, V., Sreeush, M. G., Sun, Q., Sutton, A. J., Sweeney, C., Swingedouw, D., Séférian, R., Takao, S., Tatebe, H., Tian, H., Tian, X., Tilbrook, B., Tsujino, H., Tubiello, F., van Ooijen, E., van der Werf, G. R., van de Velde, S. J., Walker, A. P., Wanninkhof, R., Yang, X., Yuan, W., Yue, X., and Zeng, J..: Supplemental data of the Global Carbon Budget 2025, ICOS-ERIC Carbon Portal, https://doi.org/10.18160/GCP-2025, 2025c.

Fu, W., Moore, J. K., Primeau, F., Collier, N., Ogunro, O. O., Hoffman, F. M., and Randerson, J. T.: Evaluation of Ocean Biogeochemistry and Carbon Cycling in CMIP Earth System Models With the International Ocean Model Benchmarking (IOMB) Software System, JGR Oceans, 127, e2022JC018965, https://doi.org/10.1029/2022JC018965, 2022.

Ganzenmüller, R., Bultan, S., Winkler, K., Fuchs, R., Zabel, F., and Pongratz, J.: Land-use change emissions based on high-resolution activity data substantially lower than previously estimated, Environ. Res. Lett., 17, 064050, https://doi.org/10.1088/1748-9326/ac70d8, 2022.

Gasser, T., Crepin, L., Quilcaille, Y., Houghton, R. A., Ciais, P., and Obersteiner, M.: Historical CO2 emissions from land use and land cover change and their uncertainty, Biogeosciences, 17, 4075–4101, https://doi.org/10.5194/bg-17-4075-2020, 2020.

Gaubert, B., Stephens, B. B., Basu, S., Chevallier, F., Deng, F., Kort, E. A., Patra, P. K., Peters, W., Rödenbeck, C., Saeki, T., Schimel, D., Van der Laan-Luijkx, I., Wofsy, S., and Yin, Y.: Global atmospheric CO2 inverse models converging on neutral tropical land exchange, but disagreeing on fossil fuel and atmospheric growth rate, Biogeosciences, 16, 117–134, https://doi.org/10.5194/bg-16-117-2019, 2019.

Gauthier, C. B., Melton, J. R., Meyer, G., Raj Deepak, S. N., and Sonnentag, O.: Parameter Optimization for Global Soil Carbon Simulations: Not a Simple Problem, J Adv Model Earth Syst, 17, e2024MS004577, https://doi.org/10.1029/2024MS004577, 2025.

GCP: The Global Carbon Budget 2007, available at: http://www. globalcarbonproject.org/carbonbudget/archive.htm, last access: 23 October 2025, 2007.

Giglio, L., Schroeder, W., and Justice, C. O.: The collection 6 MODIS active fire detection algorithm and fire products, Remote Sensing of Environment, 178, 31–41, https://doi.org/10.1016/j.rse.2016.02.054, 2016.

Gitz V, Ciais P. Amplifying effects of land-use change on future atmospheric CO2 levels. Global Biogeochemical Cycles. https://doi.org/10.1029/2002GB001963, 2003.

Gloege, L., McKinley, G. A., Landschützer, P., Fay, A. R., Frölicher, T. L., Fyfe, J. C., Ilyina, T., Jones, S., Lovenduski, N. S., Rodgers, K. B., Schlunegger, S., and Takano, Y.: Quantifying Errors in Observationally Based

Estimates of Ocean Carbon Sink Variability, Global Biogeochem. Cy., 35, e2020GB006788, https://doi.org/10.1029/2020GB006788, 2021.

Gloege, L., Yan, M., Zheng, T., and McKinley, G. A.: Improved Quantification of Ocean Carbon Uptake by Using Machine Learning to Merge Global Models and pCO2 Data, J. Adv. Model. Earth Syst., 14, e2021MS002620, https://doi.org/10.1029/2021MS002620, 2022.

Golar, G., Malik, A., Muis, H., Herman, A., Nurudin, N., and Lukman, L.: The social-economic impact of COVID-19 pandemic: implications for potential forest degradation, Heliyon, 6, e05354, https://doi.org/10.1016/j.heliyon.2020.e05354, 2020.

Goris, N., Tjiputra, J. F., Olsen, A., Schwinger, J., Lauvset, S. K., and Jeansson, E.: Constraining Projection-Based Estimates of the Future North Atlantic Carbon Uptake, J. Clim., 31, 3959–3978, https://doi.org/10.1175/JCLI-D-17-0564.1, 2018.

Grassi, G., House, J., Kurz, W. A., Cescatti, A., Houghton, R. A., Peters, G. P., Sanz, M. J., Viñas, R. A., Alkama, R., Arneth, A., Bondeau, A., Dentener, F., Fader, M., Federici, S., Friedlingstein, P., Jain, A. K., Kato, E., Koven, C. D., Lee, D., Nabel, J. E. M. S., Nassikas, A. A., Perugini, L., Rossi, S., Sitch, S., Viovy, N., Wiltshire, A., and Zaehle, S.: Reconciling global-model estimates and country reporting of anthropogenic forest CO2 sinks, Nature Clim Change, 8, 914–920, https://doi.org/10.1038/s41558-018-0283-x, 2018.

Grassi, G., Stehfest, E., Rogelj, J., van Vuuren, D., Cescatti, A., House, J., Nabuurs, G.-J., Rossi, S., Alkama, R., Viñas, R. A., Calvin, K., Ceccherini, G., Federici, S., Fujimori, S., Gusti, M., Hasegawa, T., Havlik, P., Humpenöder, F., Korosuo, A., Perugini, L., Tubiello, F. N., and Popp, A.: Critical adjustment of land mitigation pathways for assessing countries' climate progress, Nat. Clim. Chang., 11, 425–434, https://doi.org/10.1038/s41558-021-01033-6, 2021.

Grassi, G., Schwingshackl, C., Gasser, T., Houghton, R. A., Sitch, S., Canadell, J. G., Cescatti, A., Ciais, P., Federici, S., Friedlingstein, P., Kurz, W. A., Sanz Sanchez, M. J., Abad Viñas, R., Alkama, R., Bultan, S., Ceccherini, G., Falk, S., Kato, E., Kennedy, D., Knauer, J., Korosuo, A., Melo, J., McGrath, M. J., Nabel, J. E. M. S., Poulter, B., Romanovskaya, A. A., Rossi, S., Tian, H., Walker, A. P., Yuan, W., Yue, X., and Pongratz, J.: Harmonising the land-use flux estimates of global models and national inventories for 2000–2020, Earth Syst. Sci. Data, 15, 1093–1114, https://doi.org/10.5194/essd-15-1093-2023, 2023.

Grassi, G., Peters, G. P., Canadell, J. G., Cescatti, A., Federici, S., Gidden, M. J., Harris, N., Herold, M., Krug, T., O'Sullivan, M., Pongratz, J., Sanz, M. J., Schwingshackl, C., and Van Vuuren, D.: Improving land-use emission estimates under the Paris Agreement, Nat Sustain, 8, 579–581, https://doi.org/10.1038/s41893-025-01565-1, 2025.

Gregor, L., Lebehot, A. D., Kok, S., and Scheel Monteiro, P. M.: A comparative assessment of the uncertainties of global surface ocean CO2 estimates using a machine-learning ensemble (CSIR-ML6 version 2019a)–have we hit the wall?. Geoscientific Model Development, 12(12), 5113-5136, https://doi.org/10.5194/gmd-12-5113-2019, 2019.

Gregor, L., Shutler, J., and Gruber, N.: High-resolution variability of the ocean carbon sink. Global Biogeochemical Cycles, 38(8), e2024GB008127, https://doi.org/10.1029/2024GB008127, 2024.

Gruber, N., Bakker, D. C. E., DeVries, T., Gregor, L., Hauck, J., Landschützer, P., McKinley, G. A., and Müller, J. D.: Trends and variability in the ocean carbon sink, Nat. Rev. Earth Environ., 4, 119–134, https://doi.org/10.1038/s43017-022-00381-x, 2023.

Gruber, N., Clement, D., Carter, B. R., Feely, R. A., van Heuven, S., Hoppema, M., Ishii, M., Key, R. M., Kozyr, A., Lauvset, S. K., Lo Monaco, C., Mathis, J. T., Murata, A., Olsen, A., Perez, F. F., Sabine, C. L., Tanhua, T., and Wanninkhof, R.: The oceanic sink for anthropogenic CO2 from 1994 to 2007, 363, 1193–1199, https://doi.org/10.1126/science.aau5153, 2019.

Guan, D., Liu, Z., Geng, Y., Lindner, S., and Hubacek, K.: The gigatonne gap in China's carbon dioxide inventories, Nature Clim Change, 2, 672–675, https://doi.org/10.1038/nclimate1560, 2012.

Gulev, S. K., Thorne, P. W., Ahn, J., Dentener, F. J., Domingues, C. M., Gerland, S., Gong, D. S., Kaufman, S., Nnamchi, H. C., Quaas, J., Rivera, J. A., Sathyendranath, S., Smith, S. L., Trewin, B., von Shuckmann, K., and Vose, R. S.: Changing State of the Climate System. In: Climate Change 2021: The Physical Science Basis. Contribution of Working Group I to the Sixth Assessment Report of the Intergovernmental Panel on Climate

Change [Masson-Delmotte, V., Zhai, P., Pirani, A., Connors, S. L., Péan, C., Berger, S., Caud, N., Chen, Y., Goldfarb, L., Gomis, M. I., Huang, M., Leitzell, K., Lonnoy, E., Matthews, J.B.R., Maycock, T.K., Waterfield, T., Yelekçi, O., Yu, R. and Zhou, B. (eds.)]. Cambridge University Press, Cambridge, United Kingdom and New York, NY, USA, pp. 287–422, https://doi.org/10.1017/9781009157896.004, 2021.

Guo, R., Wang, J., Bing, L., Tong, D., Ciais, P., Davis, S. J., Andrew, R. M., Xi, F., and Liu, Z.: Global CO2 uptake by cement from 1930 to 2019, 13, 1791–1805, https://doi.org/10.5194/essd-13-1791-2021, 2021.

Gürses, Ö., Oziel, L., Karakuş, O., Sidorenko, D., Völker, C., Ye, Y., Zeising, M., Butzin, M., and Hauck, J.: Ocean biogeochemistry in the coupled ocean–sea ice–biogeochemistry model FESOM2.1–REcoM3, Geosci. Model Dev., 16, 4883–4936, https://doi.org/10.5194/gmd-16-4883-2023, 2023.

Gütschow, J., Jeffery, M. L., Gieseke, R., Gebel, R., Stevens, D., Krapp, M., and Rocha, M.: The PRIMAP-hist national historical emissions time series, 8, 571–603, https://doi.org/10.5194/essd-8-571-2016, 2016.

Gütschow, J., Busch, D. and Pflüger, M.: The PRIMAP-hist national historical emissions time series (1750-2023) v2.6, Zenodo [Data set], https://doi.org/10.5281/zenodo.13752654, 2023.

Hall, B. D., Crotwell, A. M., Kitzis, D. R., Mefford, T., Miller, B. R., Schibig, M. F., and Tans, P. P.: Revision of the World Meteorological Organization Global Atmosphere Watch (WMO/GAW) CO2 calibration scale, 14, 3015–3032, https://doi.org/10.5194/amt-14-3015-2021, 2021.

Hansis, E., Davis, S. J., and Pongratz, J.: Relevance of methodological choices for accounting of land use change carbon fluxes, Global Biogeochem. Cycles, 29, 1230–1246, https://doi.org/10.1002/2014GB004997, 2015.

Hauck, J., Nissen, C., Landschützer, P., Rödenbeck, C., Bushinsky, S., and Olsen, A.: Sparse observations induce large biases in estimates of the global ocean CO2 sink: an ocean model subsampling experiment, Philos. Trans. R. Soc. Math. Phys. Eng. Sci., 381, 20220063, https://doi.org/10.1098/rsta.2022.0063, 2023a.

Hauck, J., Gregor, L., Nissen, C., Patara, L., Hague, M., Mongwe, P., Bushinsky, S., Doney, S. C., Gruber, N., Le Quéré, C., Manizza, M., Mazloff, M., Monteiro, P. M. S., and Terhaar, J.: The Southern Ocean Carbon Cycle 1985–2018: Mean, Seasonal Cycle, Trends, and Storage. Global Biogeochemical Cycles, 37(11), e2023GB007848, https://doi.org/10.1029/2023GB007848, 2023b.

Hauck, J., Zeising, M., Le Quéré, C., Gruber, N., Bakker, D. C. E., Bopp, L., Chau, T. T. T., Gürses, Ö., Ilyina, T., Landschützer, P., Lenton, A., Resplandy, L., Rödenbeck, C., Schwinger, J., and Séférian, R.: Consistency and Challenges in the Ocean Carbon Sink Estimate for the Global Carbon Budget, Front. Mar. Sci., 7, 571720, https://doi.org/10.3389/fmars.2020.571720, 2020.

Haverd, V., Smith, B., Nieradzik, L., Briggs, P. R., Woodgate, W., Trudinger, C. M., Canadell, J. G., and Cuntz, M.: A new version of the CABLE land surface model (Subversion revision r4601) incorporating land use and land cover change, woody vegetation demography, and a novel optimisation-based approach to plant coordination of photosynthesis, Geosci. Model Dev., 11, 2995–3026, https://doi.org/10.5194/gmd-11-2995-2018, 2018.

Heinke, J., Rolinski, S., and Müller, C.: Modelling the role of livestock grazing in C and N cycling in grasslands with LPJmL5.0-grazing, Geosci. Model Dev., 16, 2455–2475, https://doi.org/10.5194/gmd-16-2455-2023, 2023.

Hickler, T., Smith, B., Prentice, I. C., Mjöfors, K., Miller, P., Arneth, A., and Sykes, M. T.: CO2 fertilization in temperate FACE experiments not representative of boreal and tropical forests, Glob. Change Biol., 14, 1531–1542, https://doi.org/10.1111/j.1365-2486.2008.01598.x, 2008.

Hoesly, R. M., Smith, S. J., Feng, L., Klimont, Z., Janssens-Maenhout, G., Pitkanen, T., Seibert, J. J., Vu, L., Andres, R. J., Bolt, R. M., Bond, T. C., Dawidowski, L., Kholod, N., Kurokawa, J., Li, M., Liu, L., Lu, Z., Moura, M. C. P., O'Rourke, P. R., and Zhang, Q.: Historical (1750–2014) anthropogenic emissions of reactive gases and aerosols from the Community Emissions Data System (CEDS), Geosci. Model Dev., 11, 369–408, https://doi.org/10.5194/gmd-11-369-2018, 2018.

Hoesly, R., Smith, S. J., Prime, N., Ahsan, H., Suchyta, H., O'Rourke, P., Crippa, M., Klimont, Z., Guizzardi, D., Behrendt, J., Feng, L., Harkins, C., McDonald, B., Mott, A., McDuffie, A., Nicholson, M. and Wang, S.: CEDS v_2024_07_08 Release Emission Data, Zenodo [Data set], https://doi.org/10.5281/zenodo.12803196, 2024.

Hong, C., Burney, J. A., Pongratz, J., Nabel, J. E. M. S., Mueller, N. D., Jackson, R. B., and Davis, S. J.: Global and regional drivers of land-use emissions in 1961–2017, Nature, 589, 554–561, https://doi.org/10.1038/s41586-020-03138-y, 2021.

Holding, T., Ashton, I. G., Shutler, J. D., Land, P. E., Nightingale, P. D., Rees, A. P., Brown, I., Piolle, J.-F., Kock, A., Bange, H. W., Woolf, D. K., Goddijn-Murphy, L., Pereira, R., Paul, F., Girard-Ardhuin, F., Chapron, B., Rehder, G., Ardhuin, F., and Donlon, C. J.: The FluxEngine air–sea gas flux toolbox: simplified interface and extensions for in situ analyses and multiple sparingly soluble gases, Ocean Sci., 15, 1707–1728, https://doi.org/10.5194/os-15-1707-2019, 2019.

Hoppe, J., Hinder, B., Rafaty, R., Patt, A., and Grubb, M.: Three Decades of Climate Mitigation Policy: What Has It Delivered?, Annu. Rev. Environ. Resour., 48, 615–650, https://doi.org/10.1146/annurev-environ-112321-103821, 2023.

Houghton, R. A. and Castanho, A.: Annual emissions of carbon from land use, land-use change, and forestry from 1850 to 2020, Earth Syst. Sci. Data, 15, 2025–2054, https://doi.org/10.5194/essd-15-2025-2023, 2023.

Houghton, R. A., House, J. I., Pongratz, J., van der Werf, G. R., DeFries, R. S., Hansen, M. C., Le Quéré, C., and Ramankutty, N.: Carbon emissions from land use and land-cover change, Biogeosciences, 9, 5125–5142, https://doi.org/10.5194/bg-9-5125-2012, 2012.

Houghton, R. A. and Nassikas, A. A.: Global and regional fluxes of carbon from land use and land cover change 1850-2015: Carbon Emissions From Land Use, Global Biogeochem. Cycles, 31, 456–472, https://doi.org/10.1002/2016GB005546, 2017.

Huang, B., Thorne, P. W., Banzon, V. F., Boyer, T., Chepurin, G., Lawrimore, J. H., Menne, M. J., Smith, T. M., Vose, R. S., and Zhang, H.-M.: NOAA Extended Reconstructed Sea Surface Temperature (ERSST), Version 5, https://doi.org/10.7289/V5T72FNM, 2017.

Hubau, W., Lewis, S.L., Phillips, O.L., Affum-Baffoe, K., Beeckman, H., Cuní-Sanchez, A., Daniels, A.K., Ewango, C.E.N., Fauset, S., Mukinzi, J.M., Sheil, D., Sonké, B., Sullivan, M.J.P., Sunderland, T.C.H., Taedoumg, H., Thomas, S.C., White, L.J.T., Abernethy, K.A., Adu-Bredu, S., Amani, C.A., Baker, T.R., Banin, L.F., Baya, F., Begne, S.K., Bennett, A.C., Benedet, F., Bitariho, R., Bocko, Y.E., Boeckx, P., Boundja, P., Brienen, R.J.W., Brncic, T., Chezeaux, E., Chuyong, G.B., Clark, C.J., Collins, M., Comiskey, J.A., Coomes, D.A., Dargie, G.C., de Haulleville, T., Kamdem, M.N.D., Doucet, J.-L., Esquivel-Muelbert, A., Feldpausch, T.R., Fofanah, A., Foli, E.G., Gilpin, M., Gloor, E., Gonmadje, C., Gourlet-Fleury, S., Hall, J.S., Hamilton, A.C., Harris, D.J., Hart, T.B., Hockemba, M.B.N., Hladik, A., Ifo, S.A., Jeffery, K.J., Jucker, T., Yakusu, E.K., Kearsley, E., Kenfack, D., Koch, A., Leal, M.E., Levesley, A., Lindsell, J.A., Lisingo, J., Lopez-Gonzalez, G., Lovett, J.C., Makana, J.-R., Malhi, Y., Marshall, A.R., Martin, J., Martin, E.H., Mbayu, F.M., Medjibe, V.P., Mihindou, V., Mitchard, E.T.A., Moore, S., Munishi, P.K.T., Bengone, N.N., Ojo, L., Ondo, F.E., Peh, K.S.-H., Pickavance, G.C., Poulsen, A.D., Poulsen, J.R., Qie, L., Reitsma, J., Rovero, F., Swaine, M.D., Talbot, J., Taplin, J., Taylor, D.M., Thomas, D.W., Toirambe, B., Mukendi, J.T., Tuagben, D., Umunay, P.M., van der Heijden, G.M.F., Verbeeck, H., Vleminckx, J., Willcock, S., Wöll, H., Woods, J.T., Zemagho, L.: Asynchronous carbon sink saturation in African and Amazonian tropical forests, Nature, 579, 80–87, https://doi.org/10.1038/s41586-020-2035-0, 2020.

Humphrey, V., Zscheischler, J., Ciais, P., Gudmundsson, L., Sitch, S., and Seneviratne, S. I.: Sensitivity of atmospheric CO2 growth rate to observed changes in terrestrial water storage, Nature, 560, 628–631, https://doi.org/10.1038/s41586-018-0424-4, 2018.

Humphrey, V., Berg, A., Ciais, P., Gentine, P., Jung, M., Reichstein, M., Seneviratne, S. I., and Frankenberg, C.: Soil moisture–atmosphere feedback dominates land carbon uptake variability, Nature, 592, 65–69, https://doi.org/10.1038/s41586-021-03325-5, 2021.

Huntzinger, D. N., Michalak, A. M., Schwalm, C., Ciais, P., King, A. W., Fang, Y., Schaefer, K., Wei, Y., Cook, R. B., Fisher, J. B., Hayes, D., Huang, M., Ito, A., Jain, A. K., Lei, H., Lu, C., Maignan, F., Mao, J., Parazoo, N., Peng, S., Poulter, B., Ricciuto, D., Shi, X., Tian, H., Wang, W., Zeng, N., and Zhao, F.: Uncertainty in the response of terrestrial carbon sink to environmental drivers undermines carbon-climate feedback predictions, Sci Rep, 7, 4765, https://doi.org/10.1038/s41598-017-03818-2, 2017.

Iida, Y., Takatani, Y., Kojima, A., and Ishii, M.: Global trends of ocean CO2 sink and ocean acidification: an observation-based reconstruction of surface ocean inorganic carbon variables, J Oceanogr, 77, 323–358, https://doi.org/10.1007/s10872-020-00571-5, 2021.

Ilyina, T., Li, H., Spring, A., Müller, W. A., Bopp, L., Chikamoto, M. O., Danabasoglu, G., Dobrynin, M., Dunne, J., Fransner, F., Friedlingstein, P., Lee, W., Lovenduski, N. S., Merryfield, W. j., Mignot, J., Park, J. y., Séférian, R., Sospedra-Alfonso, R., Watanabe, M., and Yeager, S.: Predictable Variations of the Carbon Sinks and Atmospheric CO2 Growth in a Multi-Model Framework, Geophys. Res. Lett., 48, e2020GL090695, https://doi.org/10.1029/2020GL090695, 2021.

IMF: International Monetary Fund: World Economic Outlook, available at: http://www.imf.org, last access: 23 October 2025, 2025.

Instituto Nacional de Pesquisas Espaciais (INPE): Portal TerraBrasilis, available at: http://terrabrasilis.dpi.inpe.br/en/home-page/, last access: 23 October 2025.

Ito, A.: Disequilibrium of terrestrial ecosystem CO2 budget caused by disturbance-induced emissions and non-CO2 carbon export flows: a global model assessment, Earth Syst. Dynam., 10, 685–709, https://doi.org/10.5194/esd-10-685-2019, 2019.

Ito, A. and Inatomi, M.: Use of a process-based model for assessing the methane budgets of global terrestrial ecosystems and evaluation of uncertainty, 9, 759–773, https://doi.org/10.5194/bg-9-759-2012, 2012.

Jackson, R. B., Canadell, J. G., Le Quéré, C., Andrew, R. M., Korsbakken, J. I., Peters, G. P., and Nakicenovic, N.: Reaching peak emissions, Nature Clim Change, 6, 7–10, https://doi.org/10.1038/nclimate2892, 2016.

Jackson, R. B., Le Quéré, C., Andrew, R. M., Canadell, J. G., Korsbakken, J. I., Liu, Z., Peters, G. P., and Zheng, B.: Global energy growth is outpacing decarbonization, Environ. Res. Lett., 13, 120401, https://doi.org/10.1088/1748-9326/aaf303, 2018.

Jackson, R. B., Friedlingstein, P., Andrew, R. M., Canadell, J. G., Le Quéré, C., and Peters, G. P.: Persistent fossil fuel growth threatens the Paris Agreement and planetary health, Environ. Res. Lett., 14, 121001, https://doi.org/10.1088/1748-9326/ab57b3, 2019.

Jackson, R. B., Friedlingstein, P., Quéré, C. L., Abernethy, S., Andrew, R. M., Canadell, J. G., Ciais, P., Davis, S. J., Deng, Z., Liu, Z., Korsbakken, J. I., and Peters, G. P.: Global fossil carbon emissions rebound near pre-COVID-19 levels, Environ. Res. Lett., 17, 031001, https://doi.org/10.1088/1748-9326/ac55b6, 2022.

Jacobson, A. R., Schuldt, K. N., Tans, P., Andrews, A., Miller, J. B., Oda, T., Basu, S., Mund, J., Weir, B., Ott, L., Aalto, T., Abshire, J. B., Aikin, K., Aoki, S., Apadula, F., Arnold, S., Baier, B., Bartyzel, J., Beyersdorf, A., Biermann, T., Biraud, S. C., Boenisch, H., Brailsford, G., Brand, W. A., Chen, G., Chen, H., Chmura, L., Clark, S., Colomb, A., Commane, R., Conil, S., Couret, C., Cox, A., Cristofanelli, P., Cuevas, E., Curcoll, R., Daube, B., Davis, K. J., De Wekker, S., Della Coletta, J., Delmotte, M., DiGangi, E., DiGangi, J. P., di Sarra, A. G., Dlugokencky, E., Elkins, J. W., Emmenegger, L., Fang, S., Fischer, M. L., Forster, G., Frumau, A., Galkowski, M., Gatti, L. V., Gehrlein, T., Gerbig, C., Gheusi, F., Gloor, E., Gomez-Trueba, V., Goto, D., Griffis, T., Hammer, S., Hanson, C., Haszpra, L., Hatakka, J., Heimann, M., Heliasz, M., Hensen, A., Hermansen, O., Hintsa, E., Holst, J., Ivakhov, V., Jaffe, D. A., Jordan, A., Joubert, W., Karion, A., Kawa, S. R., Kazan, V., Keeling, R. F., Keronen, P., Kneuer, T., Kolari, P., Komínková, K., Kort, E., Kozlova, E., Krummel, P., Kubistin, D., Labuschagne, C., Lam, D. H. Y., Lan, X., Langenfelds, R. L., Laurent, O., Laurila, T., Lauvaux, T., Lavric, J., Law, B. E., Lee, J., Lee, O. S. M., Lehner, I., Lehtinen, K., Leppert, R., Leskinen, A., Leuenberger, M., Levin, I., Levula, J., Lin, J., Lindauer, M., Loh, Z., Lopez, M., Luijkx, I. T., Lunder, C. R., Machida, T., Mammarella, I., Manca, G., Manning, A., Manning, A., Marek, M. V., Martin, M. Y., Matsueda, H., McKain, K., Meijer, H., Meinhardt, F., Merchant, L., Mihalopoulos, N., Miles, N. L., Miller, C. E., Mitchell, L., Mölder, M., Montzka, S., Moore, F., Moossen, H., Morgan, E., Morgui, J.-A., Morimoto, S., Müller-Williams, J., Munger, J. W., Munro, D., Myhre, C. L., Nakaoka, S.-I., Necki, J., Newman, S., Nichol, S., Niwa, Y., Obersteiner, F., O'Doherty, S., Paplawsky, B., Peischl, J., Peltola, O., Piacentino, S., Pichon, J.-M., Pickers, P., Piper, S., Pitt, J., Plass-Dülmer, C., Platt, S. M., Prinzivalli, S., Ramonet, M., Ramos, R., Reyes-Sanchez, E., Richardson, S. J., Riris, H., Rivas, P. P., Ryerson, T., Saito, K., Sargent, M., Sasakawa, M., Scheeren, B., Schuck, T., Schumacher, M., Seifert, T., Sha, M. K., Shepson, P., Shook, M., Sloop, C. D., Smith, P., Stanley, K., Steinbacher, M., Stephens, B., Sweeney, C., Thoning, K., Timas, H., Torn, M., Tørseth, K., Trisolino, P., Turnbull, J., van den Bulk, P., van Dinther, D., Vermeulen, A., Viner, B., Vitkova, G., Walker, S., Watson, A., Wofsy, S. C., Worsey, J., Worthy, D., Young, D., Zaehle, S., Zahn, A., and Zimnoch, M.: CarbonTracker CT2022, NOAA GML [Data set], https://doi.org/10.25925/Z1GJ-3254, 2023a.

Jacobson, A. R., Schuldt, K. N., Tans, P., Andrews, A., Miller, J. B., Oda, T., Basu, S., Mund, J., Weir, B., Ott, L., Aalto, T., Abshire, J. B., Aikin, K., Aoki, S., Apadula, F., Arnold, S., Baier, B., Bartyzel, J., Beyersdorf, A., Biermann, T., Biraud, S. C., Boenisch, H., Brailsford, G., Brand, W. A., Chen, G., Chen, H., Chmura, L., Clark, S.,

Colomb, A., Commane, R., Conil, S., Couret, C., Cox, A., Cristofanelli, P., Cuevas, E., Curcoll, R., Daube, B., Davis, K. J., De Wekker, S., Della Coletta, J., Delmotte, M., DiGangi, E., DiGangi, J. P., di Sarra, A. G., Dlugokencky, E., Elkins, J. W., Emmenegger, L., Fang, S., Fischer, M. L., Forster, G., Frumau, A., Galkowski, M., Gatti, L. V., Gehrlein, T., Gerbig, C., Gheusi, F., Gloor, E., Gomez-Trueba, V., Goto, D., Griffis, T., Hammer, S., Hanson, C., Haszpra, L., Hatakka, J., Heimann, M., Heliasz, M., Hensen, A., Hermansen, O., Hintsa, E., Holst, J., Ivakhov, V., Jaffe, D. A., Jordan, A., Joubert, W., Karion, A., Kawa, S. R., Kazan, V., Keeling, R. F., Keronen, P., Kneuer, T., Kolari, P., Komínková, K., Kort, E., Kozlova, E., Krummel, P., Kubistin, D., Labuschagne, C., Lam, D. H. Y., Lan, X., Langenfelds, R. L., Laurent, O., Laurila, T., Lauvaux, T., Lavric, J., Law, B. E., Lee, J., Lee, O. S. M., Lehner, I., Lehtinen, K., Leppert, R., Leskinen, A., Leuenberger, M., Levin, I., Levula, J., Lin, J., Lindauer, M., Loh, Z., Lopez, M., Luijkx, I. T., Lunder, C. R., Machida, T., Mammarella, I., Manca, G., Manning, A., Manning, A., Marek, M. V., Martin, M. Y., Matsueda, H., McKain, K., Meijer, H., Meinhardt, F., Merchant, L., Mihalopoulos, N., Miles, N. L., Miller, C. E., Mitchell, L., Mölder, M., Montzka, S., Moore, F., Moossen, H., Morgan, E., Morgui, J.-A., Morimoto, S., Müller-Williams, J., Munger, J. W., Munro, D., Myhre, C. L., Nakaoka, S.-I., Necki, J., Newman, S., Nichol, S., Niwa, Y., Obersteiner, F., O'Doherty, S., Paplawsky, B., Peischl, J., Peltola, O., Piacentino, S., Pichon, J.-M., Pickers, P., Piper, S., Pitt, J., Plass-Dülmer, C., Platt, S. M., Prinzivalli, S., Ramonet, M., Ramos, R., Reyes-Sanchez, E., Richardson, S. J., Riris, H., Rivas, P. P., Ryerson, T., Saito, K., Sargent, M., Sasakawa, M., Scheeren, B., Schuck, T., Schumacher, M., Seifert, T., Sha, M. K., Shepson, P., Shook, M., Sloop, C. D., Smith, P., Stanley, K., Steinbacher, M., Stephens, B., Sweeney, C., Thoning, K., Timas, H., Torn, M., Tørseth, K., Trisolino, P., Turnbull, J., van den Bulk, P., van Dinther, D., Vermeulen, A., Viner, B., Vitkova, G., Walker, S., Watson, A., Wofsy, S. C., Worsey, J., Worthy, D., Young, D., Zaehle, S., Zahn, A., and Zimnoch, M.: CarbonTracker CT-NRT.v2023-3, NOAA GML [Data set], https://doi.org/10.25925/7TAF-J322, 2023b.

Jain, A. K., Meiyappan, P., Song, Y., and House, J. I.: CO2 emissions from land-use change affected more by nitrogen cycle, than by the choice of land-cover data, Global Change Biology, 19, 2893–2906, https://doi.org/10.1111/gcb.12207, 2013.

Jain, P., Barber, Q. E., Taylor, S. W., Whitman, E., Castellanos Acuna, D., Boulanger, Y., Chavardès, R. D., Chen, J., Englefield, P., Flannigan, M., Girardin, M. P., Hanes, C. C., Little, J., Morrison, K., Skakun, R. S., Thompson, D. K., Wang, X., Parisien, M.-A.: Drivers and Impacts of the Record-Breaking 2023 Wildfire Season in Canada. Nature Communications, 15(1), p.6764, https://doi.org/10.1038/s41467-024-51154-7, 2024.

Janssens-Maenhout, G., Crippa, M., Guizzardi, D., Muntean, M., Schaaf, E., Dentener, F., Bergamaschi, P., Pagliari, V., Olivier, J. G. J., Peters, J. A. H. W., van Aardenne, J. A., Monni, S., Doering, U., Petrescu, A. M. R., Solazzo, E., and Oreggioni, G. D.: EDGAR v4.3.2 Global Atlas of the three major greenhouse gas emissions for the period 1970–2012, Earth Syst. Sci. Data, 11, 959–1002, https://doi.org/10.5194/essd-11-959-2019, 2019.

Jean-Michel, L., Eric, G., Romain, B.-B., Gilles, G., Angélique, M., Marie, D., Clément, B., Mathieu, H., Olivier, L. G., Charly, R., Tony, C., Charles-Emmanuel, T., Florent, G., Giovanni, R., Mounir, B., Yann, D., and Pierre-Yves, L. T.: The Copernicus Global 1/12° Oceanic and Sea Ice GLORYS12 Reanalysis, Front. Earth Sci., 9, 2021.

Jiang, F., Ju, W., He, W., Wu, M., Wang, H., Wang, J., Jia, M., Feng, S., Zhang, L., and Chen, J. M.: A 10-year global monthly averaged terrestrial net ecosystem exchange dataset inferred from the ACOS GOSAT v9 XCO2 retrievals (GCAS2021), Earth Syst. Sci. Data, 14, 3013–3037, https://doi.org/10.5194/essd-14-3013-2022, 2022.

Jiang, F., Wang, H., Chen, J. M., Ju, W., Tian, X., Feng, S., Li, G., Chen, Z., Zhang, S., Lu, X., Liu, J., Wang, H., Wang, J., He, W., and Wu, M.: Regional CO2 fluxes from 2010 to 2015 inferred from GOSAT XCO2 retrievals using a new version of the Global Carbon Assimilation System, Atmospheric Chem. Phys., 21, 1963–1985, https://doi.org/10.5194/acp-21-1963-2021, 2021.

Jin, Y., Keeling, R. F., Stephens, B. B., Long, M. C., Patra, P. K., Rödenbeck, C., Morgan, E. J., Kort, E. A., and Sweeney, C.: Improved atmospheric constraints on Southern Ocean CO 2 exchange. Proceedings of the National Academy of Sciences, 121(6), e2309333121, https://doi.org/10.1073/pnas.2309333121, 2024.

Jin, Z., Wang, T., Zhang, H., Wang, Y., Ding, J., and Tian, X.: Constraint of satellite CO2 retrieval on the global carbon cycle from a Chinese atmospheric inversion system, Sci. China Earth Sci., 66, 609–618, https://doi.org/10.1007/s11430-022-1036-7, 2023.

Joos, F. and Spahni, R.: Rates of change in natural and anthropogenic radiative forcing over the past 20,000 years, Proceedings of the National Academy of Sciences, 105, 1425–1430, https://doi.org/10.1073/pnas.0707386105, 2008.

Jones, C. D., Hickman, J. E., Rumbold, S. T., Walton, J., Lamboll, R. D., Skeie, R. B., Fiedler, S., Forster, P. M., Rogelj, J., Abe, M., Botzet, M., Calvin, K., Cassou, C., Cole, J. N. S., Davini, P., Deushi, M., Dix, M., Fyfe, J. C., Gillett, N. P., Ilyina, T., Kawamiya, M., Kelley, M., Kharin, S., Koshiro, T., Li, H., Mackallah, C., Müller, W. A., Nabat, P., van Noije, T., Nolan, P., Ohgaito, R., Olivié, D., Oshima, N., Parodi, J., Reerink, T. J., Ren, L., Romanou, A., Séférian, R., Tang, Y., Timmreck, C., Tjiputra, J., Tourigny, E., Tsigaridis, K., Wang, H., Wu, M., Wyser, K., Yang, S., Yang, Y., and Ziehn, T.: The Climate Response to Emissions Reductions Due to COVID-19: Initial Results From CovidMIP, Geophys. Res. Lett., 48, e2020GL091883, https://doi.org/10.1029/2020GL091883, 2021a.

Jones, M. W., Abatzoglou, J. T., Veraverbeke, S., Andela, N., Lasslop, G., Forkel, M., Smith, A. J. P., Burton, C., Betts, R. A., van der Werf, G. R., Sitch, S., Canadell, J. G., Santín, C., Kolden, C., Doerr, S. H., and Le Quéré, C.: Global and Regional Trends and Drivers of Fire Under Climate Change, Rev. Geophys., 60, e2020RG000726, https://doi.org/10.1029/2020RG000726, 2022.

Jones, M. W., Andrew, R. M., Peters, G. P., Janssens-Maenhout, G., De-Gol, A. J., Ciais, P., Patra, P. K., Chevallier, F., and Le Quéré, C.: Gridded fossil CO2 emissions and related O2 combustion consistent with national inventories 1959–2018, Sci Data, 8, 2, https://doi.org/10.1038/s41597-020-00779-6, 2021b.

Jones, M. W., Andrew, R. M., Peters, G. P., Janssens-Maenhout, G., De-Gol, A. J., Dou, X., Liu, Z., Pickers, P., Ciais, P., Patra, P. K., Chevallier, F., and Le Quéré, C.: Gridded fossil CO2 emissions and related O2 combustion consistent with national inventories, Zenodo [Data set], https://doi.org/10.5281/zenodo.17467681, 2025.

Jones, M. W., Kelley, D. I., Burton, C. A., Di Giuseppe, F., Barbosa, M. L. F., Brambleby, E., Hartley, A. J., Lombardi, A., Mataveli, G., McNorton, J. R., Spuler, F. R., Wessel, J. B., Abatzoglou, J. T., Anderson, L. O., Andela, N., Archibald, S., Armenteras, D., Burke, E., Carmenta, R., Chuvieco, E., Clarke, H., Doerr, S. H., Fernandes, P. M., Giglio, L., Hamilton, D. S., Hantson, S., Harris, S., Jain, P., Kolden, C. A., Kurvits, T., Lampe, S., Meier, S., New, S., Parrington, M., Perron, M. M. G., Qu, Y., Ribeiro, N. S., Saharjo, B. H., San-Miguel-Ayanz, J., Shuman, J. K., Tanpipat, V., van der Werf, G. R., Veraverbeke, S., and Xanthopoulos, G.: State of Wildfires 2023–2024, Earth System Science Data, 16, 3601–3685, https://doi.org/10.5194/essd-16-3601-2024, 2024b.

Jones, M.W., Veraverbeke, S., Andela, N., Doerr, S.H., Kolden, C., Mataveli, G., Pettinari, M.L., Le Quéré, C., Rosan, T.M., van der Werf, G.R. and van Wees, D.: Global rise in forest fire emissions linked to climate change in the extratropics. Science, 386(6719), p.eadl5889, 2024c.

Jung, M., Reichstein, M., Schwalm, C. R., Huntingford, C., Sitch, S., Ahlström, A., Arneth, A., Camps-Valls, G., Ciais, P., Friedlingstein, P., Gans, F., Ichii, K., Jain, A. K., Kato, E., Papale, D., Poulter, B., Raduly, B., Rödenbeck, C., Tramontana, G., Viovy, N., Wang, Y.-P., Weber, U., Zaehle, S., and Zeng, N.: Compensatory water effects link yearly global land CO2 sink changes to temperature, Nature, 541, 516–520, https://doi.org/10.1038/nature20780, 2017.

Kaiser, J. W., Heil, A., Andreae, M. O., Benedetti, A., Chubarova, N., Jones, L., Morcrette, J.-J., Razinger, M., Schultz, M. G., Suttie, M., and van der Werf, G. R.: Biomass burning emissions estimated with a global fire assimilation system based on observed fire radiative power, Biogeosciences, 9, 527–554, https://doi.org/10.5194/bg-9-527-2012, 2012.

Kato, E., Kinoshita, T., Ito, A., Kawamiya, M., and Yamagata, Y.: Evaluation of spatially explicit emission scenario of land-use change and biomass burning using a process-based biogeochemical model, J. Land Use Sci., 8, 104–122, https://doi.org/10.1080/1747423X.2011.628705, 2013.

Kawasaki, T., Hasumi, H., and Tanaka, Y.: Role of tide-induced vertical mixing in the deep Pacific Ocean circulation, J. Oceanogr., 77, 173–184, https://doi.org/10.1007/s10872-020-00584-0, 2021.

Ke, P., Ciais, P., Sitch, S., Li, W., Bastos, A., Liu, Z., Xu, Y., Gui, X., Bian, J., Goll, D. S., Xi, Y., Li, W., O'Sullivan, M., Goncalves de Souza, J., Friedlingstein, P., Chevallier, F.: Low latency carbon budget analysis reveals a large decline of the land carbon sink in 2023. National Science Review, p.nwae367, https://doi.org/10.1093/nsr/nwae367, 2024.

Keeley, J. E. and Pausas, J. G.: Distinguishing disturbance from perturbations in fire-prone ecosystems, Int. J. Wildland Fire, 28, 282–287, https://doi.org/10.1071/WF18203, 2019.

Keeling, C. D., Bacastow, R. B., Bainbridge, A. E., Ekdahl, C. A., Guenther, P. R., Waterman, L. S., and Chin, J. F. S.: Atmospheric carbon dioxide variations at Mauna Loa Observatory, Hawaii, Tellus A., 28, 538–551, https://doi.org/10.1111/j.2153-3490.1976.tb00701.x, 1976.

Keeling R.F.: Development of an Interferometric Oxygen Analyzer for Precise Measurement of the Atmospheric O2 Mole Fraction, PhD thesis, Harvard University, Cambridge, Massachusetts, available at: https://bluemoon.ucsd.edu/publications/ralph/34_PhDthesis.pdf, last access: 23 October 2025, 1988.

Keeling, R. F., Manning, A. C., Paplawsky, W. J., and Cox, A. C.: On the long-term stability of reference gases for atmospheric O2/N2 and CO2 measurements, Tellus B Chem. Phys. Meteorol., 59, 3–14, https://doi.org/10.1111/j.1600-0889.2006.00196.x, 2007.

Keeling, R. F. and Manning, A. C.: 5.15 - Studies of Recent Changes in Atmospheric O2 Content, in: Treatise on Geochemistry (Second Edition), edited by: Holland, H. D. and Turekian, K. K., Elsevier, Oxford, 385–404, https://doi.org/10.1016/B978-0-08-095975-7.00420-4, 2014.

Kelley, D. I., Burton, C., Di Giuseppe, F., Jones, M. W., Barbosa, M. L. F., Brambleby, E., McNorton, J. R., Liu, Z., Bradley, A. S. I., Blackford, K., Burke, E., Ciavarella, A., Di Tomaso, E., Eden, J., Ferreira, I. J. M., Fiedler, L., Hartley, A. J., Keeping, T. R., Lampe, S., Lombardi, A., Mataveli, G., Qu, Y., Silva, P. S., Spuler, F. R., Steinmann, C. B., Torres-Vázquez, M. Á., Veiga, R., Van Wees, D., Wessel, J. B., Wright, E., Bilbao, B., Bourbonnais, M., Gao, C., Di Bella, C. M., Dintwe, K., Donovan, V. M., Harris, S., Kukavskaya, E. A., N'Dri, A. B., Santín, C., Selaya, G., Sjöström, J., Abatzoglou, J. T., Andela, N., Carmenta, R., Chuvieco, E., Giglio, L., Hamilton, D. S., Hantson, S., Meier, S., Parrington, M., Sadegh, M., San-Miguel-Ayanz, J., Sedano, F., Turco, M., Van Der Werf, G. R., Veraverbeke, S., Anderson, L. O., Clarke, H., Fernandes, P. M., and Kolden, C. A.: State of Wildfires 2024–2025, Earth Syst. Sci. Data, 17, 5377–5488, https://doi.org/10.5194/essd-17-5377-2025, 2025.

Keppler, L. and Landschützer, P.: Regional Wind Variability Modulates the Southern Ocean Carbon Sink, Sci Rep, 9, 7384, https://doi.org/10.1038/s41598-019-43826-y, 2019.

Kharin, V. V., Boer, G. J., Merryfield, W. J., Scinocca, J. F., and Lee, W. -S.: Statistical adjustment of decadal predictions in a changing climate, Geophysical Research Letters, 39, 2012GL052647, https://doi.org/10.1029/2012GL052647, 2012.

Khatiwala, S., Primeau, F., and Hall, T.: Reconstruction of the history of anthropogenic CO2 concentrations in the ocean, Nature, 462, 346–349, https://doi.org/10.1038/nature08526, 2009.

Khatiwala, S., Tanhua, T., Mikaloff Fletcher, S., Gerber, M., Doney, S. C., Graven, H. D., Gruber, N., McKinley, G. A., Murata, A., Ríos, A. F., and Sabine, C. L.: Global ocean storage of anthropogenic carbon, Biogeosciences, 10, 2169–2191, https://doi.org/10.5194/bg-10-2169-2013, 2013.

Kong, Y., Zheng, B., Zhang, Q., and He, K.: Global and regional carbon budget for 2015–2020 inferred from OCO-2 based on an ensemble Kalman filter coupled with GEOS-Chem, Atmospheric Chem. Phys., 22, 10769–10788, https://doi.org/10.5194/acp-22-10769-2022, 2022.

Kou-Giesbrecht, S. and Arora, V. K.: Representing the Dynamic Response of Vegetation to Nitrogen Limitation via Biological Nitrogen Fixation in the CLASSIC Land Model, Global Biogeochemical Cycles, 36, e2022GB007341, https://doi.org/10.1029/2022GB007341, 2022.

Korsbakken, J. I., Peters, G. P., and Andrew, R. M.: Uncertainties around reductions in China's coal use and CO2 emissions, Nature Clim Change, 6, 687–690, https://doi.org/10.1038/nclimate2963, 2016.

Koven, C. D., Knox, R. G., Fisher, R. A., Chambers, J. Q., Christoffersen, B. O., Davies, S. J., Detto, M., Dietze, M. C., Faybishenko, B., Holm, J., Huang, M., Kovenock, M., Kueppers, L. M., Lemieux, G., Massoud, E., McDowell, N. G., Muller-Landau, H. C., Needham, J. F., Norby, R. J., Powell, T., Rogers, A., Serbin, S. P., Shuman, J. K., Swann, A. L. S., Varadharajan, C., Walker, A. P., Wright, S. J., and Xu, C.: Benchmarking and parameter sensitivity of physiological and vegetation dynamics using the Functionally Assembled Terrestrial Ecosystem Simulator (FATES) at Barro Colorado Island, Panama, Biogeosciences, 17, 3017–3044, https://doi.org/10.5194/bg-17-3017-2020, 2020.

Krinner, G., Viovy, N., de Noblet-Ducoudré, N., Ogée, J., Polcher, J., Friedlingstein, P., Ciais, P., Sitch, S., and Prentice, I. C.: A dynamic global vegetation model for studies of the coupled atmosphere-biosphere system:

DVGM for coupled climate studies, Global Biogeochem. Cycles, 19, GB1015, https://doi.org/10.1029/2003GB002199, 2005.

Lacroix, F., Ilyina, T., and Hartmann, J.: Oceanic CO2 outgassing and biological production hotspots induced by pre-industrial river loads of nutrients and carbon in a global modeling approach, Biogeosciences, 17, 55–88, https://doi.org/10.5194/bg-17-55-2020, 2020.

Lacroix, F., Ilyina, T., Mathis, M., Laruelle, G. G., and Regnier, P.: Historical increases in land-derived nutrient inputs may alleviate effects of a changing physical climate on the oceanic carbon cycle, Glob Change Biol, 27, 5491–5513, https://doi.org/10.1111/gcb.15822, 2021.

Lamboll, R. D., Nicholls, Z. R. J., Smith, C. J., Kikstra, J. S., Byers, E., and Rogelj, J.: Assessing the size and uncertainty of remaining carbon budgets, Nat. Clim. Change, https://doi.org/10.1038/s41558-023-01848-5, 2023.

Lamboll, R. D., Jones, C. D., Skeie, R. B., Fiedler, S., Samset, B. H., Gillett, N. P., Rogelj, J., Forster, P. M., 2021: Modifying emissions scenario projections to account for the effects of COVID-19: protocol for CovidMIP, Geosci. Model Dev., 14, 3683–3695, https://doi.org/10.5194/gmd-14-3683-2021, 2021.

Lan, X., Tans, P. and Thoning, K.: NOAA Greenhouse Gas Marine Boundary Layer Reference - CO2 [Data set]. NOAA Global Monitoring Laboratory, https://doi.org/10.15138/DVNP-F961, 2024.

Lan, X., Tans, P. and Thoning, K. W.: Trends in globally-averaged CO2 determined from NOAA Global Monitoring Laboratory measurements, https://doi.org/10.15138/9N0H-ZH07, 2025.

Landschützer, P., Gruber, N., Haumann, F. A., Rödenbeck, C., Bakker, D. C. E., van Heuven, S., Hoppema, M., Metzl, N., Sweeney, C., Takahashi, T., Tilbrook, B., and Wanninkhof, R.: The reinvigoration of the Southern Ocean carbon sink, Science, 349, 1221–1224, https://doi.org/10.1126/science.aab2620, 2015.

Landschützer, P., Gruber, N., and Bakker, D. C. E.: Decadal variations and trends of the global ocean carbon sink: decadal air-sea CO2 flux variability, Global Biogeochem. Cycles, 30, 1396–1417, https://doi.org/10.1002/2015GB005359, 2016.

Lapola, D. M., Pinho, P., Barlow, J., Aragão, L. E. O. C., Berenguer, E., Carmenta, R., Liddy, H. M., Seixas, H., Silva, C. V. J., Silva-Junior, C. H. L., Alencar, A. A. C., Anderson, L. O., Armenteras, D., Brovkin, V., Calders, K., Chambers, J., Chini, L., Costa, M. H., Faria, B. L., Fearnside, P. M., Ferreira, J., Gatti, L., Gutierrez-Velez, V. H., Han, Z., Hibbard, K., Koven, C., Lawrence, P., Pongratz, J., Portela, B. T. T., Rounsevell, M., Ruane, A. C., Schaldach, R., da Silva, S. S., von Randow, C., Walker, W. S.: The drivers and impacts of Amazon forest degradation. Science, 379(6630), p.eabp8622, https://doi.org/10.1126/science.abp8622, 2023.

Law, R. M., Ziehn, T., Matear, R. J., Lenton, A., Chamberlain, M. A., Stevens, L. E., Wang, Y.-P., Srbinovsky, J., Bi, D., Yan, H., and Vohralik, P. F.: The carbon cycle in the Australian Community Climate and Earth System Simulator (ACCESS-ESM1) – Part 1: Model description and pre-industrial simulation, Geosci. Model Dev., 10, 2567–2590, https://doi.org/10.5194/gmd-10-2567-2017, 2017.

Laughner, J. L., Roche, S., Kiel, M., Toon, G. C., Wunch, D., Baier, B. C., Biraud, S., Chen, H., Kivi, R., Laemmel, T., McKain, K., Quéhé, P.-Y., Rousogenous, C., Stephens, B. B., Walker, K., and Wennberg, P. O.: A new algorithm to generate a priori trace gas profiles for the GGG2020 retrieval algorithm, Atmos. Meas. Tech., 16, 1121–1146, https://doi.org/10.5194/amt-16-1121-2023, 2023.

Lauvset, S. K., Lange, N., Tanhua, T., Bittig, H. C., Olsen, A., Kozyr, A., Álvarez, M., Azetsu-Scott, K., Brown, P. J., Carter, B. R., Cotrim Da Cunha, L., Hoppema, M., Humphreys, M. P., Ishii, M., Jeansson, E., Murata, A., Müller, J. D., Pérez, F. F., Schirnick, C., Steinfeldt, R., Suzuki, T., Ulfsbo, A., Velo, A., Woosley, R. J., and Key, R. M.: The annual update GLODAPv2.2023: the global interior ocean biogeochemical data product, Earth Syst. Sci. Data, 16, 2047–2072, https://doi.org/10.5194/essd-16-2047-2024, 2024.

Lawrence, D. M., Fisher, R. A., Koven, C. D., Oleson, K. W., Swenson, S. C., Bonan, G., Collier, N., Ghimire, B., van Kampenhout, L., Kennedy, D., Kluzek, E., Lawrence, P. J., Li, F., Li, H., Lombardozzi, D., Riley, W. J., Sacks, W. J., Shi, M., Vertenstein, M., Wieder, W. R., Xu, C., Ali, A. A., Badger, A. M., Bisht, G., van den Broeke, M., Brunke, M. A., Burns, S. P., Buzan, J., Clark, M., Craig, A., Dahlin, K., Drewniak, B., Fisher, J. B., Flanner, M., Fox, A. M., Gentine, P., Hoffman, F., Keppel-Aleks, G., Knox, R., Kumar, S., Lenaerts, J., Leung, L. R., Lipscomb, W. H., Lu, Y., Pandey, A., Pelletier, J. D., Perket, J., Randerson, J. T., Ricciuto, D. M., Sanderson, B. M., Slater, A., Subin, Z. M., Tang, J., Thomas, R. Q., Val Martin, M., and Zeng, X.: The Community Land

Model Version 5: Description of New Features, Benchmarking, and Impact of Forcing Uncertainty, J. Adv. Model Earth, Sy., 11, 4245–4287, https://doi.org/10.1029/2018MS001583, 2019.

Le Quéré, C., Rödenbeck, C., Buitenhuis, E. T., Conway, T. J., Langenfelds, R., Gomez, A., Labuschagne, C., Ramonet, M., Nakazawa, T., Metzl, N., Gillett, N., and Heimann, M.: Saturation of the Southern Ocean CO2 Sink Due to Recent Climate Change, Science, 316, 1735–1738, https://doi.org/10.1126/science.1136188, 2007.

Le Quéré, C., Raupach, M. R., Canadell, J. G., Marland, G., Bopp, L., Ciais, P., Conway, T. J., Doney, S. C., Feely, R. A., Foster, P., Friedlingstein, P., Gurney, K., Houghton, R. A., House, J. I., Huntingford, C., Levy, P. E., Lomas, M. R., Majkut, J., Metzl, N., Ometto, J. P., Peters, G. P., Prentice, I. C., Randerson, J. T., Running, S. W., Sarmiento, J. L., Schuster, U., Sitch, S., Takahashi, T., Viovy, N., van der Werf, G. R., and Woodward, F. I.: Trends in the sources and sinks of carbon dioxide, Nature Geosci, 2, 831–836, https://doi.org/10.1038/ngeo689, 2009.

Le Quéré, C., Andres, R. J., Boden, T., Conway, T., Houghton, R. A., House, J. I., Marland, G., Peters, G. P., van der Werf, G. R., Ahlström, A., Andrew, R. M., Bopp, L., Canadell, J. G., Ciais, P., Doney, S. C., Enright, C., Friedlingstein, P., Huntingford, C., Jain, A. K., Jourdain, C., Kato, E., Keeling, R. F., Klein Goldewijk, K., Levis, S., Levy, P., Lomas, M., Poulter, B., Raupach, M. R., Schwinger, J., Sitch, S., Stocker, B. D., Viovy, N., Zaehle, S., and Zeng, N.: The global carbon budget 1959–2011, Earth Syst. Sci. Data, 5, 165–185, https://doi.org/10.5194/essd-5-165-2013, 2013.

Le Quéré, C., Peters, G. P., Andres, R. J., Andrew, R. M., Boden, T. A., Ciais, P., Friedlingstein, P., Houghton, R. A., Marland, G., Moriarty, R., Sitch, S., Tans, P., Arneth, A., Arvanitis, A., Bakker, D. C. E., Bopp, L., Canadell, J. G., Chini, L. P., Doney, S. C., Harper, A., Harris, I., House, J. I., Jain, A. K., Jones, S. D., Kato, E., Keeling, R. F., Klein Goldewijk, K., Körtzinger, A., Koven, C., Lefèvre, N., Maignan, F., Omar, A., Ono, T., Park, G.-H., Pfeil, B., Poulter, B., Raupach, M. R., Regnier, P., Rödenbeck, C., Saito, S., Schwinger, J., Segschneider, J., Stocker, B. D., Takahashi, T., Tilbrook, B., van Heuven, S., Viovy, N., Wanninkhof, R., Wiltshire, A., and Zaehle, S.: Global carbon budget 2013, Earth Syst. Sci. Data, 6, 235–263, https://doi.org/10.5194/essd-6-235-2014, 2014.

Le Quéré, C., Moriarty, R., Andrew, R. M., Peters, G. P., Ciais, P., Friedlingstein, P., Jones, S. D., Sitch, S., Tans, P., Arneth, A., Boden, T. A., Bopp, L., Bozec, Y., Canadell, J. G., Chini, L. P., Chevallier, F., Cosca, C. E., Harris, I., Hoppema, M., Houghton, R. A., House, J. I., Jain, A. K., Johannessen, T., Kato, E., Keeling, R. F., Kitidis, V., Klein Goldewijk, K., Koven, C., Landa, C. S., Landschützer, P., Lenton, A., Lima, I. D., Marland, G., Mathis, J. T., Metzl, N., Nojiri, Y., Olsen, A., Ono, T., Peng, S., Peters, W., Pfeil, B., Poulter, B., Raupach, M. R., Regnier, P., Rödenbeck, C., Saito, S., Salisbury, J. E., Schuster, U., Schwinger, J., Séférian, R., Segschneider, J., Steinhoff, T., Stocker, B. D., Sutton, A. J., Takahashi, T., Tilbrook, B., van der Werf, G. R., Viovy, N., Wang, Y.-P., Wanninkhof, R., Wiltshire, A., and Zeng, N.: Global carbon budget 2014, Earth Syst. Sci. Data, 7, 47–85, https://doi.org/10.5194/essd-7-47-2015, 2015a.

Le Quéré, C., Moriarty, R., Andrew, R. M., Canadell, J. G., Sitch, S., Korsbakken, J. I., Friedlingstein, P., Peters, G. P., Andres, R. J., Boden, T. A., Houghton, R. A., House, J. I., Keeling, R. F., Tans, P., Arneth, A., Bakker, D. C. E., Barbero, L., Bopp, L., Chang, J., Chevallier, F., Chini, L. P., Ciais, P., Fader, M., Feely, R. A., Gkritzalis, T., Harris, I., Hauck, J., Ilyina, T., Jain, A. K., Kato, E., Kitidis, V., Klein Goldewijk, K., Koven, C., Landschützer, P., Lauvset, S. K., Lefèvre, N., Lenton, A., Lima, I. D., Metzl, N., Millero, F., Munro, D. R., Murata, A., Nabel, J. E. M. S., Nakaoka, S., Nojiri, Y., O'Brien, K., Olsen, A., Ono, T., Pérez, F. F., Pfeil, B., Pierrot, D., Poulter, B., Rehder, G., Rödenbeck, C., Saito, S., Schuster, U., Schwinger, J., Séférian, R., Steinhoff, T., Stocker, B. D., Sutton, A. J., Takahashi, T., Tilbrook, B., van der Laan-Luijkx, I. T., van der Werf, G. R., van Heuven, S., Vandemark, D., Viovy, N., Wiltshire, A., Zaehle, S., and Zeng, N.: Global Carbon Budget 2015, Earth Syst. Sci. Data, 7, 349–396, https://doi.org/10.5194/essd-7-349-2015, 2015b.

Le Quéré, C., Andrew, R. M., Canadell, J. G., Sitch, S., Korsbakken, J. I., Peters, G. P., Manning, A. C., Boden, T. A., Tans, P. P., Houghton, R. A., Keeling, R. F., Alin, S., Andrews, O. D., Anthoni, P., Barbero, L., Bopp, L., Chevallier, F., Chini, L. P., Ciais, P., Currie, K., Delire, C., Doney, S. C., Friedlingstein, P., Gkritzalis, T., Harris, I., Hauck, J., Haverd, V., Hoppema, M., Klein Goldewijk, K., Jain, A. K., Kato, E., Körtzinger, A., Landschützer, P., Lefèvre, N., Lenton, A., Lienert, S., Lombardozzi, D., Melton, J. R., Metzl, N., Millero, F., Monteiro, P. M. S., Munro, D. R., Nabel, J. E. M. S., Nakaoka, S., O'Brien, K., Olsen, A., Omar, A. M., Ono, T., Pierrot, D., Poulter, B., Rödenbeck, C., Salisbury, J., Schuster, U., Schwinger, J., Séférian, R., Skjelvan, I., Stocker, B. D., Sutton, A. J., Takahashi, T., Tian, H., Tilbrook, B., van der Laan-Luijkx, I. T., van der Werf, G. R., Viovy, N., Walker, A. P., Wiltshire, A. J., and Zaehle, S.: Global Carbon Budget 2016, Earth Syst. Sci. Data, 8, 605–649, https://doi.org/10.5194/essd-8-605-2016, 2016.

Le Quéré, C., Andrew, R. M., Friedlingstein, P., Sitch, S., Pongratz, J., Manning, A. C., Korsbakken, J. I., Peters, G. P., Canadell, J. G., Jackson, R. B., Boden, T. A., Tans, P. P., Andrews, O. D., Arora, V. K., Bakker, D. C. E., Barbero, L., Becker, M., Betts, R. A., Bopp, L., Chevallier, F., Chini, L. P., Ciais, P., Cosca, C. E., Cross, J., Currie, K., Gasser, T., Harris, I., Hauck, J., Haverd, V., Houghton, R. A., Hunt, C. W., Hurtt, G., Ilyina, T., Jain, A. K., Kato, E., Kautz, M., Keeling, R. F., Klein Goldewijk, K., Körtzinger, A., Landschützer, P., Lefèvre, N., Lenton, A., Lienert, S., Lima, I., Lombardozzi, D., Metzl, N., Millero, F., Monteiro, P. M. S., Munro, D. R., Nabel, J. E. M. S., Nakaoka, S., Nojiri, Y., Padin, X. A., Peregon, A., Pfeil, B., Pierrot, D., Poulter, B., Rehder, G., Reimer, J., Rödenbeck, C., Schwinger, J., Séférian, R., Skjelvan, I., Stocker, B. D., Tian, H., Tilbrook, B., Tubiello, F. N., van der Laan-Luijkx, I. T., van der Werf, G. R., van Heuven, S., Viovy, N., Vuichard, N., Walker, A. P., Watson, A. J., Wiltshire, A. J., Zaehle, S., and Zhu, D.: Global Carbon Budget 2017, Earth Syst. Sci. Data, 10, 405–448, https://doi.org/10.5194/essd-10-405-2018, 2018a.

Le Quéré, C., Andrew, R. M., Friedlingstein, P., Sitch, S., Hauck, J., Pongratz, J., Pickers, P. A., Korsbakken, J. I., Peters, G. P., Canadell, J. G., Arneth, A., Arora, V. K., Barbero, L., Bastos, A., Bopp, L., Chevallier, F., Chini, L. P., Ciais, P., Doney, S. C., Gkritzalis, T., Goll, D. S., Harris, I., Haverd, V., Hoffman, F. M., Hoppema, M., Houghton, R. A., Hurtt, G., Ilyina, T., Jain, A. K., Johannessen, T., Jones, C. D., Kato, E., Keeling, R. F., Klein Goldewijk, K., Landschützer, P., Lefèvre, N., Lienert, S., Liu, Z., Lombardozzi, D., Metzl, N., Munro, D. R., Nabel, J. E. M. S., Nakaoka, S., Neill, C., Olsen, A., Ono, T., Patra, P., Peregon, A., Peters, W., Peylin, P., Pfeil, B., Pierrot, D., Poulter, B., Rehder, G., Resplandy, L., Robertson, E., Rocher, M., Rödenbeck, C., Schuster, U., Schwinger, J., Séférian, R., Skjelvan, I., Steinhoff, T., Sutton, A., Tans, P. P., Tian, H., Tilbrook, B., Tubiello, F. N., van der Laan-Luijkx, I. T., van der Werf, G. R., Viovy, N., Walker, A. P., Wiltshire, A. J., Wright, R., Zaehle, S., and Zheng, B.: Global Carbon Budget 2018, Earth Syst. Sci. Data, 10, 2141–2194, https://doi.org/10.5194/essd-10-2141-2018, 2018b.

Le Quéré, C., Korsbakken, J. I., Wilson, C., Tosun, J., Andrew, R., Andres, R. J., Canadell, J. G., Jordan, A., Peters, G. P., and van Vuuren, D. P.: Drivers of declining CO2 emissions in 18 developed economies, Nat. Clim. Chang., 9, 213–217, https://doi.org/10.1038/s41558-019-0419-7, 2019.

Le Quéré, C., Peters, G. P., Friedlingstein, P., Andrew, R. M., Canadell, J. G., Davis, S. J., Jackson, R. B., and Jones, M. W.: Fossil CO2 emissions in the post-COVID-19 era, Nat. Clim. Chang., 11, 197–199, https://doi.org/10.1038/s41558-021-01001-0, 2021.

Levitus, S., Antonov, J. I., Boyer, T. P., Baranova, O. K., Garcia, H. E., Locarnini, R. A., Mishonov, A. V., Reagan, J. R., Seidov, D., Yarosh, E. S., and Zweng, M. M.: World ocean heat content and thermosteric sea level change (0–2000 m), 1955–2010, Geophys. Res. Lett., 39, https://doi.org/10.1029/2012GL051106, 2012.

Li, H., Ilyina, T., Müller, W. A., and Sienz, F.: Decadal predictions of the North Atlantic CO2 uptake, Nat. Commun., 7, 11076, https://doi.org/10.1038/ncomms11076, 2016.

Li, H., Ilyina, T., Müller, W. A., and Landschützer, P.: Predicting the variable ocean carbon sink, Sci. Adv., 5, eaav6471, https://doi.org/10.1126/sciadv.aav6471, 2019.

Li, H., Ilyina, T., Loughran, T., Spring, A., and Pongratz, J.: Reconstructions and predictions of the global carbon budget with an emission-driven Earth system model, Earth Syst. Dyn., 14, 101–119, https://doi.org/10.5194/esd-14-101-2023, 2023.

Li, W., Ciais, P., Peng, S., Yue, C., Wang, Y., Thurner, M., Saatchi, S. S., Arneth, A., Avitabile, V., Carvalhais, N., Harper, A. B., Kato, E., Koven, C., Liu, Y. Y., Nabel, J. E. M. S., Pan, Y., Pongratz, J., Poulter, B., Pugh, T. A. M., Santoro, M., Sitch, S., Stocker, B. D., Viovy, N., Wiltshire, A., Yousefpour, R., and Zaehle, S.: Land-use and land-cover change carbon emissions between 1901 and 2012 constrained by biomass observations, Biogeosciences, 14, 5053–5067, https://doi.org/10.5194/bg-14-5053-2017, 2017.

Liao, E., Resplandy, L., Liu, J., and Bowman, K. W.: Amplification of the Ocean Carbon Sink During El Niños: Role of Poleward Ekman Transport and Influence on Atmospheric CO2, Global Biogeochem. Cy., 34, e2020GB006574, https://doi.org/10.1029/2020GB006574, 2020.

Lienert, S. and Joos, F.: A Bayesian ensemble data assimilation to constrain model parameters and land-use carbon emissions, Biogeosciences, 15, 2909–2930, https://doi.org/10.5194/bg-15-2909-2018, 2018.

Liu, J., Baskaran, L., Bowman, K., Schimel, D., Bloom, A. A., Parazoo, N. C., Oda, T., Carroll, D., Menemenlis, D., Joiner, J., Commane, R., Daube, B., Gatti, L. V., McKain, K., Miller, J., Stephens, B. B., Sweeney, C., and

Wofsy, S.: Carbon Monitoring System Flux Net Biosphere Exchange 2020 (CMS-Flux NBE 2020), 13, 299–330, https://doi.org/10.5194/essd-13-299-2021, 2021.

Liu, Z., Guan, D., Wei, W., Davis, S. J., Ciais, P., Bai, J., Peng, S., Zhang, Q., Hubacek, K., Marland, G., Andres, R. J., Crawford-Brown, D., Lin, J., Zhao, H., Hong, C., Boden, T. A., Feng, K., Peters, G. P., Xi, F., Liu, J., Li, Y., Zhao, Y., Zeng, N., and He, K.: Reduced carbon emission estimates from fossil fuel combustion and cement production in China, Nature, 524, 335–338, https://doi.org/10.1038/nature14677, 2015.

Liu, Z., Zeng, N., Liu, Y., Kalnay, E., Asrar, G., Wu, B., Cai, Q., Liu, D., and Han, P.: Improving the joint estimation of CO2 and surface carbon fluxes using a constrained ensemble Kalman filter in COLA (v1.0), Geosci. Model Dev., 15, 5511–5528, https://doi.org/10.5194/gmd-15-5511-2022, 2022.

Liu, Z., Ciais, P., Deng, Z., Lei, R., Davis, S. J., Feng, S., Zheng, B., Cui, D., Dou, X., Zhu, B., Guo, R., Ke, P., Sun, T., Lu, C., He, P., Wang, Y., Yue, X., Wang, Y., Lei, Y., Zhou, H., Cai, Z., Wu, Y., Guo, R., Han, T., Xue, J., Boucher, O., Boucher, E., Chevallier, F., Tanaka, K., Wei, Y., Zhong, H., Kang, C., Zhang, N., Chen, B., Xi, F., Liu, M., Bréon, F.-M., Lu, Y., Zhang, Q., Guan, D., Gong, P., Kammen, D. M., He, K., and Schellnhuber, H. J.: Near-real-time monitoring of global CO2 emissions reveals the effects of the COVID-19 pandemic, Nat Commun, 11, 5172, https://doi.org/10.1038/s41467-020-18922-7, 2020a.

Liu, Z., Ciais, P., Deng, Z., Davis, S. J., Zheng, B., Wang, Y., Cui, D., Zhu, B., Dou, X., Ke, P., Sun, T., Guo, R., Zhong, H., Boucher, O., Bréon, F.-M., Lu, C., Guo, R., Xue, J., Boucher, E., Tanaka, K., and Chevallier, F.: Carbon Monitor, a near-real-time daily dataset of global CO2 emission from fossil fuel and cement production, Sci Data, 7, 392, https://doi.org/10.1038/s41597-020-00708-7, 2020b.

Long, M. C., Stephens, B. B., McKain, K., Sweeney, C., Keeling, R. F., Kort, E. A., Morgan, E. J., Bent, J. D., Chandra, N., Chevallier, F., Commane, R., Daube, B. C., Krummel, P. B., Loh, Z., Luijkx, I. T., Munro, D., Patra, P., Peters, W., Ramonet, M., Rödenbeck, C., Stavert, A., Tans, P., Wofsy, S. C.: Strong Southern Ocean carbon uptake evident in airborne observations. Science, 374(6572), 1275–1280, https://doi.org/10.1126/science.abi4355, 2021.

Lovenduski, N. S., Bonan, G. B., Yeager, S. G., Lindsay, K., and Lombardozzi, D. L.: High predictability of terrestrial carbon fluxes from an initialized decadal prediction system, Environ. Res. Lett., 14, 124074, https://doi.org/10.1088/1748-9326/ab5c55, 2019a.

Lovenduski, N. S., Yeager, S. G., Lindsay, K., and Long, M. C.: Predicting near-term variability in ocean carbon uptake, Earth Syst. Dyn., 10, 45–57, https://doi.org/10.5194/esd-10-45-2019, 2019b.

Lutz, F., Herzfeld, T., Heinke, J., Rolinski, S., Schaphoff, S., von Bloh, W., Stoorvogel, J. J., and Müller, C.: Simulating the effect of tillage practices with the global ecosystem model LPJmL (version 5.0-tillage), Geosci. Model Dev., 12, 2419–2440, https://doi.org/10.5194/gmd-12-2419-2019, 2019.

Ma, L., Hurtt, G., Ott, L., Sahajpal, R., Fisk, J., Lamb, R., Tang, H., Flanagan, S., Chini, L., Chatterjee, A., and Sullivan, J.: Global evaluation of the Ecosystem Demography model (ED v3.0), Geosci. Model Dev., 15, 1971–1994, https://doi.org/10.5194/gmd-15-1971-2022, 2022.

Magi, B. I., Rabin, S., Shevliakova, E., and Pacala, S.: Separating agricultural and non-agricultural fire seasonality at regional scales, Biogeosciences, 9, 3003–3012, https://doi.org/10.5194/bg-9-3003-2012, 2012.

Maksyutov, S., Oda, T., Saito, M., Janardanan, R., Belikov, D., Kaiser, J. W., Zhuravlev, R., Ganshin, A., Valsala, V. K., Andrews, A., Chmura, L., Dlugokencky, E., Haszpra, L., Langenfelds, R. L., Machida, T., Nakazawa, T., Ramonet, M., Sweeney, C., and Worthy, D.: Technical note: A high-resolution inverse modelling technique for estimating surface CO2 fluxes based on the NIES-TM–FLEXPART coupled transport model and its adjoint, Atmos. Chem. Phys., 21, 1245–1266, https://doi.org/10.5194/acp-21-1245-2021, 2021.

Masarie, K. A. and Tans, P. P.: Extension and integration of atmospheric carbon dioxide data into a globally consistent measurement record, J. Geophys. Res., 100, 11593, https://doi.org/10.1029/95JD00859, 1995.

Mataveli, G., Jones, M.W., Carmenta, R., Sanchez, A., Dutra, D.J., Chaves, M., de Oliveira, G., Anderson, L.O. and Aragão, L.E.: Deforestation falls but rise of wildfires continues degrading Brazilian Amazon forests. Global Change Biology, 30(2), p.e17202, https://doi.org/10.1111/gcb.17202, 2024.

Mather, A. S.: The transition from deforestation to reforestation in Europe, in: Agricultural technologies and tropical deforestation (eds. Angelsen, A.; Kaimowitz, D.), CABI in association with centre for international Forestry Research, 35–52, 2001.

Mauritsen, T., Bader, J., Becker, T., Behrens, J., Bittner, M., Brokopf, R., Brovkin, V., Claussen, M., Crueger, T., Esch, M., Fast, I., Fiedler, S., Fläschner, D., Gayler, V., Giorgetta, M., Goll, D. S., Haak, H., Hagemann, S., Hedemann, C., Hohenegger, C., Ilyina, T., Jahns, T., Jimenéz-de-la-Cuesta, D., Jungclaus, J., Kleinen, T., Kloster, S., Kracher, D., Kinne, S., Kleberg, D., Lasslop, G., Kornblueh, L., Marotzke, J., Matei, D., Meraner, K., Mikolajewicz, U., Modali, K., Möbis, B., Müller, W. A., Nabel, J. E. M. S., Nam, C. C. W., Notz, D., Nyawira, S.-S., Paulsen, H., Peters, K., Pincus, R., Pohlmann, H., Pongratz, J., Popp, M., Raddatz, T. J., Rast, S., Redler, R., Reick, C. H., Rohrschneider, T., Schemann, V., Schmidt, H., Schnur, R., Schulzweida, U., Six, K. D., Stein, L., Stemmler, I., Stevens, B., von Storch, J.-S., Tian, F., Voigt, A., Vrese, P., Wieners, K.-H., Wilkenskjeld, S., Winkler, A., and Roeckner, E.: Developments in the MPI-M Earth System Model version 1.2 (MPI-ESM1.2) and Its Response to Increasing CO2, J. Adv. Model Earth Sy., 11, 998–1038, https://doi.org/10.1029/2018MS001400, 2019.

Mayot, N., Buitenhuis, E. T., Wright, R. M., Hauck, J., Bakker, D. C. E., and Le Quéré, C.: Constraining the trend in the ocean CO2 sink during 2000–2022. Nat Commun 15, 8429, https://doi.org/10.1038/s41467-024-52641-7, 2024.

McGrath, M. J., Luyssaert, S., Meyfroidt, P., Kaplan, J. O., Bürgi, M., Chen, Y., Erb, K., Gimmi, U., McInerney, D., Naudts, K., Otto, J., Pasztor, F., Ryder, J., Schelhaas, M.-J., and Valade, A.: Reconstructing European forest management from 1600 to 2010, 12, 4291–4316, https://doi.org/10.5194/bg-12-4291-2015, 2015.

McKinley, G. A., Fay, A. R., Eddebbar, Y. A., Gloege, L., and Lovenduski, N. S.: External Forcing Explains Recent Decadal Variability of the Ocean Carbon Sink, AGU Advances, 1, e2019AV000149, https://doi.org/10.1029/2019AV000149, 2020.

McKinley, G. A., Fay, A. R., Lovenduski, N. S., and Pilcher, D. J.: Natural Variability and Anthropogenic Trends in the Ocean Carbon Sink, Annu. Rev. Mar. Sci., 9, 125–150, https://doi.org/10.1146/annurev-marine-010816-060529, 2017.

Meiyappan, P., Jain, A. K., and House, J. I.: Increased influence of nitrogen limitation on CO 2 emissions from future land use and land use change, Global Biogeochem. Cycles, 29, 1524–1548, https://doi.org/10.1002/2015GB005086, 2015.

Melo, J., Rossi, S., Achard, F., Alkama, R., Canadell, J. G., Federici, S., Friedlingstein, P., Gibbs, D., Harris, N., Heinrich, V., O'Sullivan, M., Peters, G., Pongratz, J., Rose, M., Roman-Cuesta, R., Sanz Sanchez, M. J., Schwingshackl, C., Sitch, S., and Grassi, G.: The LULUCF Data Hub: translating global land use emissions estimates into the national GHG inventory framework (Version 3.0, 2025 NGHGI release) (3.0), https://doi.org/10.5281/ZENODO.17140775, 2025.

Melton, J. R., Arora, V. K., Wisernig-Cojoc, E., Seiler, C., Fortier, M., Chan, E., and Teckentrup, L.: CLASSIC v1.0: the open-source community successor to the Canadian Land Surface Scheme (CLASS) and the Canadian Terrestrial Ecosystem Model (CTEM) – Part 1: Model framework and site-level performance, Geosci. Model Dev., 13, 2825–2850, https://doi.org/10.5194/gmd-13-2825-2020, 2020.

Mercado, L. M., Bellouin, N., Sitch, S., Boucher, O., Huntingford, C., Wild, M., and Cox, P. M.: Impact of changes in diffuse radiation on the global land carbon sink, Nature, 458, 1014–1017, https://doi.org/10.1038/nature07949, 2009.

Merchant, C. J., Embury, O., Bulgin, C. E., Block, T., Corlett, G. K., Fiedler, E., Good, S. A., Mittaz, J., Rayner, N. A., Berry, D., Eastwood, S., Taylor, M., Tsushima, Y., Waterfall, A., Wilson, R., and Donlon, C.: Satellite-based time-series of sea-surface temperature since 1981 for climate applications, Sci. Data, 6, 223, https://doi.org/10.1038/s41597-019-0236-x, 2019.

Moorcroft, P. R., Hurtt, G. C., and Pacala, S. W.: A Method for Scaling Vegetation Dynamics: The Ecosystem Demography Model (ed), Ecol. Monogr., 71, 557–586, https://doi.org/10.1890/0012-9615(2001)071[0557:AMFSVD]2.0.CO;2, 2001.

Müller, J. D., Gruber, N., Carter, B., Feely, R., Ishii, M., Lange, N., Lauvset, S. K., Murata, A., Olsen, A., Pérez, F. F., Sabine, C., Tanhua, T., Wanninkhof, R., and Zhu, D.: Decadal Trends in the Oceanic Storage of Anthropogenic Carbon From 1994 to 2014, AGU Adv., 4, e2023AV000875, https://doi.org/10.1029/2023AV000875, 2023.

Müller, J. D., Gruber, N., Schneuwly, A., Bakker, D. C. E., Gehlen, M., Gregor, L., Hauck, J., Landschützer, P., and McKinley, G. A.: Unexpected decline in the ocean carbon sink under record-high sea surface temperatures in 2023, Nat. Clim. Chang., 15, 978–985, https://doi.org/10.1038/s41558-025-02380-4, 2025.

Müller, J. and Joos, F.: Committed and projected future changes in global peatlands – continued transient model simulations since the Last Glacial Maximum, Biogeosciences, 18, 3657–3687, https://doi.org/10.5194/bg-18-3657-2021, 2021.

Nayagam, L., Maksyutov, S., Oda, T., Janardanan, R., Trisolino, P., Zeng J., Kaiser, J.W. and Matsunaga, T.: A top-down estimation of subnational CO2 budget using a global high-resolution inverse model with data from regional surface networks, Environ. Res. Lett., 19, 0140312024, https://doi.org/10.1088/1748-9326/ad0f74, 2024.

NCEP: National Centers for Environmental Prediction. ONI Index. Cold & Warm Episodes by Season [Data set], available at: https://www.cpc.ncep.noaa.gov/products/analysis_monitoring/ensostuff/ONI_v5.php, last access: 23 October 2025, 2025.

Nayagam, L., Maksyutov, S., Janardanan, R., Oda, T., Tiwari, Y. K., Sreenivas, G., Datye, A., Jain, C. D., Ratnam, M. V., Sinha, V., Hakkim, H., Terao, Y., Naja, M., Ahmed, Md. K., Mukai, H., Zeng, J., Kaiser, J. W., Someya, Y., Yoshida, Y., and Matsunaga, T.: Indian Land Carbon Sink Estimated from Surface and GOSAT Observations, Remote Sensing, 17, 450, https://doi.org/10.3390/rs17030450, 2025.

Nevison, C.D., Mahowald, N.M., Doney, S.C., Lima, I.D. and Cassar, N.:. Impact of variable air-sea O 2 and CO 2 fluxes on atmospheric potential oxygen (APO) and land-ocean carbon sink partitioning. Biogeosciences, 5(3), pp.875-889, https://doi.org/10.5194/bg-5-875-2008, 2008.

Niu, G.-Y., Yang, Z.-L., Mitchell, K. E., Chen, F., Ek, M. B., Barlage, M., Kumar, A., Manning, K., Niyogi, D., Rosero, E., Tewari, M., and Xia, Y.: The community Noah land surface model with multiparameterization options (Noah-MP): 1. Model description and evaluation with local-scale measurements, J. Geophys. Res. Atmospheres, 116, https://doi.org/10.1029/2010JD015139, 2011.

Niwa, Y., Ishijima, K., Ito, A., and Iida, Y.: Toward a long-term atmospheric CO2 inversion for elucidating natural carbon fluxes: technical notes of NISMON-CO2 v2021.1, Prog. Earth Planet Sci., 9, 42, https://doi.org/10.1186/s40645-022-00502-6, 2022.

Niwa, Y., Fujii, Y., Sawa, Y., Iida, Y., Ito, A., Satoh, M., Imasu, R., Tsuboi, K., Matsueda, H., and Saigusa, N.: A 4D-Var inversion system based on the icosahedral grid model (NICAM-TM 4D-Var v1.0) – Part 2: Optimization scheme and identical twin experiment of atmospheric CO₂ inversion, Geosci. Model Dev., 10, 2201–2219, https://doi.org/10.5194/gmd-10-2201-2017, 2017.

Niwa, Y., Langenfelds, R., Krummel, P., Loh, Zoe, Worthy, Doug, Hatakka, Juha, Aalto, Tuula, Ramonet, Michel, Delmotte, Marc, Schmidt, Martina, Gheusi, Francois, Mihalopoulos, N., Morgui, J.A., Andrews, Arlyn, Dlugokencky, Ed, Lee, John, Sweeney, Colm, Thoning, Kirk, Tans, Pieter, De Wekker, Stephan, Fischer, Marc L., Jaffe, Dan, McKain, Kathryn, Viner, Brian, Miller, John B., Karion, Anna, Miller, Charles, Sloop, Christopher D., Saito, Kazuyuki, Aoki, Shuji, Morimoto, Shinji, Goto, Daisuke, Steinbacher, Martin, Myhre, Cathrine Lund, Hermanssen, Ove, Stephens, Britton, Keeling, Ralph, Afshar, Sara, Paplawsky, Bill, Cox, Adam, Walker, Stephen, Schuldt, Kenneth, Mukai, Hitoshi, Machida, Toshinobu, Sasakawa, Motoki, Nomura, Shohei, Ito, Akihiko, Iida, Yosuke, and Jones, Matthew W.: Long-term global CO2 fluxes estimated by NICAM-based Inverse Simulation for Monitoring CO2 (NISMON-CO2) (ver.2022.1), National Institute for Environmental Studies Japan [Data set], https://doi.org/10.17595/20201127.001, 2020.

Norby, R.J.: Forest productivity response to elevated CO2 in free-air CO2 enrichment experiments: the 23 percent solution, revisited, New Phytologist, https://doi.org/10.1111/nph.70162, 2025.

Obermeier, W. A., Nabel, J. E. M. S., Loughran, T., Hartung, K., Bastos, A., Havermann, F., Anthoni, P., Arneth, A., Goll, D. S., Lienert, S., Lombardozzi, D., Luyssaert, S., McGuire, P. C., Melton, J. R., Poulter, B., Sitch, S., Sullivan, M. O., Tian, H., Walker, A. P., Wiltshire, A. J., Zaehle, S., and Pongratz, J.: Modelled land use and land cover change emissions – a spatio-temporal comparison of different approaches, 12, 635–670, https://doi.org/10.5194/esd-12-635-2021, 2021.

Obermeier, W. A., Schwingshackl, C., Ganzenmüller, R., Grassi, G., Heinrich, V., Luijkx, I. T., Bastos, A., Ciais, P., Sitch, S., and Pongratz, J.: Differences and uncertainties in land-use CO2 flux estimates, Nat Rev Earth Environ, https://doi.org/10.1038/s43017-025-00730-6, 2025.

O'Dell, C. W., Eldering, A., Wennberg, P. O., Crisp, D., Gunson, M. R., Fisher, B., Frankenberg, C., Kiel, M., Lindqvist, H., Mandrake, L., Merrelli, A., Natraj, V., Nelson, R. R., Osterman, G. B., Payne, V. H., Taylor, T. E., Wunch, D., Drouin, B. J., Oyafuso, F., Chang, A., McDuffie, J., Smyth, M., Baker, D. F., Basu, S., Chevallier, F., Crowell, S. M. R., Feng, L., Palmer, P. I., Dubey, M., García, O. E., Griffith, D. W. T., Hase, F., Iraci, L. T., Kivi, R., Morino, I., Notholt, J., Ohyama, H., Petri, C., Roehl, C. M., Sha, M. K., Strong, K., Sussmann, R., Te, Y., Uchino, O., and Velazco, V. A.: Improved retrievals of carbon dioxide from Orbiting Carbon Observatory-2 with the version 8 ACOS algorithm, Atmos. Meas. Tech., 11, 6539–6576, https://doi.org/10.5194/amt-11-6539-2018, 2018.

O'Rourke, P. R., Smith, S. J., Mott, A., Ahsan, H., McDuffie, E. E., Crippa, M., Klimont, Z., McDonald, B., Wang, S., Nicholson, M. B., Feng, L., and Hoesly, R. M.: CEDS v_2021_04_21 Release Emission Data, Zenodo [Data set], https://doi.org/10.5281/zenodo.4741285, 2021.

O'Sullivan, M., Zhang, Y., Bellouin, N., Harris, I., Mercado, L. M., Sitch, S., Ciais, P., and Friedlingstein, P.: Aerosol–light interactions reduce the carbon budget imbalance, Environ. Res. Lett., 16, 124072, https://doi.org/10.1088/1748-9326/ac3b77, 2021.

O'Sullivan, M., Friedlingstein, P., Sitch, S., Anthoni, P., Arneth, A., Arora, V. K., Bastrikov, V., Delire, C., Goll, D. S., Jain, A., Kato, E., Kennedy, D., Knauer, J., Lienert, S., Lombardozzi, D., McGuire, P. C., Melton, J. R., Nabel, J. E. M. S., Pongratz, J., Poulter, B., Séférian, R., Tian, H., Vuichard, N., Walker, A. P., Yuan, W., Yue, X., and Zaehle, S.: Process-oriented analysis of dominant sources of uncertainty in the land carbon sink, Nat. Commun., 13, 4781, https://doi.org/10.1038/s41467-022-32416-8, 2022.

O'Sullivan, M., Spracklen, D. V., Batterman, S. A., Arnold, S. R., Gloor, M., and Buermann, W.: Have Synergies Between Nitrogen Deposition and Atmospheric CO2 Driven the Recent Enhancement of the Terrestrial Carbon Sink?, Glob. Biogeochem. Cycles, 33, 163–180, https://doi.org/10.1029/2018GB005922, 2019.

O'Sullivan, M., Sitch, S., Friedlingstein, P., Luijkx, I. T., Peters, W., Rosan, T. M., Arneth, A., Arora, V. K., Chandra, N., Chevallier, F., Ciais, P., Falk, S., Feng, L., Gasser, T., Houghton, R. A., Jain, A. K., Kato, E., Kennedy, D., Knauer, J., McGrath, M. J., Niwa, Y., Palmer, P. I., Patra, P. K., Pongratz, J., Poulter, B., Rödenbeck, C., Schwingshackl, C., Sun, Q., Tian, H., Walker, A. P., Yang, D., Yuan, W., Yue, X., and Zaehle, S.: The key role of forest disturbance in reconciling estimates of the northern carbon sink. Commun Earth Environ 5, 705, https://doi.org/10.1038/s43247-024-01827-4, 2024.

O'Sullivan, M., Friedlingstein, P., Sitch, S., Pongratz, J., Schwingshackl, C., Gasser, T., Ciais, P., Arora, V., Kato, E., Knauer, J., Nützel, T., Sun, Q., Yuan. W., and Zaehle, S.: An improved approach to estimate the natural land carbon sink, 27 July 2025, PREPRINT (Version 1) available at Research Square [https://doi.org/10.21203/rs.3.rs-7207206/v1], 2025.

Palmer, P. I., Feng, L., Baker, D., Chevallier, F., Bösch, H., and Somkuti, P.: Net carbon emissions from African biosphere dominate pan-tropical atmospheric CO2 signal, Nat Commun, 10, 3344, https://doi.org/10.1038/s41467-019-11097-w, 2019.

Pan, Y., Birdsey, R. A., Fang, J., Houghton, R., Kauppi, P. E., Kurz, W. A., Phillips, O. L., Shvidenko, A., Lewis, S. L., Canadell, J. G., Ciais, P., Jackson, R. B., Pacala, S. W., McGuire, A. D., Piao, S., Rautiainen, A., Sitch, S., and Hayes, D.: A Large and Persistent Carbon Sink in the World's Forests, Science, 333, 988–993, https://doi.org/10.1126/science.1201609, 2011.

Pandey, S., Miller, J. B., Basu, S., Liu, J., Weir, B., Byrne, B., Chevallier, F., Bowman, K. W., Liu, Z., Deng, F., O'Dell, C. W., and Chatterjee, A.: Toward Low-Latency Estimation of Atmospheric CO2 Growth Rates Using Satellite Observations: Evaluating Sampling Errors of Satellite and In Situ Observing Approaches, AGU Advances, 5, e2023AV001145, https://doi.org/10.1029/2023AV001145, 2024.

Pandey, S., Chevallier, F., Rödenbeck, C., Byrne, B., Chatterjee, A., Liu, J., and Frankenberg, C.: Reduction in Earth's carbon budget imbalance, Nat Commun, 16, 6818, https://doi.org/10.1038/s41467-025-61588-2, 2025.

Patra, P. K., Takigawa, M., Watanabe, S., Chandra, N., Ishijima, K., and Yamashita, Y.: Improved Chemical Tracer Simulation by MIROC4.0-based Atmospheric Chemistry-Transport Model (MIROC4-ACTM), SOLA, 14, 91–96, https://doi.org/10.2151/sola.2018-016, 2018.

Pendrill, F., Persson, U. M., Godar, J., Kastner, T., Moran, D., Schmidt, S., and Wood, R.: Agricultural and forestry trade drives large share of tropical deforestation emissions, Global Environmental Change, 56, 1–10, https://doi.org/10.1016/j.gloenvcha.2019.03.002, 2019.

Pérez, F. F., Becker, M., Goris, N., Gehlen, M., López-Mozos, M., Tjiputra, J., Olsen, A., Müller, J. D., Huertas, I. E., Chau, T. T. T., Cainzos, V., Velo, A., Benard, G., Hauck, J., Gruber, N., and Wanninkhof, R.: An Assessment of CO 2 Storage and Sea-Air Fluxes for the Atlantic Ocean and Mediterranean Sea Between 1985 and 2018. Global Biogeochemical Cycles, 38(4), e2023GB007862, https://doi.org/10.1029/2023GB007862, 2024.

Peters, G. P., Minx, J. C., Weber, C. L., and Edenhofer, O.: Growth in emission transfers via international trade from 1990 to 2008, Proceedings of the National Academy of Sciences, 108, 8903–8908, https://doi.org/10.1073/pnas.1006388108, 2011a.

Peters, G. P., Marland, G., Le Quéré, C., Boden, T., Canadell, J. G., and Raupach, M. R.: Rapid growth in CO2 emissions after the 2008–2009 global financial crisis, Nature Clim Change, 2, 2–4, https://doi.org/10.1038/nclimate1332, 2012a.

Peters, G. P., Andrew, R. M., Boden, T., Canadell, J. G., Ciais, P., Le Quéré, C., Marland, G., Raupach, M. R., and Wilson, C.: The challenge to keep global warming below 2 °C, Nature Clim Change, 3, 4–6, https://doi.org/10.1038/nclimate1783, 2013.

Peters, G. P., Le Quéré, C., Andrew, R. M., Canadell, J. G., Friedlingstein, P., Ilyina, T., Jackson, R. B., Joos, F., Korsbakken, J. I., McKinley, G. A., Sitch, S., and Tans, P.: Towards real-time verification of CO2 emissions, Nature Clim Change, 7, 848–850, https://doi.org/10.1038/s41558-017-0013-9, 2017a.

Peters, G. P., Andrew, R. M., Canadell, J. G., Fuss, S., Jackson, R. B., Korsbakken, J. I., Le Quéré, C. and Nakicenovic, N.: Key indicators to track current progress and future ambition of the Paris Agreement, 7, 118–122, https://doi.org/10.1038/nclimate3202, 2017b.

Peters, G. P., Andrew, R. M., Canadell, J. G., Friedlingstein, P., Jackson, R. B., Korsbakken, J. I., Le Quéré, C., and Peregon, A.: Carbon dioxide emissions continue to grow amidst slowly emerging climate policies, Nat. Clim. Chang., 10, 3–6, https://doi.org/10.1038/s41558-019-0659-6, 2020.

Peters, W., Miller, J. B., Whitaker, J., Denning, A. S., Hirsch, A., Krol, M. C., Zupanski, D., Bruhwiler, L., and Tans, P. P.: An ensemble data assimilation system to estimate CO2 surface fluxes from atmospheric trace gas observations, J. Geophys. Res. Atmospheres, 110, https://doi.org/10.1029/2005JD006157, 2005.

Petrescu, A. M. R., Peters, G. P., Janssens-Maenhout, G., Ciais, P., Tubiello, F. N., Grassi, G., Nabuurs, G.-J., Leip, A., Carmona-Garcia, G., Winiwarter, W., Höglund-Isaksson, L., Günther, D., Solazzo, E., Kiesow, A., Bastos, A., Pongratz, J., Nabel, J. E. M. S., Conchedda, G., Pilli, R., Andrew, R. M., Schelhaas, M.-J., and Dolman, A. J.: European anthropogenic AFOLU greenhouse gas emissions: a review and benchmark data, Earth Syst. Sci. Data, 12, 961–1001, https://doi.org/10.5194/essd-12-961-2020, 2020.

Pfeil, B., Olsen, A., Bakker, D. C. E., Hankin, S., Koyuk, H., Kozyr, A., Malczyk, J., Manke, A., Metzl, N., Sabine, C. L., Akl, J., Alin, S. R., Bates, N., Bellerby, R. G. J., Borges, A., Boutin, J., Brown, P. J., Cai, W.-J., Chavez, F. P., Chen, A., Cosca, C., Fassbender, A. J., Feely, R. A., González-Dávila, M., Goyet, C., Hales, B., Hardman-Mountford, N., Heinze, C., Hood, M., Hoppema, M., Hunt, C. W., Hydes, D., Ishii, M., Johannessen, T., Jones, S. D., Key, R. M., Körtzinger, A., Landschützer, P., Lauvset, S. K., Lefèvre, N., Lenton, A., Lourantou, A., Merlivat, L., Midorikawa, T., Mintrop, L., Miyazaki, C., Murata, A., Nakadate, A., Nakano, Y., Nakaoka, S., Nojiri, Y., Omar, A. M., Padin, X. A., Park, G.-H., Paterson, K., Perez, F. F., Pierrot, D., Poisson, A., Ríos, A. F., Santana-Casiano, J. M., Salisbury, J., Sarma, V. V. S. S., Schlitzer, R., Schneider, B., Schuster, U., Sieger, R., Skjelvan, I., Steinhoff, T., Suzuki, T., Takahashi, T., Tedesco, K., Telszewski, M., Thomas, H., Tilbrook, B., Tjiputra, J., Vandemark, D., Veness, T., Wanninkhof, R., Watson, A. J., Weiss, R., Wong, C. S., and Yoshikawa-Inoue, H.: A uniform, quality controlled Surface Ocean CO2 Atlas (SOCAT), Earth Syst. Sci. Data, 5, 125–143, https://doi.org/10.5194/essd-5-125-2013, 2013.

Piao, S., Ciais, P., Friedlingstein, P., de Noblet-Ducoudré, N., Cadule, P., Viovy, N., and Wang, T.: Spatiotemporal patterns of terrestrial carbon cycle during the 20th century, Global Biogeochem. Cy., 23, GB4026, https://doi.org/10.1029/2008GB003339, 2009.

Piao, S., Huang, M., Liu, Z., Wang, X., Ciais, P., Canadell, J. G., Wang, K., Bastos, A., Friedlingstein, P., Houghton, R. A., Le Quéré, C., Liu, Y., Myneni, R. B., Peng, S., Pongratz, J., Sitch, S., Yan, T., Wang, Y., Zhu, Z., Wu, D., and Wang, T.: Lower land-use emissions responsible for increased net land carbon sink during the slow warming period, Nature Geosci, 11, 739–743, https://doi.org/10.1038/s41561-018-0204-7, 2018.

Pongratz, J., Reick, C.H., Raddatz, T. and Claussen, M.: Effects of anthropogenic land cover change on the carbon cycle of the last millennium. Global Biogeochemical Cycles, 23(4), doi:10.1029/2009GB003488, 2009.

Pongratz, J., Reick, C. H., Houghton, R. A., and House, J. I.: Terminology as a key uncertainty in net land use and land cover change carbon flux estimates, Earth Syst. Dynam., 5, 177–195, https://doi.org/10.5194/esd-5-177-2014, 2014.

Pongratz, J., Smith, S. M., Schwingshackl, C., Dayathilake, L., Gasser, T., Grassi, G. and Pilli, R.: Chapter 7: Current levels of CDR. in The State of Carbon Dioxide Removal 2024 – 2nd Edition, https://doi.org/10.17605/OSF.IOZXSKB, 2024.

Poulter, B., Bastos, A., Canadell, J., Ciais, P., Gruber, N., Hauck, J., Jackson, R., Ishii, M., Müller, J., Patra, P., and Tian, H.: Inventorying Earth's Land and Ocean Greenhouse Gases, Eos, 103, https://doi.org/10.1029/2022EO179084, 2022.

Poulter, B., Frank, D. C., Hodson, E. L., and Zimmermann, N. E.: Impacts of land cover and climate data selection on understanding terrestrial carbon dynamics and the CO2 airborne fraction, Biogeosciences, 8, 2027–2036, https://doi.org/10.5194/bg-8-2027-2011, 2011.

Poulter, B., Freeborn, P. H., Jolly, W. M., and Varner, J. M.: COVID-19 lockdowns drive decline in active fires in southeastern United States, PNAS, 118, e2105666118, https://doi.org/10.1073/pnas.2105666118, 2021.

Powis, C. M., Smith, S. M., Minx, J. C., and Gasser, T.: Quantifying global carbon dioxide removal deployment, Environ. Res. Lett., 18, 024022, https://doi.org/10.1088/1748-9326/acb450, 2023.

Prentice, I. C., Farquhar, G. D., Fasham, M. J. R., Goulden, M. L., Heimann, M., Jaramillo, V. J., Kheshgi, H. S., Le Quéré, C., Scholes, R. J., and Wallace, D. W. R.: The Carbon Cycle and Atmospheric Carbon Dioxide, in Climate Change 2001: The Scientific Basis. Contribution of Working Group I to the Third Assessment Report of the Intergovernmental Panel on Climate Change, edited by: Houghton, J. T., Ding, Y., Griggs, D. J., Noguer, M., van der Linden, P. J., Dai, X., Maskell, K., and Johnson, C. A., Cambridge University Press, Cambridge, United Kingdom and New York, NY, USA, 183–237, ISBN: 978-0521014953, 2001.

Price, J. T. and Warren, R.: Literature Review of the Potential of "Blue Carbon" Activities to Reduce Emissions, available at: https://avoid-net-uk.cc.ic.ac.uk/wp-content/uploads/delightful-downloads/2016/03/Literature-review-of-the-potential-of-blue-carbon-activities-to-reduce-emissions-AVOID2-WPE2.pdf, last access: 23 October 2025, 2016.

Qin, Y., Xiao, X., Wigneron, J.-P., Ciais, P., Brandt, M., Fan, L., Li, X., Crowell, S., Wu, X., Doughty, R., Zhang, Y., Liu, F., Sitch, S., and Moore, B.: Carbon loss from forest degradation exceeds that from deforestation in the Brazilian Amazon, Nat. Clim. Chang., 11, 442–448, https://doi.org/10.1038/s41558-021-01026-5, 2021.

Qin, Z., Zhu, Y., Canadell, J.G., Chen, M., Li, T., Mishra, U. and Yuan, W.: Global spatially explicit carbon emissions from land-use change over the past six decades (1961–2020). One Earth, 7(5), pp.835-847, https://doi.org/10.1016/j.oneear.2024.04.002, 2024.

Qiu, C., Ciais, P., Zhu, D., Guenet, B., Peng, S., Petrescu, A. M. R., Lauerwald, R., Makowski, D., Gallego-Sala, A. V., Charman, D. J., and Brewer, S. C.: Large historical carbon emissions from cultivated northern peatlands, Sci. Adv., 7, eabf1332, https://doi.org/10.1126/sciadv.abf1332, 2021.

Randerson, J. T., Chen, Y., van der Werf, G. R., Rogers, B. M., and Morton, D. C.: Global burned area and biomass burning emissions from small fires: BURNED AREA FROM SMALL FIRES, J. Geophys. Res. Biogeosciences, 117, n/a-n/a, https://doi.org/10.1029/2012JG002128, 2012.

Randerson, J. T., Li, Y., Fu, W., Primeau, F., Kim, J. E., Mu, M., Hoffman, F. M., Trugman, A. T., Yang, L., Wu, C., Wang, J. A., Anderegg, W. R. L., Baccini, A., Friedl, M. A., Saatchi, S. S., Denning, A. S., and Goulden, M. L.: The weak land carbon sink hypothesis, Sci. Adv., 11, eadr5489, https://doi.org/10.1126/sciadv.adr5489, 2025.

Raupach, M. R., Marland, G., Ciais, P., Le Quere, C., Canadell, J. G., Klepper, G., and Field, C. B.: Global and regional drivers of accelerating CO2 emissions, Proceedings of the National Academy of Sciences, 104, 10288–10293, https://doi.org/10.1073/pnas.0700609104, 2007.

Regnier, P., Resplandy, L., Najjar, R. G., and Ciais, P.: The land-to-ocean loops of the global carbon cycle, Nature, 603, 401–410, https://doi.org/10.1038/s41586-021-04339-9, 2022.

Reick, C. H., Gayler, V., Goll, D., Hagemann, S., Heidkamp, M., Nabel, J. E. M. S., Raddatz, T., Roeckner, E., Schnur, R., 110 and Wilkenskjeld, S.: JSBACH 3 – The land component of the MPI Earth System Model: documentation of version 3.2, available at: https://doi.org/10.17617/2.3279802, 2021.

Remaud, M., Chevallier, F., Cozic, A., Lin, X., and Bousquet, P.: On the impact of recent developments of the LMDz atmospheric general circulation model on the simulation of CO2 transport, 11, 4489, https://doi.org/10.5194/gmd-11-4489-2018, 2018.

Resplandy, L., Keeling, R. F., Rödenbeck, C., Stephens, B. B., Khatiwala, S., Rodgers, K. B., Long, M. C., Bopp, L., and Tans, P. P.: Revision of global carbon fluxes based on a reassessment of oceanic and riverine carbon transport, Nature Geosci, 11, 504–509, https://doi.org/10.1038/s41561-018-0151-3, 2018.

Resplandy, L., Keeling, R. F., Eddebbar, Y., Brooks, M., Wang, R., Bopp, L., Long, M. C., Dunne, J. P., Koeve, W., and Oschlies, A.: Quantification of ocean heat uptake from changes in atmospheric O2 and CO2 composition, Scientific Reports, 9, 20244, https://doi.org/10.1038/s41598-019-56490-z, 2019.

Rödenbeck, C., Houweling, S., Gloor, M., and Heimann, M.: CO2 flux history 1982–2001 inferred from atmospheric data using a global inversion of atmospheric transport, Atmos Chem Phys, 3, 1919–1964, 2003.

Rödenbeck, C., Bakker, D. C. E., Metzl, N., Olsen, A., Sabine, C., Cassar, N., Reum, F., Keeling, R. F., and Heimann, M.: Interannual sea–air CO2 flux variability from an observation-driven ocean mixed-layer scheme, 11, 4599–4613, https://doi.org/10.5194/bg-11-4599-2014, 2014.

Rödenbeck, C., Zaehle, S., Keeling, R., and Heimann, M.: History of El Niño impacts on the global carbon cycle 1957–2017: a quantification from atmospheric CO2 data, 373, 20170303, https://doi.org/10.1098/rstb.2017.0303, 2018.

Rödenbeck, C., DeVries, T., Hauck, J., Le Quéré, C., and Keeling, R. F.: Data-based estimates of interannual sea–air CO2 flux variations 1957–2020 and their relation to environmental drivers, Biogeosciences, 19, 2627–2652, https://doi.org/10.5194/bg-19-2627-2022, 2022.

Rosan, T. M., Klein Goldewijk, K., Ganzenmüller, R., O'Sullivan, M., Pongratz, J., Mercado, L. M., Aragao, L. E. O. C., Heinrich, V., Randow, C. V., Wiltshire, A., Tubiello, F. N., Bastos, A., Friedlingstein, P., and Sitch, S.: A multi-data assessment of land use and land cover emissions from Brazil during 2000–2019, Environ. Res. Lett., 16, 074004, https://doi.org/10.1088/1748-9326/ac08c3, 2021.

Rosan, T. M., Sitch, S., O'Sullivan, M., Basso, L. S., Wilson, C., Silva, C., Gloor, E., Fawcett, D., Heinrich, V., Souza, J. G. and Bezerra, F.G.S.: Synthesis of the land carbon fluxes of the Amazon region between 2010 and 2020. Communications Earth & Environment, 5(1), p.46. https://doi.org/10.1038/s43247-024-01205-0, 2024.

Sakamoto, K., H. Nakano, S. Urakawa, T. Toyoda, Y. Kawakami, H. Tsujino, G. Yamanaka, 2023: Reference manual for the Meteorological Research Institute Community Ocean Model version 5 (MRI.COMv5), Technical Reports of the Meteorological Research Institute, No.87, https://doi.org/10.11483/mritechrepo.87.

Sarma, V. V. S. S., Sridevi, B., Metzl, N., Patra, P. K., Lachkar, Z., Chakraborty, K., Goyet, C., Levy, M., Mehari, M., and Chandra, N.: Air-Sea Fluxes of CO2 in the Indian Ocean Between 1985 and 2018: A Synthesis Based on Observation-Based Surface CO2, Hindcast and Atmospheric Inversion Models, Glob. Biogeochem. Cycles, 37, e2023GB007694, https://doi.org/10.1029/2023GB007694, 2023.

Schaphoff, S., von Bloh, W., Rammig, A., Thonicke, K., Biemans, H., Forkel, M., Gerten, D., Heinke, J., Jägermeyr, J., Knauer, J., Langerwisch, F., Lucht, W., Müller, C., Rolinski, S., and Waha, K.: LPJmL4 – a dynamic

global vegetation model with managed land – Part 1: Model description, Geosci. Model Dev., 11, 1343–1375, https://doi.org/10.5194/gmd-11-1343-2018, 2018.

Schimel, D., Alves, D., Enting, I. G., Heimann, M., Joos, F., Raynaud, D., Wigley, T., Prater, M., Derwent, R., Ehhalt, D., Fraser, P., Sanhueza, E., Zhou, X., Jonas, P., Charlson, R., Rodhe, H., Sadasivan, S., Shine, K. P., Fouquart, Y., Ramaswamy, V., Solomon, S., Srinivasan, J., Albritton, D., Derwent, R., Isaksen, I., Lal, M., and Wuebbles, D.: Radiative Forcing of Climate Change, in: Climate Change 1995: The Science of Climate Change, Contribution of Working Group I to the Second Assessment Report of the Intergovernmental Panel on Climate Change [Houghton, J. T., Meira Rilho, L. G., Callander, B. A., Harris, N., Kattenberg, A., and Maskell, K. (eds.)], Cambridge University Press, Cambridge, United Kingdom and New York, NY, USA, ISBN: 978-0521559621, 1995.

Schimel, D., Stephens, B. B., and Fisher, J. B.: Effect of increasing CO 2 on the terrestrial carbon cycle, Proc Natl Acad Sci USA, 112, 436–441, https://doi.org/10.1073/pnas.1407302112, 2015.

Schuh, A. E., Jacobson, A. R., Basu, S., Weir, B., Baker, D., Bowman, K., Chevallier, F., Crowell, S., Davis, K. J., Deng, F., Denning, S., Feng, L., Jones, D., Liu, J., and Palmer, P. I.: Quantifying the Impact of Atmospheric Transport Uncertainty on CO 2 Surface Flux Estimates, Global Biogeochem. Cycles, 33, 484–500, https://doi.org/10.1029/2018GB006086, 2019.

Schuldt, K. N., Mund, J., Aalto, T., Abshire, J. B., Aikin, K., Allen, G., Andrade, M., Andrews, A., Apadula, F., Arnold, S., Baier, B., Bakwin, P., Bartyzel, J., Bentz, G., Bergamaschi, P., Beyersdorf, A., Biermann, T., Biraud, S. C., Blanc, P.-E., Boenisch, H., Bowling, D., Brailsford, G., Brand, W. A., Brunner, D., Bui, T. P., Burban, B., Bäni, L., Calzolari, F., Chang, C. S., Chen, H., Chen, G., Chmura, L., Clark, S., Climadat, S., Colomb, A., Commane, R., Condori, L., Conen, F., Conil, S., Couret, C., Cristofanelli, P., Cuevas, E., Curcoll, R., Daube, B., Davis, K. J., De Mazière, M., De Wekker, S., Dean-Day, J. M., Della Coletta, J., Delmotte, M., Di Iorio, T., DiGangi, E., DiGangi, J. P., Dickerson, R., Elsasser, M., Emmenegger, L., Fang, S., Forster, G., France, J., Frumau, A., Fuente-Lastra, M., Galkowski, M., Gatti, L. V., Gehrlein, T., Gerbig, C., Gheusi, F., Gloor, E., Goto, D., Griffis, T., Hammer, S., Hanisco, T. F., Hanson, C., Haszpra, L., Hatakka, J., Heimann, M., Heliasz, M., Heltai, D., Henne, S., Hensen, A., Hermans, C., Hermansen, O., Hintsa, E., Hoheisel, A., Holst, J., Iraci, L. T., Ivakhov, V., Jaffe, D. A., Jordan, A., Joubert, W., Kang, H.-Y., Karion, A., Kawa, S. R., Kazan, V., Keeling, R. F., Keronen, P., Kim, J., Klausen, J., Kneuer, T., Ko, M.-Y., Kolari, P., Kominkova, K., Kort, E., Kozlova, E., Krummel, P. B., Kubistin, D., Kulawik, S. S., Kumps, N., Labuschagne, C., Lam, D. H., Lan, X., Langenfelds, R. L., Lanza, A., Laurent, O., Laurila, T., Lauvaux, T., Lavric, J., Law, B. E., Lee, C.-H., Lee, J., Lehner, I., Lehtinen, K., Leppert, R., Leskinen, A., Leuenberger, M., Leung, W. H., Levin, I., Levula, J., Lin, J., Lindauer, M., Lindroth, A., Loh, Z. M., Lopez, M., Lunder, C. R., Löfvenius, M. O., Machida, T., Mammarella, I., Manca, G., Manning, A., Manning, A., Marek, M. V., Marklund, P., Marrero, J. E., Martin, M. Y., Martin, D., Martins, G. A., Matsueda, H., McKain, K., Meijer, H., Meinhardt, F., Merchant, L., Metzger, J.-M., Mihalopoulos, N., Miles, N. L., Miller, C. E., Miller, J. B., Mitchell, L., Monteiro, V., Montzka, S., Moossen, H., Moreno, C., Morgan, E., Morgui, J.-A., Morimoto, S., Munger, J. W., Munro, D., Mutuku, M., Myhre, C. L., Mölder, M., Müller-Williams, J., Nakaoka, S.-I., Necki, J., Newman, S., Nichol, S., Nisbet, E., Niwa, Y., Njiru, D. M., Noe, S. M., Nojiri, Y., O'Doherty, S., Obersteiner, F., Paplawsky, B., Parworth, C. L., Peischl, J., Peltola, O., Peters, W., Philippon, C., Piacentino, S., Pichon, J. M., Pickers, P., Piper, S., Pitt, J., Plass-Dülmer, C., Platt, S. M., Prinzivalli, S., Ramonet, M., Ramos, R., Ren, X., Reyes-Sanchez, E., Richardson, S. J., Rigouleau, L.-J., Riris, H., Rivas, P. P., Rothe, M., Roulet, Y.-A., Ryerson, T., Ryoo, J.-M., Sargent, M., Sasakawa, M., Schaefer, H., Scheeren, B., Schmidt, M., Schuck, T., Schumacher, M., Seibel, J., Seifert, T., Sha, M. K., Shepson, P., Shin, D., Shook, M., Sloop, C. D., Smale, D., Smith, P. D., Spain, G., St. Clair, J. M., Steger, D., Steinbacher, M., Stephens, B., Sweeney, C., Sørensen, L. L., Taipale, R., Takatsuji, S., Tans, P., Thoning, K., Timas, H., Torn, M., Trisolino, P., Turnbull, J., Vermeulen, A., Viner, B., Vitkova, G., Walker, S., Watson, A., Weiss, R., Weyrauch, D., Wofsy, S. C., Worsey, J., Worthy, D., Xueref-Remy, I., Yates, E. L., Young, D., Yver-Kwok, C., Zaehle, S., Zahn, A., Zellweger, C., Zimnoch, M., de Souza, R. A., di Sarra, A. G., van Dinther, D., van den Bulk, P.: Multi-laboratory compilation of atmospheric carbon dioxide data for the period 1957-2023; obspack_co2_1_GLOBALVIEWplus_v10.1_2024-11-13, https://doi.org/10.25925/20241101, 2024.

Schuldt, K. N., Jacobson, A. R., Aalto, T., Aaltonen, H., Andrews, A., Apadula, F., Arnold, S., Bakwin, P., Bartyzel, J., Bergamaschi, P., Biermann, T., Biraud, S. C., Blanc, P.-E., Brunner, D., Bäni, L., Calzolari, F., Chen, H., Chmura, L., Colomb, A., Condori, L., Conen, F., Conil, S., Couret, C., Cristofanelli, P., Cuevas, E., De Mazière, M., De Wekker, S., Della Coletta, J., Delmotte, M., Di Iorio, T., Elsasser, M., Emmenegger, L., Forster, G., Frumau, A., Fuente-Lastra, M., Galkowski, M., Gheusi, F., Hammer, S., Haszpra, L., Hatakka, J., Heliasz, M., Heltai, D., Henne, S., Hensen, A., Hermans, C., Hermansen, O., Hoheisel, A., Holst, J., Jaffe, D. A., Karion, A., Kazan, V., Keronen, P., Kneuer, T., Kolari, P., Kominkova, K., Krummel, P. B., Kubistin, D., Kumps, N., Lan, X., Langenfelds, R. L., Lanza, A., Laurent, O., Lee, J., Lehner, I., Lehtinen, K., Leskinen, A., Leuenberger, M., Levin,

I., Levula, J., Lindauer, M., Lindroth, A., Loh, Z. M., Lopez, M., Lunder, C. R., Löfvenius, M. O., Mammarella, I., Manca, G., Manning, A., Manning, A., Marek, M. V., Marklund, P., McKain, K., Meijer, H., Meinhardt, F., Metzger, J.-M., Miller, J. B., Miller, C. E., Myhre, C. L., Mölder, M., Müller-Williams, J., Necki, J., Noe, S. M., O'Doherty, S., Peltola, O., Philippon, C., Piacentino, S., Pichon, J. M., Pickers, P., Pitt, J., Plass-Dülmer, C., Platt, S. M., Ramonet, M., Ramos, R., Reyes-Sanchez, E., Rigouleau, L.-J., Rivas, P. P., Roulet, Y.-A., Scheeren, B., Schmidt, M., Schumacher, M., Sha, M. K., Sloop, C. D., Smith, P. D., Steger, D., Steinbacher, M., Sweeney, C., Sørensen, L. L., Taipale, R., Tans, P., Thoning, K., Trisolino, P., Vermeulen, A., Viner, B., Vitkova, G., Weyrauch, D., Worthy, D., Xueref-Remy, I., Young, D., Yver-Kwok, C., Zimnoch, M., di Sarra, A. G., van den Bulk, P.: Multi-laboratory compilation of atmospheric carbon dioxide data for the year 2024; obspack_co2_1_NRT_v10.1_2025-02-07, https://doi.org/10.25925/20250101, 2025.

Schwinger, J., Goris, N., Tjiputra, J. F., Kriest, I., Bentsen, M., Bethke, I., Ilicak, M., Assmann, K. M., and Heinze, C.: Evaluation of NorESM-OC (versions 1 and 1.2), the ocean carbon-cycle stand-alone configuration of the Norwegian Earth System Model (NorESM1), Geosci. Model Dev., 9, 2589–2622, https://doi.org/10.5194/gmd-9-2589-2016, 2016.

Schwingshackl, C., Obermeier, W. A., Bultan, S., Grassi, G., Canadell, J. G., Friedlingstein, P., Gasser, T., Houghton, R. A., Kurz, W. A., Sitch, S., and Pongratz, J.: Differences in land-based mitigation estimates reconciled by separating natural and land-use CO2 fluxes at the country level, One Earth, 5, 1367–1376, https://doi.org/10.1016/j.oneear.2022.11.009, 2022.

Séférian, R., Nabat, P., Michou, M., Saint-Martin, D., Voldoire, A., Colin, J., Decharme, B., Delire, C., Berthet, S., Chevallier, M., Sénési, S., Franchisteguy, L., Vial, J., Mallet, M., Joetzjer, E., Geoffroy, O., Guérémy, J.-F., Moine, M.-P., Msadek, R., Ribes, A., Rocher, M., Roehrig, R., Salas-y-Mélia, D., Sanchez, E., Terray, L., Valcke, S., Waldman, R., Aumont, O., Bopp, L., Deshayes, J., Éthé, C., and Madec, G.: Evaluation of CNRM Earth System Model, CNRM-ESM2-1: Role of Earth System Processes in Present-Day and Future Climate, Journal of Advances in Modeling Earth Systems, 11, 4182–4227, https://doi.org/10.1029/2019MS001791, 2019.

Seiler, C., Melton, J. R., Arora, V. K., Sitch, S., Friedlingstein, P., Anthoni, P., Goll, D., Jain, A. K., Joetzjer, E., Lienert, S., Lombardozzi, D., Luyssaert, S., Nabel, J. E. M. S., Tian, H., Vuichard, N., Walker, A. P., Yuan, W., and Zaehle, S.: Are Terrestrial Biosphere Models Fit for Simulating the Global Land Carbon Sink?, J. Adv. Model. Earth Syst., 14, e2021MS002946, https://doi.org/10.1029/2021MS002946, 2022.

Sellar, A. A., Jones, C. G., Mulcahy, J. P., Tang, Y., Yool, A., Wiltshire, A., O'Connor, F. M., Stringer, M., Hill, R., Palmieri, J., Woodward, S., Mora, L., Kuhlbrodt, T., Rumbold, S. T., Kelley, D. I., Ellis, R., Johnson, C. E., Walton, J., Abraham, N. L., Andrews, M. B., Andrews, T., Archibald, A. T., Berthou, S., Burke, E., Blockley, E., Carslaw, K., Dalvi, M., Edwards, J., Folberth, G. A., Gedney, N., Griffiths, P. T., Harper, A. B., Hendry, M. A., Hewitt, A. J., Johnson, B., Jones, A., Jones, C. D., Keeble, J., Liddicoat, S., Morgenstern, O., Parker, R. J., Predoi, V., Robertson, E., Siahaan, A., Smith, R. S., Swaminathan, R., Woodhouse, M. T., Zeng, G., and Zerroukat, M.: UKESM1: Description and Evaluation of the U.K. Earth System Model, J. Adv. Model. Earth Syst., 11, 4513–4558, https://doi.org/10.1029/2019MS001739, 2019.

Ship and Bunker, 2026. Bunker demand change, Q3 2025, at key global bunkering locations. Available at: https://shipandbunker.com/bi/bunker-volumes, last access: 23 March 2026.

Shu, S., Jain, A. K., Koven, C. D., and Mishra, U.: Estimation of Permafrost SOC Stock and Turnover Time Using a Land Surface Model With Vertical Heterogeneity of Permafrost Soils, Global Biogeochem. Cy., 34, e2020GB006585, https://doi.org/10.1029/2020GB006585, 2020.

Shutler, J. D., Land, P. E., Piolle, J.-F., Woolf, D. K., Goddijn-Murphy, L., Paul, F., Girard-Ardhuin, F., Chapron, B., and Donlon, C. J.: FluxEngine: A Flexible Processing System for Calculating Atmosphere–Ocean Carbon Dioxide Gas Fluxes and Climatologies, J. Atmospheric Ocean. Technol., 33, 741–756, https://doi.org/10.1175/JTECH-D-14-00204.1, 2016.

Silva Junior, C.H., Anderson, L.O., Silva, A.L., Almeida, C.T., Dalagnol, R., Pletsch, M.A., Penha, T.V., Paloschi, R.A. and Aragão, L.E.: Fire responses to the 2010 and 2015/2016 Amazonian droughts. Frontiers in Earth Science, 7, p.97, https://doi.org/10.3389/feart.2019.00097, 2019.

Sitch, S., V. Brovkin, W. von Bloh, D. Van Vuuren, B. Eickhout, and Ganopolski, A.: Impacts of future land cover on atmospheric CO2 and climate. Global Biogeochemical Cycles, 19, GB2013. doi:10.1029/2004GB002311, 2005.

Sitch, S., Huntingford, C., Gedney, N., Levy, P. E., Lomas, M., Piao, S. L., Betts, R., Ciais, P., Cox, P., Friedlingstein, P., Jones, C. D., Prentice, I. C., and Woodward, F. I.: Evaluation of the terrestrial carbon cycle, future plant geography and climate-carbon cycle feedbacks using five Dynamic Global Vegetation Models (DGVMs): Uncertainty In Land Carbon Cycle Feedbacks, Glob. Change Biol., 14, 2015–2039, https://doi.org/10.1111/j.1365-2486.2008.01626.x, 2008.

Sitch, S., O'Sullivan, M., Robertson, E., Friedlingstein, P., Albergel, C., Anthoni, P., Arneth, A., Arora, V. K., Bastos, A., Bastrikov, V., Bellouin, N., Canadell, J. G., Chini, L., Ciais, P., Falk, S., Harris, I., Hurtt, G., Ito, A., Jain, A. K., Jones, M. W., Joos, F., Kato, E., Kennedy, D., Klein Goldewijk, K., Kluzek, E., Knauer, J., Lawrence, P. J., Lombardozzi, D., Melton, J. R., Nabel, J. E. M. S., Pan, N., Peylin, P., Pongratz, J., Poulter, B., Rosan, T. M., Sun, Q., Tian, H., Walker, A. P., Weber, U., Yuan, W., Yue, X., Zaehle, S.: Trends and Drivers of Terrestrial Sources and Sinks of Carbon Dioxide: An Overview of the TRENDY Project, Global Biogeochemical Cycles, 38(7), e2024GB008102, https://doi.org/10.1029/2024GB008102, 2024.

Smallman, T. L., Milodowski, D. T., Neto, E. S., Koren, G., Ometto, J., and Williams, M.: Parameter uncertainty dominates C-cycle forecast errors over most of Brazil for the 21st century, Earth Syst. Dyn., 12, 1191–1237, https://doi.org/10.5194/esd-12-1191-2021, 2021.

Smith, B., Wårlind, D., Arneth, A., Hickler, T., Leadley, P., Siltberg, J., and Zaehle, S.: Implications of incorporating N cycling and N limitations on primary production in an individual-based dynamic vegetation model, Biogeosciences, 11, 2027–2054, https://doi.org/10.5194/bg-11-2027-2014, 2014.

Smith, S. M., Geden, O., Gidden, M. J., Lamb, W. F., Nemet, G. F., Minx, J. C., Buck, H., Burke, J., Cox, E., Edwards, M. R., Fuss, S., Johnstone, I., Müller-Hansen, F., Pongratz, J., Probst, B. S., Roe, S., Schenuit, F., Schulte, I., and Vaughan, N. E. The State of Carbon Dioxide Removal 2024 - 2nd Edition, http://dx.doi.org/10.17605/OSF.IO/F85QJ, 2024.

Sospedra-Alfonso, R., Merryfield, W. J., Boer, G. J., Kharin, V. V., Lee, W.-S., Seiler, C., and Christian, J. R.: Decadal climate predictions with the Canadian Earth System Model version 5 (CanESM5), Geosci. Model Dev., 14, 6863–6891, https://doi.org/10.5194/gmd-14-6863-2021, 2021.

Steele, L. P., Dlugokencky, E. J., Lang, P. M., Tans, P. P., Martin, R. C., and Masarie, K. A.: Slowing down of the global accumulation of atmospheric methane during the 1980s, Nature 358, 313–316, https://doi.org/10.1038/358313a0, 1992.

Stephens, B. B., Gurney, K. R., Tans, P. P., Sweeney, C., Peters, W., Bruhwiler, L., Ciais, P., Ramonet, M., Bousquet, P., Nakazawa, T., Aoki, S., Machida, T., Inoue, G., Vinnichenko, N., Lloyd, J., Jordan, A., Heimann, M., Shibistova, O., Langenfelds, R. L., Steele, L. P., Francey, R. J., and Denning, A. S.: Weak Northern and Strong Tropical Land Carbon Uptake from Vertical Profiles of Atmospheric CO2, Science, 316, 1732–1735, https://doi.org/10.1126/science.1137004, 2007.

Stephens, B. B., Keeling, R. F., Heimann, M., Six, K. D., Murnane, R., and Caldeira, K.: Testing global ocean carbon cycle models using measurements of atmospheric O2 and CO2 concentration, Glob. Biogeochem. Cycles, 12, 213–230, https://doi.org/10.1029/97GB03500, 1998.

Stock, C. A., Dunne, J. P., Luo, J. Y., Ross, A. C., Van Oostende, N., Zadeh, N., Cordero, T. J., Liu, X., and Teng, Y.: Photoacclimation and Photoadaptation Sensitivity in a Global Ocean Ecosystem Model, J Adv Model Earth Syst, 17, e2024MS004701, https://doi.org/10.1029/2024MS004701, 2025.

Stocker, T., Qin, D., and Platner, G.-K.: Climate Change 2013: The Physical Science Basis. Contribution of Working Group I to the Fifth Assessment Report of the Intergovernmental Panel on Climate Change [Intergovernmental Panel on Climate Change (eds.)], Cambridge University Press, Cambridge, ISBN: 9789291691388, 2013.\

Swart, N. C., Cole, J. N. S., Kharin, V. V., Lazare, M., Scinocca, J. F., Gillett, N. P., Anstey, J., Arora, V., Christian, J. R., Hanna, S., Jiao, Y., Lee, W. G., Majaess, F., Saenko, O. A., Seiler, C., Seinen, C., Shao, A., Sigmond, M., Solheim, L., von Salzen, K., Yang, D., and Winter, B.: The Canadian Earth System Model version 5 (CanESM5.0.3), Geosci. Model Dev., 12, 4823–4873, https://doi.org/10.5194/gmd-12-4823-2019, 2019.

SX Coal: Monthly coal consumption estimates, http://www.sxcoal.com/, last access: 23 October 2025, 2022.

Takahashi, T., Sutherland, S. C., Wanninkhof, R., Sweeney, C., Feely, R. A., Chipman, D. W., Hales, B., Friederich, G., Chavez, F., Sabine, C., Watson, A., Bakker, D. C. E., Schuster, U., Metzl, N., Yoshikawa-Inoue, H., Ishii, M., Midorikawa, T., Nojiri, Y., Körtzinger, A., Steinhoff, T., Hoppema, M., Olafsson, J., Arnarson, T. S., Tilbrook, B., Johannessen, T., Olsen, A., Bellerby, R., Wong, C. S., Delille, B., Bates, N. R., and de Baar, H. J. W.: Climatological mean and decadal change in surface ocean pCO2, and net sea–air CO2 flux over the global oceans, Deep Sea Research Part II: Topical Studies in Oceanography, 56, 554–577, https://doi.org/10.1016/j.dsr2.2008.12.009, 2009.

Terhaar, J., Frölicher, T. L., and Joos, F.: Southern Ocean anthropogenic carbon sink constrained by sea surface salinity, Sci. Adv., 7, eabd5964, https://doi.org/10.1126/sciadv.abd5964, 2021.

Terhaar, J., Frölicher, T. L., and Joos, F.: Observation-constrained estimates of the global ocean carbon sink from Earth system models, Biogeosciences, 19, 4431–4457, https://doi.org/10.5194/bg-19-4431-2022, 2022.

Terhaar, J., Goris, N., Müller, J. D., DeVries, T., Gruber, N., Hauck, J., Perez, F. F., and Séférian, R.: Assessment of Global Ocean Biogeochemistry Models for Ocean Carbon Sink Estimates in RECCAP2 and Recommendations for Future Studies. Journal of Advances in Modeling Earth Systems, 16(3), e2023MS003840, https://doi.org/10.1029/2023MS003840, 2024.

Tian, H., Xu, X., Lu, C., Liu, M., Ren, W., Chen, G., Melillo, J., and Liu, J.: Net exchanges of CO2, CH4, and N2O between China's terrestrial ecosystems and the atmosphere and their contributions to global climate warming, J. Geophys. Res. Biogeosciences, 116, G02011, https://doi.org/10.1029/2010JG001393, 2011.

Tian, H., Chen, G., Lu, C., Xu, X., Hayes, D. J., Ren, W., Pan, S., Huntzinger, D. N., and Wofsy, S. C.: North American terrestrial CO2 uptake largely offset by CH4 and N2O emissions: toward a full accounting of the greenhouse gas budget, Climatic Change, 129, 413–426, https://doi.org/10.1007/s10584-014-1072-9, 2015.

Tjiputra, J. F., Schwinger, J., Bentsen, M., Morée, A. L., Gao, S., Bethke, I., Heinze, C., Goris, N., Gupta, A., He, Y.-C., Olivié, D., Seland, Ø., and Schulz, M.: Ocean biogeochemistry in the Norwegian Earth System Model version 2 (NorESM2), Geosci. Model Dev., 13, 2393–2431, https://doi.org/10.5194/gmd-13-2393-2020, 2020.

Tsujino, H., Nakano, H., Sakamoto, K., Urakawa, L.S., Toyama, K., Kosugi, N., Kitamura, Y., Ishii, M., Nishikawa, S., Nishikawa, H., Sugiyama, T., and Ishikawa, Y.: Impact of increased horizontal resolution of an ocean model on carbon circulation in the North Pacific Ocean. Journal of Advances in Modeling Earth Systems, 16, e2023MS003720, https://doi.org/10.1029/2023MS003720, 2024.

Tubiello, F. N., Conchedda, G., Wanner, N., Federici, S., Rossi, S., and Grassi, G.: Carbon emissions and removals from forests: new estimates, 1990–2020, Earth Syst. Sci. Data, 13, 1681–1691, https://doi.org/10.5194/essd-13-1681-2021, 2021.

Tubiello, F., Pekkarinen, A., Branthomme, A., Piccoli, M., Obli-Laryea, G., Ramadan, N., and Conchedda, G.: New FAOSTAT forest emissions and removals estimates: 1990–2025, Earth Syst. Sci. Data Discussions, https://doi.org/10.5194/essd-2025-635, 2025.

Tuck, C.: 2022 Mineral Commodity Summary: Iron Ore, Tech. rep., U.S. Geological Survey, https://pubs.usgs.gov/periodicals/mcs2022/mcs2022-iron-ore.pdf, 2022.

UNFCCC: Synthesis report for the technical assessment component of the first global stocktake, available at: https://unfccc.int/documents/461466, last access: 23 October 2025, 2022.

Vale, M. M., Berenguer, E., Argollo de Menezes, M., Viveiros de Castro, E. B., Pugliese de Siqueira, L., and Portela, R. de C. Q.: The COVID-19 pandemic as an opportunity to weaken environmental protection in Brazil, Biological Conservation, 255, 108994, https://doi.org/10.1016/j.biocon.2021.108994, 2021.

van der Laan-Luijkx, I. T., van der Velde, I. R., van der Veen, E., Tsuruta, A., Stanislawska, K., Babenhauserheide, A., Zhang, H. F., Liu, Y., He, W., Chen, H., Masarie, K. A., Krol, M. C., and Peters, W.: The CarbonTracker Data Assimilation Shell (CTDAS) v1.0: implementation and global carbon balance 2001–2015, Geosci. Model Dev., 10, 2785–2800, https://doi.org/10.5194/gmd-10-2785-2017, 2017.

van der Velde, I. R., van der Werf, G. R., Houweling, S., Maasakkers, J. D., Borsdorff, T., Landgraf, J., Tol, P., van Kempen, T. A., van Hees, R., Hoogeveen, R., Veefkind, J. P., and Aben, I.: Vast CO2 release from Australian

fires in 2019–2020 constrained by satellite, Nature, 597, 366–369, https://doi.org/10.1038/s41586-021-03712-y, 2021.

van der Werf, G. R., Randerson, J. T., Giglio, L., Collatz, G. J., Mu, M., Kasibhatla, P. S., Morton, D. C., DeFries, R. S., Jin, Y., and van Leeuwen, T. T.: Global fire emissions and the contribution of deforestation, savanna, forest, agricultural, and peat fires (1997–2009), Atmospheric Chem. Phys., 10, 11707–11735, https://doi.org/10.5194/acp-10-11707-2010, 2010.

van der Werf, G. R., Randerson, J. T., Giglio, L., van Leeuwen, T. T., Chen, Y., Rogers, B. M., Mu, M., van Marle, M. J. E., Morton, D. C., Collatz, G. J., Yokelson, R. J., and Kasibhatla, P. S.: Global fire emissions estimates during 1997–2016, Earth Syst. Sci. Data, 9, 697–720, https://doi.org/10.5194/essd-9-697-2017, 2017.

van Wees, D., van der Werf, G. R., Randerson, J. T., Andela, N., Chen, Y., and Morton, D. C.: The role of fire in global forest loss dynamics, Glob. Change Biol., 27, 2377–2391, https://doi.org/10.1111/gcb.15591, 2021.

von Bloh, W., Schaphoff, S., Müller, C., Rolinski, S., Waha, K., and Zaehle, S.: Implementing the nitrogen cycle into the dynamic global vegetation, hydrology, and crop growth model LPJmL (version 5.0), Geosci. Model Dev., 11, 2789–2812, https://doi.org/10.5194/gmd-11-2789-2018, 2018.

Vaittinada Ayar, P., Bopp, L., Christian, J. R., Ilyina, T., Krasting, J. P., Séférian, R., Tsujino, H., Watanabe, M., Yool, A., and Tjiputra, J.: Contrasting projections of the ENSO-driven CO2 flux variability in the equatorial Pacific under high-warming scenario, Earth Syst. Dynam., 13, 1097–1118, https://doi.org/10.5194/esd-13-1097-2022, 2022.

Vuichard, N., Messina, P., Luyssaert, S., Guenet, B., Zaehle, S., Ghattas, J., Bastrikov, V., and Peylin, P.: Accounting for carbon and nitrogen interactions in the global terrestrial ecosystem model ORCHIDEE (trunk version, rev 4999): multi-scale evaluation of gross primary production, Geosci. Model Dev., 12, 4751–4779, https://doi.org/10.5194/gmd-12-4751-2019, 2019.

Walker, A. P., Quaife, T., Bodegom, P. M., De Kauwe, M. G., Keenan, T. F., Joiner, J., Lomas, M. R., MacBean, N., Xu, C., Yang, X., and Woodward, F. I.: The impact of alternative trait-scaling hypotheses for the maximum photosynthetic carboxylation rate (V cmax) on global gross primary production, New Phytol., 215, 1370–1386, https://doi.org/10.1111/nph.14623, 2017.

Walker, A. P., De Kauwe, M. G., Bastos, A., Belmecheri, S., Georgiou, K., Keeling, R. F., McMahon, S. M., Medlyn, B. E., Moore, D. J. P., Norby, R. J., Zaehle, S., Anderson-Teixeira, K. J., Battipaglia, G., Brienen, R. J. W., Cabugao, K. G., Cailleret, M., Campbell, E., Canadell, J. G., Ciais, P., Craig, M. E., Ellsworth, D. S., Farquhar, G. D., Fatichi, S., Fisher, J. B., Frank, D. C., Graven, H., Gu, L., Haverd, V., Heilman, K., Heimann, M., Hungate, B. A., Iversen, C. M., Joos, F., Jiang, M., Keenan, T. F., Knauer, J., Körner, C., Leshyk, V. O., Leuzinger, S., Liu, Y., MacBean, N., Malhi, Y., McVicar, T. R., Penuelas, J., Pongratz, J., Powell, A. S., Riutta, T., Sabot, M. E. B., Schleucher, J., Sitch, S., Smith, W. K., Sulman, B., Taylor, B., Terrer, C., Torn, M. S., Treseder, K. K., Trugman, A. T., Trumbore, S. E., van Mantgem, P. J., Voelker, S. L., Whelan, M. E., and Zuidema, P. A.: Integrating the evidence for a terrestrial carbon sink caused by increasing atmospheric CO2, New Phytol., 229, 2413–2445, https://doi.org/10.1111/nph.16866, 2021.

Watanabe, M., Tatebe, H., Koyama, H., Hajima, T., Watanabe, M., and Kawamiya, M.: Importance of El Niño reproducibility for reconstructing historical CO2 flux variations in the equatorial Pacific, Ocean Sci., 16, 1431–1442, https://doi.org/10.5194/os-16-1431-2020, 2020.

Watson, A. J., Schuster, U., Shutler, J. D., Holding, T., Ashton, I. G. C., Landschützer, P., Woolf, D. K., and Goddijn-Murphy, L.: Revised estimates of ocean-atmosphere CO2 flux are consistent with ocean carbon inventory, Nat Commun, 11, 4422, https://doi.org/10.1038/s41467-020-18203-3, 2020.

Watson, R. T., Rohde, H., Oeschger, H., and Siegenthaler, U.: Greenhouse Gases and Aerosols, in: Climate Change: The IPCC Scientific Assessment. Intergovernmental Panel on Climate Change (IPCC), edited by: Houghton, J. T., Jenkins, G. J., and Ephraums, J. J., Cambridge University Press, Cambridge, ISBN: 978-0521403603, 1990.

Wenzel, S., Cox, P. M., Eyring, V., and Friedlingstein, P.: Projected land photosynthesis constrained by changes in the seasonal cycle of atmospheric CO2, Nature, 538, 499–501, https://doi.org/10.1038/nature19772, 2016.

Wilkenskjeld, S., Kloster, S., Pongratz, J., Raddatz, T., and Reick, C. H.: Comparing the influence of net and gross anthropogenic land-use and land-cover changes on the carbon cycle in the MPI-ESM, Biogeosciences, 11, 4817–4828, https://doi.org/10.5194/bg-11-4817-2014, 2014.

Wiltshire, A. J., Burke, E. J., Chadburn, S. E., Jones, C. D., Cox, P. M., Davies-Barnard, T., Friedlingstein, P., Harper, A. B., Liddicoat, S., Sitch, S., and Zaehle, S.: JULES-CN: a coupled terrestrial carbon–nitrogen scheme (JULES vn5.1), 14, 2161–2186, https://doi.org/10.5194/gmd-14-2161-2021, 2021.

Winkler, K., Yang, H., Ganzenmüller, R., Fuchs, R., Ceccherini, G., Duveiller, G., Grassi, G., Pongratz, J., Bastos, A., Shvidenko, A., Araza, A., Herold, M., Wigneron, J.-P., and Ciais, P.: Changes in land use and management led to a decline in Eastern Europe's terrestrial carbon sink, Commun. Earth Environ., 4, 1–14, https://doi.org/10.1038/s43247-023-00893-4, 2023.

Woodward, F. I. and Lomas, M. R.: Vegetation dynamics – simulating responses to climatic change, Biol. Rev., 79, 643–670, https://doi.org/10.1017/S1464793103006419, 2004.

Wright, R. M., Le Quéré, C., Buitenhuis, E., Pitois, S., and Gibbons, M. J.: Role of jellyfish in the plankton ecosystem revealed using a global ocean biogeochemical model, 18, 1291–1320, https://doi.org/10.5194/bg-18-1291-2021, 2021.

Wunch, D., Wennberg, P. O., Osterman, G., Fisher, B., Naylor, B., Roehl, C. M., O'Dell, C., Mandrake, L., Viatte, C., Kiel, M., Griffith, D. W. T., Deutscher, N. M., Velazco, V. A., Notholt, J., Warneke, T., Petri, C., De Maziere, M., Sha, M. K., Sussmann, R., Rettinger, M., Pollard, D., Robinson, J., Morino, I., Uchino, O., Hase, F., Blumenstock, T., Feist, D. G., Arnold, S. G., Strong, K., Mendonca, J., Kivi, R., Heikkinen, P., Iraci, L., Podolske, J., Hillyard, P. W., Kawakami, S., Dubey, M. K., Parker, H. A., Sepulveda, E., García, O. E., Te, Y., Jeseck, P., Gunson, M. R., Crisp, D., and Eldering, A.: Comparisons of the Orbiting Carbon Observatory-2 (OCO-2) X CO2 measurements with TCCON, Atmos. Meas. Tech., 10, 2209–2238, https://doi.org/10.5194/amt-10-2209-2017, 2017.

Wunder, S., Kaimowitz, D., Jensen, S., and Feder, S.: Coronavirus, macroeconomy, and forests: What likely impacts?, For. Policy Econ., 131, 102536, https://doi.org/10.1016/j.forpol.2021.102536, 2021.

Xi, F., Davis, S. J., Ciais, P., Crawford-Brown, D., Guan, D., Pade, C., Shi, T., Syddall, M., Lv, J., Ji, L., Bing, L., Wang, J., Wei, W., Yang, K.-H., Lagerblad, B., Galan, I., Andrade, C., Zhang, Y., and Liu, Z.: Substantial global carbon uptake by cement carbonation, Nature Geosci, 9, 880–883, https://doi.org/10.1038/ngeo2840, 2016.

Xia, J., Chen, Y., Liang, S., Liu, D., and Yuan, W.: Global simulations of carbon allocation coefficients for deciduous vegetation types, Tellus B, 67, 28016, https://doi.org/10.3402/tellusb.v67.28016, 2015.

Xia, X., Ren, P., Wang, X., Liu, D., Chen, X., Dan, L., He, B., He, H., Ju, W., Liang, M., Lu, X., Peng, J., Qin, Z., Xia, J., Zheng, B., Wei, J., Yue, X., Yu, G., Piao, S., and Yuan, W.: The carbon budget of China: 1980–2021, Science Bulletin, 69, 114–124, https://doi.org/10.1016/j.scib.2023.11.016, 2024.

Yang, D., Liu, Y., Feng, L., Wang, J., Yao, L., Cai, Z., Zhu, S., Lu, N., and Lyu, D.: The First Global Carbon Dioxide Flux Map Derived from TanSat Measurements, Adv. Atmospheric Sci., 38, 1433–1443, https://doi.org/10.1007/s00376-021-1179-7, 2021.

Yang, X., Thornton, P., Ricciuto, D., Wang, Y., and Hoffman, F.: Global evaluation of terrestrial biogeochemistry in the Energy Exascale Earth System Model (E3SM) and the role of the phosphorus cycle in the historical terrestrial carbon balance, Biogeosciences, 20, 2813–2836, https://doi.org/10.5194/bg-20-2813-2023, 2023.

Yao, Y., Joetzjer, E., Ciais, P., Viovy, N., Cresto Aleina, F., Chave, J., Sack, L., Bartlett, M., Meir, P., Fisher, R., and Luyssaert, S.: Forest fluxes and mortality response to drought: model description (ORCHIDEE-CAN-NHA r7236) and evaluation at the Caxiuanã drought experiment, Geosci. Model Dev., 15, 7809–7833, https://doi.org/10.5194/gmd-15-7809-2022, 2022.

Yao, Y., Ciais, P., Viovy, N., Joetzjer, E. and Chave, J.: How drought events during the last century have impacted biomass carbon in Amazonian rainforests. Global Change Biology, 29(3), pp.747-762, https://doi.org/10.1111/gcb.16504, 2023.

You, Y., Tian, H., Pan, S., Shi, H., Bian, Z., Gurgel, A., Huang, Y., Kicklighter, D., Liang, X.-Z., Lu, C., Melillo, J., Miao, R., Pan, N., Reilly, J., Ren, W., Xu, R., Yang, J., Yu, Q., and Zhang, J.: Incorporating dynamic crop

growth processes and management practices into a terrestrial biosphere model for simulating crop production in the United States: Toward a unified modeling framework, Agricultural and Forest Meteorology, 325, 109144, https://doi.org/10.1016/j.agrformet.2022.109144, 2022.

Yu, Z., Ciais, P., Piao, S., Houghton, R. A., Lu, C., Tian, H., Agathokleous, E., Kattel, G. R., Sitch, S., Goll, D., Yue, X., Walker, A., Friedlingstein, P., Jain, A. K., Liu, S., and Zhou, G.: Forest expansion dominates China's land carbon sink since 1980, Nat. Commun., 13, 5374, https://doi.org/10.1038/s41467-022-32961-2, 2022.

Yue, X. and Unger, N.: The Yale Interactive terrestrial Biosphere model version 1.0: description, evaluation and implementation into NASA GISS ModelE2, Geosci. Model Dev., 8, 2399–2417, https://doi.org/10.5194/gmd-8-2399-2015, 2015.

Yue, X., Zhou, H., Tian, C., Ma, Y., Hu, Y., Gong, C., Zheng, H., and Liao, H.: Development and evaluation of the interactive Model for Air Pollution and Land Ecosystems (iMAPLE) version 1.0, Geosci. Model Dev., 17, 4621–4642, https://doi.org/10.5194/gmd-17-4621-2024, 2024.

Yuan, W., Liu, D., Dong, W., Liu, S., Zhou, G., Yu, G., Zhao, T., Feng, J., Ma, Z., Chen, J., Chen, Y., Chen, S., Han, S., Huang, J., Li, L., Liu, H., Liu, S., Ma, M., Wang, Y., Xia, J., Xu, W., Zhang, Q., Zhao, X., and Zhao, L.: Multiyear precipitation reduction strongly decreases carbon uptake over northern China, J. Geophys. Res.-Biogeo., 119, 881–896, https://doi.org/10.1002/2014JG002608, 2014.

Yue, C., Ciais, P., Zhu, D., Wang, T., Peng, S. S., and Piao, S. L.: How have past fire disturbances contributed to the current carbon balance of boreal ecosystems?, Biogeosciences, 13, 675–690, https://doi.org/10.5194/bg-13-675-2016, 2016.

Zaehle, S. and Friend, A. D.: Carbon and nitrogen cycle dynamics in the O-CN land surface model: 1. Model description, site-scale evaluation, and sensitivity to parameter estimates: Site-scale evaluation of a C-N model, Global Biogeochem. Cycles, 24, GB1005, https://doi.org/10.1029/2009GB003521, 2010.

Zaehle, S., Ciais, P., Friend, A. D., and Prieur, V.: Carbon benefits of anthropogenic reactive nitrogen offset by nitrous oxide emissions, Nature Geosci, 4, 601–605, https://doi.org/10.1038/ngeo1207, 2011.

Zaehle, S., Medlyn, B. E., De Kauwe, M. G., Walker, A. P., Dietze, M. C., Hickler, T., Luo, Y., Wang, Y.-P., El-Masri, B., Thornton, P., Jain, A., Wang, S., Warlind, D., Weng, E., Parton, W., Iversen, C. M., Gallet-Budynek, A., McCarthy, H., Finzi, A., Hanson, P. J., Prentice, I. C., Oren, R., and Norby, R. J.: Evaluation of 11 terrestrial carbon–nitrogen cycle models against observations from two temperate Free-Air CO2 Enrichment studies, New Phytol., 202, 803–822, https://doi.org/10.1111/nph.12697, 2014.

Zeng, J., Iida, Y., Matsunaga, T., and Shirai, T.: Surface ocean CO2 concentration and air-sea flux estimate by machine learning with modelled variable trends, Front. Mar. Sci., 9, https://doi.org/10.3389/fmars.2022.989233, 2022.

Zheng, B., Ciais, P., Chevallier, F., Chuvieco, E., Chen, Y., and Yang, H.: Increasing forest fire emissions despite the decline in global burned area, Sci. Adv., 7, eabh2646, https://doi.org/10.1126/sciadv.abh2646, 2021.

Zhu, Y., Xia, X., Canadell, J. G., Piao, S., Lu, X., Mishra, U., Wang, X., Yuan, W., and Qin, Z.: China's carbon sinks from land-use change underestimated, Nat. Clim. Chang., 15, 428–435, https://doi.org/10.1038/s41558-025-02296-z, 2025.

Zou, Y., Wang, Y., Ke, Z., Tian, H., Yang, J., and Liu, Y.: Development of a REgion-Specific Ecosystem Feedback Fire (RESFire) Model in the Community Earth System Model, J. Adv. Model. Earth Syst., 11, 417–445, https://doi.org/10.1029/2018MS001368, 2019.

Zscheischler, J., Mahecha, M. D., Avitabile, V., Calle, L., Carvalhais, N., Ciais, P., Gans, F., Gruber, N., Hartmann, J., Herold, M., Ichii, K., Jung, M., Landschützer, P., Laruelle, G. G., Lauerwald, R., Papale, D., Peylin, P., Poulter, B., Ray, D., Regnier, P., Rödenbeck, C., Roman-Cuesta, R. M., Schwalm, C., Tramontana, G., Tyukavina, A., Valentini, R., van der Werf, G., West, T. O., Wolf, J. E., and Reichstein, M.: Reviews and syntheses: An empirical spatiotemporal description of the global surface–atmosphere carbon fluxes: opportunities and data limitations, Biogeosciences, 14, 3685–3703, https://doi.org/10.5194/bg-14-3685-2017, 2017.

Tables

Table 1. Factors used to convert carbon in various units (by convention, Unit 1 = Unit 2 × conversion).

Unit 1	Unit 2	Conversion	Source
GtC (gigatonnes of carbon)	ppm (parts per million) (a)	2.124 (b)	Ballantyne et al. (2012)
GtC (gigatonnes of carbon)	PgC (petagrams of carbon)	1	SI unit conversion
GtCO2 (gigatonnes of carbon dioxide)	GtC (gigatonnes of carbon)	3.664	44.01/12.011 in mass equivalent
(a) Measurements of atmospheric CO_2 concentration have units of dry-air mole fraction. 'ppm' is an abbreviation for micromole/mol, dry air.			
(b) The use of a factor of 2.124 assumes that all the atmosphere is well mixed within one year. In reality, only the troposphere is well mixed and the growth rate of CO_2 concentration in the less well-mixed stratosphere is not measured by sites from the NOAA network. Using a factor of 2.124 makes the approximation that the growth rate of CO_2 concentration in the stratosphere equals that of the troposphere on a yearly basis.			

Table 2. How to cite the individual components of the global carbon budget presented here.

Component	**Primary reference**
Global fossil CO_2 emissions (EFOS), total and by fuel type	Andrew and Peters (2025)
National territorial fossil CO_2 emissions (EFOS)	Erb and Marland (2025), UNFCCC (2022)
National consumption-based fossil CO_2 emissions (EFOS) by country (consumption)	Peters et al. (2011a) updated as described in this paper
Net land-use change flux (ELUC)	This paper (see Table 4 for individual model references).
Growth rate in atmospheric CO_2 concentration (GATM)	Lan et al. (2025)
Ocean and land CO_2 sinks (SOCEAN and SLAND)	This paper (see Table 4 for individual model and data products references).

Table 3. Main methodological changes in the global carbon budget this year (GCB2025). Empty cells mean there were no methodological changes introduced that year. Table S10 lists methodological changes from the first global carbon budget publication up to 2024.

Fossil fuel emissions		**LUC emissions**	**Reservoirs**			**Other changes**
Global	Country (territorial)		Atmosphere	Ocean	Land	
	Projection available for Japan for the first time	Bookkeeping estimates derived from models that estimate ELUC based on transient carbon densities responding to environmental changes (BLUE, OSCAR, LUCE).	Include an assessment of satellite-derived growth rates	Adjustments applied for known underestimation of GOBMs and cool surface skin effect in fCO2-product. Suspension of 19 ocean data sets from SOCAT.	Include the RSS adjustment.	

Table 4. References for the process models, bookkeeping models, ocean data products, and atmospheric inversions. All models and products are updated with new data to the end of year 2024.

Model/data name	Reference	Change from Global Carbon Budget 2024 (Friedlingstein et al., 2025a)
Bookkeeping models for land-use change emissions		
BLUE	Hansis et al. (2015)	Transient C densities used to estimate ELUC
OSCAR	Gasser et al. (2020)	No change
LUCE	Qin et al. (2024)	Transient C densities used to estimate ELUC
Dynamic global vegetation models		
CABLE-POP	Haverd et al. (2018)	corrected N deposition input data, minor parameter changes
CLASSIC	Melton et al. (2020), Gauthier et al. (2025), Kou-Giesbrecht and Arora (2022)	
CLM6.0	Lawrence et al. (2019)	New dust scheme, new BGC fire method, updates to MEGAN for BVOCs, parameter updates, new surface datasets, new N fixation method
CLM-FATES	Fisher et al. (2015), Koven et al. (2020)	New model
DLEM	Tian et al. (2015), You et al. (2022)	No change
EDv3	Moorcroft et al. (2001), Ma et al. (2022)	Updated meteorology inputs (i.e. hourly air temperature)
ELM	Yang et al.(2023), Burrows et al.(2020)	No change
ELM-FATES	Fisher et al. (2015), Koven et al. (2020), Needham et al. (2025)	New model
GDSTEM	Felzer et al. (2009), Felzer et al. (2011), Felzer (2012), Felzer and Jiang (2018)	New model
IBIS	Xia et al., (2024)	No change
iMAPLE	Yue et al. (2024)	No change.

ISAM	Jain et al. (2013), Meiyappan et al. (2015), Shu et al. (2020)	Vertically resolved soil biogeochemistry (carbon and nitrogen) module, following Shu et al. (2020)
JSBACH	Mauritsen et al. (2019), Reick et al. (2021)	No change
JULES-ES	Wiltshire et al. (2021), Sellar et al. (2019), Burton et al. (2019)	Minor updates to wildfire parameters
LPJ-GUESS	Smith et al. (2014)	Wood harvest without the LUH2 secondary mature, young, and non-forest harvest fraction info
LPJmL	Schaphoff et al. (2018), von Bloh et al. (2018), Lutz et al., (2019), Heinke et al. (2023)	Switch from version 5.7.5 to 5.10.0 incorporating updates to soil temperature scheme, revised N demand and N uptake processes, revised tree phenology, as well as bugfixes and code improvements
LPJ-EOSIM	Poulter et al. (2011) (d)	Incorporation of new respiration temperature responses and leaf respiration acclimation, updated the soil temperature and water scheme to have 8 layers
LPX-Bern	Lienert and Joos (2018)	No change
ORCHIDEEv3	Krinner et al. (2005), Zaehle and Friend (2010), Vuichard et al. (2019)	No change
SDGVM	Woodward and Lomas (2004), Walker et al. (2017)	Reverted to version used in Friedlingstein et al. (2022), but retaining the recent bug fix to monthly heterotrophic respiration output
VISIT	Ito and Inatomi (2012), Kato et al. (2013)	No change
VISIT-UT	Ito (2019)	New model
Intermediate complexity land carbon cycle model		
CARDAMOM	Bloom et al. (2016), Smallman et al. (2021)	Analysis resolution increased from 1 x1 to 0.5x0.5 degree. Estimates of fAPAR from MODIS collection 6.1. New prior constraint on the leaf carbon per unit area parameter (LCA). MODIS burned area forcing was replaced by GFEDv5 burned area estimate
Global ocean biogeochemistry models		
NEMO-PlankTOM12	Wright et all (2021)	No change
NEMO4.2-PISCES (IPSL)	Aumont et al. (2015)	No change to the model version, but switch to ERA5 forcing - A,B,C,D simulations have been re-run starting from GCB2024 simulation restart fields from 1940 onwards
MICOM-HAMOCC (NorESM1-OCv1.2)	Schwinger et al. (2016)	No change, model has been re-run to provide monthly CFC/SF_6 outputs
MPIOM-	Lacroix et al. (2021)	No change

HAMOCC6		
NEMO3.6-PISCESv2-gas (CNRM)	Berthet et al. (2019), Séférian et al. (2019)	Updated simulations using 1750 preindustrial conditions instead of 1850. No change in model configuration, except nudging of surface ocean fields applied to minimize the change of atm forcing. The methodology used is based on Sanchez-Gomez et al. (2024)
FESOM2.1-REcoM3	Gürses et al. (2023)	Switched to ERA5 forcing - A,B,C,D simulations have been re-run starting from GCB2024 simulation restart fields
MOM6-COBALTv3 (Princeton)	Stock et al., (2025)	New model configuration MOM6-COBALTv3 with ~1° horizontal resolution (360x210). 1) updated ocean biogeochemical module COBALTv3 with an additional fixed nitrogen removal process - anaerobic ammonium oxidation (anammox); 2) updated air-sea gas exchange scheme - wind-wave-bubble formulation; 3) updated riverine carbon and nutrient inputs following R2OMIP protocol (Lacroix et al., 2024, https://zenodo.org/records/13799103); 4) updated river water discharge files.
CESM-ETHZ	Doney et al. (2009)	Compared to the 2024 submission, we changed the forcing to ERA5. To this end, a new spinup was performed, extending over 500 years.
MRI-ESM2-4	Tsujino et al. (2024), Sakamoto et al. (2023)	Iron circulation is modified according to Moore and Braucher (2008) and iron limitation on primary production is adjusted according to this change. Updated atmospheric CO2 for simulations A and C. The JRA-3Q reanalysis (Kosaka et al. 2024) is used to physically force the model. The model is spun up for 1925 years with xCO2=278ppm.
ACCESS (CSIRO)	Law et al. (2017)	No change in model since GCB2024, but switched to ERA5 forcing and extended spinup.
fCO2-products		
VLIZ-SOMFFN	Landschützer et al. (2016)	Time period extended to 2024
Jena-MLS	Rödenbeck et al. (2014) updated to Rödenbeck et al (2022)	Time period extended to 2024
CMEMS-LSCE-FFNNv2	Chau et al. (2022)	Time period extended to 2024
UExP-FNN-U	Watson et al. (2020) and Ford et al. (2024)	Updated to recalculated SOCATv2025 dataset (Ford et al. 2025). Updated salinity dataset to use a tiered approach (described in Gregor et al. 2024) including ESA CCI-SSS (v5.51) and CMEMS GLORYS12V1. Updated time period to 1980 to 2024
NIES-ML3	Zeng et al. (2022)	Time period extended to 2024.
JMA-MLR	Iida et al. (2021)	Time period extended to 2024. Updated to recalculated SOCATv2025 dataset (Ford et al. 2025)
OceanSODA-ETHZv2	Gregor et al. (2024)	Time period extended to 2024

LDEO-HPD	Gloege et al. (2022) and Bennington et al. (2022)	Time period extended to 2024
CSIR-ML6	Gregor et al. (2019)	Time period extended to 2024
Atmospheric inversions		
Jena CarboScope	Rödenbeck et al. (2018) & Stephens et al. (2007).	Slight change in station set. Numerical flux resolution 2x2. TM3 run on spatial resolution 6x4 (multiple of 2x2)
CarbonTracker Europe (CTE)	van der Laan-Luijkx et al. (2017)	Update of prior fluxes and assimilated observations.
NISMON-CO2	Niwa et al. (2022), Niwa et al. (2017).	Update of prior fluxes, specifically changed GFED to GBEI. Update of the meteorological input to JRA-3Q. Including more CO2 observations.
CT-NOAA	Jacobson et al. (2025), Byrne et al. (2023), Krol et al. (2005), Peiro et al. (2022)	New air-sea gas exchange and new terrestrial NBE (Jacobson et al., 2025). Unlike previous submissions, CT2025 uses only one set of priors.
CMS-Flux	Liu et al. (2021)	Update of prior fluxes and assimilated observations.
CAMS-Satellite	Chevallier et al. (2005) and Chevallier et al. (2025)	Update of the prior fluxes and assimilated observations.
GONGGA	Jin et al. (2024)	Update of the prior fluxes and assimilated observations.
COLA	Liu et al. (2022)	Update of the prior fluxes and assimilated observations.
GCASv2	Jiang et al. (2021) & Emmons et al. (2010)	Update of the prior fluxes and assimilated observations.
UoE	Feng et al. (2016) & Palmer et al. (2019)	Update of the prior fluxes and assimilated observations.
MIROC-ACTM	Chandra et al. (2022) & Patra et al. (2018)	Update of assimilated observations and prior fluxes, specifically changed to MiCASA and GFED. Update of the meteorological input to JRA-3Q.
NTFVAR	Nayagam et al. (2025) & Maksyutov et al. (2021)	Update of prior fluxes and assimilated observations.
THU	Kong et al. (2022)	New this year, after missing out 1 year. Compared to the previous submission: update of prior fluxes and assimilated observations.
NISMON-CO2_GOSAT	Niwa et al. (2022), Niwa et al. (2017).	New this year.
Earth System Models		
CanESM5	Swart et al. (2019), Sospedra-Alfonso et al. (2021)	No change
EC-Earth3-CC	Döscher et al. (2021), Bilbao et al. (2021), Bernardello et al. (2024)	No change
IPSL-CM6A-CO2-LR	Boucher et al. (2020)	No change
MIROC-ES2L	Watanabe et al. (2020)	No change

MPI-ESM1-2-LR	Mauritsen et al. (2019), Li et al. (2023)	No change
NorCPM-CC	Tjiputra et al. (2020), Bethke et al. (2021)	New this year.

8

Table 5. Comparison of results from the bookkeeping method and budget residuals with results from the DGVMs, as well as additional estimates from atmospheric oxygen, atmospheric inversions and Earth System Models (ESMs) for different periods, the last decade, and the last year available. All values are in GtC yr^{-1}. The best estimate for GCB2025 (E_{LUC}) is calculated with the bookkeeping models (1a) and used in the budget Table 7, see Section 2 and Figure 7 for description of the bookkeeping component fluxes. The best estimate for GCB2025 (S_{LAND}) is calculated with the DGVMs including the RSS correction (2b), and used in the budget Table 7. The DGVM uncertainties represent ±1σ of the decadal or annual (for 2024) estimates from the individual DGVMs. For the inverse systems the mean and range of available results is given when the number of systems is less than 10, otherwise the ±1σ is provided. All values are rounded to the nearest 0.1 GtC and therefore columns do not necessarily add to zero.

Mean (GtC yr^{-1})

		1960s	1970s	1980s	1990s	2000s	2010s	2015-2024	2024
Land-use change emissions (E_{LUC})	Bookkeeping (BK) Net flux (1a)	1.9±0.7	1.7±0.7	1.7±0.7	1.7±0.7	1.7±0.7	1.6±0.7	1.4±0.7	1.3±0.7
	BK - deforestation (total)	1.8 [1.6,2.1]	1.8 [1.6,2.1]	1.7 [1.5,1.9]	1.9 [1.6,2.1]	2 [1.7,2.2]	2 [1.6,2.4]	1.9 [1.5,2.3]	1.9 [1.4,2.4]
	BK - forest regrowth (total)	-0.9 [-1,-0.7]	-0.9 [-1,-0.8]	-0.9 [-1,-0.8]	-1 [-1.1,-0.8]	-1.1 [-1.2,-0.9]	-1.3 [-1.4,-1]	-1.3 [-1.5,-1]	-1.3 [-1.6,-1]
	BK - other transitions	0.3 [0.3,0.3]	0.2 [0.2,0.3]	0.2 [0.1,0.3]	0.1 [0.1,0.2]	0.1 [0,0.1]	0.2 [0.1,0.2]	0.1 [0.1,0.1]	0.1 [0.1,0.1]
	BK - peat drainage & peat fires	0.2 [0.1,0.2]	0.2 [0.1,0.2]	0.2 [0.2,0.2]	0.3 [0.2,0.3]	0.2 [0.2,0.3]	0.3 [0.3,0.3]	0.2 [0.2,0.3]	0.2 [0.2,0.2]
	BK - wood harvest & forest management	0.4 [0.1,0.6]	0.4 [0.1,0.6]	0.5 [0.1,0.7]	0.5 [0.1,0.7]	0.5 [0.1,0.7]	0.4 [0.1,0.7]	0.4 [0.1,0.7]	0.4 [0.1,0.7]
	DGVMs-net flux (1b)	1.3±0.5	1.2±0.5	1.2±0.5	1.2±0.5	1.2±0.6	1.1±0.6	1±0.6	0.9±0.5
Terrestrial sink (S_{LAND})	Residual sink from global budget (E_{FOS}+E_{LUC}(1a)-G_{ATM}-S_{OCEAN}) (2a)	1.9±0.8	2±0.8	1.7±0.9	2.6±0.9	2.9±0.9	3±0.9	2.4±0.9	0.3±1
	DGVMs (2b)	0.9±0.3	1.6±0.5	1.4±0.6	2±0.5	2.2±0.6	2.5±0.7	2.4±0.8	1.9±0.9
Net land fluxes (S_{LAND}-E_{LUC})	GCB2025 Budget (2b-1a)	-0.9±0.8	-0.1±0.9	-0.3±0.9	0.2±0.9	0.5±0.9	0.9±1	1±1	0.7±1.1
	Atmospheric O_2	---	---	---	1.3±0.6	0.9±0.7	1±0.8	0.7±0.8	-

		1960s	1970s	1980s	1990s	2000s	2010s	2015-2024	2024
	DGVMs-net (2b-1b)	-0.3±0.4	0.4±0.6	0.2±0.5	0.8±0.4	1±0.4	1.4±0.6	1.4±0.7	1.1±0.8
	Inversions*	- [-,-]	- [-,-]	- [-,-]	0.7 [0.6,0.8] (2)	1.4 [1.3,1.6] (3)	1.5 [1.3,2.3] (8)	1.3±0.3 (14)	0.2±0.7 (14)
	ESMs	0 [-0.7,0.5]	1.5 [1.2,2]	1.1 [0.5,1.4]	1.8 [1.2,2.4]	1.8 [0.4,2.7]	2 [0.7,3]	2.3 [-0.1,3.6]	0.8 [-2.9-3.3]

*Estimates are adjusted for the pre-industrial influence of river fluxes, for the cement carbonation sink, and adjusted to common EFOS (Sect. 2.7). The ranges given include varying numbers (in parentheses) of inversions in each decade (Table S4)

20

Table 6: Comparison of results for the un-adjusted ocean sinks from the fCO_2-products, from global ocean biogeochemistry models (GOBMs), the best estimate for GCB2025 (adjusted S_{OCEAN}) calculated from fCO_2-products and GOBMs) and used in the budget Table 7, as well as additional estimates from ocean interior observation-based changes in the dissolved inorganic carbon (DIC) inventory, atmospheric oxygen, atmospheric inversions and Earth System Models (ESMs) for different periods, the last decade, and the last year available. All values are in GtC yr^{-1}. Uncertainties represent ±1σ of the estimates from the GOBMs and inversions (n>10) and range of ensemble members is given for ensembles with n<10 (fCO_2-products, inversions, ocean interior, ESMs). The uncertainty of the GCB2025 budget estimate is based on expert judgement (Section 2 and Supplement S1 to S4) and for oxygen it is the standard deviation of a Monte Carlo ensemble (Section 2.8). Note that adjustments were applied to the fCO_2-products and two of the ocean interior estimates to match the definition of S_{OCEAN} (see section 2.5.1 and S3.6).

Mean (GtC yr^{-1})

Product	1960s	1970s	1980s	1990s	2000s	2010s	2015-2024	2024
GCB2025 Budget	1.3±0.4	1.6±0.4	2.1±0.4	2.3±0.4	2.6±0.4	3.1±0.4	3.2±0.4	3.4±0.4
fCO_2-products	---	---	---	2.3 [2,3]	2.5 [2.4,2.9]	3.1 [2.9,3.5]	3.3 [2.9,3.9]	3.5 [2.8,4.2]
GOBMs	1.1±0.2	1.3±0.3	1.8±0.3	2.0±0.3	2.2±0.3	2.6±0.3	2.7±0.3	2.9±0.3
Atmospheric O_2	---	---	---	2.0±0.4	2.8±0.4	3.4±0.5	3.5±0.5	-
Inversions	- [-,-]	- [-,-]	- [-,-]	2.4 [2.2,2.5] (2)	2.3 [2.2,2.4] (3)	2.9 [2.1,3.1] (8)	3±0.3 (14)	3±0.4 (14)
Ocean interior	1.1 [-,-]	1.3 [-,-]	1.8 [-,-]	2.1 [2,2.3]	2.2 [1.7,2.5]	3.3 [2.7,4]	---	-
ESMs	0.7 [0.1,1.1]	1 [0.4,1.4]	1.5 [0.7,2]	1.7 [1.1,2.1]	1.9 [1.5,2.2]	2.4 [2,2.7]	2.5 [2.2,2.8]	2.6 [2.2-3.1]

Table 7: Decadal mean in the five components of the anthropogenic CO_2 budget for different periods, and last year available. All values are in GtC yr^{-1}, and uncertainties are reported as ±1σ. Fossil CO_2 emissions include cement carbonation. The table also shows the budget imbalance (B_{IM}), which provides a measure of the discrepancies among the nearly independent estimates. A positive imbalance means the emissions are overestimated and/or the sinks are too small. All values are rounded to the nearest 0.1 GtC and therefore columns do not necessarily add to zero.

Mean (GtC yr^{-1})

		1960s	1970s	1980s	1990s	2000s	2010s	2015-2024	2024	2025 (Projection)
Total emissions (E_{FOS} + E_{LUC})	Fossil CO2 emissions (E_{FOS})*	3±0.2	4.7±0.2	5.4±0.3	6.4±0.3	7.8±0.4	9.5±0.5	9.8±0.5	10.3±0.5	10.4±0.5
	Land-use change emissions (E_{LUC})	1.9±0.7	1.7±0.7	1.7±0.7	1.7±0.7	1.7±0.7	1.6±0.7	1.4±0.7	1.3±0.7	1.1±0.7
	Total emissions	4.9±0.7	6.4±0.7	7.1±0.8	8.1±0.8	9.5±0.8	11.1±0.8	11.2±0.9	11.6±0.9	11.5±0.9
Partitioning	Growth rate in atmos CO2 (G_{ATM})	1.7±0.07	2.8±0.07	3.4±0.02	3.1±0.02	4±0.02	5.1±0.02	5.6±0.02	7.9±0.2	4.9±0.2
	Ocean sink (S_{OCEAN})	1.3±0.4	1.6±0.4	2.1±0.4	2.3±0.4	2.6±0.4	3.1±0.4	3.2±0.4	3.4±0.4	3.2±0.4
	Terrestrial sink (S_{LAND})	0.9±0.3	1.6±0.5	1.4±0.6	2±0.5	2.2±0.6	2.5±0.7	2.4±0.8	1.9±0.9	3.4±1
Budget Imbalance	BIM= E_{FOS}+ E_{LUC}- (G_{ATM} +S_{OCEA}	0.9	0.5	0.3	0.7	0.7	0.4	0	-1.7	

	1960s	1970s	1980s	1990s	2000s	2010s	2015-2024	2024	2025 (Projection)
$_{N}$+S$_{LAND}$)									

*Fossil emissions excluding the cement carbonation sink amount to 3±0.2 GtC yr^{-1}, 4.7±0.2 GtC yr^{-1}, 5.5±0.3 GtC yr^{-1}, 6.4±0.3 GtC yr^{-1}, 7.9±0.4 GtC yr^{-1}, and 9.7±0.5 GtC yr^{-1} for the decades 1960s to 2010s respectively and to 10±0.5 GtC yr^{-1} for 2024, and 10.5±0.5 GtC yr^{-1} for 2025.

41

Table 8. Cumulative CO_2 for different time periods in gigatonnes of carbon (GtC). Fossil CO_2 emissions include cement carbonation. The budget imbalance (B_{IM}) provides a measure of the discrepancies among the nearly independent estimates. All values are rounded to the nearest 5 GtC and therefore columns do not necessarily add to zero. Uncertainties are reported as follows: E_{FOS} is 5% of cumulative emissions; E_{LUC} prior to 1959 is 1σ spread from the DGVMs, E_{LUC} post-1959 is 0.7*number of years (where 0.7 GtC yr^{-1} is the uncertainty on the annual E_{LUC} flux estimate); G_{ATM} uncertainty is held constant at 5 GtC for all time periods; S_{OCEAN} uncertainty is 20% of the cumulative sink (20% relates to the annual uncertainty of 0.4 GtC yr^{-1}, which is ~20% of the current ocean sink); and S_{LAND} is the 1σ spread from the DGVMs estimates.

Mean (GtC yr^{-1})

		1750-2024	1850-2014	1850-2024	1960-2024	1850-2025
Emissions	Fossil CO2 emissions (E_{FOS})	500±25	400±20	495±25	415±20	510±25
	Land-use change emissions (E_{LUC})	280±65	235±55	250±60	110±45	250±60
	Total emissions	780±70	635±60	745±65	525±50	755±65
Partitioning	Growth rate in atmos CO2 (G_{ATM})	310±5	235±5	290±5	230±5	295±5
	Ocean sink (S_{OCEAN})	210±40	170±35	200±40	145±30	205±40
	Terrestrial sink (S_{LAND})	190±50	150±40	175±50	120±30	175±50
Budget imbalance	BIM=E_{FOS}+E_{LUC}-(G_{ATM}+S_{OCEAN}+S_{LAND})	65	80	80	35	80

Table 9. Average annual growth rate in fossil CO_2 emissions over the most recent decade (2015-2024) and the previous decade (2005-2014). The data for the World include the cement carbonation sink. IAS are emissions from international aviation and shipping. The rest of the world is defined as World minus China, USA, India, EU27, and IAS.

	World	China	USA	India	EU27	OECD	Non-OECD	IAS	Rest of the World
2005-2014	2.1%	6.7%	-1.4%	6.4%-	2.2%	-1.0%	4.6%	1.9%	1.8%
2015-2024	0.8%	2.5%	-1.2%	3.6%	-2.5%	-1.5%	2.1%	-1.4%	0.6%

Table 10. Major known sources of uncertainties in each component of the Global Carbon Budget, defined as input data or processes that have a demonstrated effect of at least ±0.3 GtC yr^{-1}.

Source of uncertainty	Time scale (years)	Location	Evidence
Fossil CO2 emissions (EFOS; Section 2.1)			
energy statistics	annual to decadal	global, but mainly China & major developing countries	(Korsbakken et al., 2016, Guan et al., 2012)
carbon content of coal	annual to decadal	global, but mainly China & major developing countries	(Liu et al., 2015)
system boundary	annual to decadal	all countries	(Andrew, 2020a)
Net land-use change flux (ELUC; section 2.2)			
land-cover and land-use change statistics	continuous	global; in particular tropics	(Houghton et al., 2012, Gasser et al., 2020, Ganzenmüller et al., 2022, Yu et al. 2022)
sub-grid-scale transitions	annual to decadal	global	(Wilkenskjeld et al., 2014, Bastos et al., 2021)
vegetation biomass	annual to decadal	global; in particular tropics	(Houghton et al., 2012, Bastos et al., 2021)
forest degradation (fire, selective logging)	annual to decadal	tropics; Amazon	(Aragão et al., 2018, Qin et al., 2021, Lapola et al., 2023)
wood and crop harvest	annual to decadal	global; SE Asia	(Arneth et al., 2017, Erb et al., 2018)
peat burning	multi-decadal trend	global	(van der Werf et al., 2010, 2017)
Atmospheric growth rate (GATM; section 2.4) no demonstrated uncertainties larger than ±0.3 GtC yr-1 . The uncertainties in annual GATM have been estimated as ±0.2 GtC yr-1, although the conversion of the growth rate into a global annual flux assuming instantaneous mixing throughout the atmosphere introduces additional errors (see Section 2.4.2).			
Ocean sink (SOCEAN; section 2.5)			
sparsity in surface fCO2 observations	mean, decadal variability and trend	global, in particular southern hemisphere	(Gloege et al., 2021, Denvil-Sommer et al., 2021, Hauck et al., 2023a; Dong et al., 2024b)

riverine carbon outgassing and its anthropogenic perturbation	annual to decadal	global, in particular partitioning between Tropics and South	(Aumont et al., 2001, Lacroix et al., 2020, Crisp et al., 2022)
Models underestimate interior ocean anthropogenic carbon storage	annual to decadal	global	(Friedlingstein et al., 2022a, this study, DeVries et al., 2023, Müller et al., 2023)
near-surface temperature and salinity gradients	mean on all time-scales	global	(Watson et al., 2020, Dong et al., 2022, Bellenger et al., 2023, Dong et al., 2024a)
Land sink (SLAND; section 2.6)			
strength of CO2 fertilisation	multi-decadal trend	global	(Wenzel et al., 2016; Walker et al., 2021)
response to variability in temperature and rainfall	annual to decadal	global; in particular tropics	(Cox et al., 2013; Jung et al., 2017; Humphrey et al., 2018; 2021)
nutrient limitation and supply	annual to multi-decadal	global	(Zaehle et al., 2014)
carbon allocation and tissue turnover rates	annual to decadal	global	(De Kauwe et al., 2014; O'Sullivan et al., 2022)
tree mortality	annual	global in particular tropics	(Hubau et al., 2021; Brienen et al., 2020)
response to diffuse radiation	annual	global	(Mercado et al., 2009; O'Sullivan et al., 2021)

63

64

Figures

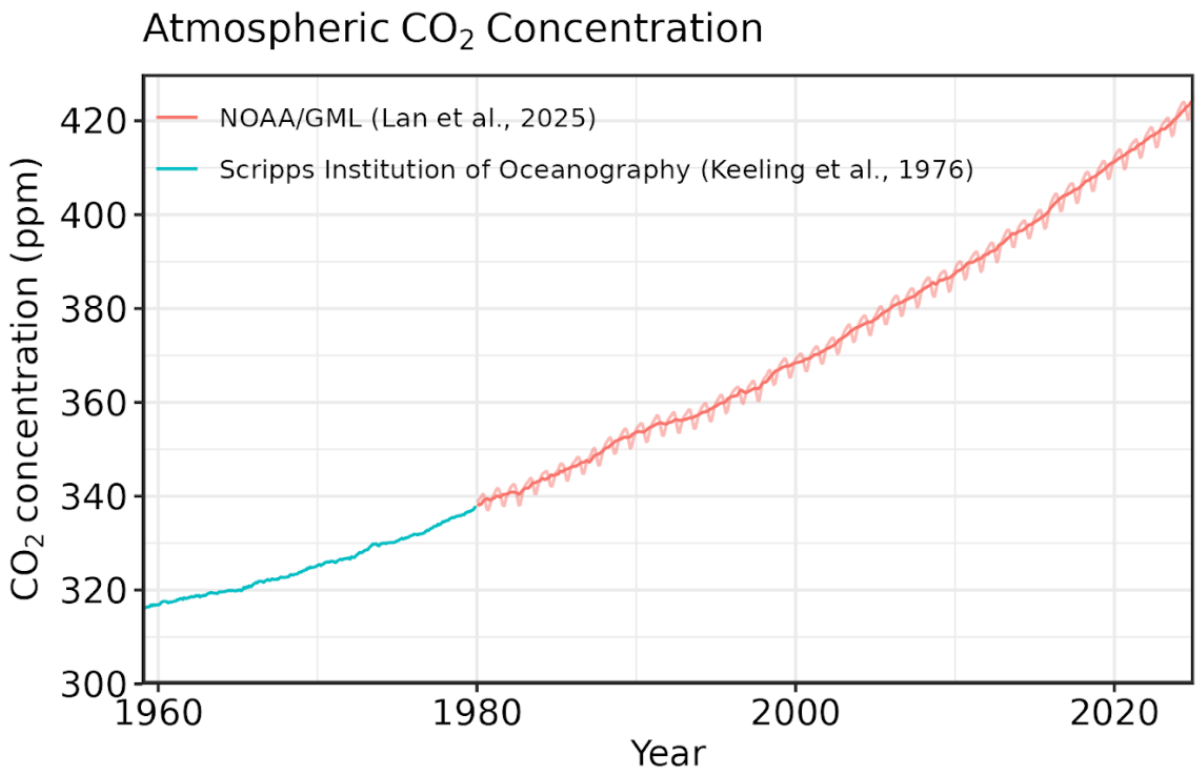

Figure 1. Surface average atmospheric CO_2 concentration (ppm). Since 1980, monthly data are from NOAA/GML (Lan et al., 2025) and are based on an average of direct atmospheric CO_2 measurements from multiple stations in the marine boundary layer (Masarie and Tans, 1995). The 1958-1979 monthly data are from the Scripps Institution of Oceanography, based on an average of direct atmospheric CO_2 measurements from the Mauna Loa and South Pole stations (Keeling et al., 1976). To account for the difference of mean CO_2 and seasonality between the NOAA/GML and the Scripps station networks used here, the Scripps surface average (from two stations) was de-seasonalised and adjusted to match the NOAA/GML surface average (from multiple stations) by adding the mean difference of 0.667 ppm, calculated here from overlapping data during 1980-2012.

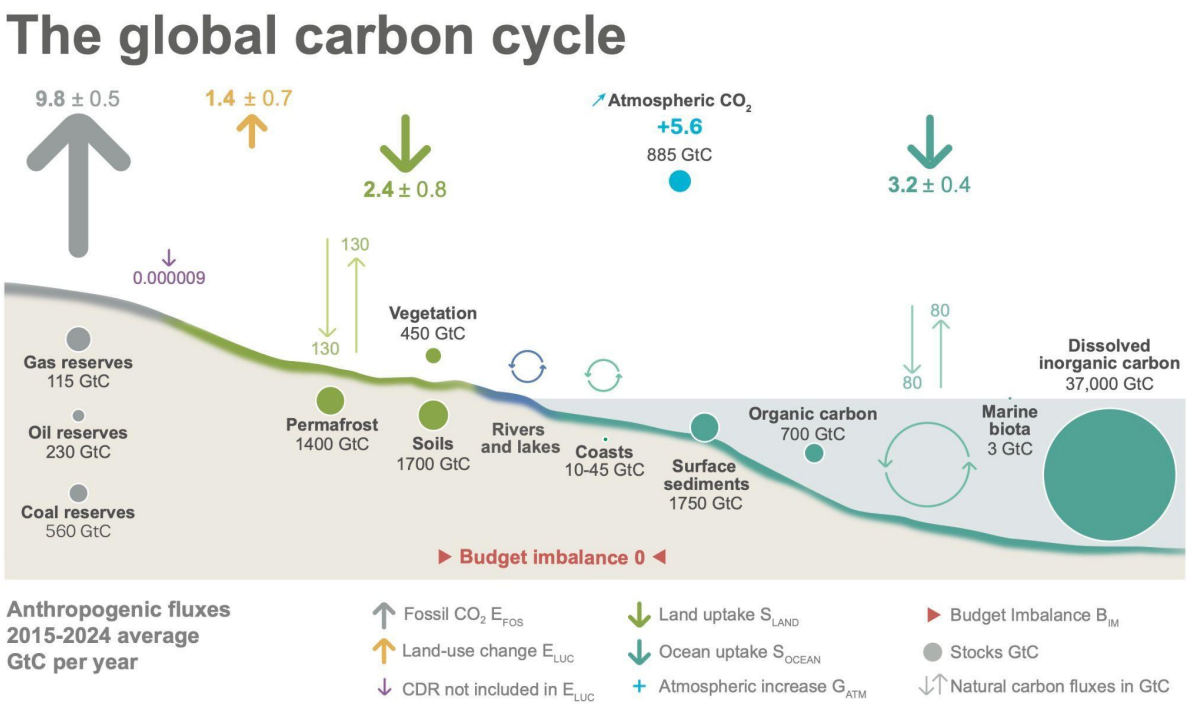

Figure 2. Schematic representation of the overall perturbation of the global carbon cycle caused by anthropogenic activities, averaged globally for the decade 2015-2024. See legends for the corresponding arrows. Fluxes estimates and their 1 standard deviation uncertainty are as reported in Table 7. The CDR estimate is for the year 2024. The uncertainty in the atmospheric CO_2 growth rate is very small (±0.02 GtC yr^{-1}) and is neglected for the figure. The anthropogenic perturbation occurs on top of an active carbon cycle, with fluxes and stocks represented in the background and taken from Canadell et al. (2021) for all numbers, except for the carbon stocks in coasts which is from a literature review of coastal marine sediments (Price and Warren, 2016). Fluxes are in GtC yr^{-1} and reservoirs in GtC. This figure was produced by Nigel Hawtin.

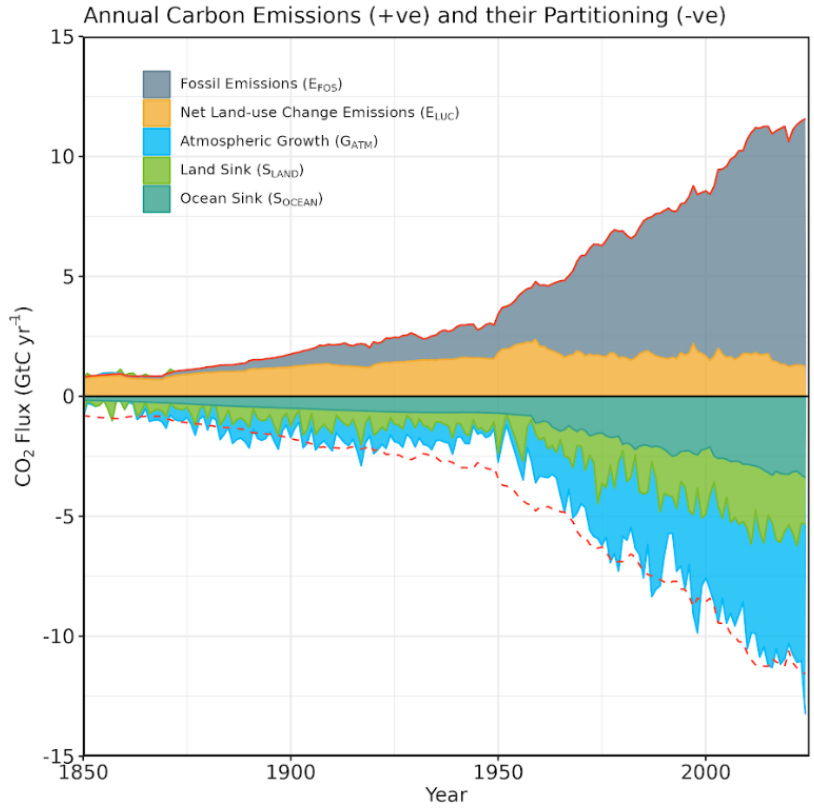

Figure 3. Combined components of the global carbon budget as a function of time, for fossil CO_2 emissions (E_{FOS}, including a small sink from cement carbonation; grey) and emissions from land-use change (E_{LUC}; brown), as well as their partitioning among the atmosphere (G_{ATM}; cyan), ocean (S_{OCEAN}; blue), and land (S_{LAND}; green). The figure shows annual estimates of each flux (in GtC yr^{-1}) since the year 1850. The partitioning is based on nearly independent estimates from observations (for G_{ATM}) and from process model ensembles constrained by data (for S_{OCEAN} and S_{LAND}) and does not exactly add up to the sum of the emissions, resulting in a budget imbalance (B_{IM}) which is represented by the difference between the bottom red line (mirroring total emissions) and the sum of carbon fluxes in the ocean, land, and atmosphere reservoirs. The E_{FOS} estimate is based on a mosaic of different datasets and has an uncertainty of ±5% (±1σ). The E_{LUC} estimate is from three bookkeeping models (Table 4) with uncertainty of ±0.7 GtC yr^{-1}. The G_{ATM} estimates prior to 1959 are from Joos and Spahni (2008) with uncertainties equivalent to about ±0.1-0.15 GtC yr^{-1} and from Lan et al. (2025) since 1959 with uncertainties of about +-0.07 GtC yr^{-1} during 1959-1979 and ±0.02 GtC yr^{-1} since 1980. The S_{OCEAN} estimate prior to 1959 is the average from Khatiwala et al. (2013) and DeVries (2014) with uncertainty of about ±30%. After 1959, it is the average of an ensemble of models (GOBMs) and an ensemble of fCO_2-products (with adjustments, Table 4) with uncertainties of about ±0.4 GtC yr^{-1}. The S_{LAND} estimate is the average of an ensemble of models (DGVMs) (Table 4) with uncertainties of about ±1 GtC yr^{-1}. See the text for more details of each component and their uncertainties.

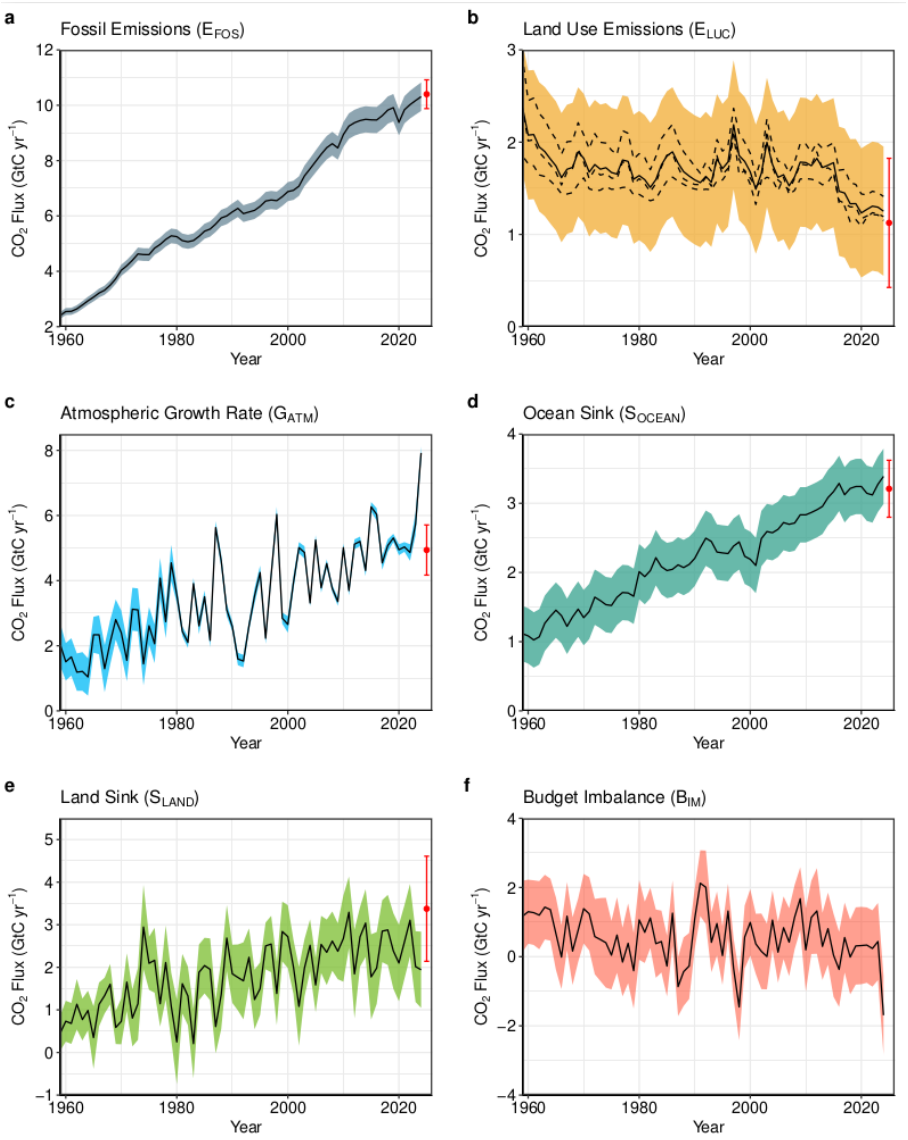

104

105 **Figure 4.** Components of the global carbon budget and their uncertainties as a function of time, presented
106 individually for (a) fossil CO_2, including cement carbonation emissions (E_{FOS}), (b) emissions from land-use
107 change (E_{LUC}), (c) growth rate in atmospheric CO_2 concentration (G_{ATM}), (d) the ocean CO_2 sink (S_{OCEAN}), (e)
108 the land CO_2 sink (S_{LAND}), (f) the budget imbalance (B_{IM}) that is not accounted for by the other terms. Individual
109 estimates from the three bookkeeping models are shown as dashed lines for E_{LUC} in panel (b). Positive values of
110 S_{LAND} and S_{OCEAN} represent a flux from the atmosphere to land or the ocean. All data are in GtC yr^{-1} with the
111 uncertainty bounds representing ±1 standard deviation in shaded colour. Data sources are as in Figure 3. The red
112 dots indicate our projections for the year 2025 and the red error bars the uncertainty in the 2025 projections (see
113 methods).

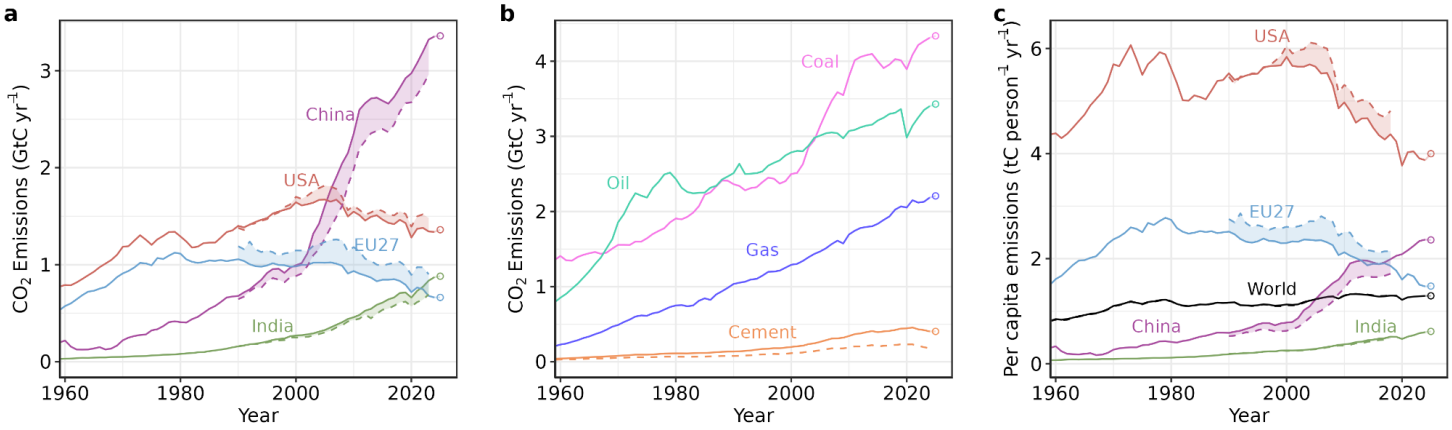

114

115 **Figure 5.** Fossil CO_2 emissions for (a) territorial (solid lines) and consumption (dashed lines) emissions for the
116 top three country emitters (USA, China, India) and for the European Union (EU27), (b) global emissions by fuel
117 type, including coal, oil, gas, and cement, and cement minus cement carbonation (dashed), and (c) per-capita
118 emissions the world and for the large emitters as in panel (a). Territorial emissions are from Andrew & Peters
119 (2025), while consumption-based emissions are updated from Peters et al. (2011a). See Section 2.1 and
120 Supplement S.1 for details of the calculations and data sources.

121

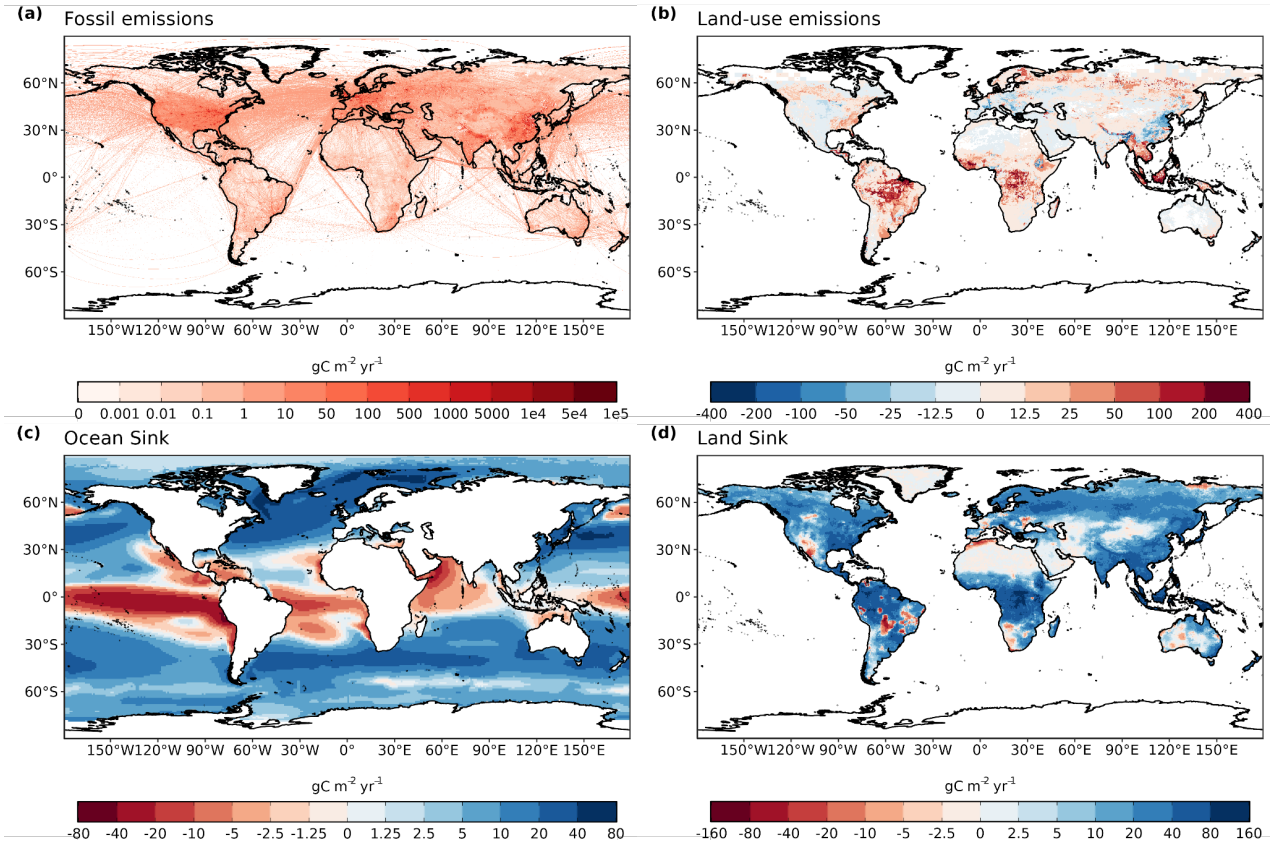

Figure 6. The 2015-2024 decadal mean components of the global carbon budget, presented for (a) fossil CO_2 emissions (E_{FOS}), (b) land-use change emissions (E_{LUC}), (c) the ocean CO_2 sink (S_{OCEAN}), and (d) the land CO_2 sink (S_{LAND}). Positive values for E_{FOS} and E_{LUC} represent a flux to the atmosphere, whereas positive values of S_{OCEAN} and S_{LAND} represent a flux from the atmosphere to the ocean or the land (carbon sink). In all panels, red colours represent a source (flux from the land/ocean to the atmosphere), blue colours represent a sink (flux from the atmosphere into the land/ocean). All units are in gC m^{-2} yr^{-1}. Note the different scales in each panel. E_{FOS} data shown is from GCP-GridFEDv2025.0 and does not include cement carbonation. The E_{LUC} map shows the average E_{LUC} from the three bookkeeping models plus emissions from peat drainage and peat fires. BLUE and LUCE provide spatially explicit estimates at 0.25° resolution. Gridded E_{LUC} estimates for OSCAR are derived by spatially distributing their national data based on the spatial patterns of BLUE gross fluxes in each country (see Schwingshackl et al., 2022, for more details about the methodology). S_{OCEAN} data shown is the average of un-adjusted GOBMs and fCO_2-products means, using GOBMs simulation A, no adjustment for bias and drift applied to the gridded fields (see Section 2.5). S_{LAND} data shown is the average of the DGVMs for simulation S2, no adjustment for bias and drift applied to the gridded fields (see Section 2.6).

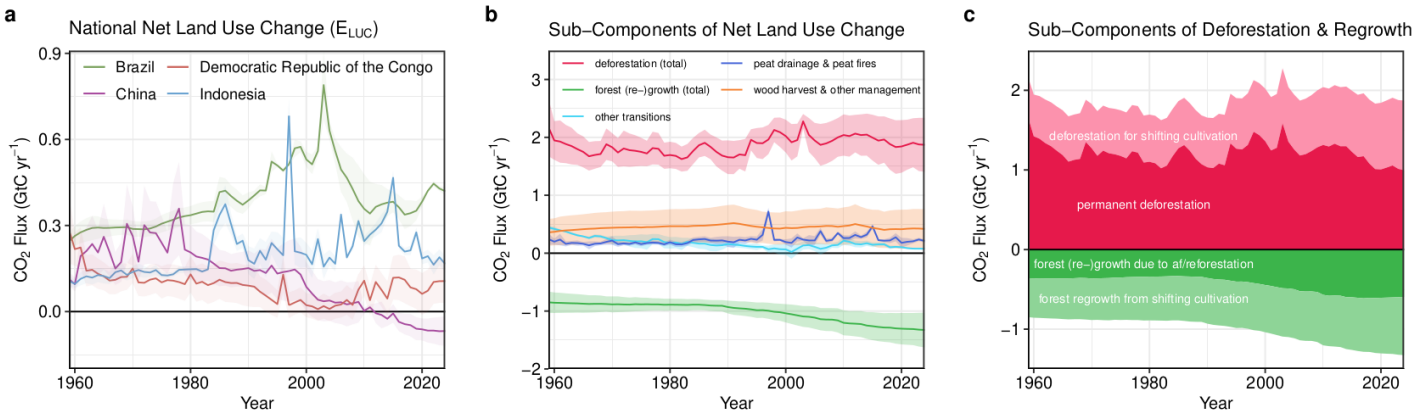

Figure 7. Net CO_2 exchanges between the atmosphere and the terrestrial biosphere related to land use change. (a) Net CO_2 emissions from land-use change from the four countries with largest cumulative emissions since 1959. Values shown are the average of the three bookkeeping models, with shaded regions as ±1σ uncertainty. (b) Sub-components of E_{LUC}: (i) emissions from deforestation (including permanent deforestation and deforestation in shifting cultivation cycles), (ii) emissions from peat drainage & peat fires, (iii) removals from forest (re-)growth (including forest (re-)growth due to afforestation and reforestation and forest regrowth in shifting cultivation cycles), (iv) fluxes from wood harvest and other forest management (comprising slash and product decay following wood harvest, regrowth after wood harvest, and fire suppression), and (v) emissions and removals related to other land-use transitions. The sum of the five components is E_{LUC} shown in Figure 4b. (c) Sub-components of 'deforestation (total)' and of 'forest (re-)growth (total)': (i) deforestation in shifting cultivation cycles, (ii) permanent deforestation, (iii) forest (re-)growth due to afforestation and/or reforestation, and (iv) forest regrowth in shifting cultivation cycles.

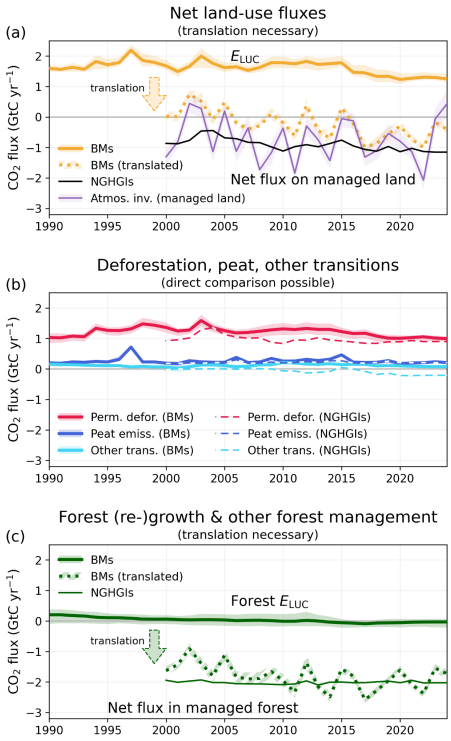

151

152 **Figure 8.** Comparison of land-use flux estimates from bookkeeping models (BMs; following the GCB
153 definition of E_{LUC}), national GHG inventories (NGHGIs; following IPCC guidelines and thus including all
154 carbon fluxes on managed land), and atmospheric inversion systems (considering fluxes on managed land only).
155 To compare BM results with NGHGIs, a translation is necessary for some subcomponents. (a) Net land-use
156 fluxes, for which a translation of BMs is necessary, (b) subcomponents permanent deforestation, peat drainage
157 & peat fires, and other transitions, which can be directly compared and (c) subcomponent forest (re-)growth &
158 other forest management, for which a translation is necessary. The lines represent the mean of 3 BMs and 14
159 atmospheric inversion estimates, respectively; Shaded areas denote the full range across BM estimates and the
160 standard deviation for atmospheric inversions, respectively. The subcomponent forest (re-)growth & other forest
161 management includes removals from forest (re-)growth (permanent), emissions and removals from wood
162 harvest & other forest management, and emissions and removals in shifting cultivation cycles. The translation of
163 BM estimates to NGHGI estimates in (a) and (c) is done by adding the natural land sink in managed forests to
164 the BM estimates (see also Table S11). The GCB definition of E_{LUC} and the NGHGI definition of land-use
165 fluxes are equally valid, each in its own context. For illustrative purposes we only show the translation of BM
166 estimates to the NGHGI definition. NGHGI data are from the LULUCF data hub V3.1 (Melo et al. 2025).

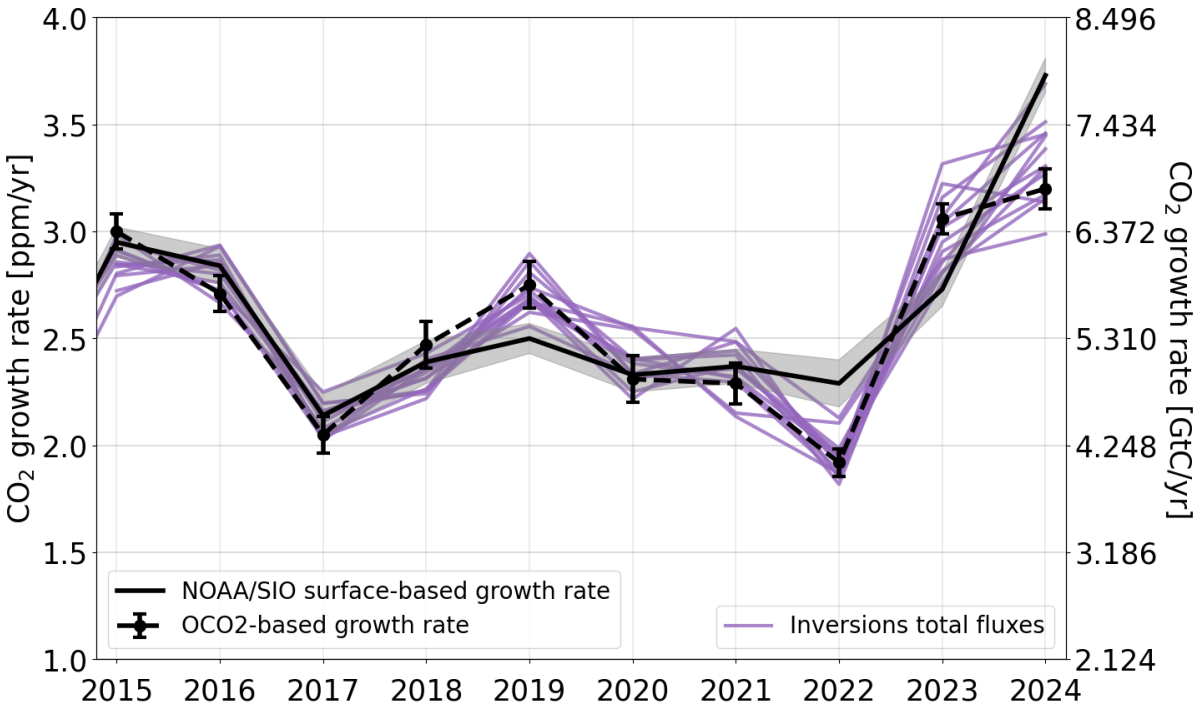

167

168 **Figure 9:** Annual atmospheric CO_2 growth rates based on observations from the surface network (by NOAA
169 (National Oceanic and Atmospheric Administration) and SIO (Scripps Institution of Oceanography), as well as
170 using the Growth Rate from Satellite Observations (GRESO) approach using OCO-2 based XCO_2 observations
171 in ppm yr^{-1} with uncertainties. To obtain G_{ATM}, the surface observation-based growth rate in units of ppm yr^{-1} is
172 converted to units of GtC yr^{-1} by multiplying by a conversion factor (CF) of 2.124 GtC per ppm, assuming
173 instantaneous mixing of CO_2 throughout the atmosphere. The purple lines are the atmospheric growth rates (in
174 GtC yr^{-1}) calculated as the sum of the fluxes derived by the atmospheric inversions. Note that the right hand axis
175 shows the growth rate in GtC yr^{-1}, with intervals of the conversion factor.

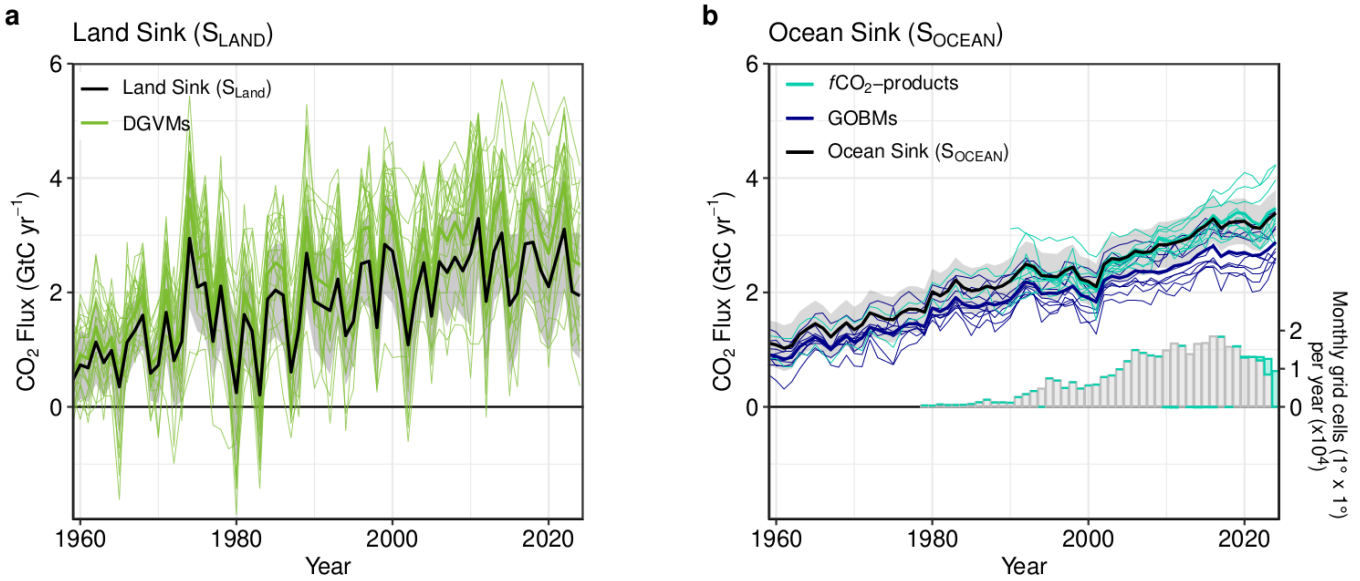

Figure 10. (a) The land CO_2 sink (S_{LAND}) estimated by individual DGVMs (thin green lines). The DGVM multi-model mean is shown as the thick green line. The S_{LAND} budget estimate (black with ±1σ uncertainty), is the DGVM multi-model mean adjusted for the RSS bias (i.e. reduced by 19%). (b) Comparison of the anthropogenic atmosphere-ocean CO_2 flux showing the budget values of S_{OCEAN} (black; with the uncertainty in grey shading), individual ocean models (royal blue), and the ocean fCO_2-products (cyan). Adjustments were applied to S_{OCEAN} (black) for the known underestimation in GOBMs and the warm layer/cool skin effect for fCO_2-products. Individual model lines as well as GOBM and fCO_2-product ensemble means (thick cyan and royal blue lines) do not include these adjustments, with the exception of 2 fCO_2-products (UExP-FNN-U and JMA-MLR) that include temperature corrections as part of their air-sea CO_2 flux calculation (see section 2.5). Two fCO_2-products (Jena-MLS, LDEO-HPD) extend back to 1959. All fCO_2-products were adjusted for the pre-industrial ocean source of CO_2 from river input to the ocean, by subtracting a source of 0.65 GtC yr^{-1} to make them comparable to S_{OCEAN} (see Section 2.5). The bar-plot in the lower right illustrates the number of monthly gridded values in the SOCAT v2025 dataset (Bakker et al., 2025a). Grey bars indicate the number of grid cells in SOCAT v2024, and coloured bars indicate the newly added grid cells in v2025.

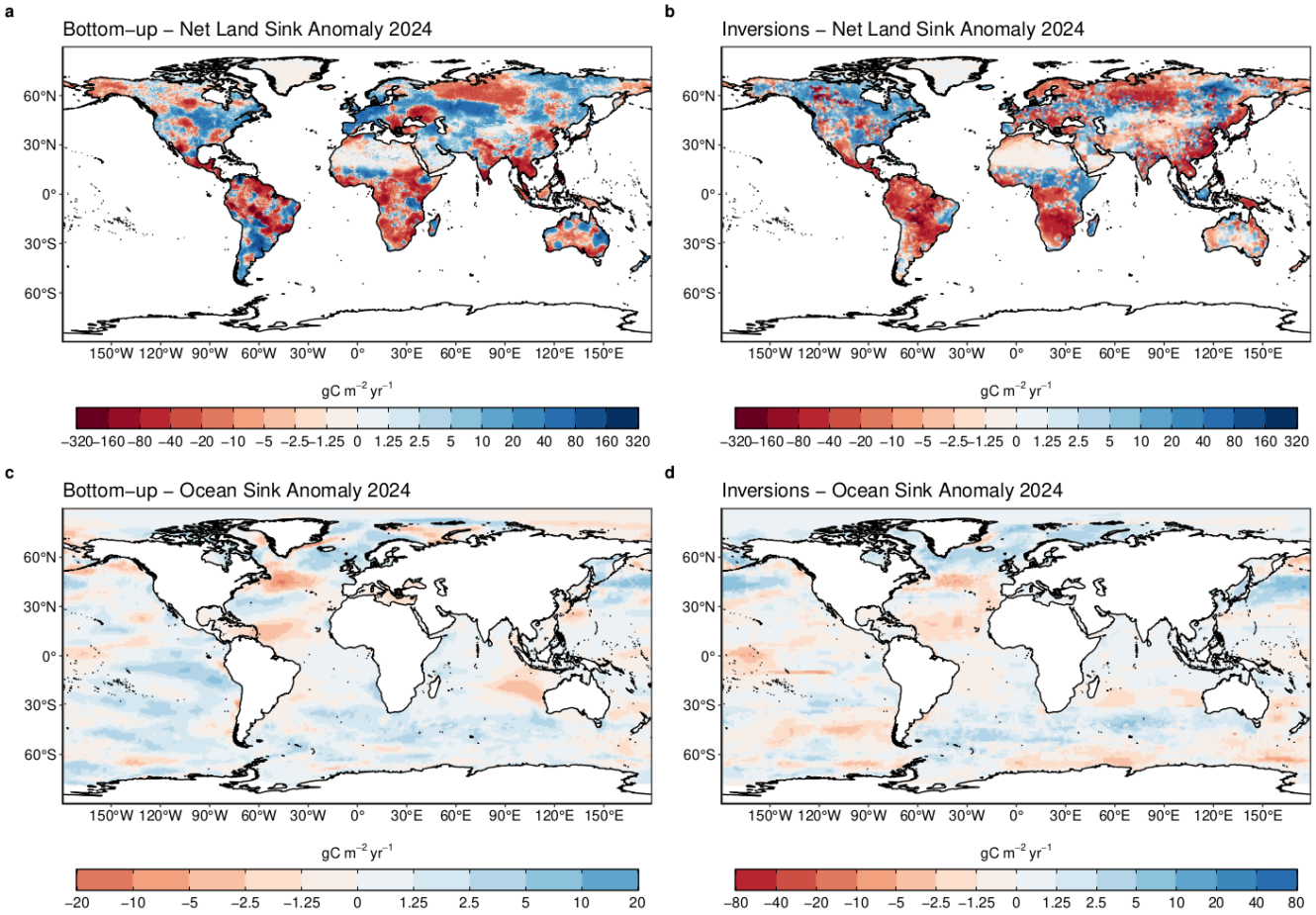

Figure 11. Anomalies in land and ocean sinks for 2024. Maps show the 2024 fluxes relative to the 2015-2024 decadal mean. Units are gC m^{-2} yr^{-1}. (a) The bottom-up anomaly in the net land flux combines both the anomaly in S_{LAND} from DGVMs and in E_{LUC} from bookkeeping models, although the E_{LUC} contribution to the anomaly is minimal. Panel (b) shows the mean anomaly in the net land flux across 14 inversions. Panel (c) shows the mean anomaly from GOBMs and fCO_2 product ensemble means. The mean anomaly for GOBMs and fCO_2 products is first calculated, and then the mean of the two products is shown. Panel (d) shows the mean anomaly in ocean fluxes across 14 inversions.

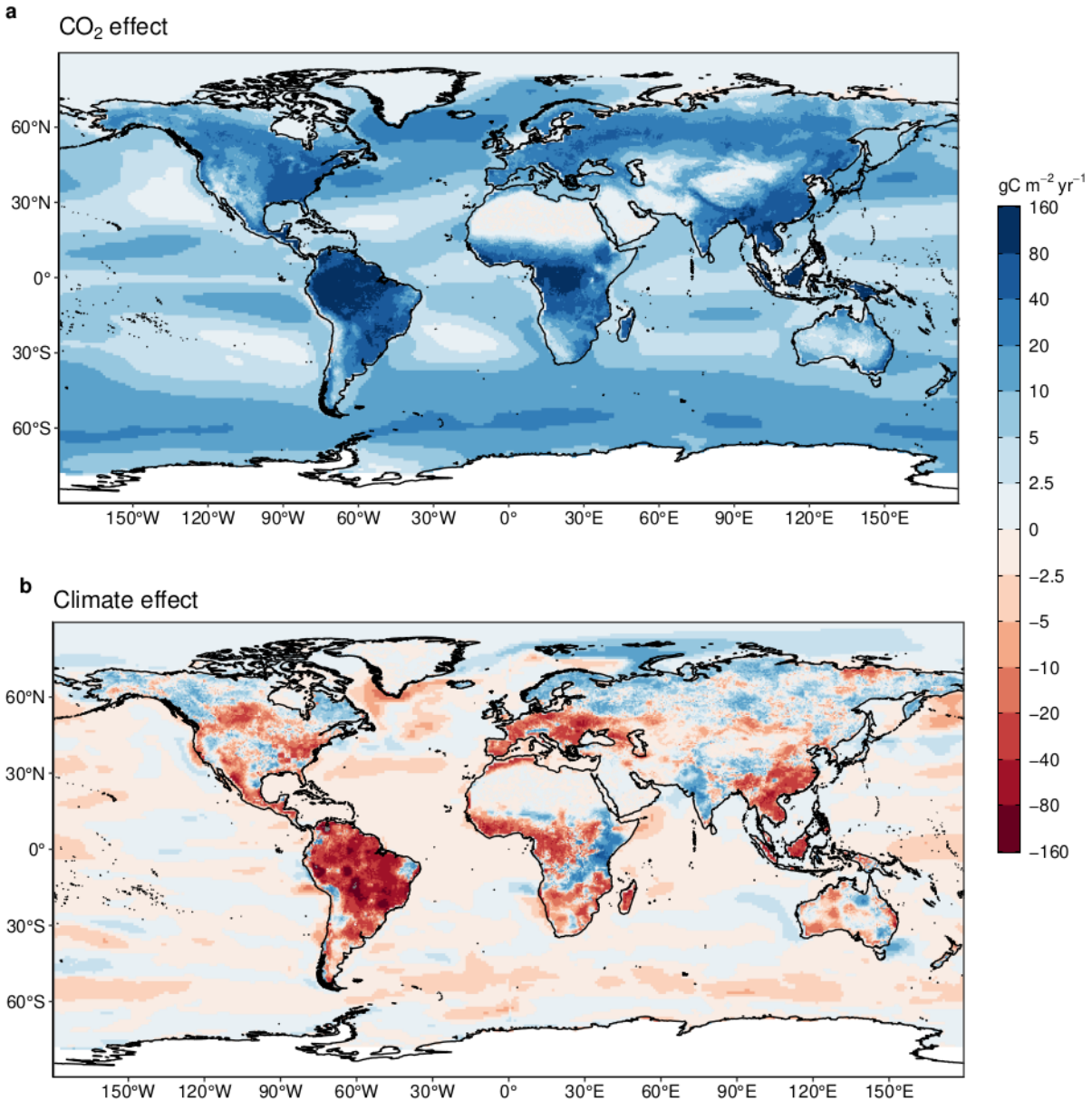

198

199 **Figure 12.** Attribution of the atmosphere-ocean (S_{OCEAN}) and atmosphere-land (S_{LAND}) CO_2 fluxes to (a)
200 increasing atmospheric CO_2 concentrations and (b) changes in climate, averaged over the previous decade 2015-
201 2024. All data shown is from the processed-based GOBMs and DGVMs. Note that the sum of ocean CO_2 and
202 climate effects shown here will not equal the ocean sink shown in Figure 6, which includes the *f*CO_2-products.
203 No adjustments were applied to the DGVMs or GOBMs. See Supplement S.3.2 and S.4.1 for attribution
204 methodology. Units are in gC m^{-2} yr^{-1} (note the non-linear colour scale). Positive values (blue) are CO_2 sinks,
205 negative values (red) are CO_2 sources.

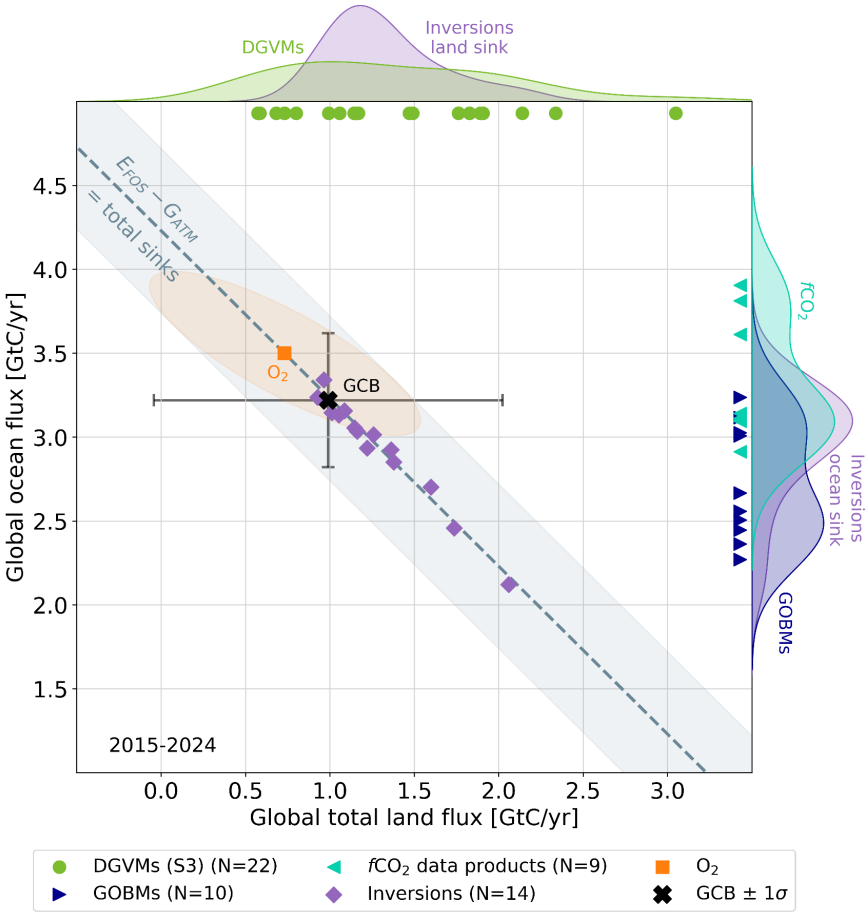

206

207 **Figure 13.** The 2015-2024 decadal mean global net atmosphere-ocean and net atmosphere-land fluxes derived
208 from the ocean models and fCO_2 products (y-axis, right and left pointing blue triangles respectively), and from
209 the DGVMs (x-axis, green symbols), and the same fluxes estimated from the atmospheric inversions (purple
210 symbols). The shaded distributions show the densities of the ensembles of individual estimates. The black
211 central cross ('GCB') is the mean (±1σ) of S_{OCEAN} and ($S_{LAND} - E_{LUC}$) as assessed in this budget. The grey
212 diagonal line represents the constraint on the global land + ocean net flux, i.e. global fossil fuel emissions minus
213 the atmospheric growth rate from this budget ($E_{FOS} - G_{ATM}$). The orange square represents the same global net
214 atmosphere-ocean and atmosphere-land fluxes as estimated from the atmospheric O_2 constraint (the ellipse
215 drawn around the central atmospheric O_2 estimate is a contour representing the 1σ uncertainty of the land and
216 ocean fluxes as a joint probability distribution). Positive values are CO_2 sinks. Note that the inverse estimates
217 have been scaled for a minor difference between E_{FOS} and GridFEDv2025.1 (Jones et al., 2025). The 'GCB'
218 central mean estimate includes the S_{LAND} and S_{OCEAN} global adjustments. The inversions and fCO_2 products
219 include the river adjustment (see Section 2). No further adjustments were applied to the individual bottom-up
220 estimates.

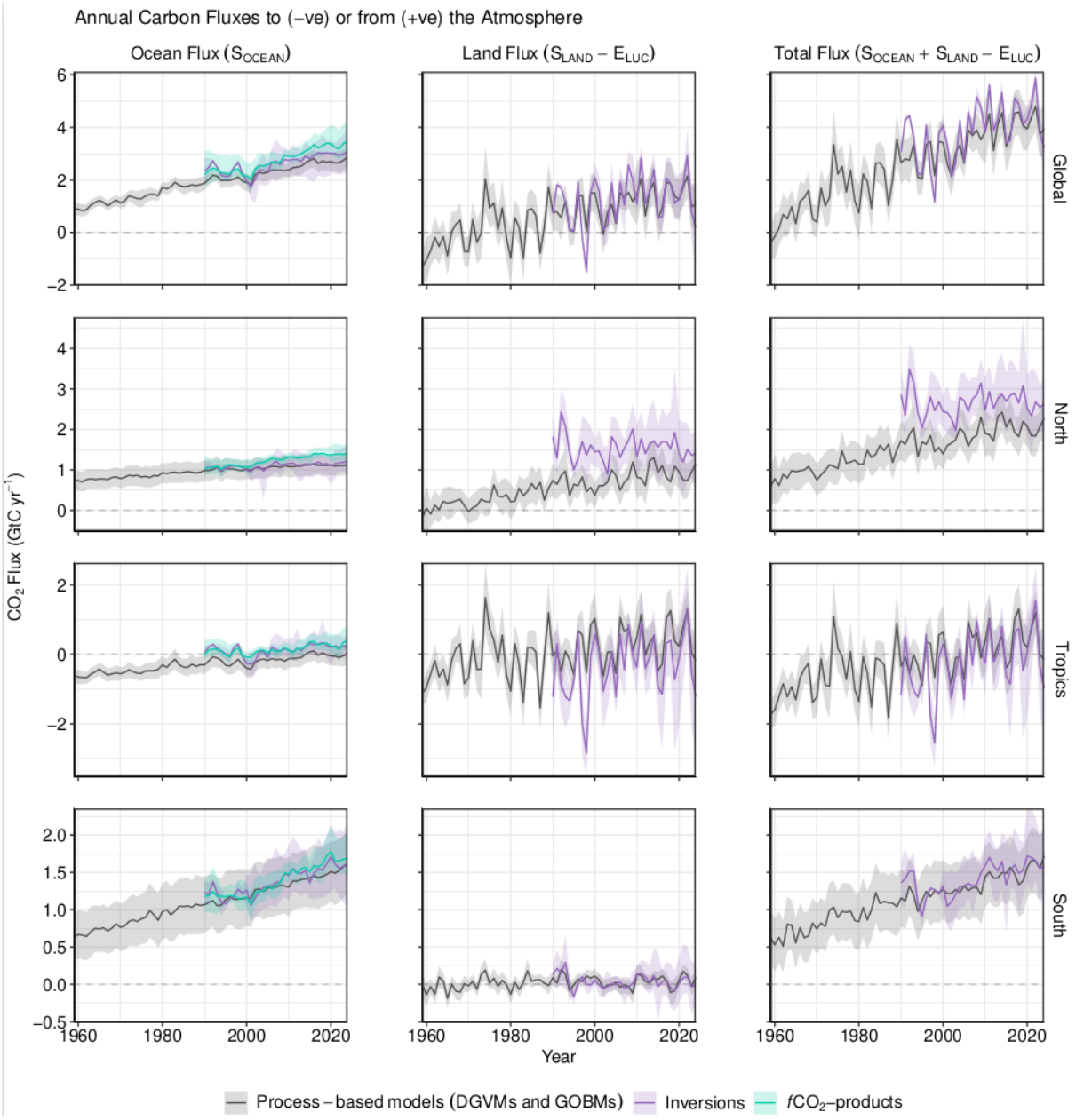

221

222 **Figure 14.** CO_2 fluxes between the atmosphere and the Earth's surface separated between land and oceans,
223 globally and in three latitude bands. The ocean flux is S_{OCEAN} and the land flux is the net atmosphere-land fluxes
224 from the DGVMs. The latitude bands are (top row) global, (2nd row) north (>30°N), (3rd row) tropics (30°S-
225 30°N), and (bottom row) south (<30°S), and over ocean (left column), land (middle column), and total (right
226 column). Estimates are shown for: process-based models (DGVMs for land, GOBMs for oceans); inversion
227 systems (land and ocean); and fCO_2-products (ocean only). Positive values are CO_2 sinks. Mean estimates from
228 the combination of the process models for the land and oceans are shown (black line) with ±1 σ of the model
229 ensemble (grey shading). For the total uncertainty in the process-based estimate of the total sink, uncertainties
230 are summed in quadrature. Mean estimates from the atmospheric inversions are shown (purple lines) with their
231 full spread (purple shading). Mean estimates from the fCO_2-products are shown for the ocean domain (light blue

lines) with full model spread (light blue shading). The global S_{OCEAN} (upper left) and the sum of S_{OCEAN} in all three regions represents the anthropogenic atmosphere-to-ocean flux based on the assumption that the pre-industrial ocean sink was 0 GtC yr^{-1} when riverine fluxes are not considered. This assumption does not hold at the regional level, where pre-industrial fluxes can be significantly different from zero. Hence, the regional panels for S_{OCEAN} represent a combination of natural and anthropogenic fluxes.

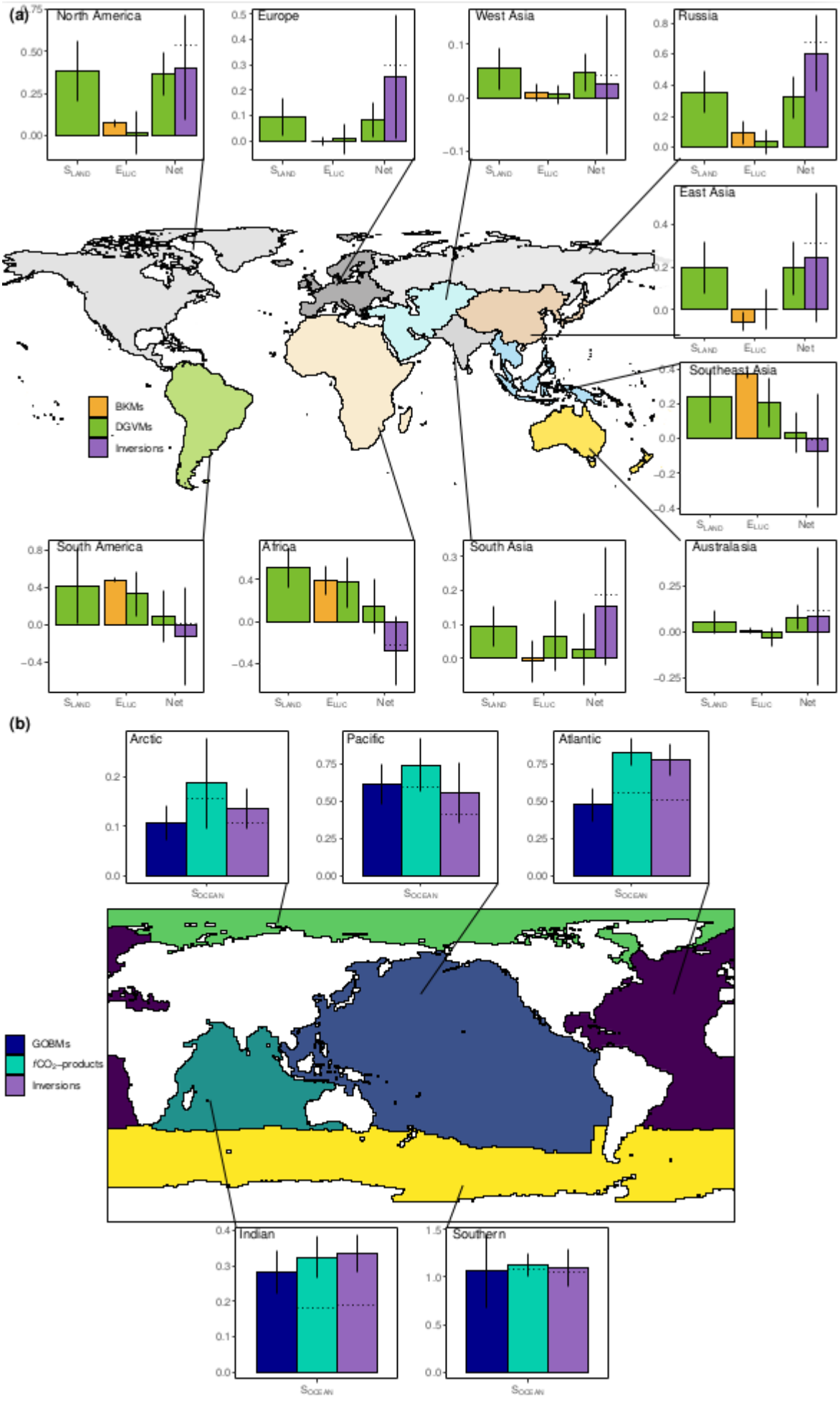
(a)
North America
Europe
West Asia
Russia
East Asia
Southeast Asia
South America
Africa
South Asia
Australasia
BIMs
DGVMs
Inversions
(b)
Arctic
Pacific
Atlantic
Indian
Southern
GOBMs
fCO2−products
Inversions

Figure 15. Decadal mean (a) land and (b) ocean fluxes for RECCAP-2 regions over 2015-2024. For land fluxes, S_{LAND} is estimated by the DGVMs (green bars), with the error bar as ±1σ spread among models. A positive S_{LAND} is a net transfer of carbon from the atmosphere to the land. E_{LUC} fluxes are shown for both DGVMs (green) and bookkeeping models (orange), again with the uncertainty calculated as the ±1σ spread. Note, a positive E_{LUC} flux indicates a loss of carbon from the land. For the DGVMs, S_{LAND} and E_{LUC} are adjusted for RSS bias. The net land flux is shown for both DGVMs (green) and atmospheric inversions (purple), including the full model spread for inversions. The ocean sink (S_{OCEAN}) is estimated by GOBMs (royal blue), fCO_2-products (cyan), and atmospheric inversions (purple). No adjustments were applied to GOBMs and fCO_2-products at regional scale. Uncertainty is estimated as the ±1σ spread for GOBMs, and the full model spread for the other two datasets. The dotted lines show the fCO_2-products and inversion results without river flux adjustment. Positive values are CO_2 sinks.